FACULDADE DE CIÊNCIAS E TECNOLOGIA
UNIVERSIDADE NOVA DE LISBOA

Influence of Constraining and Confinement in the Molecular Mobility of Low Molecular Weight Materials

Ana Rita Elias Brás

(Graduated in Chemical Engineering)

Dissertation presented to obtain a Ph.D. Degree in Chemical Physics

Supervisors: Dr. Madalena Dionísio (U.N.L. – Portugal)
Dr. Andreas Schönhals (B.A.M. – Germany)

Examiners:
Dr. Simone Capaccioli
Dr. Carlos Jorge Mariano Miranda Dias
Dr. Pedro Manuel Corrêa Calvente Barahona
Dr. Natália de Fátima Teixeira Correia
Dr. João Filipe Colardelle Luz Mano

Lisbon
2009

À minha querida Mãe,

ao Thomas,

à Avó Júlia e ao Avô Cristovão,

ao Pai.

"A Ciência é a razão do Mundo, a Arte a sua alma."

Máximo Gorki

"*A finalidade da Ciência é a Verdade. A finalidade das Artes é, pelo contrário, o prazer."*

Gotthold Ephraim Lessing

"Unsere Hauptaufgabe ist nicht, zu erkennen, was unklar in weiter Entfernung liegt sondern: Zu tun, was klar vor uns liegt."

Thomas Carlyle

REPORTS BY EXTERNAL ASSESSORS

Dr. Kia L. Ngai
Naval Research Laboratory
DC 20375-5320 Washington, DC, (USA)
email: ngai@df.unipi.it

EVALUATION FORM OF THE Ph.D. THESIS WHICH DATA ARE INDICATED IN THE FOLLOWING

AUTHOR OF THE Ph.D. THESIS: Ana Rita Elias Brás

TITLE OF THE Ph.D. THESIS: *Influence of constraining and confinement in the molecular dynamics of low molecular weight materials*

ADVISERS: Maria Madalena Alves Campos de Sousa Dionísio Andrade (Assistant Professor of the Chemistry Department, of Faculdade de Ciências e Tecnologia da Universidade Nova de Lisboa) and Priv. Doz. Dr. Habil. **Andreas Schönhals** (BAM-Federal Institute of Materials Research and Testing, Germany)

Dr. K.L. Ngai , selected as external evaluator of the Ph.D. Thesis described before, provides the respective EVALUATION FORM.

Naval Research Laboratory, Washington DC, USA , the 15th of December of 2009

Signature: 

Specifications of the Evaluation Form

1. Existence of concrete objectives and interest in the subject of the Thesis:

Definitely the thesis work has concrete objectives, and the subject matter is of current interest in the research community.

2. Existence of a methodologic strategy suited to the proposed objectives:

The candidate used techniques well suitable for the investigation of the dynamics of soft matter, and followed some previously established methods to investigate the dynamics of several materials. Her advisors are experts in the field and the methodology she followed are well suited for the objectives.

3. Interest of the achieved results and conclusions:

The results obtained by the candidate are of great interest not only to the glass transition research community, but also to pharmaceutical research, and to nano-science. The conclusions have impact on the current understanding.

4. Formal characteristics of the doctoral memory:

The thesis is well written, rich in content, and reflects many months of hard work by the candidate. She is well trained and ready to go on to do bigger things.

5. Observations (use as many as blank pages as necessary):

The thesis has the quality that it can be accepted for the Ph.D. degree at prominent American Universities. I congratulate her for a job well done.

6. Global evaluation

Excellent

Dr. Simone Capaccioli
Researcher and Lecturer- Dynamics of Soft Matter Lab
Dipartimento di Fisica, Università degli Studi di Pisa,
Largo B.Pontecorvo n.3 - I-56127 Pisa (Italy)
tel. 0039-0502214537; tel. 0039-0502214322 (lab)
fax 0039-0502214333
email: Simone.Capaccioli@df.unipi.it

EVALUATION FORM OF THE Ph.D. THESIS WHICH DATA ARE INDICATED IN THE FOLLOWING

AUTHOR OF THE Ph.D. THESIS: Ana Rita Elias Brás

TITLE OF THE Ph.D. THESIS: *Influence of constraining and confinement in the molecular dynamics of low molecular weight materials*

ADVISERS: Maria Madalena Alves Campos de Sousa Dionísio Andrade (Assistant Professor of the Chemistry Department, of Faculdade de Ciências e Tecnologia da Universidade Nova de Lisboa) and Priv. Doz. Dr. Habil. **Andreas Schönhals** (BAM-Federal Institute of Materials Research and Testing, Germany)

Dr. SIMONE CAPACCIOLI , selected as external evaluator of the Ph.D. Thesis described before, provides the respective EVALUATION FORM.

PISA, the 10th of December of 2009

Signature: Simone Capaccioli .

Specifications of the Evaluation Form

1. Existence of concrete objectives and interest in the subject of the Thesis:

The main objective of this work is the experimental study of the effects of nano-scale confinement on the dynamics of glass forming materials.
This issue is one of the most debated and hot topic in current literature and it is one of the most interesting subject for basic research in condensed matter study. In fact, although this subject has been studied since several decades and by several top scientists and laboratories (I could mention the Nobel Prize laureate J.P. De Gennes, but also J. Forrest, Greg McKenna, Friedrich Kremer, Andreas Schönals, etc.), an overall shared rationale about the observed results is still missing. The challenge is actually very general and regards also the concepts used to explain the properties of supercooled liquids in the bulk state: to understand what happened when matter is confined at the nanoscale, where the size of the confinement is approaching that typical for several dynamic and thermodynamic phenomena is of impact for all the field. The interest from the point of view of the basic research is well justified.
Actually Science is more valuable if it has a specific accountability for the overall society. Well, this thesis can attract also a strong interest for the applied point of view. In fact, the three systems chosen for testing the effect of confinement on dynamics are very important for nanotechnology applications:
a) Liquid crystals are of interest by themselves, for instance for their applications for displays and electro-optical devices, but the study of a partially ordered phase in nano-pores is a subject relevant for the study of the interfacial effect in soft matter and biomimetic materials;
b) The confinement of drugs, like ibuprofen, are important for medicine and pharmaceutical research, especially because the nano-confinement can allow their preparation or reinforce their stability in the amorphous state, that is the fundamental state to have a good bioavailability and prompt solubility. Concerning this issue, the idea of study dynamics in the supercooled and glassy state of confined ibuprofen is striking. Also the matrix used for nano-confinement is an excellent choice, as similar systems are used for controlling drug delivery and release in the organisms;
c) The study of partially crystallized polymers and in particular the mobility in the rigid amorphous phase (RAP) of PLLA is also of strong applied interest for several reason. PLLA is a biodegradable materials that recently is often preferred to other poly-esters, like PET, of difficult recycling. Moreover, it is one of the most used polymeric materials for gas barrier film membranes in packaging (both food and drug) industry. Concerning the last issue, it has to be mentioned that the nano-scale confined rigid amorphous phase is the most responsible for gas permeation in the polymeric membrane. Controlling its mobility means to tune the properties of gas barrier of the film. Finally, PLLA is a biopolymer of strong use in biomedical applications, like scaffolds for tissue engineering prosthetic implants. Again, mobility in RAP can controlled mechanical properties and it is clear that this can be of interest for applications.
Summarizing, the objectives of the thesis are clear, well chosen and concrete. Its interest is strong for both the fundamental and applied research.

2. **Existence of a methodologic strategy suited to the proposed objectives:**

The thesis is a nice example of experimental work. All the best methods were used to prepare nano-porous matrices, characterized them and optimizing the filling procedure with the materials under study. This work was carried out according careful and advanced procedures and using the best experimental techniques. Concerning dynamics, a lot of work have been done first on the materials (E7 and ibuprofen) in their bulk state, in order to obtain information completely lacking in the literature or only present in a marginal form. This part, on its own, would be original and valuable. All the other part, related to confinement, is of striking accuracy. The main experimental technique used was (DS) dielectric spectroscopy, very often conducted on a very broad band (more than 11 decades) and always the results were completely analysed, taking into account information coming from the temperature dependence of (i) dielectric strength, (ii) characteristic relaxation times, (iii) shape parameters and, in some cases, also the conductivity contribution was considered. Very often, several experimental techniques were used and combined in order to get information and rationalizing the results. For instance, in the case of E7, the combined used of specific heat spectroscopy and DS was able to reveal that the process related to the glass transition is the tumbling motion. Again in the case of confined E7, infrared spectroscopy provided information about the state of interaction of cyano group to the interface. In the case of ibuprofen, the tendency to form aggregates by H-bonding was proofed by DSC, HPLC, ESI Spectrometry, IR spectroscopy and also predicted by molecular dynamic simulations.
Finally, let me affirm that it is very rare to see how many results coming from different techniques were well rationalized in a thesis.

3. **Interest of the achieved results and conclusions:**

The interest of the specific results and of the conclusions provided by the candidate is multifold. Concerning E7 and ibuprofen in their bulk state, the dielectric study, combined with other techniques, was able to deepen some aspect still unclear in literature due to the few data available until now. In Ibuprofen, some important aspects concerning sub-glass relaxations and their relationship to the glass transition were clarified. For E7, all the dynamics is now more clear: among the many results, let me mention the assignment of the tumbling mode as the α-relaxation that brings to the glass transition. Concerning the confinement of the systems (and also the study of the constrained rigid amorphous phase in semicrystalline PLLA) it is important that all the studies revealed common and different points. Always a slower process coming from the guest molecules interacting with the pore walls (or with the crystals in PLLA) was found. On the other hand the behaviour of the other dynamic processes was found to be sensitive to both confinement (finite size effect or density effect) and interfacial (like bonding or ordering to the surface) effect. Actually, the interface determined dynamics of the system, introducing a gradient of relaxation times across the cooperativity length scale of the guest molecules. The way how the different dynamic processes are affected was rationalized in the thesis, providing useful information for further theoretical studies. I evaluate that the

experimental results coming from this thesis work are of extreme impact for our scientific community.

4. Formal characteristics of the doctoral memory:

The dissertation is clear, correct, well written in English, and easy to be read also by somebody that is not expert in the specific field. Considering the wide and multidisciplinary interest in the subject, the last mentioned quality is extremely valuable. The quality of the figures, graphs, tables and picture is high and they are always provided by clear and useful captions. References, provided at the end of each chapter, are really extensive and always relevant.
Among the 200 pages, the different parts are well identified, distributed and well balanced. Theoretical and general introduction, mainly introducing the main concepts related to glass transition, dynamics, nano-scale confinement and dielectric relaxation, occupies less than 50 pages. Nevertheless the introduction is correct and very efficient to deliver the basic ideas useful for the subsequent discussion. I appreciated a lot the part about the linear response theory, introduced without too many detailed mathematic formalisms. It is also valuable, in order to clarify the state of the art, the fact that the candidate provided in the introduction also a very extensive and updated review of the existing studies on confinement effect for liquid crystals, pharmaceutical drugs and semi-crystalline polymers. The part about the experimental techniques and materials used is also very clear and useful. The choice to move in this part all the experimental details is excellent. Also it was a good idea to present the results and discussion concerning bulk dynamics of the supercooled materials in a chapter and the effect of the confinement in a subsequent chapter, since the most of the results concerning the dynamics of the bulk materials are presented here for the first time.
I did not find any negative aspects from the formal point of view: I might quote only few typing errors that I found into the text and equations that, considering the large size of the dissertation, are much less than what one could reasonably expect. These errors are essentially typing errors, as the correct meaning is preserved.
Summarizing, my evaluation on the formal point of view is that the thesis is formally excellent. I appreciated, in particular, the communication strategy used by the candidate in the original part, that of results and discussion: to give a short outline at the beginning, then to discuss into details and eventually to summarize at the end of chapters or sub-chapters in the conclusion. It is the common procedure followed to write a good article but I never found that was easy to be done for a doctoral thesis, where usually the amount of information to be managed is much larger.

5. Observations (use as many as blank pages as necessary):

There are actually no important observations to be done. The thesis has solid contents and important results, and it is well written and presented. I could mention the following few typing and formal errors in the following. These are in no way changing my positive evaluation of this thesis. There are maybe more typos in this my report.
Specific observations:

- Pag. 24, line 2 after the §1.3.1.1., “The concepts…is shortly outlined below”;
- Pag. 36, equation 1.34 is the same as equation 1.33 just with β_{DC} replacing α_{CC}. The correct one should have at the denominator the bracket including all the terms of the sum: $(1+i\omega\tau)^{\beta DC}$;
- Pag.37, equation 1.35: α_{HN} and β_{HN} should exchange their respective position;
- Pag.43, equation 1.49: there should be $<\cos^2\theta>$ instead of $\cos\theta$;
- Pag.43, two lines below eq.1.49 “anispotropic” should be changed to “isotropic”;
- Pag.45, Ref.42 “McGrun” should be replaced with “McCrum”;
- Pag.48, Ref.118, “Hemperl” should be replaced with “Hempel”;
- Pag. 54, Ref.267, “Bets” should be replaced with “Best”;
- Pag.75, Ref.9 and 10: “Shaumburg” should be replaced with “Schaumburg”;
- Pag.97, 6 lines from the bottom: “..advantage of being not being..” should be replaced with “..advantage of being ...”;
- Pag.114, Ref.63, two authors are missing: S. Capaccioli and R. Casalini;
- Pag. 162, 4 lines from the bottom: “..which compare..” should be replaced with “…which compares…”;
- Pag. 169, Ref.15, “Bets” should be replaced with “Best”;

Moreover, in chapter 3, §3.1.x, there is a mention to bulk E7 sample oriented both in parallel and perpendicular direction to the electric field, but no specific details are provided on the experimental method used to obtain such a condition.

6. Global evaluation

X Excellent
□ Good
□ Acceptable
□ Not acceptable

RESUMO

Apesar da importância que o estado vítreo tem na actualidade, a *transição* do líquido para o vidro, *transição* vítrea, continua a ser uma matéria de debate constituindo um dos grandes desafios da física da matéria condensada. Uma vez que este facto se encontra intimamente relacionado com a dinâmica de cooperatividade, o estudo deste fenómeno em líquidos formadores de vidro sujeitos a confinamento, em nano-escala, surgiu recentemente como uma estratégia para o esclarecimento de factores como a existência de uma escala de tamanho inerente para o movimento cooperativo que determina a transição vítrea. Neste contexto, a presente tese representa uma contribuição adicional para o estudo da dinâmica molecular de líquidos formadores de vidro sob confinamento em materiais inorgânicos nanoporosos. Como compostos alvo, foram seleccionados o cristal líquido E7 e o fármaco Ibuprofeno. O primeiro devido às múltiplas transições que exibe torna-o mais susceptível a perturbações e desse modo aparece como o candidato ideal para avaliação de efeitos de confinamento. O estudo do 2º composto, o Ibuprofeno, reveste-se de particular interesse uma vez que o confinamento surge como uma forma de estabilizar a fase amorfa que assume especial relevância em aplicações farmacêuticas. A técnica principal que se utilizou para obter informação detalhada acerca da mobilidade molecular foi a Espectroscopia de Relaxação Dieléctrica (*DRS*), utilizando uma larga gama de frequências (10^{-2}-10^{9}Hz) (Capítulo I e II).

A primeira parte da tese é dedicada à caracterização dos dois compostos alvo no seu estado original. Para o E7, a combinação de DRS, com a espectroscopia de calor específico permitiu determinar qual dos processos de relaxação típicos deste (um processo na fase isotrópica ou líquida e dois processos na fase nemática: δ e *tumbling*) é responsável pela transição vítrea T_g (processo *tumbling*). O estudo detalhado da mobilidade molecular do ibuprofeno no estado líquido, líquido sobrearrefecido e vítreo, é apresentado ainda neste capítulo, tendo-se observado quatro processos de relaxação: dois processos secundários (γ e β), o processo cooperativo relacionado com a T_g (α) e o processo de Debye (D), este último provavelmente relacionado com a dinâmica das pontes de hidrogénio. Este estudo foi antecedido por uma optimização das condições necessárias para amorfizar o Ibuprofeno que no seu estado natural é um cristal (capítulo III).

No capítulo seguinte (capítulo IV), avaliou-se a dinâmica molecular do E7 confinado em membranas inorgânicas rígidas de 20 nm de diâmetro de poro quer revestidas com o fosfolípido, *lecitina*, quer no seu estado natural. Verificou-se que tanto o alinhamento do cristal líquido, como a dinâmica são influenciados pelo confinamento e pelo tratamento da superfície dos poros. Em seguida, o estudo do confinamento do E7 prosseguiu para materiais mesoporosos, do

tipo MCM-41 e SBA-15 de composição 100% sílica e de tamanho de poro entre os 2.8 e 6.8 nm. O estudo da dinâmica molecular por DRS revelou uma multiplicidade de processos de relaxação, incluindo os modos já observados no E7 original. Além destes, dois novos processos, S e I, a frequências inferiores aos anteriores foram detectados e atribuídos às moléculas de cristal líquido ancoradas à superfície interior e exterior dos poros, respectivamente.

O Ibuprofeno foi igualmente confinado naquelas matrizes com o tamanho de poro 3.6 e 6.8 nm. Este estudo revelou o confinamento como uma forma eficaz de obter o Ibuprofeno no estado amorfo. Por DRS observaram-se para além de dois processos secundários (γ e β) semelhantes aos encontrados para o Ibuprofeno livre, dois outros processos, sendo que um deles, o mais lento, é atribuído às moléculas de Ibuprofeno ancoradas à superfície interior do poro. O outro processo (α) revelou que a dinâmica do Ibuprofeno confinado é acelerada relativamente ao composto original.

Por fim, no capítulo V descreve-se o estudo do constrangimento da mobilidade da relaxação α associada à transição vítrea durante a cristalização do PLLA. Verificou-se que a mobilidade molecular durante a cristalização isotérmica pode ser descrita como um somatório de dois processos de relaxação, que progridem de forma independente, um com as características do processo de relaxação associado á transição vítrea já detectado no PLLA amorfo, e outro, de menor mobilidade, associado às regiões amorfas rígidas adjacentes à fase cristalina. O confinamento exercido pela fase amorfa rígida foi estudado em amostras de diferentes graus de cristalinidade compreendidos entre 0.43 e 0.65. Observou-se ainda que o processo de relaxação associado à transição vítrea sofre um aumento de mobilidade com o aumento da cristalinidade. Este facto, quase contra-intuitivo, foi racionalizado em termos de i) aumento da espessura da fase amorfa rígida que diminui a influência da parede cristalina nos movimentos cooperativos das cadeias poliméricas e ii) uma fase amorfa menos densa que permanece após a cristalização. Adicionalmente encontrou-se um carácter multi-modal para o processo de relaxação associado a movimentos localizados. A natureza multi-componente deste processo secundário revelou-se como uma sonda da morfologia atingida.

Palavras-Chave: confinamento, transição vítrea, relaxação dieléctrica, cristalização

ABSTRACT

Despite the importance that the glassy state has nowadays, the *transition* from liquid to the glass, glass *transition*, still remains a matter of debate which constitutes one of the great condensed matter physics challenges. Since this fact is closely related to the cooperativity dynamics, the study of this phenomenon in glass-forming liquids under confinement in the nanometer scale, has recently emerged as a strategy to clarify factors such as the existence of an inherent length scale of the cooperative dynamics that determines the glass transition temperature. In this context, this thesis represents an additional contribution to the study of molecular dynamics of glass-forming liquids under confinement in nanoporous inorganic materials. As target compounds the liquid crystal E7 and the drug Ibuprofen were selected. Since the first exhibit various transitions makes it more sensitive to perturbations and thus appears as the ideal candidate to evaluate confinement effects. The study of ibuprofen is of particular interest because confinement emerges as a method of stabilizing the amorphous phase that is mostly important in pharmaceutical applications. Dielectric Relaxation Spectroscopy (DRS) is the main technique used to obtain detailed information about the molecular mobility in a wide range of frequencies (10^{-2}-10^{9}Hz) (Chapter I and II).

The first part of the thesis is devoted to the characterization of the two target compounds in the bulk state. The combination of DRS with the specific heat spectroscopy allowed to determine which of the E7 observed relaxation processes (a process in the isotropic phase and two processes in the nematic phase: δ and tumbling) is responsible for the glass transition temperature T_g (tumbling process). Detailed studies of ibuprofen molecular mobility in the liquid, supercooled liquid and glassy states are also presented in this chapter, where four relaxation processes are detected: two secondary processes (γ and β), the cooperative process related to T_g (α) and the Debye process (D), probably related to the hydrogen bonding dynamics. This study was preceded by an optimization of the conditions to obtain amorphous Ibuprofen which is a crystal in its natural state (Chapter III).

In the next chapter (Chapter IV), the molecular dynamics of E7 confined to untreated and phospholipid lecithin treated rigid inorganic membranes with 20 nm pore diameter was evaluated. It was found that both the liquid crystal alignment, as well as the dynamics is influenced by confinement and treatment of the surface pores. Additionally, E7 was further studied confined to the mesoporous materials MCM-41 and SBA-15 type, 100% silica composition and pore size between the 2.8 and 6.8 nm. A multiplicity of relaxation processes was revealed by DRS, including the modes already observed in the bulk E7. In addition, two

new processes, S and I, at frequencies lower than the previous ones were detected and attributed to the liquid crystal molecules anchored to the inner and outer pore surface, respectively.

Ibuprofen was also confined to the molecular sieves with pore size 3.6 and 6.8 nm. This study revealed to be an effective way to obtain Ibuprofen in the amorphous state. Besides two secondary processes (γ and β) similar to those found for bulk ibuprofen, it was observed two other processes, the slower one is assigned to the ibuprofen molecules anchored to the inner surface of the pore. The other process revealed that the dynamics of confined Ibuprofen is faster as compared to the bulk α-relaxation.

Finally, Chapter V describes the mobility study of the α-relaxation associated to the glass transition constrained during crystallization of PLLA. It was found that the molecular mobility during the isothermal crystallization can be described as a sum of two relaxation processes that evolve independently, one characteristic of the process associated to glass transition already detected in the amorphous PLLA, and another, with lower mobility, associated with the amorphous regions adjacent to the rigid crystalline phase. The confinement due to the rigid amorphous phase was studied in samples of crystallinity degrees between 0.43 and 0.65. It was observed that the mobility of the relaxation process associated to the glass transition temperature increased with the increase of crystallinity. This fact, almost counterintuitive, was rationalized in terms of both i) thicker rigid amorphous phase that decreases the influence of the rigid crystalline wall on the cooperative motions of the main relaxation process and ii) less dense mobile amorphous phase that remains after crystallization. Additionally, a multi-modal character was found for the secondary relaxation process, associated with localized movements. The multi-component nature of this secondary process turned to be a probe of the morphology attained.

Keywords: confinement, glass transition, dielectric relaxation, crystallization

AGRADECIMENTOS

Agora, no último dia que me resta antes de entregar este meu trabalho e com a pressão natural destes momentos, quero pensar nos agradecimentos, mas o meu pensamento voa e começo a recordar como todo o meu percurso começou.

O Erasmus e a minha ida para a Alemanha, o final do curso, a entrada como bolseira para dar início àquilo que viria a ser a minha vida, o que gosto de fazer e que está a culminar com a entrega da minha tese de doutoramento.

A todas as pessoas com quem partilhei estes quatro anos…todas mesmo, estou grata e nomeando apenas alguns nomes, os mais importantes e decisivos, não esqueço, todos aqueles que das mais diferentes formas me deram o seu incentivo e apoio, todos os meus colegas, amigos, e família que ajudaram a concretizar e a chegar ao fim desta etapa da minha vida.

À Celina, Sofia, Inês, do laboratório, e em especial a Maite, que me apoiou desde o início. Aos queridos, Mafalda e João Dias que estão sempre comigo. Ao João Fernandes, à Lili, ao Márcio, à Sofia e à Ana, pelos almoços e jantares de convívio. Ao Hugo e à Andreia, pelo incentivo e mensagens encorajadoras. À Pia da Alemanha até hoje, pela sempre presença, ao longe.

Ao Frédéric e à Emeline pela partilha sempre generosa dos seus conhecimentos, que muito contribuíram para esta tese, assim como pelo seu apoio, muito importante, durante a minha estadia em Lille.

E por fim…

À Natália, paciente e querida Natália, com os seus ensinamentos, conselhos, o seu saber científico, que seria deste trabalho sem a sua persistência e amizade. Foi e será sempre um privilégio tê-la do meu lado.

Ao meu co-orientador alemão Andreas, sempre interessado e gentil, com as suas sugestões e conhecimentos científicos, que contribuíram de forma crucial para que esta tese se aperfeiçoasse*.

À PROFESSORA Madalena, que tornou real e possível este meu sonho. Fica para além do aqui descrito a minha gratidão pela sua amizade, pelos seus ralhos, pelas suas canseiras comigo, mesmo quando por vezes o seu cansaço era evidente. Comecei a trabalhar com ela, antes do inicio desta tese e assim com o seu muito saber e apoio, consegui aprender e desenvolver as minhas capacidades tanto pessoais, como científicas nesta área de trabalho que me permitiu ter aqui chegado.

Dou graças a Deus por tudo o que me deu, o que me fez conseguir e por ter encontrado a Professora Madalena.

*Hiermit möchte ich bei allen bedanken, die seitens der BAM im besonderen Maße zum Gelingen dieser Arbeit beigetragen haben.
An erster Stelle möchte ich mich bei Priv.-Doz. Dr. Andreas Schönhals für die sehr gute Betreuung meiner Arbeit bedanken. Es war ein ganz besonderes Privileg für mich, mit einem der führenden Experten auf dem Gebiet „confinement and dielectrics“ zusammenzuarbeiten. Die Arbeit mit ihm war sehr angenehm. Zudem waren fachliche Diskussionen immer sehr fruchtbar gaben mir wichtige Denkanstöße. Ein ganz besonderer Dank noch einmal für die intensive Betreuung vor allem bei der endgültigen Ausarbeitung der Doktorarbeit und dem hohen persönlichen Einsatz, der auf Grund der externen Betreuung sicherlich einiges an Mehraufwand mit sich brachte.
Persönlich danken möchte ich auch Ligia und Stefan Frunza, Hao Ning, Ole Hölck und Diana Labahn für die nette Unterstützung während meiner Aufenthalte und die gute Arbeitsatmosphäre. Ein weiterer Dank geht an Frau Bertus und Herrn Audi für die Hilfe im Labor.

I would like to thank “Fundação para a Ciência e Tecnologia” for the financial support by means of the PhD grant SFRH/BD/23829/2005.

To the Chemistry Department of “Faculdade de Ciências e Tecnologia da Universidade Nova de Lisboa” (Portugal), to BAM- Federal Institute of Materials Research and Testing (Germany) and to “Laboratoire de Dynamique et Structure des Matériaux Moléculaires, Université des Sciences et Technologies de Lille” (France).

GENERAL INDEX

FIGURE INDEX

CHAPTER 2| EXPERIMENTAL

CHAPTER 3| MOLECULAR MOBILITY OF BULK MATERIALS

CHAPTER 5| CHANGES IN PLLA MOLECULAR MOBILITY UPON CONSTRAINING

CHAPTER 6| CONCLUSIONS

TABLE INDEX

CHAPTER 1| THEORETICAL ASPECTS

CHAPTER 2| EXPERIMENTAL

CHAPTER 3| MOLECULAR MOBILITY OF BULK MATERIALS

LIST OF SYMBOLS

α	…	Polarizability $(C.m^2.V^{-1})$
ΔC_p	…	Molar heat capacity increment $(J.mol^{-1}.K^{-1})$
d	…	Pore diameter (m)
d_a	…	Amorphous layer thickness (m)
D	…	Dielectric displacement $(C.m^{-2})$
E	…	Outer electrical field $(V.m^{-1})$
E_A	…	Activation energy $(J.mol^{-1})$
E_L	…	Electric field strength $(V.m^{-1})$
E_0	…	Field amplitude of electric field
ε_s	…	Permittivity at low frequency $(F.m^{-1} = A.s.V^{-1}.m^{-1})$
ε_0	…	Vacuum permittivity $(\varepsilon_0 = 8.854x10^{-12}\ F.m^{-1})$
ε_∞	…	Instantaneous relative permittivity $(F.m^{-1})$
ε^*	…	Dielectric permittivity (Complex dielectric function)
ε'	…	Real component of dielectric permittivity
ε''	…	Imaginary component of dielectric permittivity
$\Delta\varepsilon$	…	Dielectric strength
f	…	Frequency (Hz)
f_v	…	Fractional free-volume
ψ	…	Dielectric function
Φ	…	Dielectric decay function
g_k	…	Kirkwood g-factor
G_g	…	Glass modulus $(Pa = N/m^2)$
ΔG_i^*	…	Gibbs free enthalpy (J)
h	…	Planck constant $(h = 6.626068 \times 10^{-34}.m^2.kg.s^{-1})$
H	…	Enthalpy (J)
ΔH_i^*	…	Activation enthalpy (J)

k	…	Boltzmann constant ($k = 1.381 \times 10^{-23}.m^2.kg.s^{-2}.K^{-1}$)
L	…	Relaxation time distribution (s)
L_c	…	Crystalline thickness (m)
L_{ma}	…	Mobile amorphous thicknesses (m)
L_{ra}	…	Rigid amorphous thicknesses (m)
m	…	Dimensionless “steepness index”
$\langle M \rangle$	…	Average dipole component
μ	…	Electric dipole moment ($Debye$)
$\overrightarrow{\mu_L}$	…	Longitudinal component of dipole moment vector ($Debye$)
$\overrightarrow{\mu_T}$	…	Transverse component of dipole moment vector ($Debye$)
μ_0	…	Permanent dipole moment ($Debye$)
$\Delta\mu$	...	Free energy barrier ($J.mol^{-1}$)
N	…	Number of particles
N_0	…	Number of molecules per unit volume ($mol.m^{-3}$)
P	…	Polarization
P_0	…	Polarization at moment of field removal
P_∞	…	Induced polarization
R	…	Ideal gas constant ($R = 8.314\, J.mol^{-1}.K^{-1}$)
ρ	…	Number density (m^{-3})
S_C	...	Molar configuration entropy
ΔS_i^*	…	Activation entropy ($J.mol^{-1}.K^{-1}$)
σ	…	Conductivity ($S \cdot m^{-1}$)
t	…	Time (s)
t_c	…	Crossover time from localized to cooperative fluctuations (s)
T	…	Temperature (K)
T_g	…	Glass transition temperature (K)
T_c	…	Crystallization temperature (K)
T_B	…	Crossover temperature (K)

T_{IN}	…	Isotropic to nematic transition temperature (K)
T_K	…	Kauzmann temperature (K)
T_m	…	Melting point temperature (K)
T_{ref}	…	Reference temperature (K)
T_0	…	Ideal glass transition or Vogel temperature (K)
$\dot{T}$	…	Cooling rate ($K.min^{-1}$)
τ	…	Relaxation time (s)
v	…	Measured specific volume of a polymer ($m^3.g^{-1}$)
v_f	…	Free-volume per gram ($m^3.g^{-1}$)
v_f^*	…	Critical free volume (m^3)
v_0	…	Occupied volume (m^3)
V	…	Volume (m^3)
ω	…	Angular frequency (s^{-1})
ω_{max}	…	Characteristic relaxation rate (s)
y	…	System response
y_0	…	Dimensionless dipole strength function
z^*	…	Minimal size for cooperative transitions
ξ_α	…	Characteristic length of the glass transition (m)
Θ	…	Filling degree (%)

CHAPTER 1|THEORETICAL ASPECTS

INDEX

1.1 Introduction

The nature of the glass transition is still a matter of debate and it remains a challenge to modern experimental physics to find out under what conditions an ensemble of a few molecules starts to behave like a liquid [1,2,3,4,5,6,7,8]. This question can be approached by measuring over a broad frequency range the molecular dynamics of guest molecules embedded in nanoporous host systems of well controlled confining geometry [6,7,9,10]. The dynamical behavior of the confined guest can significantly deviate from the dynamics of the bulk state. It is now evident that this problem is intimately related to the perception of the cooperative dynamics and its inherent length scale in glass-forming liquids [4-9,11,12,13,14,15].

This work is mainly devoted to the understanding of the impact of geometrical constraints in glass formers under confinement, from both fundamental and practical perspectives in addition to the characterization of the molecular mobility of the bulk glass formers themselves. Being subject to the influence of a continuously changing environment, the molecules of a fluid undergo an irregular motion with respect to both their orientation and position in space. In microporous systems such as zeolites [16,17] molecular mobility is well-known to be dominated by the architecture of the solid and the nature of the interaction. So far, however, only a few systematic investigations have been carried out on the transition from the surface-dominated adsorbate- adsorbent system to the bulk liquid, especially in the case of pharmaceutical compounds, which are now becoming a new practical field of interest, specially as tool to control and stabilize otherwise unstable forms [18,19,20]. In polymers, an additional approach to evaluate nanometer confinement effects on the dynamical behavior other than impregnate the material in a nanoporous matrix, is the induction of crystallization. In this case, the amorphous phase will be entrapped between crystaline lamellae under nanoscale dimensions [21,22,23].

Dielectric spectroscopy, as an ideal tool to study molecular dynamics and charge transport, was chosen the main technique to evaluate the dynamical behavior of the guest in both bulk and confined states in the present work. In its modern form it is broadband in frequency and covers the range from 10^{-6} to 10^{12} Hz. This study applied almost all the frequency range available, from 10^{-2} to 10^{9} Hz.

1.2 Glass Transition

The research of glass transition has a long history that can be traced back to the Babylonians who documented their recipe of making glasses from dessert sand, and to the study of dynamics of alkali silicate glass and a natural polymer by R. Kohlrausch in Göttingen in mid 1800's. Since then, glass transition and its phenomena were found in many kinds of materials including inorganic substances with widely different chemical compositions, organic small molecules, synthetic polymers, side chain liquid crystalline polymers, metallic compounds, plastic crystals, and some biomaterials. The thermodynamic and dynamic properties of glass-forming liquids and glasses are similar, falling into

well-defined patterns [24,25] to suggest some common fundamental physics are at work. The lure of uncovering the basic physics of glass transition has led many scientists from various disciplines to join in the research. Many modern experimental techniques have been applied to study glass transition in more previously known and newly discovered glass-formers [26].

Theoretically, when the temperature is decreased, the velocity of thermal fluctuations in substances with molecular disorder slows down dramatically. If no phase transition occurs to change the disorder, the present has no typical times. Instead the **relaxation time τ** increases continuously fifteen orders of magnitude, from the picoseconds to several minutes. Such variation of τ is concomitant with changes in density or structure which at a typical experimental time (for example minutes), when cooling is continued, the substance vitrifies. A **glass** is then an amorphous solid formed by cooling from the melt to rigidity without crystallization. A material for which crystallization can be circumvented undergoing vitrification upon further cooling is called a **glass-former**.

Rigidity means weak steady response to a permanent shear stress, which in liquids is seen as the viscosity η. To a certain extent connects with τ by the mechanical Maxwell equation [27],

$$\eta \approx G_g \cdot \tau \qquad \textbf{Equation 1. 1}$$

where G_g is a glass modulus of order 10^9 to 10^{12} Pa.

The increase in viscosity reflects the increase in relaxation time [27].

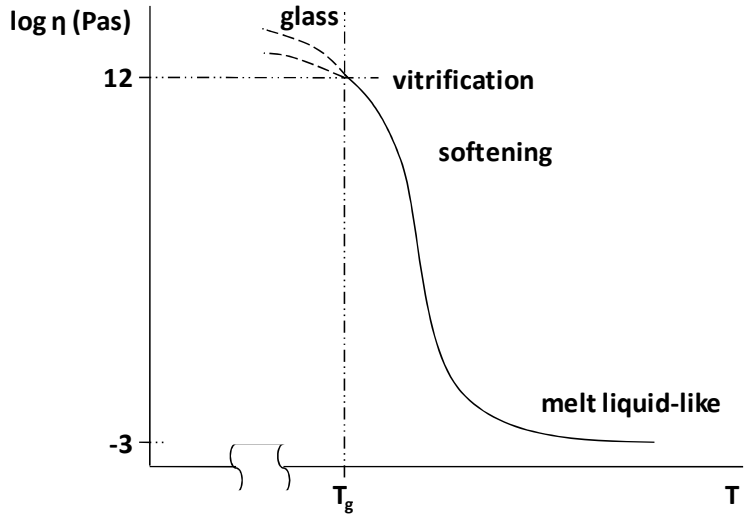

Figure 1. 1- Viscosity temperature dependence and interruption of glass solidification. The properties of the glass below vitrification depend on the cooling rate near T_g (redrawn from [27]).

The solidification of glasses is gradual, with no discontinuity if crystallization doesn't take place. Vitrification is characterized by a "transition" point (normalized at $\eta = 10^{12.3}\text{Pa} \cdot \text{s}$) which is

normally called the **glass transition temperature T_g** (not a proper thermodynamic transition, it is a kinetic process).

1.2.1 Thermal Glass Transition

If a liquid is cooled down (Figure 1. 2) with a given cooling rate $\dot{T} = dT/dt$, below the melting point T_m, molecular motion slows down and if the liquid is cooled sufficiently fast, crystallization can be avoided [27,28,29]; the liquid in such state is called supercooled. At a certain point, molecules will reorganize so slowly that they cannot adequately use configurations in the available time allowed by the cooling rate. Therefore the liquid seems to freeze on a laboratory time scale. The structure of the **supercooled liquid** is retained in a non-equilibrium metastable state, and the material becomes a glass. The transition to a glass occurs across a narrow transformation range where the characteristic molecular relaxation time becomes of the order of 100 seconds. The rate of change of volume or enthalpy with respect to temperature decreases continuously but abruptly to a value comparable to that of a crystalline solid. The intersection of the liquid and glass portions of the volume versus temperature curve provides another definition of T_g, ($T \approx \frac{2}{3}T_m$) [30,31]. In fact, Figure 1. 2 doesn't illustrate a true phase transition behavior, since no discontinuous changes in any physical property is involved.

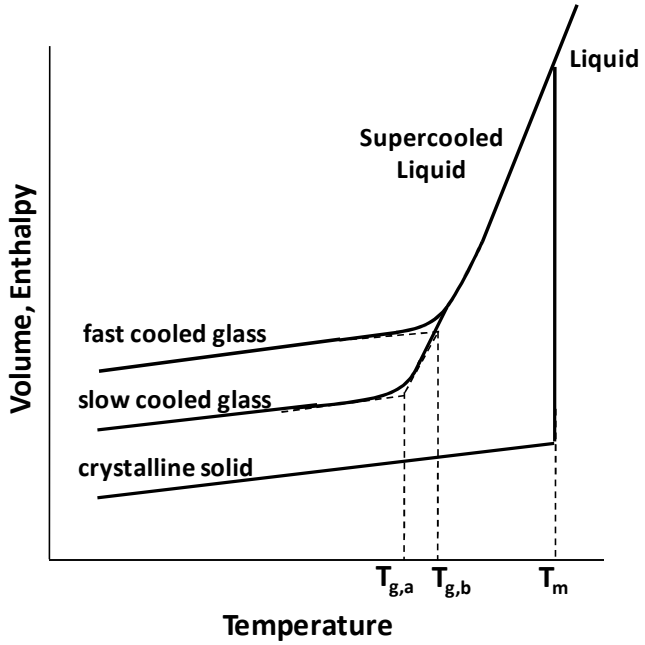

Figure 1. 2- Temperature dependence of a liquid's volume *V* or enthalpy *H* at constant pressure. T_m is the melting temperature. A slow cooling rate produces a glass transition at $T_{g,a}$; a faster cooling rate leads to a glass transition at $T_{g,b}$.(redrawn from [31]).

The properties of a glass depend on the process by which it is formed, as T_g increases with the cooling rate [32,33] (T_g changes by 3-5 K when the cooling rate changes by one order of magnitude [34]) and the transformation rate is narrow, so that T_g is an important material characteristic.

In principle, there are two possible primary concepts for the thermal glass transition: firstly, the primary concept may be a continuous slowing down of the dynamic glass transition in the liquid, consequently the thermal glass transition is then simply a consequence of the fact that thermal fluctuations become too slow to be determined in the present time as described above; secondly, the primary concept may be an ideal glass transition, which means a kinetic phase transition below T_g, therefore, the thermal glass transition is then a dynamic precursor of this ideal transition [27,35]. An old example of these long-running issues given by Gibbs and DiMarzio [36] is the corresponding interpretation of the Kauzmann temperature [37] according to their thermodynamic lattice theory of the glass transition.

In Figure 1. 3 a quantity such as the viscosity can be compared with a crystallization rate after a suitable reduction of the two quantities to comparable time scales. For case A shown in the figure, the crystallization rate in the forming interval is slow so that it is easy to get a clear glass by sufficiently quick action. For case B, the reciprocal crystallization rate at the "edge" is comparable with the viscosity time scale in the forming interval so that a reasonable interaction can be organized.

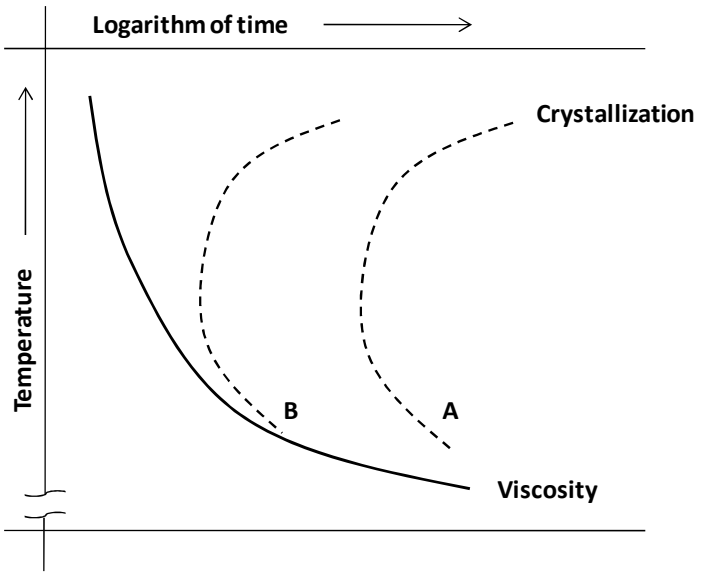

Figure 1. 3- Diagram of time, temperature and transition which compares times from viscosity with times for a suitable crystallization rate (redrawn from[38]).

The viscosity curve in the diagram is associated with the dynamic glass transition and the solidification at T_g is then called the **thermal glass transition**. Above T_g the glass transition is a dynamic phenomenon in the liquid. The diagram shows that one has a "slow dynamics" near T_g that becomes faster and faster at higher temperatures.

The **dynamic glass transition** is then a high temperature precursor of the glass transition.

1.2.2 Dynamic Glass Transition

When a supercooled liquid enters at the glass transition temperature T_g, is characterized by a viscosity of the order 10^{13} Poise, which implies a relaxation time τ exceeding 100 s as explained above (see Equation 1. 1 for $G_g \sim 10^{11}$Pa). For glass-forming materials the range of relaxation times within the liquid state thus covers the entire spectrum from local vibrational processes at ≈ 10^{-14} s to highly cooperative molecular motion with time scales of 10^6 s or more. These latter primary relaxations have been studied for many years by means of a wide spectrum of experimental techniques in order to gain insight into the molecular dynamics of liquids and supercooled liquids as a function of temperature. Some examples are NMR techniques, light scattering, viscosity measurements, tracer or self-diffusion experiments, ultrasonic attenuation, and dielectric relaxation spectroscopy [39], which is the main technique used in this work.

To a first approximation, these techniques reveal identical temperature dependencies for a given material and unambiguously show that the dynamics cannot be rationalized within the simple picture of thermal activation over a well defined barrier with a height quantified by the activation energy E_A.

Phenomenologically, the apparent activation energy of a typical relaxation process in the liquid phase tends to increase significantly while approaching the glass transition and indicates a divergence well above $T = 0$ if extrapolated to below T_g [40].

The α-relaxation is related to the glass transition of the system and for that reason is also called dynamic glass transition.

1.2.2.1 α- Relaxation

Although the glass transition remains an unsolved problem of the physics of condensed matter [41], it is well accepted that its dynamics is cooperative in nature, which means that a specific unit moves together with its environment. In polymers, is generally attributed to micro-brownian segmental motions (segmental mobility) [42].

In dielectric experiments performed at a given frequency, f(Hz), the α-relaxation takes place in response to the dielectric field reaching a value in the order of $(2\pi f)^{-1}$ seconds.

The temperature dependence of the relaxation time of the α-relaxation in a logarithmic plot of the relaxation time as a function of the reciprocal of temperature shows a departure from linearity, presenting some curvature near T_g. The most widely used empirical temperature law which seems capable of reproducing such findings is that established by Vogel–Fulcher–Tammann-Hesse [43,44,45] (VFTH):

$$\tau(T) = \tau_\infty exp\left(\frac{A}{T - T_0}\right),\ T_0 < T_g \qquad \textbf{Equation 1. 2a}$$

or

$$\log f = \log f_\infty - \left(\frac{A}{T - T_0}\right) \qquad \textbf{Equation 1. 2b}$$

where $\log f_\infty$ ($f_\infty \approx 10^{10}$ Hz -10^{13} Hz) and A are constants, and T_0 is the so-called ideal glass transition or Vogel temperature, which is generally 30-70 K below T_g. This T_0, corresponding to the value where the relaxation time diverges, has been identified with T_k, the **Kauzmann temperature** [46].

T_k is the temperature at which the glass transition must intervene to impede thermodynamic crisis for supercooled liquids[1]. Equation 1. 2 indicates that the α-relaxation is not an activated process. An apparent, temperature-dependent activation energy can be calculated formally from this equation. The apparent activation energy is given by:

$$E_A(T) = R\frac{d\ln\tau}{d(1/T)} \qquad \textbf{Equation 1. 3}$$

where R is the ideal gas constant, increases dramatically as T_g is approached. The term **apparent activation energy**, is used since it does not refer to a true activation barrier: its value is usually much greater than the dissociation energy of the $C-C$ bond, and consequently if it would represent a true activation energy, it will imply the broken of the chemical bond. Therefore it has no physical or chemical meaning, it just reflects the cooperativity of the underlying molecular motions where R is the ideal gas constant, increases dramatically as T_g is approached [47].

To analyse the temperature dependence of the relaxation rate in more detail a derivative method is applied [48]. This method is sensitive to the functional form of $f(T)$ irrespective of the pre-factor. For a dependency according to the VFTH equation one gets:

$$\left[\frac{d\log f}{dT}\right]^{-1/2} = A^{-1/2}\cdot(T - T_0) \qquad \textbf{Equation 1. 4}$$

[1] In 1948 Kauzmann pointed out that the entropy of supercooled liquid decreases rapidly on cooling towards the kinetic glass transition temperature, and extrapolates to the entropy of the crystal not far below T_g [13]. Temperature dependence of the entropy of glass intersects that of crystal at so called Kauzmann temperature, T_K. If the entropy of the supercooled liquid becomes lower than that of the stable crystal, it would eventually become negative at sufficiently low temperature, thereby violating the Third Law of Thermodynamics. This situation is named Kauzmann's paradox or entropy crisis. To avoid the entropy crisis, the glass transition must intervene, in order for the entropy of the glass to remain positive, forming an "ideal glass" at T_K.

In a plot $\left[\frac{\mathrm{dlog}\, f}{dT}\right]^{-1/2}$ versus T a VFT-behavior shows up as a straight line with $T_0 > 0$.
For a dependence according to the Arrhenius law [49], i.e,:

$$\tau\,(T) = \tau_\infty\, exp\,\left[\frac{E_A}{RT}\right] \qquad \textbf{Equation 1. 5}$$

where τ_∞ is the relaxation time at infinite temperature, a straight line is observed but with intersection at the origin ($T_0 = 0$).
Although the physical meaning of T_0 is up to know not yet clear the universality of the VFTH equation near T_g suggests that T_0 is a significant temperature for the dynamics of the glass transition. At higher temperatures ($T \approx T_0 + 100$ K) and higher frequencies, a change may occur in the temperature dependence of $\log \tau$ from VFTH behavior to another behavior [50,51].
Different approaches have been proposed to understand the physical origin of the VFTH-equation. Among those are the Free Volume and the Adam-Gibbs theories.

1.2.2.1.1 Free-Volume Theory

Although the **free-volume** has no unique or rigorous definition, it is a useful semiquantitative concept which has been employed in statistical thermodynamical theories of the liquid state (Glasstone, Laidler and Eyring 1941, and others). According to Glasstone, Laidler and Eyring the free-volume may be regarded as the volume in which each molecule of a liquid moves in an average potential field due to its neighbours. However, theoretical estimates of the free-volume depend on postulates regarding the compressibilities of the molecules and the nature of their packing in the liquid state. A definition of free-volume often used in polymer studies is that employed by Doollitle (1951,1952) [52, 53]:

$$\nu_f = \nu - \nu_0 \qquad \textbf{Equation 1. 6}$$

where ν_f is the free-volume per gram and ν the measured specific volume of the polymer at temperature T. ν_0 has been termed the "occupied volume". In Doolittle's studies ν_0 was taken to as the value of ν extrapolated to 0 K and was therefore regarded as a constant independent of temperature. This definition assumes that ν_f must tend to zero as the temperature tends to absolute zero, and that the increase of ν with temperature, due to thermal expansion, is associated entirely with an increase in ν_f.
The free-volume is a time averaged quantity which can be determined from equilibrium experiments. In a liquid-like system, however, the local free-volume is continually being redistributed throughout the medium, the redistribution occurring simultaneously with the random thermal motions of the molecules. The basic idea underlying the free-volume approach to relaxation phenomena is that the

molecular mobility at any temperature is dependent on the available free-volume at that temperature. As the temperature increases, the free volume increases and molecular motions become more rapid.

A few molecular theories based on this free-volume concept have been proposed, with the ultimate aim of relating dynamic quantities such as the diffusion coefficient, viscosity or relaxation time to the equilibrium quantity, the free volume. However, the purpose of this sub-section is not to describe all this models, instead it is more instructive to consider some relevant empirical expressions.

It was assumed that the flow viscosity of low molecular weight hydrocarbon liquids could be represented by an empirical equation which, with the aid of Equation 1. 6, can be written in the form:

$$\eta = a \cdot e^{-\frac{b}{f}} \qquad \textbf{Equation 1. 7}$$

where a and b are constants and $f = v_f/v$ is the fractional free-volume. Like v_f, f depends on variables such as temperature and external pressure.

Considering the case of a polymer, whose segmental movement rates r_1 and r_2 at two different temperatures, T_1 and T_2, where the segmental free volumes are v_{f1} and v_{f2} , respectively, with the following ratio:

$$\ln\frac{r_1}{r_2} = v_f^*\left(\frac{1}{v_{f1}} - \frac{1}{v_{f2}}\right) \qquad \textbf{Equation 1. 8}$$

Where v_f^* is the critical free volume which is needed for a segmental jump to take place, like in the theory of Cohen and Turnbull (1959) [54], where the molecular transport in liquids occurs with the movement of molecules into voids having a volume greater than some critical volume v_f^* formed by the redistribution of free volume.

Now assuming that for polymers the excess rate over that of the glass is entirely attributable to an increasing free volume, the following expression can be derived:

$$v_{f2} = v_{f1} + \alpha \cdot v_1 \cdot (T_2 - T_1) \qquad \textbf{Equation 1. 9}$$

where α is the difference between the cubical expansion coefficients above and below the glass transition temperature, and v_1 is the actual segmental volume at temperature T_1. The substituting for v_{f2} in Equation 1. 8 delivers:

$$\ln\frac{r_1}{r_2} = \frac{\left(\frac{v_f^*}{v_{f1}}\right)(T_2 - T_1)}{\left(\frac{v_{f1}}{\alpha \cdot v_1}\right) + T_2 - T_1} \qquad \textbf{Equation 1. 10}$$

This equation has the same form as the well-known WLF (William, Landel and Ferry, 1955) equation [55] which correlates the mechanical behavior of all polymers near their glass transition temperature, T_g; if $T_1 = T_g$. The temperature dependence may then be written in the form:

$$\log a_T = \log \frac{\tau_1}{\tau_2} = -\frac{C_1 \cdot (T - T_g)}{C_2 + T - T_g} \qquad \textbf{Equation 1. 11}$$

where a_T is the shift factor, τ is the relaxation time, T_{ref} is the chosen reference temperature and C_1 and C_2 are constants of the material dependent on the value chosen for T_0 [47]. This empirical equation is usually valid over the temperature range $T_g < T < T_g + 100\ K$ [56]. In this equation it is implicit the time-temperature superposition principle that establishes the equivalence between these two variables [56]. Applying this principle, in the case of dielectric relaxation spectroscopy, the relaxation curves obtained at different temperatures can be superimposed by horizontal shifts along a logarithmic time scale to give a single master curve covering a large range of times.
The WLF and the VFTH parameters are related by the following expressions [55]:

$$C_1 = \frac{A}{2.303\,(T - T_{ref})} \qquad \textbf{Equation 1. 12a}$$

$$C_2 = T_{ref} - T_0 \qquad \textbf{Equation 1. 12b}$$

The WLF and VFTH equations are the most frequently applied for describing non-Arrhenius behavior, although there exists a wide variety of mathematical representations. In a work of Stickel *et al*. some of the more important formulations are presented and compared [40].

1.2.2.1.2 Adam-Gibbs Theory

As a second approach that will be outlined here is the Adam-Gibbs theory, that is the first to deal with the α-relaxation as a cooperative process [57].
The changes in the relaxation time in the glass-transition region could be interpreted as a change in the length scale of the segmental motions that are increasing as the temperature decreases [58]. This increase of the length scale with temperature decrease is associated with the cooperativity enhancement as described by Adam and Gibbs [59]. The Adam and Gibbs paper is considered as the turning point from rare free volume to small configurational entropy as the reason for slow molecular mobility in glass formers [60]. Their theory assumes that the molecular dynamics on approaching T_g is controlled by cooperative rearrangements of particles in different regions, *CRR*, and it asserts that the relaxation time, τ for cooperative rearrangements is determined by entropy according to:

$$\tau = \tau_\infty \cdot \exp\left(\frac{z^*\Delta\mu}{kT}\right) = \tau_\infty \cdot exp\left(\frac{A}{S_C(T)\cdot T}\right) \qquad \textbf{Equation 1. 13}$$

where A is a constant, $\Delta\mu$ is the free energy barrier hindering the cooperative rearrangement per molecule and z^* is the minima size allowed in regions for the majority of the cooperative transitions to occur. In other words, z^*monomeric unities must rearrange in order to allow a transition between two states inside a *CRR*. S_C is the temperature-dependent molar configuration entropy defined as the molar entropy subtracted of the contribution arising from intramolecular and intermolecular vibrations.

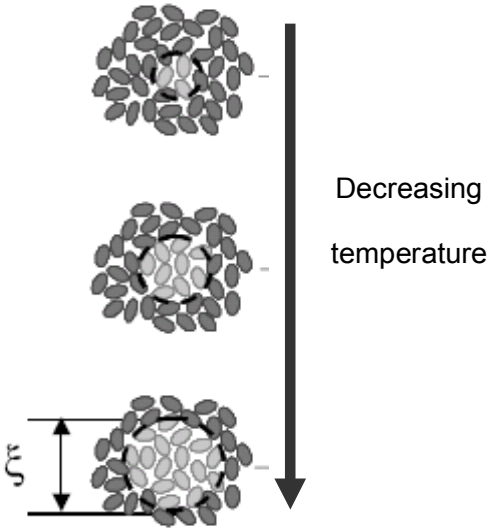

Figure 1. 4- Schematic representation for the increasing cooperative region with decreasing *T* near the glass transition (reproduced from ref [61]).

The value of $S_C(T)$ is computed from:

$$S_C(T) = \int_{T_2}^{T_1} \frac{\Delta C_p(T')}{T'}\, dT' \qquad \textbf{Equation 1. 14}$$

Where T_2 is the temperature at which the configurational component of the total entropy goes to zero and $\Delta C_p(T)$ is the molar heat capacity increment due to gaining access to the configurational states. $\Delta C_p(T)$ is usually identified with the experimentally difference between liquid-rubber and glass-crystal molar heat capacities [62].

The number of particles that rearrange cooperatively, N, designated as cooperativity, increases with the temperature decrease. The CRR size is $V_\alpha = {\xi_\alpha}^3$, with ξ_α being the characteristic length of the glass transition.

Therefore, in glass formers, the spatial aspect of the dynamic heterogeneity of the α-relaxation may be described as a consequence of a mobility contrast between an island of high mobility [11] where local

mobility persists even below T_g assisted by a cooperative shell of low mobility [63,64], that constitutes the *CRR*. The reorientations of molecules forming the cage, corresponds to the dynamic glass transition being a cooperative process because the fluctuations of the molecules forming the cage cannot be independent from each other [65].

1.2.2.1.3 Fragility

In the above section equations used to describe the dynamic glass transition or α-relaxation including the working interval and T_g were presented, like the VFTH equation (Equation 1. 2), a three-parameter equation for the $\log f - T$ relation. However, this property can be simply characterized by one parameter [66] that may then be determined from properties near T_g. This parameter was called **fragility** [67,68,69]. It reflects the stability of the liquid structure to temperatures changes in the supercooled regime [70]. Briefly, the fragility of the α-relaxation is considered as a measure for generation of configurational entropy in the liquid [27,71,72].

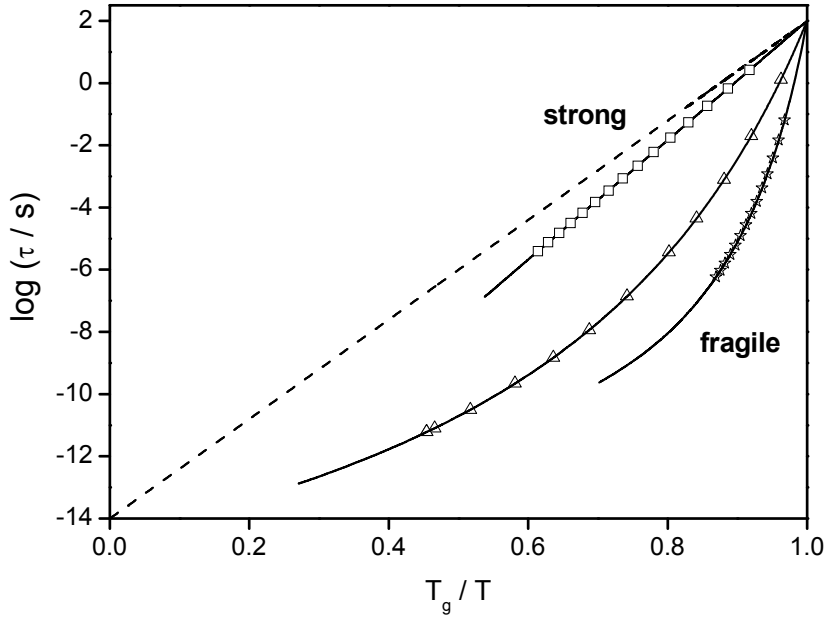

Figure 1. 5- Strong-fragile classification of glass-forming liquids according to their relaxation times *versus* reciprocal temperature scaled with $T_g(\tau = 100s)$. Near the limit of strong behavior is depicted the T_g-scaled plot of caffeine (squares) with $m = 19$ [73]. Glycerol (triangles) shows an intermediate fragility with $m = 53$ [1]. Acetaminophen (stars) is presented as an example of a fragile glass, $m = 128$ [74].

In other words, fragility is this structural weakness of the glass formers that is in the origin of their departure from the Arrhenius behaviour. Materials are called "fragile" if their temperature dependence of the relaxation time deviates strongly from an Arrhenius-type behavior and "strong" if that

dependence is close to the latter [75,76]. A quantitative measure of fragility is the dimensionless "steepness index" m, defined as:

$$m = \left[\frac{d\log\tau(T)}{d\left(T_g/T\right)}\right]_{T=T_g} \qquad \textbf{Equation 1. 15}$$

By this definition, m corresponds to the slope of the plot $\log\tau(T)$ versus $1/T$, measured at T_g, divided by T_g exemplified in the Figure 1. 5.

The fragility index ranges from about 15, referred to as strong, up to about 200, for fragile glass formers. This limits for the fragility index comes from the fact that the strong glasses are characterized by a $\tau(T)$ with an Arrhenius behavior and a pre-exponential factor of 10^{-13}-10^{-14} s and the fact that $\tau(T_g) \cong 100$ s.

The above **fragility diagram** (Figure 1.5) was translated by Angell [27,77] guided by the concept of configurational-entropy, from viscosity η to reciprocal configurational entropy: $\log[\eta(T)/\eta(T_g)] \rightarrow S_c(T_g)/S_c(T)$.

Relating m to a current temperature T instead of T_g:

$$m(T) = m(T_g)\cdot\frac{T}{T_g}\cdot\frac{(T_g - T_0)^2}{(T - T_0)^2} \qquad \textbf{Equation 1. 16}$$

decreasing with increasing temperature. The actual steepness index $m(T)$ in the working interval is another quantitative measure of fragility.

D is the fragility parameter entering the modified Vogel-Fulcher-Tamman (VFT) law:

$$\tau = \tau_\infty \exp\left[\frac{DT_0}{(T - T_0)}\right] \qquad \textbf{Equation 1. 17}$$

where the product DT_0 replaces the parameter A in the conventional expression (Equation 1. 2a).

In these terms, the relationship between the steepness index m and the parameter D can be expressed as [78]:

$$m = \left[\frac{d\log\tau(T)}{d\left(T_g/T\right)}\right]_{T=T_g} = \frac{T_g}{2.3}\frac{DT_0}{\left(T_g - T_0\right)^2}$$ **Equation 1. 18**

The limits for D are much smaller than for $m(T_g)$ [27]. Strong glasses present low values of m and high values of D, whereas the reverse occurs for fragile ones (e.g. $m = 81$ and $D = 6.8$ for o-terphenyl) [79].

1.2.3 Open Items in the Understanding of Glass Transition

The glass transition phenomena are observed in many different classes of materials and have been studied in various disciplines. It is a long-standing problem due to the increasing number of important and general experimental facts that challenge conventional theories to explain [80]. The α-relaxation is the slowest and the dominant relaxation process in viscous liquids, closely linked to the glass transition because it sets the time scale for equilibration. Most important unsolved problems regarding viscous liquids concern properties of the α process. This section aims to describe some problems, classically referred as "three canonical features".

(1) Nonlinearity- The classical recovery experiments near the transformation interval, starting from equilibrium above or below the experimental temperature, are differently influenced by partial freezing and are not therefore symmetrical; This one has been presented in the previous section;

(2) Non-Arrhenius- To find a way to explain the temperature dependence of the α-relaxation time τ, which for some liquids increases by more than a factor of 10 when temperature is lowered by just 1% [24,81]. This one has also been presented earlier;

(3) Non-exponentiality- To clarify the observed shape of the α loss peak which was recognized already more than 40 years ago to be always asymmetric compared to Debye's exponential decay which correspond to broader dynamic loss peaks.

1.2.3.1 β Process and αβ–Splitting

An open question that remains controversial is the nature of the relaxation process well above the glass transition and also how localized mobility and cooperative motions correlate at low temperatures. Moreover, the different crossover profiles assumed by the respective temperature dependencies of relaxation times found are still a matter of debate. In the following sections, these different relaxation processes are described and its correlations as well.

1.2.3.1.1 β-Relaxation (or any sub-glass relaxation)

Below T_g, in the glassy state, two types of dynamical processes are observed: localized motions that are the origin of the secondary relaxation processes and a very slow dynamic process due to structural recovery as evidenced by physical ageing processes.

Sub-glass relaxations are thermally activated processes. Therefore, the temperature dependence of their relaxation times is of Arrhenius-type (Equation 1. 5). The value of τ_∞ for a Debye process, is of the order of 10^{-12} s up to 10^{-14} s. Also, E_A is representing the potential barrier resisting the molecular rearrangement [25] that can arise from either intramolecular (e.g. two different orientations of a side-group relative to the main chain in a polymeric material) or intermolecular forces. Whatever the origin of the potential barriers, intermolecular or intramolecular, the associated motions must be much simpler and more local than the α-relaxation in order to present an Arrhenius behavior. E_A usually varies between 20 and 60 kJ·mol^{-1}, depending also on the environment of the group that undergoes the conformational changes. The above values of τ_∞ and E_A are associated with strictly local processes due to individual mobility of sub-units, and thus involve independent molecular motion with nearly no activation entropy. A similar formulation is based on the thermal activated states by Eyring [82].

The activation Gibbs free enthalpy ΔG_i^* can then be written as:

$$\Delta G_i^* = \Delta H_i^* - T \cdot \Delta S_i^* \qquad \textbf{Equation 1. 19}$$

In Eyring's theory of absolute reaction rates [83], the relaxation time τ_i can be written in function of the activation enthalpy, ΔH_i^* and entropy, ΔS_i^*:

$$\tau_i(T) = \frac{h}{kT}\exp\left(\frac{\Delta G_i^*}{kT}\right) = \frac{h}{kT}\exp\left(\frac{\Delta H_i^*}{kT} - \frac{\Delta S_i^*}{T}\right) \qquad \textbf{Equation 1. 20}$$

where h and k are the Planck and the Boltzmann constants, respectively. The activation entropy ΔS_i^* is related to the fraction of available sites when comparing activated states to the inactivated ones, ΔH_i^* is directly related to the height of the potential barrier to be overcome by the reorienting entity.

Values of τ_∞ lower than 10^{-14} ($\approx 10^{-16}$-10^{-18} s) imply an activation entropy greater than zero, being associated with more complex mobility mechanisms for which the activation energy could be of the order of 160 - 210 kJ mol^{-1}, as is the case for the β-relaxation in polysaccharides [84,85] and in polymers where the conformational mobility of the main chain is severely restricted [86].

Moreover, it should be noted that other techniques such as Thermally Stimulated Discharge Current (TSDC) which is able to deconvolute a relaxation process, found that complex secondary relaxations, apparently cooperative, are in fact non-cooperative, originated by local motional processes only. The claimed cooperativity is due to the fact that it is an energy distributed process, as was recently reported by Diogo and Moura-Ramos [87].

In polymeric materials, the secondary processes correspond to either limited in-chain movements or hindered rotations of side groups, laterally attached to the main chain (or of its subunits) that can occur independently of the backbone movements, or even conformational changes in cyclic side groups [42]. Heijboer [88] suggested that the β-relaxation time is determined by a local barrier within the molecule. This is a reasonable assumption in polymers. Nevertheless, the molecular origin of the β-relaxation is not completely understood, being observed in a variety of materials other than polymers, including glass-forming liquids made of simple molecules that do not have internal modes of motion [89,90] including ionic liquids [91]. It seems then to be a near-universal feature of the amorphous state, as proposed by Goldstein and Johari [89], and thus called the Johari-Goldstein process.

1.2.3.1.1 $\alpha\beta$-Splitting Region

As mentioned before, the relaxation times of the α process show a strong temperature dependence, described by the VFTH equation (Equation 1. 2), while the temperature dependence of the secondary processes follows an Arrhenius-type behavior (Equation 1. 5). Therefore, in a logarithmic plot of the relaxation time versus the reciprocal of temperature (activation plot), the α process corresponds to a curved line, while the β process is a straight line (Figure 1. 6 [58]).

At temperatures well above T_g the time scales of both relaxation processes tend to converge, because $\log \tau_\alpha$ increases faster than $\log \tau_\beta$ with the temperature increase. Consequently, the two lines in the activation plot come close together and eventually merge in a single process – the α process - or, with decreasing temperature, the α-relaxation process bifurcates into two processes, α and β, and the frequency and temperature, T_β, region where the separation occurs is designated by **αβ splitting**. The **crossover region** is a more general designation due to the detection of multiple secondary processes, and thus the occurrence of more than one merging region, and is defined as *the temperature-frequency region where changes take place in the dynamic behaviour of the system* [92]. The temperature interval where crossover effects are felt is about ($1.2\,T_g$ - $1.4\,T_g$). The different methods used to estimate it for a specific substance have typical uncertainties of ±10 K, and the corresponding relaxation times are of the order of 10^{-6} s, with uncertainty of about ±1 decade, but large variances occur for different substances (in reference [93] Beiner *et al*. compiled data for 38 different glasses) [58].

Figure 1. 6 gives the two principal profiles schematized in accordance with Schönhals [47] and Garwe [94, 95]. The first example at the left side shows the classical true merging of the α- and β-relaxations at high temperatures as suggested by Goldstein and Johari, whereas $log\,\tau(\alpha\beta)$ should have an activated temperature dependence with the same activation energy as the low temperature β process.

In all scenarios, it is accepted that two distinct processes occur above and below the crossover S, as shown clearly for poly(hexyl methacrylate) (PHMA) by dielectric, shear and calorimetric measurements that established that the cooperativity onset took place in the crossover region [63].

In scenario A, the main feature in this landscape is that at a certain temperature the trace of the a process changes in such a way that two new processes are originated, the α and β. This clear differentiation between a and α has been perceived as an indication of the onset of the intermolecular cooperativity [63] and in accordance with Sokolov [96], it is a demonstration of the non monotonic nature of the glass transition. Also some recent studies, in which a derivative data evaluation method [40] is used, show that the temperature T_B (crossover temperature defined by the intersection of two VFTH laws) is very close to that corresponding to τ_β (the time where structural and secondary processes approach each other). In other words, the coupling of the secondary relaxation leads to changes in the cooperativity. This differentiation between the processes below and above τ_β was already noted by G. Williams in 1966 [97] for poly(ethyl methacrylate) (PEMA). Measurements made with heat capacity spectroscopy for example in poly(n-hexyl methacrylate) (PnHMA), also confirm that the main relaxation consists of two calorimetrically distinct parts [98]. Because of this, the application of temperature-time superposition holding below $\alpha\beta$-splitting region cannot be recommended for the characterization of the high temperature a process above the crossover region [99].

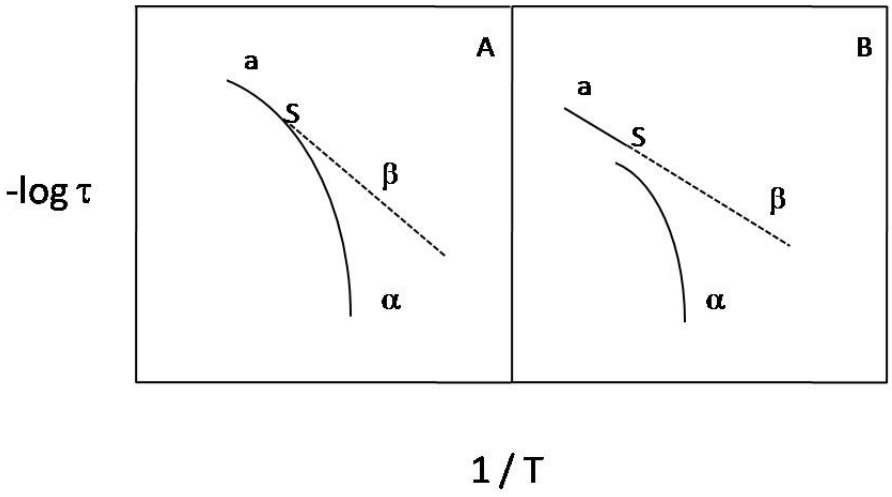

Figure 1. 6- Two possible scenarios for the splitting of the α and β processes (redrawn from [47]).

In scenario B, an extrapolation of the low temperature behavior of τ_α and τ_β shows that the two processes are always separated, *i.e.* the relaxation time of the α process is always higher than the corresponding to the β process. The slope of the β process trace in the Arrhenius diagram does not change significantly when the α approaches. The separate α onset (*i.e.* the starting temperature for this process) can possibly be characterized by a minimal cooperativity for the α process that can not be continued by a local, non-cooperative process [94,95,100]. The poly(*n*-butyl methacrylate) (PnBMA) [94] and the low molecular weight epoxy resin EPON828 [101] are two well structurally different materials presenting a separate onset according to the topology of Figure 1. 6 B. Even in crosslinked

poly(butyl methacrylate) (PBMA) with 10% wt. of ethylene glycol dimethacrylate (EGDMA) this scenario is kept [102].

This behavior was also predicted by Schultz [103] that considered the β process as a Johari-Goldstein relaxation, supporting the idea that this process is generated by a second process which is partially independent from the main relaxation processes.

Anyway, this landscape does not admit that the α process is a simple continuation of the β, but it is strongly determined by the β-relaxation.

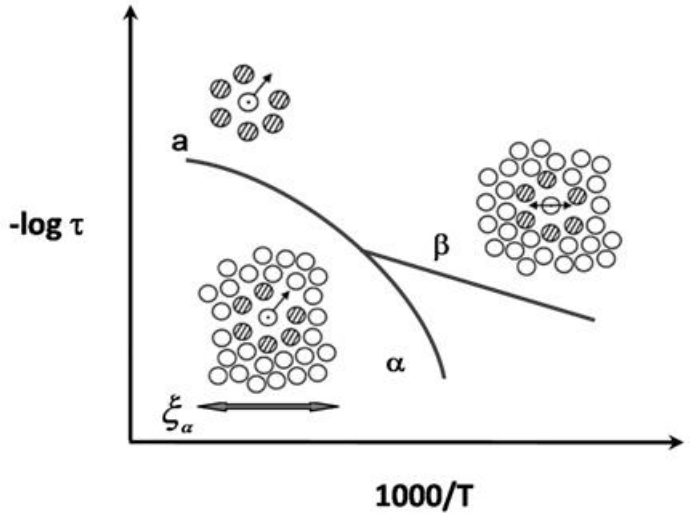

Figure 1. 7- Schematic molecular pictures for the diffusive high temperature a process (cage escape), the diffusive low-temperature α process (cooperatively-assisted cage escape), and the finite β process (adapted from ref.[59]).

Below the α and β crossover region (T_{on}, see further on), the island of mobility scenario from Johari [104] together with the concept of cooperatively rearranging regions, *CRR*'s [11] introduced by Adam and Gibbs, the β process is assumed to be a localized motion in the inner, less dense and more mobile part of the *CRR*. A schematic picture for the density/mobility situation in glasses at different temperatures relative to T_{on} is shown in the Figure 1. 7, which is reproduced from [59, 105].

Theoretical developments [64] within the so-called coupling model (CM) introduced by Ngai and co-workers [106] seem to point in the direction of a universal slow β-relaxation closely connected to the glass transition process, precursor of the α process; in this context the term 'slow' is used to distinguish from 'fast' β process, observed in a variety of glass formers in the GHz region ([107] and refs. cited therein).

More recently, a special relevance has been given to the quantitative determination of the number of molecules or monomeric units in a cooperatively rearranging region, N_α, and its dependence with the temperature. Calorimetric parameters obtained from heat capacity spectroscopy (HCS) has been used to calculate N_α, as the ratio between the volume of the *CRR*, $V_\alpha = \xi_\alpha^3$, and the mean volume of one molecule [108,109,100,110]. This parameter becomes very useful in the study of the crossover region

because it allows the estimation of the temperature at which the cooperativity starts, from the extrapolation for $N_\alpha(T) \rightarrow 0$ [111,112]. An open and debated question is whether the trace of the process α follows a VFTH or an Arrhenius behavior. Goldstein and Johari [89,90], for example, considered that above a certain temperature (higher than T_g) no cooperative rearrangement is required [113] and the activation energy of the merged process was the same as the β one. Garwe *et al.* [95] found also an Arrhenius behavior in poly(ethyl methacrylate) (PEMA), but with larger activation energy than that of the β process. The later seemed to act as a precursor of the cooperativity of the α process, what was interpreted as an indication of a locally coordinative mobility in the origin of the β process. Studies carried on alkyl acrylates and alkyl methacrylates interpenetrating polymer networks also shown this coalescence scenario where the secondary β-relaxation and the main α process merge to a single process [114,115].

1.3 Dynamics under confinement

A challenge that research into the confined glass transition nowadays face is an independent confirmation of the characteristic length of the glass transition in the bulk material without confinement. Confining geometries can be realized in various ways: by containing the system under study in molecular sieves, in nanoporous sol-gel glasses, in mesoporous membranes, in block copolymers, in semi-crystalline polymers, etc.

In 1981, in the book "Glasübergang", Donth idealized a situation for the glass transition. In such case, it was assumed that the molecular motions which cause the dynamic glass transition are not affected by the confining walls as long as all three dimensions are larger than the characteristic length $\xi_\alpha(T)$. If a spherical pore with given diameter d and volume V_d of nanometer size is considered (Figure 1. 8), while the temperature is decreasing the volume $V_\alpha = {\xi_\alpha}^3(T)$ of a cooperatively rearranging region *CRR* of the dynamic glass transition increases.

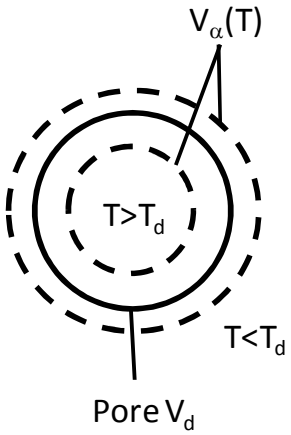

Figure 1. 8- Glass Transition in confining geometries. Comparison of a given spherical volume V_d with increasing volume $V_\alpha(T)$ of a cooperatively rearranging region *CRR* (redrawn from reference [27]).

In the ideal case, the WLF curve (Equation 1. 11) is undisturbed for $T > T_d$, and at low temperatures $T < T_d$ shows a modified trace in the Arrhenius diagram, where T_d is implicitly given by the coincidence of the two volumes, $V_d = V_\alpha(T_d)$. According to Adam and Gibbs, the WLF curvature for the α process is connected with increasing cooperativity, i.e. increasing $V_\alpha(T)$. At $T = T_d$, this increase is stopped and the glass transition cooperativity must overcome constant volume. If this situation occurs for a fixed molecular mechanism with a given activation energy equal to the apparent activation energy of the WLF curve at $T = T_d$, the glass transition for given $T < T_d$, in the pore is then faster than in the bulk (Figure 1. 9A). Having a set of pores with different diameters, T_d shifts increasing with decreasing pore diameter (Figure 1. 9B). Below T_d, there is higher mobility $\log \tau$, in smaller pores, i.e., lower glass temperatures in smaller pores. This idealized case was called **hindered glass transition** [4]

In preliminary experiments it was evident for Donth [27], the limitations of the idealization. The glass transition is affected by the pore walls even at much larger diameters than $\xi_\alpha(T)$, starting at about $d = 10$ nm, and its parameters, including T_g, depend seriously on pore surface properties [27].

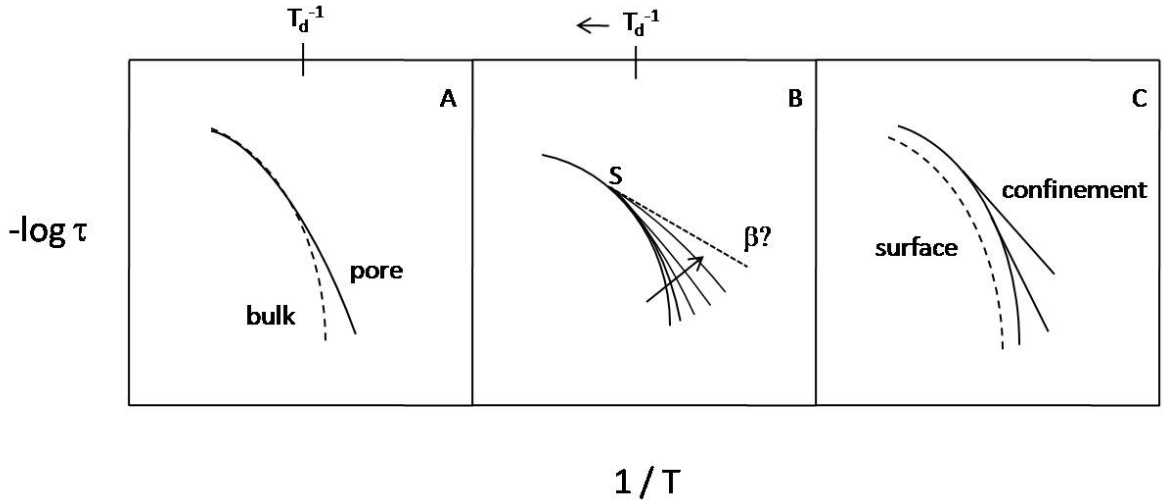

Figure 1. 9- Glass Transition in confining geometries. A- Comparison of traces of a hindered glass transition in a pore and a non-confined glass transition in bulk; B- Hindered glass transition in a series of pores. The arrow is directed towards smaller diameters and S is the crossover region; C- Example of the relationship between the hindered glass transition and the α process modified by the structure near the surface for strong interaction between surface and glass former (redrawn from reference [27]).

The Arrhenius diagram of semicrystalline polyethylene PE, presenting similar features to the behavior plotted in Figure 1. 9A were observed, led Schick to use semicrystalline terephthalate PET to test ξ_α against the thickness of the amorphous layer d_a [116]. The foreign boundaries of the pores are thus substituted by a self-organized interface in the same material. The crystallization regime could

considerably vary the thickness layer d_a, but the T_g variation against the bulk material was moderate ($\Delta T = 5$ K lower than the bulk T_g). This suggests that the molecular mechanisms in the bulk and in the layer (in a one-dimensional $D = 1$ confined geometry) are quite the same. Systematic experiments reviewed in [117] on semicrystalline poly(ethylene terephtalate) were done correlating ξ_α with d_a and predicting a bulk length near $d_a \approx 2\xi_\alpha$. However, the higher mobilities, predicted by the hindered glass transition, were not observed in this "weak" $D = 1$ confinement [27].

Moreover, for a small molecule glass former, benzoin isobutylether, in a series of porous glasses with pore diameters between 7.5 and 2.0 nm [118], decreasing characteristic lengths with decreasing but larger pore sizes were observed. Speculating about the small D limit relaxation, in this situation the environment for cooperative relaxation is not so extremely optimized, since we have more free volume than in the bulk, which means that the β process should be found in the small pore if this process can be localized at all.

Experiments in small $d < 10$ nm uncoated and silanized zeolite pores are first reported by F. Kremer group [8] in 1999 for H-bond-forming liquids ethylene glycol (EG) and propylene glycol (PPG) and for "quasi"-van der Waals liquid salol, where the question "how many molecules form a liquid" does not have a general answer.

Also, concerning PPG, in 1998, Schönhals and Stauga [119] reported a slow down of the whole chain motion in silanized nanoporous glass and attributed the observed shift to the hydrogen bonding interactions between PPG and hydroxyl groups on the glass surface. Interestingly, this effect is dramatically reduced when a non-chemically treated glass is used.

Any serious attempt to confirm the bulk characteristic length for the glass transition in confining geometries must try to separate or eliminate effects from the pore or layer interface [120], since strong interaction between the glass former and the interface material causes the glass transition T_g to increase [38], and weak interaction causes T_g to decrease. The latter effect, in the ideal case, the hindered glass transition, is normally called the **confinement effect** on the glass transition, while the other effect is called **surface or interaction effect** [121]. The interaction effect has three parts [27]:

1) Structure effect- when the glass former in the pore may have a structure different from that in the bulk. This may concern the near wall regions (as indicated by an extra ε'' peak [9]), but also the core regions (as indicated by different T_g values);

2) Density effect- the density of a glass former in the pores must not be the same as in the bulk. Thermodynamically, there is a curved surface so that the pressure inside, and thus the density, should be different from a material with large plane surfaces (as for $D = 1$ confinement). The shift of ΔT_g would be then proportional to the reciprocal pore diameter $1/d$.

3) Process effect- normally at low viscosity, the glass transition in the pores would be also isobaric (constant pressure thermodynamic process) like in bulk glass formers. If the glass transition at low temperatures, where the viscosity gets very high, is an isochoric transition (constant volume process) remains an open question.

The three effects are interlaced in such a way that it is believed to be an independent phenomenon, and the glass transition in confining geometries could never be used to confirm or disprove bulk characteristic lengths. It is evident that this counterbalance also must depend sensitively on the type of confined molecules (glass-forming organic liquids, polymers, liquid crystals, proteins, lipids and more recently ionic liquids), on the properties of the (inner and outer) surfaces (wetting, non-wetting) and on the architecture of the molecules with respect to the walls (grafted, layered or amorphous systems) [27].

For example, a T_g depression of the order of $\Delta T_g \approx 10$ K, from bulk to pores of a few nanometers in size were first reported in 1991 by Mckenna *et al* [122]. This depression is proportional to the inverse pore diameter $\Delta T_g \sim 1/d$, which therefore could be interpreted as a density effect.

While it is unambiguously established that finite size effects are favorable for the depression of the first-order phase transitions, leading for instance to a considerable shift of the melting point [123], the effects on the glass transition have been studied less extensively. It strongly affects their physical properties as documented by a variety of experimental techniques and theoretical approaches [12,124,125]. However, both experimental and theoretical developments regarding glass transitions in liquids confined to small pores with diameters in the range of several 10 Å seem to be also rather contradictory. A finite size induced decrease of the glass transition temperature T_g is reported by Jackson and McKenna (122) for o-terphenyl and benzyl embedded in Vycor glasses and later by Zhang, Liu and Jonas [126] for several organic liquids confined to the pores of silica glasses. The opposite effect, a small increase of T_g, has been observed by Dubochet et al.[127] for o-xylene and toluene if dispersed in glass-forming liquids microemulsions and by Hofer, Mayer and Johari [128] for pure ethylene glycol and solutions of LiCl in H_2O in poly(2-hydroxyethyl methacrylate) hydrogels. $\Delta T_g = T_{g,pore} - T_{g,bulk}$ range from -18 to $+15$ K.

To discuss the pore size dependence, a detailed study by Schönhals et al. [129,130,131] found for PPG (MW=3000) confined in nanoporous sol-gel glasses, two competitive effects: for pore sizes between 20 and 5 nm a decrease in T_g was observed while for the lowest pore size an increase of T_g relative to bulk was determined.

When ΔT_g is positive, in dielectric experiments, the loss curve $\varepsilon''(\log \tau)$ often consists of two components, the proper α process and, usually at lower frequencies, the α process modified by the structure of the surface (Figure 1. 9C), especially if the pore surface is not treated by a surfactant with high molecular mobility. Figure 1. 9C corresponds to an old rule that more structure results in higher T_g, and thus, lower mobility because more structure diminishes the free volume [27].

In a later paper, Binder and co-workers [132] performed MD simulations to study the dynamics of supercooled liquids close to smooth walls as well as close to rough walls. In that work, very interesting results were reported: in the case of strong interaction with the wall an increase of the relaxation times was observed whereas a decrease in relaxation times was reported for smooth surfaces. As the distance from the wall increases, the behaviour of the confined liquid is the same as in

the bulk. Two important remarks have to be emphasized here. First, in the case where there is an interaction between the particles and the rough surface, the glass transition increases for molecules adsorbed in the pore wall whereas T_g bulk is observed for molecules in the middle of the pore, far from the wall. Second, a decrease in the glass transition is observed close to the smooth wall and a bulk glass transition is observed when the distance increases from the wall into the pore centre. It is obvious that a gradient in the glass transition as a function of the distance from the wall is observed [133]. Concerning the glass transition itself, Park and Mackenna after some studies on the calorimetry glass transition observed that there are two different glass transitions for o-terphenyl (o-TP) and polystyrene/*o*-terphenyl (*o*-TP/PS) solutions confined in pore glasses [120]. After such results Park and Mackenna have then raised an important question about the existence of two glass transitions in confined geometries. Both increased and decreased transitions have been observed in dielectric spectroscopy (two relaxations at lower frequencies for confined liquids in nanopores were observed) [6,7,9,134,135].

This discussion shows that the problem put forward in the beginning of the section has not yet been completely settled and remains the subject of continuing research.

1.3.1 Confinement Effects- A Literature Review

1.3.1.1 Liquid Crystals

Studies on systems like liquid crystals might be useful to shine light to the glass transition phenomena in general. The concepts associated to the liquid crystals (LC's) are shortly outlined below.

Liquid-crystal materials consist of anisotropic molecules that self-assemble into phases with orientational order, but often no positional order, in their simplest form. Thermotropic liquid crystals (LC) are materials which have structures between the crystalline and the isotropic state [136,137]. In crystals the molecules have maximal (positional and translational) order and minimal mobility while in liquids the reverse is the case. In LC's aspects of both states are combined and mesomorphic phases are formed in which order and mobility compete. They are formed for instance by molecules which have a stiff, rod-like mesogenic unit in their structure [138], showing a high degree of shape anisotropy, which manifests itself in many ways, such as dielectric and optical anisotropies. The most important liquid crystalline structures are the nematic and the smectic mesophases. The nematic phase is the liquid crystalline state with the lowest order.

Due to the fact that liquid crystals exhibit various mesophases and phase transitions between them which are sensitive to perturbations, it appear as ideal candidates when confined in porous media for the study of the quenched random disorder effects upon phase transitions and critical phenomena [139,140], and they have been studied extensively in the last 20 years [141-142143,144,145,146,147,148,149,150].

Many of the physical properties of LC's remain open when the confinement reaches nanometric sizes. At this length scale, thermodynamic equilibrium states are strongly affected, and new rules appear to govern the nature and the temperature of phase transitions. In particular, theoreticians have argued that the presence of disorder in such systems leads to the formation of glasses, for example the so-called smectic glasses [151]. Apart from these more advanced considerations, a number of liquid crystals are themselves glass-forming liquids, such as the well-studied case of 4-(2-methylbutyl)-4-cyanobiphenyl ($CB15$) [152], and the example of 4-pentyl-4'-cyanobiphenyl ($5CB$) [141]. These considerations drive the application of liquid crystals in the interesting area of glass physics. Multiple types of confinement have been used and multiple techniques have been applied to confined LC's. In 1996, a book on the subject appeared, reviewing the knowledge available at that time [10]. Important examples are calorimetric studies on aerogel systems [153], where shifts in the phase transition temperatures and the appearance of double, broadened heat capacity peaks were the main observations. Comparable results were observed in aerosil dispersions [154], however, the behavior was somewhat different because of the more flexible nature of the aerosil network as compared to aerogels. A review on calorimetric data for 4-n-octyl-4-cyanobiphenyl ($8CB$) is given in [140]. Structural information was obtained from X-ray diffraction [155] and NMR [156]. These measurements gave information on the alignment of LC's in Anopore membranes [157], the disorder in Vycor porous glass [158], and disordering effects as well as certain critical phenomena at the phase transitions in aerosol dispersions. Disorder was also the main subject in a number of optical experiments and computer simulations [159]. The general picture, put forward by all these results, is that the close interaction with the surfaces of the confining materials results in a number of changes which can mainly be understood by the formation of domains and the disturbance of the long range order. Also dielectric spectroscopy has been applied, elucidating aspects of the dynamics and the structure of confined LC's [7,9,160,161,162,163,164]. In particular, it was observed that the interaction of the LC's molecules with surfaces can induce structures different from the bulk giving rise to additional relaxation processes, which are not characteristic for the bulk system. For instance the molecular dynamics of a guest forming a strongly adsorbed surface layer with a partial ordering is essentially slower relative to bulk molecules [163,165]. In cyanobiphenyl-aerosil composites having high silica densities, an additional process to the bulk-like relaxation was observed [166]. This process was assigned to cyanobiphenyl molecules forming a layer with high density packing anchored at the surface of the aerosil particles. Recently 4-n-octyl-4'-cyanobiphenyl ($8CB$) was confined to the nanopores of a series of AlMCM-41 molecular sieves with different pore sizes but constant composition [167]. Besides a process which is related to bulk like $8CB$ again a second relaxation peak related to molecules forming a surface layer at walls of the pores (inner surface) is observed. This relaxation process is influenced by both the interaction of the molecules with the surface and by the confinement**.** The behavior of this process related to the inner surface was compared with the one observed for the outer surface in the case of the composites. This comparison shows that both behave similarly at high temperatures. At low temperatures, the relaxation times have a weaker temperature dependence for the $8CB$/aerosil composites than for $8CB$ confined inside the

pores, since the molecules at the outer surface layer experience weaker interactions than when embedded in pores. On the basis of this result a confinement parameter is defined [167].
Moreover, under confinement, the surface interaction acts as an external field that couples to the LC's order parameters. This effect may induce partial order at the pore wall, which persists well above the clearing temperature [168]. Therefore the phase behaviors are considerably affected by spatial confinement and interface effects as well. For instance, the *I*-*N* transition can be weakened and its character could change from a strong first order transition in bulk to a weak first-order or continuous paranematic-to-nematic (*P*-*N*) transition depending on the strength of surface interaction [169,170]. The smectic translational order can be also inhibited and the *N*-Sm*A* suppressed or considerably broadened [139,171].
Additionally, the physics of confined LC's reveal several original features, many of which are still open fundamental questions, such as the theoretical treatment of phase behaviors under external fields induced by confinement or the interfacial properties of soft-matter and biomimetic materials. Thus, many experimental and theoretical studies focused on this scientific case were carried out during the last decade [10,139,163,164,169].

1.3.1.2 Pharmaceutical Drugs

The need for safe, therapeutically effective and patient-compliant drug delivery systems, lead researchers to design novel tools and strategies among which the use of mesoporous silica-based materials attract a great interest due to their particular physical properties [172]. In fact, such materials have been proposed as drug delivery systems due to its biocompatibility, ordered pore network, high internal surface area, silanol containing surface, chemical and mechanical stability [173,174]. One of the most important characteristics of mesoporous materials is that the diameter of the pores can be tuned from 1.5 nm to several tens of nanometers by changing the chain length of the surfactant, employing polymeric structure-directing agents, or solubilizing auxiliary substances into micelles [175,176]. Recently several studies involving these type of inorganic nanoporous matrices have been used to confine different pharmaceutics, such as: MCM-41 (Ibuprofen [177,178,179], erythromycin [180], alendronate [198], aspirin [181], captopril [182], sertraline [183]), MCM-48 (erythromycin [184]), SBA-15 (ibuprofen [185], alendronate [198,177], erythromycin [184], gentamicin [186], amoxicillin [187], captopril [182]), FSM-16 (Flurbiprofen [188]), montmorillonite (Sertraline [183], Timolol [172], Ibuprofen [189], fluorouracil [190]) and porous glasses (acetaminophen [18,19]).
Among the pharmaceutical compounds, those that are glass formers, i.e. for which crystallization is easily avoided, can play a crucial role concerning the therapeutic activity. In fact, a growing interest is devoted to the development of amorphous solid pharmaceuticals since the amorphous form of a drug often shows an improved solubility, accelerated dissolution and bioavailability promoting therapeutic activity when compared to the ordered crystalline material as underscored in recent publications [191,192]. However, the amorphous solid state is out of equilibrium, and therefore unstable. Thus

confinement in nanoporous host systems emerged recently as a strategy to overcome this problem and as a way to increase the lifetime of amorphous drugs for real-life applications [18,19]. For instance, in ibuprofen, the drug tested in this work, it was observed that when encapsulated in MCM-41 molecular sieves, it does not crystallize and therefore it exists in the supercooled liquid state as confirmed by NMR [193] and X-ray diffraction [194].

The interaction of the guest molecules with the pore surface is a key question in studies involving the confinement of pharmaceuticals. Solid- state neutron magnetic resonance (NMR) [195] showed that Ibuprofen molecules when confined in silica matrices can interact through weak hydrogen bonds between its carboxylic acid group and the silanol groups, which reflects in a high mobility [194,196,197]. In the case of phenyl salicylate (Salol) confined to nanoporous sol/gel glasses, the interaction with the inner pore surface led to the formation of an interfacial layer, having a dynamics which is slowed down compared to the bulk liquid, while for the Salol molecules localized in the centre of the pores, a faster dynamics is observed as revealed by dielectric spectroscopy [9,131].

In drug delivery systems when specific host-guest interactions are present, the drug release kinetic profiles are influenced [186,187], being demonstrated that the delivery rate can be modulated through modification of the surface pore walls. This was verified for Alendronate confined in amino-functionalized MCM-41 and SBA-15 [198]. The same effect was also observed for captropril [199] and Ibuprofen incorporated in the same porous hosts modified by silylation [200].

Moreover another practical approach to confinement that recently became important in the scientific community is that it can be used as a tool to study early stages of crystallization [18,19,20].

Crystalline forms that are metastable, transient, or inaccessible in bulk samples are found under nanoscopic confinement [18,19,20]. A common thermodynamic reason for the occurrence of usually metastable crystalline forms under nanoscopic confinement is that the stability of certain crystalline forms depends on the size [201,202]. Therefore, the systematic investigation of crystallization under confinement unveils thermodynamic properties of metastable polymorphs which are not accessible otherwise. Consequently it enhances the understanding of the crystallization behavior of pharmaceuticals in general. Beiner et al. [18] have shown by both calorimetric and X-ray scattering that nanoconfinement is a handle to rationally produce and stabilize otherwise metastable or transient polymorphs of pharmaceuticals, in particular, from the three different crystalline forms found for acetaminophen, one of these is only stable under confinement [20]. The stabilization of these metastable forms in pharmaceuticals is crucial for controllable and efficient drug delivery.

1.3.1.3 Semi-crystalline Polymers

In the light of the ongoing discussion about confinement, semicrystalline polymers can also be used as model systems to investigate the dynamical behavior of the amorphous phase that lyes entrapped between crystalline lamellae [57,203,204]. The molecular mobility associated with this amorphous phase in partially crystalline systems, can present similar features to the one described for low

molecular weight materials under nanoconfinement. However, the situation of the amorphous phase in semicrystalline polymers is more complex since there is a strong interaction between the polymer segments in the amorphous phase and the crystals. In fact some of the polymer chains even pertain both to the crystallites and the amorphous phase. Thus there are covalent bonds between amorphous and crystalline segments. This imposes strong restriction to the amorphous material in the inter-lamellae spaces, which is frequently called rigid amorphous phase to differentiate it of the amorphous polymer situated far from the crystals. As mentioned, in semicrystalline polymers the amorphous regions are placed within the spherulitic structures and confined between the crystalline lamellae or lamellae stacks, as directly evidenced by transmission electron microscopy for poly(ethylene terephthalate) (PET [205]). When confined in geometry with length scales of some nanometers, polymeric chains exhibit a conformational dynamics different from the bulk as reported for polystyrene thin films ([206] and references therein). The effect of the confinement in the glassy dynamics is still controversial, despite the great amount of experimental and theoretical results [207], and more insights into other systems are still needed. Therefore, semicrystalline polymers may also constitute a valuable model to study the dynamic behavior of polymeric chains in nanoconfined conditions [208].

The evolution of crystallization can be monitored by looking at the changes within the crystalline phase, using different techniques such as DSC, X-ray diffraction or density measurements. However, such studies can be complemented by assessing by DRS the changes occurring in the amorphous phase upon crystalline development. Usually, during isothermal crystallization a reduction of the dielectric strength of the α-relaxation is observed when monitored by dielectric spectroscopy [209,210,211,212,213,214]. In general, a broadening of the loss α-peak and a shift to lower frequencies is reported [210,215 ,216]. However, this is not always the case. For instance, for poly(L-lactic acid), the biopolymer investigated in this work, some controversial results are reported: for PLA the progress of crystallization occurs with no significant changes in the average relaxation time [209]; for isothermal crystallization of PLLA ($\overline{M}_w$ =151 000) the general impression is that the α process shifts to lower relaxation rates together with a considerable broadening of the relaxation function, very similar to the behavior observed for poly(aryl ether ketone ketone) [210], however the behavior was rationalized as the sum of an invariant, in shape and location, α process and an emergent more hindered relaxation. This was supported by the detection of two glass transitions by DSC [217], as also found for semicrystalline poly(ethylene terephtalate) [218]. More strangely, there has also been reported that the α-relaxation could be shifted to higher frequencies with crystallinity development [219].

The emergence of a second relaxation lying on the low frequency side of the bulk-like α process has been evidenced by DRS also in PET [211,218,220,221], poly(3-hydroxybutyrate) [222], PLLA [212,217], polycarbonate/poly(ε-caprolactone) blends [213], poly(propylene succinate) and poly(propylene adipate [223] and poly(butylene isophthalate) [224]. This process was assigned to the presence of a highly confined amorphous fraction located within the spherulites and on their surfaces:

a rigid amorphous region called α'-relaxation. Thus, semicrystalline polymers are usually considered as three phase systems: a bulk-like mobile amorphous region (MAP), a constrained or rigid amorphous fraction (RAP), and a crystalline phase [225]; the concept of RAP was introduced to elucidate the discrepancies between the theoretical and experimental heat capacities at T_g, determined by DSC [222,226,227]. This has several implications for dielectric measurements since the crystalline phase is regarded as immobile and no relaxation processes occurs associated with it. Thus, regarding the amorphous phase, not the whole amount of this phase contributes to the α-relaxation, being a part amorphous in structure but rigid concerning the molecular mobility responsible for the dynamic glass transition, the so-called RAP.

The influence of this rigid amorphous fraction on the dynamical properties of PLLA will be evaluated in the present work. In fact, it is one of the most extensively studied biopolymers that easily crystallize, being a biodegradable and biocompatible linear aliphatic polyester. Its applicability in different fields, such as biomedical applications, including in wound closures, prosthetic implants, controlled delivery systems and three-dimensional porous scaffolds for tissue engineering, as well as in environmental applications makes this material also interesting to be studied in a more fundamental point of view [228]. Moreover, the fact that PLLA crystallizes slowly [229], allowing preparing materials with tuned degrees of crystallinity and lamellar morphologies, by changing the thermal history, are the reason for a deeper dielectric investigation in this work.

1.4 Dielectric Relaxation Spectroscopy

Dielectric spectroscopy is one of the most commonly used techniques for the investigation of the dynamic response of glass-forming materials. One of the mainly important applications of dielectric spectroscopy is the investigation of relaxational processes which are due to rotational fluctuations of molecular dipoles [238]. In fact, broadband dielectric spectroscopy is a versatile tool to analyze details of the scaling of relaxation processes.

Figure 1. 10 represents a schematic plot of dielectric loss spectra at constant frequency as a function of temperature demonstrating the most common contributions for glass-forming materials [230].

As the temperature is raised, molecular mobilities of various types become successively energized and available for dipolar orientation. By convention the detected relaxation processes at a fixed frequency are designated α, β, γ… in order of decreasing temperature (or in order of increasing frequency for a fixed temperature). Thus, besides the α main relaxation, the β-relaxation is located at the highest temperatures, in comparison with the other sub-glass processes, with even more local mobility and shorter relaxation times. If mobile charges carriers are present, conductivity contributions lead to a divergence of $\varepsilon''(\omega)$ for low frequencies, the same happening if an interface is formed between two different dielectric media.

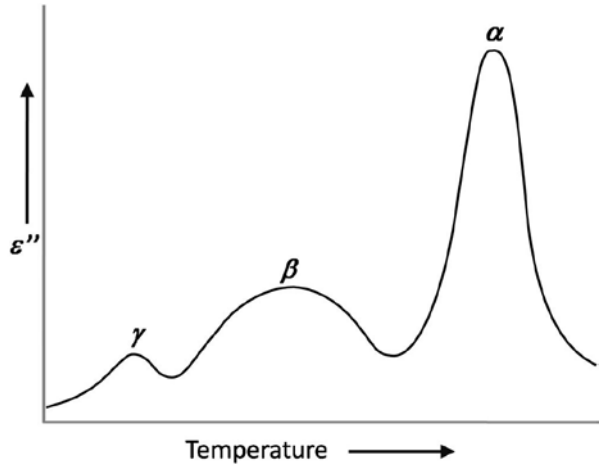

Figure 1. 10- A schematic dielectric loss curve (taken from reference [231]).

All these contributions such as dipolar orientation, conductivity and interfacial polarization should be taken in account to a proper analysis of the dielectric spectra and will be described in the following.

1.4.1.1 Polarization Mechanisms

If polarization is thought on the molecular level, the effect of the electric field is to induce an electric dipole μ on each individual molecule, the magnitude depending on the local electric field strength E_L at the molecule:

$$\mu = \alpha \cdot E_L \qquad \textbf{Equation 1. 21}$$

The constant of proportionality α is called the polarizability of the molecule. Except in certain anisotropic cases, the average direction of the induced molecular dipoles is in the direction of the applied field, since the local field is proportional to the overall applied field ($\mu \propto E$). The total dipole moment per unit volume, the polarisation P, is then related to the number of molecules per unit volume N_0:

$$P \propto N_0 \propto E \qquad \textbf{Equation 1. 22}$$

When an electric field is applied across the faces of a parallel plate capacitor containing a dielectric (a material that restricts the flow of current), the atomic and molecular charges in the dielectric are displaced from their equilibrium positions and the material is said to be polarized. There are two major polarization mechanisms in materials [232]:

1) Induced Polarization due to charge migration.

Two types of polarization results from induced dipoles: 1) electronic polarization which arises when electrons are displaced from their equilibrium positions with respect to the atomic nucleus. 2) atomic polarization which is found in molecules that consist of two different atoms, for example, carbon and oxygen. The electron distribution in these molecules is not symmetrically shared. Application of an external field will cause deflection of their equilibrium positions and create an induce dipole moment.
Both electronic and atomic polarization have a resonant frequency in the ultraviolet or visible and in the infrared range of the electromagnetic spectrum respectively, meaning that they are too fast, even instantaneous, to be studied by dielectric relaxation. However, induced polarization presents two additional aspects that should be taken into account for the dielectric measurements interpretation: i) the accumulation of ions at the material-electrode-interface results on the electrode polarization; ii) the polarization which is created due to the buildup of charges at the interface (or in the interphase) between components in heterogeneous systems is known as interfacial, space charge or Maxwell-Wagner-Sillars Polarization.
Another aspect to be taken into account is the fact that migration of charges gives rise to conductivity, which is when charge carriers are electrons and holes.

2) Orientational Polarization due to alignment of permanent dipoles.

A permanent dipole moment is caused by unbalanced sharing of electrons by atoms of a molecule. In an absence of an external electric field, these moments are oriented in a random order such that no net polarization is present. Under an external electric field, the dipoles rotate to align with the electric field causing orientation polarization to occur. The orientation of permanent dipoles involves cooperative motions of molecular segments in a viscous medium with times scales measurable by dielectric spectroscopy. The time-dependent loss of orientation of dipoles upon removal of the electric field is called dipole relaxation.
Figure 1. 11 shows, the characteristic stepwise fall in polarization of a material as the measurement frequency is raised, rendering impossible for successive components of molecular polarization to make their contribution. The dielectric permittivity follows a similar pattern.
As illustrated, the orientation of molecular dipoles is a relatively slow process compared to electronic transitions or molecular vibrations, which have frequencies above 10^{12} Hz. It does not consist of a uniform switch in the arrangement of all molecules but only of a slight adjustment of the average dipole orientation in face of a constant thermal agitation.

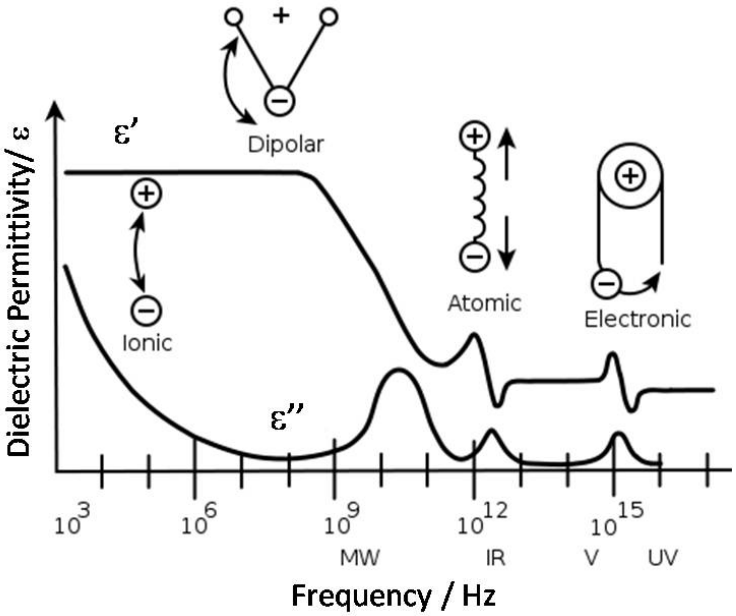

Figure 1. 11- A dielectric permittivity spectrum over a wide range of frequencies. ε′ and ε″ denote the real and the imaginary part of the permittivity, respectively. Various processes are labeled on the image: ionic and dipolar relaxation, and atomic and electronic resonances at higher energies (redrawn from reference [233]).

If the polarization is measured immediately after the field is applied, nearly no dipole orientation is actually present since it appears only with a short delay. Instantaneous response is due to induced polarization, P_∞. In the same way, the instantaneous relative permittivity, denoted ε_∞, will be low and due to the induced dipoles. It is also known as the unrelaxed or permittivity at infinite frequency, ε_∞. Therefore, the contribution of the orientation of the dipoles to the polarization is linked to the difference between the permittivity at low frequency, ε_s and at high frequencies, ε_∞.The difference of both extreme cases (arbitrary orientation and aligned orientation before and after the field application, respectively), $\Delta\varepsilon = \varepsilon_s - \varepsilon_\infty$, is called dielectric strength ($\Delta\varepsilon$). Obviously, in between these extremes of timescale the dispersion from a low to a high relative permittivity takes place.

1.4.2 Dielectrics in Time Dependent Fields

Essentially in a dielectric relaxation spectroscopy measurement, the sample is submitted to an alternate current (a.c.) electrical field and the response is measured in form of a frequency-dependent complex dielectric permittivity, which is a macroscopic quantity reflecting the microscopic event of polarization.

The mathematical formalism that describes, under field application, the built up of orientational polarization, which is a time dependent quantity, will be explained below.

When an isolator material is placed between the plates of a condensator, the charges within it are redistributed and the dipoles will be preferentially oriented along the electric field. For an outer electrical field $E(t)$, the dielectric permittivity or complex dielectric function, ε^*, will be a time (or

frequency) dependent quantity, given that time-dependent processes take place within the sample. This will cause a difference between the time-dependencies of the applied field and the resulting dielectric displacement, $D(t)$. Assuming the validity of the linear response theory, in the case of isotropic systems under a disturbance caused by a time dependent external electrical field $E(t)$, the time dependent response $y(t)$ of the system, can be described by a linear equation [234]. Therefore, the increment in $D(t)$ resulting from the increment in dE at time $t = u$ can be calculated from Equation 1. 23:

$$dD(t) = \varepsilon_0 \cdot \varepsilon_\infty \cdot dE + \varepsilon_0 \cdot (\varepsilon_s - \varepsilon_\infty)\psi(t-u) \cdot dE \qquad \textbf{Equation 1. 23}$$

Where ε_0 is the vacuum permittivity, and the $\varepsilon_0 \cdot \varepsilon_\infty \cdot dE$ term corresponds to the *instantaneous response* of the material to the electric field, whereas the $\varepsilon_0(\varepsilon_S - \varepsilon_\infty)\psi(t-u) \cdot E$ term is related to the slower response assigned to dipolar polarization.

The dielectric function $\psi(t)$ describes the temporal development of the dipole orientation, also described by $\psi(t) = 1 - e^{-t/\tau}$. By this definition $\psi(0) = 0$ and $\psi(\infty) = 1$.

According to the Boltzmann superposition principle [235], the response of a system to a time-dependent external field can be expressed by the superposition of responses of fields at different times. Each response is only dependent on the magnitude of the fields and on time. By knowing the time dependence of the field, Equation 1. 23 may be integrated, resulting in:

$$\begin{aligned} D(t) &= \varepsilon_0 \cdot \varepsilon_\infty \cdot E(t) + \varepsilon_0 \cdot (\varepsilon_s - \varepsilon_\infty) \int_{-\infty}^{t} \frac{dE(u)}{du} \psi(t-u) du \\ &= \varepsilon_0 \cdot \varepsilon_\infty \cdot E(t) + \varepsilon_0 \cdot (\varepsilon_s - \varepsilon_\infty) \int_0^{\infty} E(t-t')\, \Phi(t')\, dt' \end{aligned} \qquad \textbf{Equation 1. 24}$$

where $t - u = t'$and $\Phi(t') = \frac{d\psi(t')}{dt'}$ and is called the dielectric decay function.

A useful practical case is to consider an alternating electric field, described, in the complex form, by $E(t) = E_0 exp(i\omega t)$, where $i = \sqrt{(-1)}$, ω is the angular frequency (in rad s^{-1}) and E_0 is the field amplitude. Therefore one obtains as a response:

$$\frac{D(t)}{\varepsilon_0 \cdot E(t)} = \varepsilon_\infty + (\varepsilon_s - \varepsilon_\infty) \int_0^{\infty} e^{-i\omega t'} \cdot \Phi(t') dt' \qquad \textbf{Equation 1. 25}$$

The relation between the time dependent electric field and the dielectric displacement is expressed by the complex dielectric function or dielectric permittivity:

$$\varepsilon^* = D(t)/(\varepsilon_0 \cdot E(t)) \qquad \textbf{Equation 1. 26}$$

Inserting this in Equation 1. 25, the angular dependency of the dielectric permittivity is given:

$$\frac{\varepsilon^*(\omega)-\varepsilon_\infty}{\varepsilon_s-\varepsilon_\infty}=\int_0^\infty e^{-i\omega t}\cdot\Phi\,(t)\,dt \qquad \textbf{Equation 1. 27}$$

The integral is an imaginary Laplace transform of $\Phi(t)$ that gives rise to the complex permittivity, with real and imaginary components: $\varepsilon^*(\omega)=\varepsilon'(\omega)-i\cdot\varepsilon''(\omega)$.
The real and imaginary parts are functionally related to each other by the Kramers-Kronig relations [236,237]. This means that both $\varepsilon'(\omega)$ and $\varepsilon''(\omega)$ carry the same information. However, because of the limited frequency range and conductivity contributions including Maxwell/Wagner or electrode polarization the practical applicability of the Kramers–Kronig transformation is limited for dielectric measurements.

Debye Model

In the model of Debye to calculate a time dependent dielectric behavior it is assumed a change in the polarization following a first-order differential equation, where its time variation is proportional to its actual value:

$$\frac{dP(t)}{dt}=-\frac{P(t)}{\tau} \qquad \textbf{Equation 1. 28}$$

where τ is the characteristic relaxation time. Therefore, upon removing the electric field at $t=0$, the orientational polarization will be given by $P(t)=P_0 exp(-t/\tau)$, where P_0 is the value of the polarization at the moment of field removal. In this simplest case, $\Phi(t)$ in Equation 1. 27 is given by $k\cdot e^{-t/\tau}$ (page 215 in ref. [42], page 41 in ref. [231]), the exponential decay for the correlation function, where k is equal to $1/\tau$. Thus, the solution for the frequency dependence of $\varepsilon^*(\omega)$ maybe written as [2]:

$$\varepsilon^*(\omega)=\varepsilon_\infty+\frac{\varepsilon_s-\varepsilon_\infty}{1+i\cdot\omega\cdot\tau}=\varepsilon_\infty+\frac{\Delta\varepsilon}{1+i\cdot\omega\cdot\tau} \qquad \textbf{Equation 1. 29}$$

which is called the Debye dispersion equation, where $\Delta\varepsilon=\varepsilon_s-\varepsilon_\infty$, as already described. The real and imaginary components are given by:

[2] $\frac{\varepsilon^*(\omega)-\varepsilon_\infty}{\varepsilon_s-\varepsilon_\infty}=\int_0^\infty e^{-i\omega t}\cdot\Phi\,(t)\,dt=\int_0^\infty e^{-i\omega t}\cdot\frac{1}{\tau}\cdot e^{-t/\tau}\cdot dt=\frac{1}{\tau}\cdot\int_0^\infty e^{-i\omega t}\cdot e^{-t/\tau}\cdot dt=\frac{1}{\tau}\cdot\frac{\tau}{1+i\omega\tau}$

$$\varepsilon'(\omega) = \varepsilon_\infty + \frac{\varepsilon_s - \varepsilon_\infty}{1 + i \cdot \omega^2 \tau^2} \qquad \textbf{Equation 1. 30a}$$

$$\varepsilon''(\omega) = \frac{\varepsilon_s - \varepsilon_\infty}{1 + i \cdot \omega^2 \tau^2} \cdot \omega \cdot \tau \qquad \textbf{Equation 1. 30b}$$

Figure 1. 12 shows the typical shape of both $\varepsilon'(\log f)$ and $\varepsilon''(\log f)$ where f is the frequency in Hz, whereas the frequency of the applied outer electric field is given by $f = \omega / 2\pi$. With increasing $\log f$ the real part $\varepsilon'(\log f)$ decreases step-like whereas the imaginary part $\varepsilon''(\log f)$ exhibits a maximum. The essential quantities which characterize a dielectric relaxation process can be extracted from that behavior. The relaxation time of the fluctuation dipoles is given by $\tau = 1 / (2\pi \cdot f_{max})$, where f_{max} is the frequency at maximum ε'' [238].

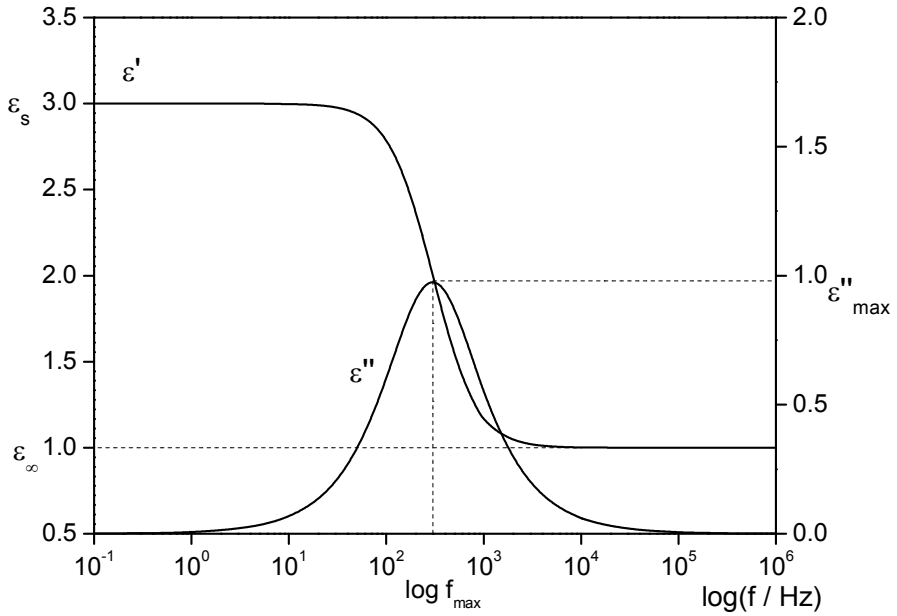

Figure 1. 12- Frequency dependence of the real and imaginary permittivities in a simple Debye process. The half-height width of $\varepsilon''(\log f)$ can be shown to be 1.14 ($\varepsilon_S = 3, \varepsilon_\infty = 1$, $f = 300\ Hz$).

1.4.2.1 Empirical Models for Non-Debye Relaxation

Only in rare cases a Debye –like relaxation behavior according to Equation 1. 29 and Equation 1. 30a is observed. Usually the measured dielectric functions are much broader than predicted by the Debye function. Moreover, in many cases the dielectric function is asymmetric. That means that the short time (high frequency) behavior is more pronounced than the long time (low frequency) one. This is called non Debye or non-ideal dielectric behavior.

A phenomenological approach to deal with this observation is to consider that this enlargement in the response is the result of a superposition of Debye-functions with a relaxation time distribution $L(\tau)$:

$$\phi(t) = \int_{-\infty}^{+\infty} e^{-t/\tau}\, L(\tau)\, d(\ln \tau) \qquad \textbf{Equation 1. 31}$$

In the frequency domain, the relaxation time distribution changes Equation 1. 31 to:

$$\frac{\varepsilon^*(\omega)-\varepsilon_\infty}{\varepsilon_s-\varepsilon_\infty} = \int_{-\infty}^{+\infty} \frac{L(\tau)}{1+i\cdot\omega\cdot t}\, d(\ln \tau) \qquad \textbf{Equation 1. 32}$$

It is possible to obtain $L(\tau)$ from experimental data, but this is a difficult problem. Therefore, the fit of several empirical model functions to the $\varepsilon^*(\omega)$ data have been proposed in the literature enabling a description of broadened and/ or asymmetric loss peaks.

The first attempt to modify the Debye function was the Cole/Cole function [239] where the broadening of the dielectric function was described by introducing a shape parameter α_{CC}, though keeping the symmetry ($\omega_{max}\cdot\tau_{CC}=1$):

$$\varepsilon_{CC}{}^*(\omega) = \varepsilon_\infty + \frac{\Delta\varepsilon}{1+(i\cdot\omega\cdot\tau_{CC})^{\alpha_{CC}}} \;; 0<\alpha_{CC}\leq 1 \qquad \textbf{Equation 1. 33}$$

For $\alpha_{CC}=1$ the Debye function is obtained.

Many experimental results in liquids and in low molecular glass-forming materials have shown that the complex dielectric function can also have asymmetric broadening, therefore Fuoss/Kirkwood [240] and later in 1950 through the Davidson/Cole [241,242] function the Debye model was also improved:

$$\varepsilon_{DC}{}^*(\omega) = \varepsilon_\infty + \frac{\Delta\varepsilon}{(1+i\cdot\omega\cdot\tau_{DC})^{\beta_{DC}}} \;; 0<\beta_{DC}\leq 1 \qquad \textbf{Equation 1. 34}$$

It should be noted that this empirical equation presents the maximum loss not at $\omega_{max}\cdot\tau_{DC}=1$, but instead at $\omega_{max}\cdot\tau_{DC}=\tan[\pi/2\cdot(1+\beta_{DC})]$, therefore the relationship between the characteristic relaxation time and the relaxation time which is related to the position of maximal loss depends on the shape parameter β_{DC}. For $\beta_{DC}=1$ the Debye function is again recovered.

Figure 1. 13 illustrates both the real and imaginary parts of the complex dielectric permittivity for the Cole/Cole and Davidson/Cole functions giving examples for selected shape parameters.

Nowadays, a more general model function was introduced by Havriliak and Negami in 1966 [243] which in fact combines both the Cole/Cole and Davidson/Cole functions:

$$\varepsilon_{HN}{}^*(\omega) = \varepsilon_\infty + \frac{\Delta\varepsilon}{(1+(i\cdot\omega\cdot\tau_{HN})^{\alpha_{HN}})^{\beta_{HN}}} \;; 0<\beta_{HN}\;; \alpha_{HN}\cdot\beta_{HN}\leq 1 \qquad \textbf{Equation 1. 35}$$

The fractional shape parameters α_{HN} and β_{HN} describe the symmetric and asymmetric broadening of the complex dielectric function and are related to the slopes of the ε'' peak at low and high frequencies relative to that corresponding to ε''_{max} as established by Jonscher [244]: $\alpha_{HN} = \partial \log \varepsilon'' / \log \omega$ for $\omega \ll 1/\tau_{HN}$, and $\alpha_{HN} \cdot \beta_{HN} = -\partial \log \varepsilon'' / \log \omega$ for $\omega \gg \frac{1}{\tau_{HN}}$.

The position of the characteristic relaxation rate, ω_{max} or relaxation time $\tau_{max} = 1/\omega_{max}$ can be obtained by τ_{HN}, the following model-independent parameter equation [245,246]:

$$\omega_{max} = 2 \cdot \pi \cdot f_{max} = \frac{1}{\tau_{max}}$$
$$= \frac{1}{\tau_{HN}} \cdot \left[\sin\left(\frac{\alpha_{HN} \cdot \pi}{2 + 2 \cdot \beta_{HN}}\right)\right]^{\frac{1}{\alpha_{HN}}} \cdot \left[\sin\left(\frac{\alpha_{HN} \cdot \beta_{HN} \cdot \pi}{2 + 2 \cdot \beta_{HN}}\right)\right]^{\frac{1}{\alpha_{HN}}} \quad \textbf{Equation 1. 36}$$

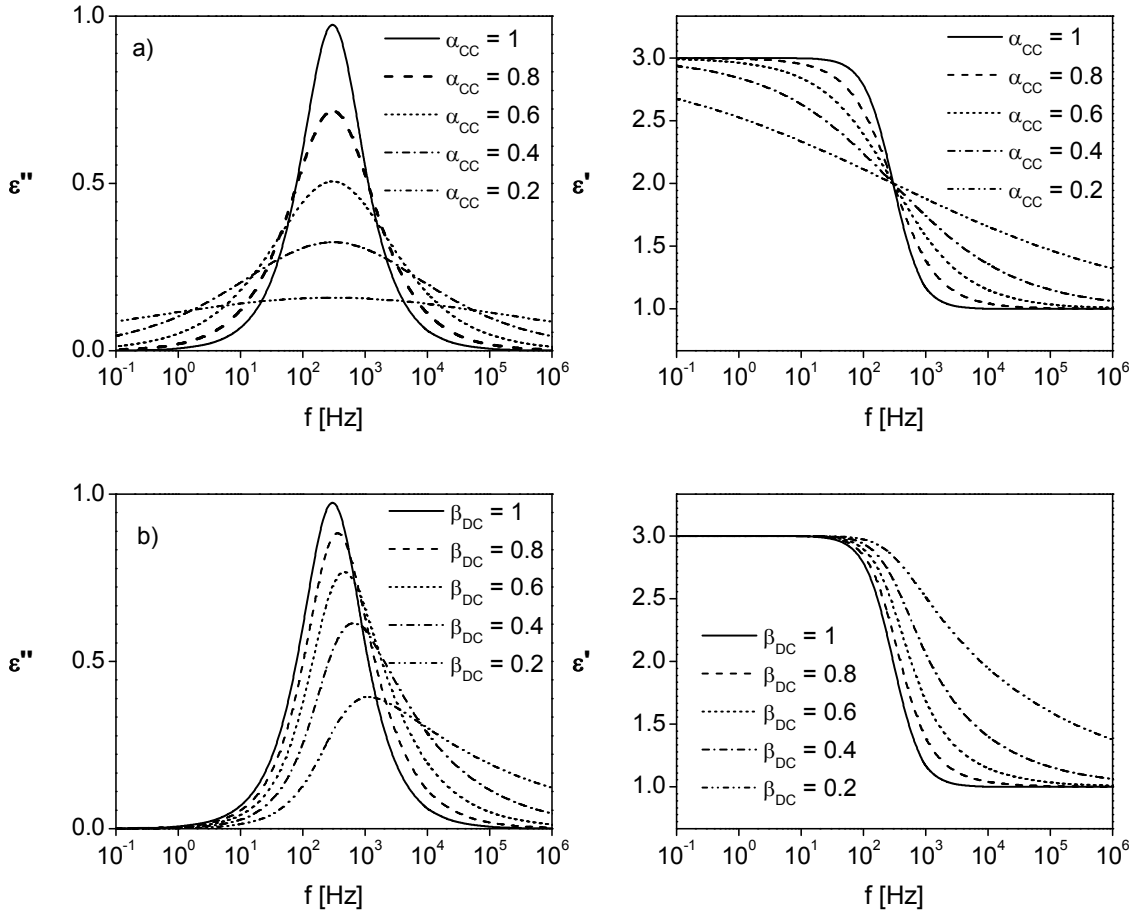

Figure 1. 13- Complex dielectric permittivity for the a) Cole/Cole and b) Davidson/Cole functions ($\Delta\varepsilon = 2$, $\varepsilon_\infty = 1$, $f = 300\ Hz$).

A compilation of the separation of the $\varepsilon^*(\omega)$ in the real and imaginary part for all the models described above is given in Table 1. 1.

Within the framework of linear response theory the dielectric behavior in the frequency domain is related to that in the time domain by a Fourier Transform. Therefore another way to describe a non-Debye relaxation behavior in the time domain is to extract information on $\Phi(t)$ assuming a stretched exponential function, as illustrated by the empirical Kohlrausch/Williams/Watts (KWW) model [247,248] which reads:

$$\Phi(t) = \exp\left[-\left(\frac{t}{\tau_{KWW}}\right)^{\beta_{KWW}}\right]; 0 < \beta_{KWW} \leq 1 \qquad \textbf{Equation 1. 37}$$

where τ_{KWW} is a characteristic time and β_{KWW} is a parameter that describes the non-exponential behavior of the decay function. A decrease of β_{KWW} may be related to a broadening of the distribution of relaxation times, which also present an asymmetric shape.

Model Function	*Real part*	*Imaginary part*
Debye	$\frac{1}{1+(\omega\cdot\tau)^2}$	$\frac{\omega\cdot\tau}{1+(\omega\cdot\tau)^2}$
Cole/Cole	$(1+\omega\cdot\tau)\alpha\cdot\cos\left(\frac{\alpha\cdot\pi}{2}\right)\cdot r^{-1}(\omega)$	$(\omega\cdot\tau)\alpha\cdot\sin\left(\frac{\alpha\cdot\pi}{2}\right)\cdot r^{-1}(\omega)$
	$r(\omega)=1+2\cdot(\omega\cdot\tau)^{\alpha}\cdot\cos\left(\frac{\alpha\cdot\pi}{2}\right)+(\omega\cdot\tau)^{2\cdot\alpha}$	
Davidson/Cole	$\cos(\Phi)^{\beta}\cdot\cos\beta\cdot\Phi$	$\cos(\Phi)^{\beta}\cdot\sin\beta\cdot\Phi$
	$\tan\Phi=\omega\cdot\tau$	
Havriliak/Negami	$r(\omega)\cos[\beta\cdot\Psi(\omega)]$	$r(\omega)\sin[\beta\cdot\Psi(\omega)]$
	$r(\omega)=\left[1+2\cdot(\omega\cdot\tau)^{\alpha}\cdot\cos\left(\frac{\alpha\cdot\pi}{2}\right)+(\omega\cdot\tau)^{2\cdot\alpha}\right]^{-\frac{\beta}{2}}$	
	$\Psi(\omega)=\arctan\left[\frac{\sin\left(\frac{\alpha\cdot\pi}{2}\right)}{(\omega\cdot\tau)^{-\alpha}+\cos\left(\frac{\alpha\cdot\pi}{2}\right)}\right]$	

Table 1. 1- Compilation of the real and imaginary parts of different model functions for the frequency domain.

A relationship between the Davidson/Cole function and the KWW formula, both having only one shape parameter, has been derived by Patterson and Lindsay [249]. This was later extended by Alegria and co-workers [250], which proposed an interrelation between both the HN and KWW function leading to the following empirical approximation:

$$\ln\frac{\tau_{HN}}{\tau_{KWW}} \approx 2.61 \cdot (1-\beta_{KWW})^{0.5} \cdot \exp(-3 \cdot \beta_{KWW}) \qquad \textbf{Equation 1. 38}$$

Also, between the fitting shape parameters of the two models:

$$\alpha_{HN} \cdot \beta_{HN} = {\beta_{KWW}}^{1.23} \qquad \textbf{Equation 1. 39}$$

It is important to note that the HN-function has two shape parameters while the KWW formula has only one. Hence during the transformation from the frequency to the time domain, information is lost.
The KWW parameter has been used in the framework of the coupling model (CM) theory [251] that postulates a so-called primitive relaxation process as a precursor of the α-relaxation in the sense of "genuine"[252] Johari-Goldstein (JG) process [253]. The CM predicts a correlation of the relaxation time of the JG process, τ_{JG}, with that of the α process which reads:

$$\boldsymbol{\tau_{JG} \approx \tau_0(T) = t_c^n[\tau_\alpha(T)]^{1-n}} \qquad \textbf{Equation 1. 40}$$

τ_0 is the primitive relaxation time of the CM, the coupling parameter $n = 1-\beta_{KWW}$, τ_α is the relaxation time of the KWW function τ_{KWW} in Equation 1. 37 and t_c is a time characterizing the crossover from localized to cooperative fluctuations found to be close to $2\times10^{-12}\ s$ for molecular glass-formers [252].

1.4.2.2 Dielectric Strength Models

The classical theories of the dielectric constant founded by Kirkwood [254], Onsager [255], and Debye [256] use a *continuum approach*: they place the molecule in a cavity surrounded by the material treated as a continuum.
The Clausius-Mosotti equation is valid for apolar molecules, while the Debye equation holds approximately well to gases and dilute solutions of molecules carrying a permanent dipole. The Debye equation for a spherical shaped sample is:

$$\frac{\varepsilon_s-1}{\varepsilon_s+2} = \frac{4\cdot\pi}{3}\cdot\alpha\cdot\rho + y_0 \qquad \textbf{Equation 1. 41}$$

where α is the polarizability of the molecule, $\rho = N/V$ is the number density, and y_0 is the dimensionless dipole strength function, $y_0 = 4\pi\cdot\rho\cdot{\mu_0}^2/\,9\cdot k\cdot T$, where μ_0 is the permanent dipole moment, k is the Boltzmann factor and T is the temperature (for μ_0 = 0, Equation 1. 41 yields the Clausius-Mosotti equation).

The Debye equation (Equation 1. 41) has been very successful for very dilute dipolar gases, but it cannot be used to evaluate dipole moments for dense gases or pure liquids.

Onsager in 1936 gave the first derivation of the static dielectric constant for a condensed phase of dipolar molecules. Onsager placed a point dipole in the centre of a cavity of dielectric constant ε_∞ and the effect of the surrounding dielectric is measured by the dielectric response of the polarization charges induced on the wall of the cavity. The resulting equation is:

$$\mu_0{}^2 = \frac{9 \cdot k \cdot T}{4 \cdot \pi \cdot \rho} \; \frac{(\varepsilon_s - \varepsilon_\infty) \cdot (2\varepsilon_s + \varepsilon_\infty)}{\varepsilon_s \cdot (\varepsilon_\infty + 2)^2} \qquad \textbf{Equation 1. 42}$$

where ε_∞ is the high frequency dielectric constant, which is related to the molecular polarisability via the Clausius-Mosotti equation

$$\frac{\varepsilon_\infty - 1}{\varepsilon_\infty + 2} = \frac{4 \cdot \pi}{3} \cdot \alpha \cdot \rho \qquad \textbf{Equation 1. 43}$$

The Onsager equation works quite well for liquids when the dipole moment is not too high and if there is no orientation correlation between the individual molecules.

When the molecules have a large permanent dipole moment, the correlation between a central dipole and the surrounding dipoles cannot be replaced by the response of a continuum dielectric.

In 1939, Kirkwood attempted to extend the Onsager theory by taking into account short-range intermolecular interactions that lead to specific static dipole-dipole orientations of the molecule and therefore has introduced the so-called Kirkwood g-factor to take into account these short range correlations.

The g-factor is obtained from the average dipole component $\langle M \rangle$ in the direction of the field due to the dipoles in the sphere:

$$g_k = \frac{\langle M \rangle}{N \cdot \mu_0{}^2} \qquad \textbf{Equation 1. 44}$$

g_k will be different from 1 if there is correlation between the orientations of neighboring molecules: for predominantly parallel or anti-parallel correlations between neighboring dipoles, $g_k > 1$ or $0 < g_k < 1$, respectively, while for a random orientation of dipoles $g_k = 1$ holds.

For a liquid consisting of non-polarizable molecules the Kirkwood-equation reads as:

$$\frac{(\varepsilon_s - 1) \cdot (2\varepsilon_s + 1)}{\varepsilon_s} = \frac{4 \cdot \pi \cdot \rho \cdot \mu_0{}^2}{k \cdot T} \cdot g_k \qquad \textbf{Equation 1. 45}$$

The deformation polarization of Equation 1. 45 was not included in Kirkwood's statistical mechanical theory, but was merely added in an empirical manner. As a result, for $g_k = 1$, indicating that there is no orientation correlation, Equation 1. 45 does not reduce to the Onsager equation.

In 1949 Fröhlich developed a very general dielectric theory which took into account the molecular polarisability together with the *continuum approach* used by Onsager. The advantages of this approach are that the deformation polarization is included at the initial stage of the theory and the cavity and reaction fields are treated in a macroscopic manner, which is more realistic than the model considered by Onsager.

Based on this model, the final Kirkwood-Fröhlich (KF) [257] equation can be obtained:

$$\Delta\varepsilon = (\varepsilon_s - \varepsilon_\infty) = g_k \cdot \frac{\rho \cdot {\mu_0}^2}{9 \cdot k \cdot T \cdot \varepsilon_0} \frac{\varepsilon_s \cdot (\varepsilon_\infty + 2)^2}{2 \cdot (\varepsilon_s + \varepsilon_\infty)} \qquad \textbf{Equation 1. 46}$$

For the special case $\varepsilon_s \gg \varepsilon_\infty$, the numerical values of $g_k \cdot \mu_0^2$ obtained from the Kirkwood equation (Equation 1. 45) and from Equation 1. 46 will not differ significantly.

1.4.2.3 Charge Carriers

Charge carriers block effects and d.c. conductivity are typical observable at low frequencies and high temperatures in dielectric spectra. Due to the parallel measurement of the translational component (d.c. conductivity) that is observed simultaneously with the most frequently analyzed rotational dynamic component (orientational relaxation) [258], dielectric relaxation spectroscopy is still adequate to study conductivity effects. These are the frequency dependent charge-carrier motion within the sample, known as electric conductivity relaxation [259,260], the trapping of charge carriers as interfaces within the bulk of the sample (interfacial Maxwell-wagner-Sillars polarization [261,262]) and the blocking of charge carriers at the interface between the ion-conducting material and the electron-conducting metallic electrode (electrode polarization) [263].

When these effects are present in the sample, the HN equation must be slightly changed by adding the conductivity term as:

$$\varepsilon^*(\omega) = -i \cdot a \cdot \left(\frac{\sigma_0}{\varepsilon_0 \cdot \omega^s}\right) + {\varepsilon_{HN}}^*(\omega) \qquad \textbf{Equation 1. 47}$$

where a has dimensions of $(\mathrm{Hz})^{-1}.(\mathrm{rad}\ .\ \mathrm{Hz})^s$. The exponent s is used to take into account a low frequency tail that is influenced by either electrode or interfacial polarization (when the conductivity is not pure d.c. $s < 1$, usually, $0.5 \leq s < 1$) [238].

Figure 1. 14 delineates some different contributions.

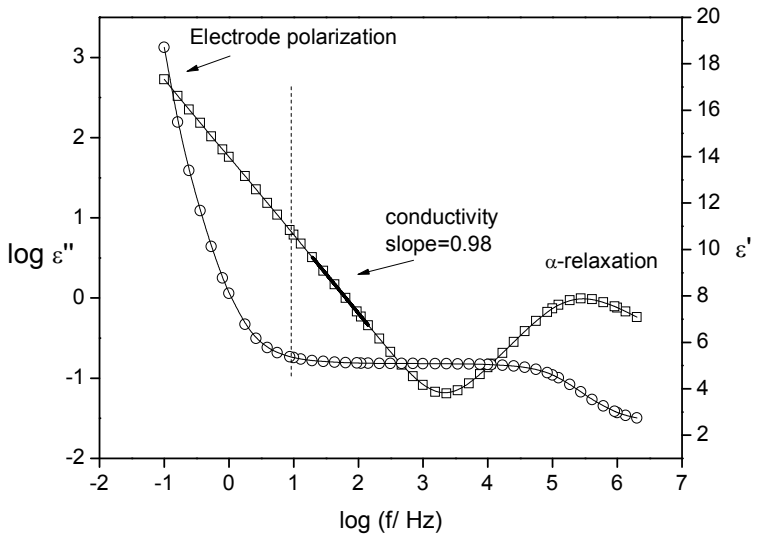

Figure 1. 14- Real part ε' (open circles) and imaginary part ε'' (open squares) of complex dielectric function for PVAc at T= 373 K. The strong increase of ε' at low frequencies is due to electrode polarization.

When the conductivity is of pure electronic origin the slope of a plot of $\log \varepsilon''$ versus $\log f$ should be equal to -1.

1.4.3 Dielectrics in Liquid Crystals

The dielectric properties of LC's are anisotropic and the complex dielectric function $\varepsilon^*(\omega)$ (ω - angular frequency) has to be described by a tensor. For uniaxial nematic phases this tensor has two main components $\varepsilon_{\parallel}^*(\omega)$ and $\varepsilon_{\perp}^*(\omega)$ parallel and perpendicular to the nematic director. The theory of dielectric relaxation of liquid crystals is shortly outlined in [264]. A more refined discussion can be found in [265,266]. The mesogenic unit has two components of the molecular dipole vector which are oriented longitudinal (L) and transverse (T) to its long axis. The dielectric response is due to correlation functions of the polarization fluctuations parallel and perpendicular to the nematic director. In that semi-microscopic treatment the measured dielectric function parallel $\varepsilon_{\parallel}^*(\omega)$ and perpendicular $\varepsilon_{\perp}^*(\omega)$ to the director comprises different weighted sums of the four underlying relaxation modes depending on the macroscopic orientation of the sample (Figure 1. 15). The relaxation mode with the lowest frequencies is due to rotational fluctuations of the molecule around its short axis. This process determines mainly $\varepsilon_{\parallel}^*(\omega)$ and is called δ-relaxation. The other three relaxation modes (different tumbling fluctuations of the molecules around their long axis) have nearly the same relaxation time and form one broad relaxation process, which is mostly related to $\varepsilon_{\perp}^*(\omega)$. This process is observed at higher frequencies than the δ process. The intensity or the dielectric strength of the δ-relaxation relative to that of the tumbling mode depends on the order parameter S of the sample under investigation [264]. In detail:

$$\varepsilon_{\parallel}^{*}(\omega) = \varepsilon_{\infty,\parallel} + \frac{G}{3k_BT}\left[(1+2S)\,\mu_L^2\,C_{\parallel}^{L}(\omega) + (1-S)\;\mu_T^2\,C_{\parallel}^{T}(\omega)\right] \qquad \textbf{Equation 1. 48a}$$

$$\varepsilon_{\perp}^{*}(\omega) = \varepsilon_{\infty,\perp} + \frac{G}{3k_BT}\left[(1-S)\,\mu_L^2\,C_{\perp}^{L}(\omega) + \left(1+\frac{S}{2}\right)\;\mu_T^2\,C_{\perp}^{T}(\omega)\right] \qquad \textbf{Equation 1. 48b}$$

is obtained. $\varepsilon_{\infty,\parallel}$ and $\varepsilon_{\infty,\perp}$ are the limiting high frequency permittivities parallel and perpendicular to the local director and G is a constant. $C_j^i(\omega)$ $(i = L,T\ ;j = \parallel,\perp)$ denote the one-sided Fourier transformations of the correlation functions of the longitudinal and transverse component of the dipole moment vector of the mesogenic unit projected parallel $\overrightarrow{\mu_L}$ and perpendicular $\overrightarrow{\mu_T}$ to the nematic director. Their long axes are preferentially aligned with respect to a common unit vector, the nematic director, n. The degree of orientation of the molecules is described by the order parameter S defined by:

$$S = \frac{1}{2}(3\cdot\langle\cos^2\theta\rangle - 1) \qquad \textbf{Equation 1. 49}$$

where θ is the angle between the direction of the long axis of the molecule and the director n the brackets denote the statistical average. For an isotropic liquid $S = 0$ holds and for a fully aligned LC phase $S = 1$ [48].

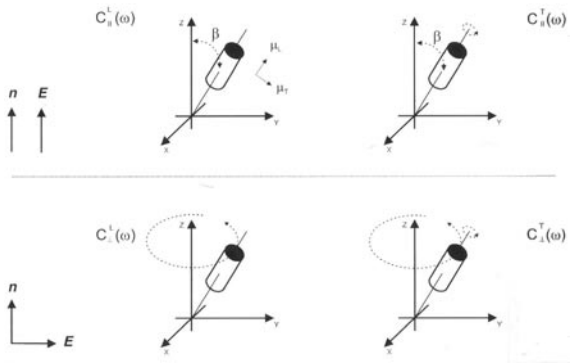

Figure 1. 15-Possible relaxation modes for a mesogenic unit in a uniaxial nematic phase depending on its orientation with regard to an outer electric field (reproduced from ref [264]).

In regard to the temperature dependence of the relaxation times of the δ- and tumbling modes deviations from the theoretically predicted Arrhenius-like dependence in the range of liquid crystalline mesophases have been already reported for cyanobiphenyl systems and other nematics [141,142,143,144,145,146,147,148,149,150], as also found for conventional glass formers. In respect to the liquid crystal studied in this work, E7, dielectric studies in a limited frequency range were already reported by some of us [147,150] and also by others [144-145,146,147,148,149,150], where these two expected processes are observed and a slow one lying on the low frequency tail of the δ, has been reported for the first time by [150,267].

1.5 References

[1] BÖHMER R, NGAI KL, ANGELL CA, PLAZEK DJ (1993) J. CHEM. PHYS. 99, 4201.

[2] HANSEN J-P (1990) "THEORY OF SIMPLE LIQUIDS" 2ND EDN. LONDON, ACADEMIC.

[3] JOHARI GP (1984) "RELAXATIONS IN COMPLEX SYSTEMS" EDS. NGAI KL AND WRIGHT GB, WASHINGTON DC: ONA.

[4] DONTH E (1981) "GLASÜBERGANG", BERLIN, AKADEMIE.

[5] GÖTZE W (1991) "LIQUIDS, FREEZING AND GLASS TRANSITION" EDS. D LEVESQUE, J-P HANSEN AND J ZINN-JUSTIN, AMSTERDAM: NORTH-HOLLAND.

[6] GORBATSCHOW W, ARNDT M, STANNARIUS R , KREMER F (1996) EUROPHYS. LETT. 35, 719.

[7] ARNDT M, STANNARIUS R, GORBATSCHOW W , KREMER F (1996) PHYS. REV. E 54, 5377.

[8] KREMER F, HUWE A, ARNDT M, BEHRENS P, SCHWIEGER W (1999) J. PHYS.: CONDENS. MATTER. 11, A175.

[9] ARNDT M, STANNARIUS R, GROOTHUES H, HEMPEL E, KREMER F (1997) PHYS. REV. LETT. 79, 2077.

[10] ALIEV FM (1996) "COMPLEX GEOMETRIES" EDS. GP CRAWFORD AND S. ŽUMER, LONDON, TAYLOR AND FRANCIS, CH. 17.

[11] ADAM G, GIBBS JH (1965) J. CHEM. PHYS. 43, 139.

[12] NGAI KL (1993) "DISORDER EFFECTS ON RELAXATIONAL PROCESSES" EDS. R RICHERT AND A BLUMEN, BERLIN, SPRINGER.

[13] WILLIAMS G, FOURNIER J (1996) J. CHEM. PHYS. 184, 5690.

[14] SAPPELT D, JÄCKLE J (1993) J. PHYS. A: MATH. GEN. 26, 7325.

[15] FISCHER EW, DONTH E, STEFFEN W (1992) PHYS. REV. LETT. 68, 2344.

[16] PFEIFER H (1976) PHYS. REP. 26, 293.

[17] KÄRGER J, RUTHVEN DM (1992) "DIFFUSION IN ZEOLITES AND OTHER POROUS SOLIDS", WILEY, NEW YORK.

[18] BEINER M, RENGARAJAN GT, PANKAJ S, ENKE D, STEINHART M (2007) NANO LETT. 7, 5.

[19] RENGARAJAN GT, ENKE D, STEINHART M, BEINER M (2008) J. MATER. CHEM. 18, 2537.

[20] BEINER M (2008) J. POLYM. SCI.: PART B, POLYM. PHYS. 46, 1556.

[21] ZHU L, CALHOUN BH, GE Q, QUIRK RP, CHENG SZD, THOMAS EL, HSIAO BS, YEH F, LIU L, LOTZ B (2001) MACROMOLECULES 34, 1244.

[22] ZHU L, CHENG SZD, CALHOUN BH, GE Q, QUIRK RP, THOMAS EL, HSIAO BS, YEH F, LOTZ B (2001) POLYMER 42, 5847; ZHU L, CHENG SZD, CALHOUN BH, GE Q, QUIRK RP, THOMAS EL, HSIAO BS, YEH F, LOTZ B (2000) J. AM. CHEM. SOC. 122, 5957.

[23] WEIMANN PA, HAJDUK DA, CHU C, CHAFFIN KA, BRODIL JC, BATES FS (1999) J. POLYM SCI, POLYM PHYS ED 37, 2053.

[24] ANGELL CA, NGAI KL, MCKENNA GB, MCMILLAN PF, MARTIN SW (2000) J. APPL. PHYS. 88, 3113.

[25] NGAI KL (2000) J.NON-CRYST.SOLIDS 275, 7.

[26] RZOSKA SJ, ZHELEZNY VP (EDS.) (2004) "NONLINEAR DIELECTRIC PHENOMENA IN COMPLEX LIQUIDS" 247-258, KLUWER ACADEMIC PUBLISHERS. PRINTED IN THE NETHERLANDS.

[27] DONTH E (2001) "THE GLASS TRANSITION, RELAXATION DYNAMICS IN LIQUIDS AND DISORDERED MATERIALS", SPRINGER-VERLAG, BELRIN, HEIDELBERG, CH. 2.

[28] TURNBULL D (1969) CONTEMP. PHYS. 10, 473.

[29] ANGELL CA (1988) J. NON-CRYST. SOLIDS 102, 205.

[30] BRAWER S (1985) "RELAXATION IN VISCOUS LIQUIDS AND GLASSES" AM. CERAM. SOC., COLUMBUS.

[31] DEBENEDETTI PG, STILLINGER FH (2001) NATURE VOL.410, 259.

[32] MOYNIHAN CT, ET AL. (1976) "THE GLASS TRANSITION AND THE NATURE OF THE GLASSY STATE" EDS. M. GOLDSTEIN AND R SIMHA, ANN. NY ACAD. SCI. 279, 15.

[33] BRÜNING R, SAMWER K (1992) PHYS. REV. B 46, 318.

[34] EDIGER MD, ANGELL CA, NAGEL SR (1996) J. PHYS. CHEM. 100, 13200.

[35] KRÜGER, JK, MESQUIDA P, BALLER J (1999), PHYS REV B, 60, 10037; KRÜGER JK, BOHN KP, JIMENEZ R, SCHREIBER J (1996) COLLOID & POLYMER SCI. 274, 490.

[36] GIBBS JH (1956) J CHEM PHYS, 25, 185; GIBB JH S, DIMARZIO EA (1958) J. CHEM. PHYS. 28, 373; DIMARZIO EA, GIBBS JH, FLEMMING PD, SANCHES IC (1976) MACROMOLECULES, 9, 763.

[37] ANGELL, CA, RAO KJ (1972) J. CHEM. 57, 470.

[38] DONTH E (2001) "THE GLASS TRANSITION, RELAXATION DYNAMICS IN LIQUIDS AND DISORDERED MATERIALS" SPRINGER-VERLAG, BELRIN, HEIDELBERG, CH. 1.

[39] RICHERT R, BLUMEN A (EDS.) (1994) "DISORDER EFFECTS ON RELAXATIONAL PROCESSES" SPRINGER, BERLIN.

[40] STICKEL F, FISHER EW, RICHERT R (1995) J. CHEM. PHYS. 102, 15, 6251.

[41] ANDERSON PW (1995) SCIENCE 267 1615; ANGEL CA (1995) SCIENCE 267 1924.

[42] MCGRUM NG, READ BE, WILLIAMS G (1991) "ANELASTIC AND DIELCTRIC EFFECTS IN POLYMERIC SOLIDS", WILEY, NEW YORK (REPRINTED BY DOVER, NEW YORK).

[43] VOGEL H (1921) PHYS. Z. 22, 645.

[44] FULCHER GS (1923) J. AM. CERAM. SOC. 8,339.

[45] TAMMANN G, HESSE WZ (1926) ANORG. ALLG. CHEM 156, 245.

[46] KAUZMANN W (1990) CHEM. REV. LETT. 64, 1549.

[47] SCHÖNHALS A, "DIELECTRIC SPECTROSCOPY OF POLYMERIC MATERIALS- FUNDAMENTALS AND APPLICATION" (EDS.) JP RUNT, JJ FITZGERALD, AMERICAN CHEMICAL SOCIETY, WASHINGTON, DC, PAGE 89.

[48] KREMER F, SCHÖNHALS A (2003) "BROADBAND DIELECTRIC RELAXATION" EDS. F KREMER AND A SCHÖNHALS, SPRINGER-VERLAG, BERLIN, CH. 10.

[49] GLASSTONE S, LAIDER KJ, EYRING H. (1941) "THE THEORY OF RATE PROCESSES" MCGRAW-HILL, NEW YORK.

[50] DIXON P (1990) PHYS REV B 42, 8179.

[51] SCHÖNHALS A, KREMER F, HOFMANN A, FISCHER EW, SCHLOSSER E (1993) PHYS REV LETT. 70, 3459.

[52] MCGRUN NG, READ BE, WILLIAMS G (1991) "ANELASTIC AND DIELCTRIC EFFECTS IN POLYMERIC SOLIDS", WILEY, NEW YORK (REPRINTED BY DOVER, NEW YORK), CH. 5.

[53] DOOLITTLE AK (1951) J. APPL. PHYS., 22, 1471; DOOLITTLE AK (1952) J. APPL. PHYS. 23, 236.

[54] COHEN MH, TURNBULL D (1959) J. CHEM. PHYS. 31, 1164.

[55] WILLIAMS ML, LANDEL RF, FERRY JD (1955) J. AM. CHEM. SOC. 77, 3701.

[56] FERRY JD (1970) "VISCOELASTIC PROPERTIES OF POLYMERS", WILEY, NEW YORK.

[57] SCHÖNHALS A (2003) "BROADBAND DIELECTRIC RELAXATION" (EDS.) F KREMER AND A SCHÖNHALS, SPRINGER-VERLAG, BERLIN, CH. 7.

[58] DIONISIO M, MANO J (2008) "HANDBOOK OF THERMAL ANALYSIS AND CALORIMETRY VOL.5 RECENT ADVANCES, TECHNIQUES AND APPLICATIONS" EDS M BROWN AND P GALLAGHER, ELSEVIER, CH. 7.

[59] KAHLE S, HEMPEL E, BEINER M, UNGER R, SCHRÖTER K, DONTH E (1999) J. MOL. STRUCT. 479, 149.

[60] HUTH H, BEINER M, DONTH E (2000) PHYS. REV. B 61, 15092.

[61] WÜBBENHORST M, LUPASCU V (2005) PROCEEDINGS OF THE ISE-12, BRAZIL.

[62] COREZZI S, FIORETTO D, SANTUCCI SC, CAPACCIOLI S, CASALINI R, LUCCHESI M, HEMPEL E, BEINER M (2002) PHYL. MAG. B 82, 3, 339.

[63] BEINER M (2001) MACROMOL. RAPID COMMUN. 22, 869.

[64] NGAI KL (1998) PHYS. REV. E 57, 7346.

[65] KREMER F, SCHÖNHALS A (2003) "BROADBAND DIELECTRIC RELAXATION" EDS. F KREMER AND A SCHÖNHALS, SPRINGER-VERLAG, BERLIN, CH.4.

[66] ANGELL CA, SICHINA W (1976) ANN. NEW YORK ACAD. SCI. 279, 53.

[67] THE T_G SCALED VISCOSITY PLOT THAT IS IN THE ORIGIN OF THE FRAGILITY CONCEPT WAS ORIGINALLY GIVEN BY LAUGHLIN WT, UHLMANN DR (1972) J. PHYS. CHEM. 76, 2317 AND OLDEKOP W (1957) GLASSTECHNISCHE BERICHTE 30, 8 BEING REVISED IN NGAI KL (2000) J. NON-CRYST. SOLIDS 275,7.

[68] ANGELL CA (1985) "RELAXATIONS IN COMPLEX SYSTEMS" (EDS.) KL NGAI AND GB WRIGHT, NATIONAL TECHNICAL INFORMATION SERVICE, SPRINGFIELD, PAGE 3.

[69] HODGE IM (1996) J. NON-CRYST. SOLIDS 202, 164.

[70] DEBENEDETTI PG (1997) "METASTABLE LIQUIDS: CONCEPTS AND PRINCIPLES" PRINCETON UNIVERSITY PRESS.

[71] RICHERT R, ANGELL CA (1998) J. CHEM. PHYS. 108, 9016.

[72] ANGELL CA, RICHARDS BE, VELIKOV V (1999) J. PHYS. CONDENS. MATTER. 11, A75.

[73] DESCAMPS M, CORREIA NT, DEROLLEZ P, DANEDE F, CAPET F (2005) J. PHYS. CHEM. B 109, 16092.

[74] JOHARI GP, KIM S, SHANKER RM (2005) J. PHARM. SCI. 94, 2207.

[75] ANGELL CA (1991) J. NON-CRYST. SOLIDS 131-133, 13.

[76] ANGELL CA (1997) J. RES. NATL. INST. STAND. TECHNOL. 102, 171.

[77] MOYNIHAN CT, ANGELL CA (2000) J. OF NON-CRYST. SOLIDS 274, 131.

[78] ABOU ELFADL A, HERRMANN A, HINTERMEYER J, PETZOLD N, NOVIKOV VN, RÖSSLER EA (2009) MACROMOLECULES 42, 6816.

[79] BATTEZZATI M, KUSÝ M, PALUMBO M, RONTO V (2005) "PROPERTIES AND APPLICATIONS OF NANOCRYSTALLINE ALLOYS FROM AMORPHOUS PRECURSORS" (EDS.) B. IDZIKOWSKI ET AL., KLUWER ACADEMIC PUBLISHERS, NETHERLANDS, PAGE 267.

[80] NGAI KL, CAPACCIOLI S (2008) J.OF THE AMERICAN CER. SOC. 91, 3, 709.

[81] KAUZMANN W (1948) CHEM. REV. 43, 219; HARRISON G (1976) "THE DYNAMIC PROPERTIES OF SUPERCOOLED LIQUIDS", ACADEMIC, NEW YORK; BRAWER S (1985) "RELAXATION IN VISCOUS LIQUIDS AND GLASSES", AMERICAN CERAMIC SOCIETY, COLUMBUS, OHIO; SCHERER GW (1990) J. NON-CRYST. SOLIDS, 123, 75; DYRE JC (1998) J. NON-CRYST. SOLIDS 235, 142; DYRE JC (2004) NATURE MATER. 3, 749.

[82] EYRING H (1936) J. CHEM. PHYS. 4, 183.

[83] EYRING HJ (1944) J. CHEM. PHYS. 4, 283.

[84] EINFELDT J, MAIßNER D, KWASNIEWSKI A (2001) PROG. POLYM. SCI. 26, 1419.

[85] VICIOSA MT, DIONÍSIO M, SILVA RM, REIS RL, MANO JF (2004) BIOMACROMOLECULES, 5, 2073.

[86] DIAZ-CALLEJA R, SAIZ E, RIANDE E, GARGALLO L, RADIC D (1993) MACROMOLECULES, 26, 3795.

[87] DIOGO HP, MOURA-RAMOS JJ (2009) J POLYM SCI PART B: POLYM PHYS 47, 820.

[88] HEIJBOER J (1976) ANN. NY ACAD. SCI. 279, 104.

[89] JOHARI GP, GOLDSTEIN M (1970) J. CHEM. PHYS., 53, 2372.

[90] JOHARI GP, GOLDSTEIN M (1972) J. CHEM. PHYS. 55, 4245; JOHARI GP (1973) J. CHEM. PHYS. 58,1766; JOHARI GP, PATHMANATHAN K (1986) J. CHEM. PHYS. 85, 6811; CHUNG SH, JOHARI GP, PATHMANATHAN K (1986) J. POLYM. SCI. B 24, 2655.

[91] RIVERA A, RÖSSLER EA (2006) PHYS. REV. B 73, 212201.

[92] COREZZI S, BEINER M, HUTH H, SCHRÖTER K, CAPACCIOLI S, CASALINI R, FIORETTO D, DONTH E (2002) J. CHEM. PHYS. 117, 2435.

[93] BEINER M, HUTH H, SCHRÖTER K (2001) J. NON-CRYST. SOLIDS, 279, 126.

[94] GARWE F, SCHÖNHALS A, BEINER M, SCHRÖTER K, DONTH E (1994) J. PHYS.: CONDENS. MATTER 6, 6941.

[95] GARWE F, SCHÖNHALS A, LOCKWENZ H, BEINER M, SCHRÖTTER K, DONTH E (1996) MACROMOLECULES 29, 247.

[96] SOKOLOV AP (1998) J. NON-CRYST. SOLIDS 235–237, 190.

[97] WILLIAMS G (1966) TRANS. FARAD. SOC. 62, 2091.

[98] BEINER M, KAHLE S, HEMPEL E, SCHRÖTER K, DONTH E (1998) EUROPHYS. LETTERS 44, 321.

[99] BEINER M, KORUS J, DONTH E (1997) MACROMOLECULES 30, 8420.

[100] DONTH E (1992) "RELAXATION AND THERMODYNAMICS IN POLYMERS, GLASS TRANSITION", AKADEMIE-VERLAG, BERLIN.

[101] CASALINI R, FIORETTO D, LIVI A, LUCHESI M, ROLLA (1997) PA PHYSICAL REVIEW B 56(6), 3016.

[102] MESEGUER DUEÑAS JM, TORRES ESCURIOLA D, GALLEGO FERRER G, MONLEÓN PRADAS M, GÓMEZ RIBELLES JL, PISSIS P, KYRITSIS A (2001) MACROMOLECULES 34, 5525.

[103] SCHULTZ M (1999) PHYS. LETTER A 251, 269.

[104] JOHARI GP, WHALLEY E (1972) FARADAY SYMP. CHEM. SOC. 6, 42.

[105] COREZZI S, CAPACCIOLI S, GALLONE G, LIVI A, ROLLA PA (1997) J. PHYS.: CONDENS. MATTER 9, 6199.

[106] NGAI KL, CAPACCIOLI S (2004) PHYS. REV. E 69, 31501; NGAI KL, PALUCH M (2004) J. CHEM. PHYS. 120(2), 857.

[107] SCHNEIDER U, LUNKENHEIMER P, BRAND R, LOIDL A (1999) PHYS. REV. E 59(6), 6924.

[108] DONTH E (1982) J. NON-CRYST. SOLIDS 53(3), 325.

[109] HEMPEL E, HEMPEL G, HENSEL A, SCHICK C, DONTH E (2000) J. PHYS. CHEM. B 104(11), 2460.

[110] VON LAUE M (1917) PHYS. Z. 18, 542.

[111] DONTH E, HUTH H, BEINER M (2001) J. PHYS.: CONDENS. MATTER 13, L451.

[112] KORUS J, HEMPEL E, BEINER M, KAHLE S, DONTH E (1997) ACTA POLYM. 48(9) 369.

[113] JOHARI GP (1976) ANN. NEW YORK ACAD. SCI. 279(1), 117.

[114] KYRITSIS A, GÓMEZ RIBELLES JL, MESEGUER DUEÑAS JM, SOLER CAMPILLO N, GALLEGO FERRER G, MONLEÓN PRADAS M (2004) MACROMOLECULES 37(2) 446.

[115] ESPADERO BERZOSA A, GÓMEZ RIBELLES JL, KRIPOTOU S, PISSIS P (2004) MACROMOLECULES 37 6472-6479.

[116] GORENINCKX G, REYNAERS H, BERGHMANS H, SMETS G (1980), J. POLYM. SCI.,POLYM. PHYS. ED. 18, 1311; GORENINCKX G, REYNAERS (1980), J. POLYM. SCI.,POLYM. PHYS. ED. 18, 1325.

[117] SCHICK C, DONTH E (1991) PHYSICA SCRIPTA 43, 423.

[118] HEMPEL E, HUWE A, OTTO K, JANOWSKI F, SCHRÖTER K, DONTH E (1999) THERMOCHIM. ACTA, 337, 163.

[119] SCHÖNHALS A, STAUGA R (1998) J. OF NON-CRYST. SOLIDS 235-237, 450.

[120] PARK J-Y, MCKENNA GB (1999) PHYS REV B, 61, 6667.

[121] MCKENNA GB (2000) J. PHYS. IV FRANCE 10, 343.

[122] JACKSON CL, MCKENNA GB (1991) J. NON-CRYST. SOLIDS, 131-133, 221.

[123] JACKSON CL, MCKENNA GB (1990) J. CHEM. PHYS. 93, 9002.

[124] KLAFTER J AND DRAKE JM (EDS.) (1989) "MOLECULAR DYNAMICS IN RESTRICTED GEOMETRIES", JOHN WILEY, NEW YORK.

[125] RICHTER D, DIANOUX AJ, PETRY W, TEIXEIRA J (1989) "DYNAMICS OF DISORDERED MATERIALS", SPRINGER PROCEEDINGS IN PHYSICS 37, SPRINGER-VERLAG, BERLIN.

[126] ZHANG J, LIU G, JONAS J (1992) J. PHYS. CHEM. 96, 3478.

[127] DUBOCHET J, ALBA CM, MACFARLANE DR, ANGELL CA, KADIYALA RK, ADRIAN M, TEIXEIRA J (1984) J. PHYS. CHEM. 88, 6727.

[128] HOFER K, MAYER E, JOHARI GP (1991) J. PHYS. CHEM. 95, 7100.

[129] SCHÖNHALS A, GOERING H, SCHICK CH, FRICK B, ZORN R (2005) J. NON-CRYST. SOLIDS 351, 33-36, 2668.

[130] SCHÖNHALS A, GOERING H, SCHICK CH (2002) J. NON-CRYST. SOLIDS 305, 1-3, 140.

[131] KREMER F, SCHÖNHALS A (2003) "BROADBAND DIELECTRIC RELAXATION" (EDS.) F KREMER AND A SCHÖNHALS, SPRINGER-VERLAG, BERLIN, CH.6.

[132] SCHEIDLER P, KOBWAND BINDER K (2002) EUROPHYS. LETT. 59, 701.

[133] ALCOUTLABI M, MCKENNA GB (2005) J. PHYS.: CONDENS. MATTER 17, R461.

[134] SCHULLER J, MEL'NICHENKO YU B, RICHERT R AND FICHER E W (1994) PHYS. REV. LETT. 73, 2224.

[135] SCHULLER J, RICHERT R AND FICSHER EW (1995) PHYS. REV. B 52 15232.

[136] DE GENNES PG (1975) THE PHYSICS OF LIQUID CRYSTALS, CLARENDON PRESS, OXFORD.

[137] CHANDRASEKHAR S (1992) LIQUID CRYSTALS, CAMBRIDGE UNIVERSITY PRESS.

[138] DEMUS D, GOODBY J, GRAY GW, SPIESS HW, VILL V (EDS) (1998) "HANDBOOK OF LIQUID CRYSTALS" WILEY-VCH WEINHEIM.

[139] BELLINI T, RADZIHOVSKY L, TONER J, CLARK NA (2001) SCIENCE 294, 1074.

[140] IANNACCHIONE GS (2004) FLUID PHASE EQUILIB. 222-223, 177.

[141] ZELLER HR (1982) PHYS. REV. LETT. 48, 334

[142] BENGUIGUI L, (1983) PHYS. REV. A 28, 1852; IDEM (1984) PHYS. REV. A 29, 2968; IDEM (1984) MOL. CRYST. LIQ. CRYST. 114, 51.

[143] DIOGO AC, MARTINS AF (1982) J. PHYS. (PARIS) 43, 779.

[144] ZHONG ZZ, SCHUELE DE, GORDON WL, ADAMIC KJ, AKINS RB (1992) J. POLYM. SCI. B: POLYM PHYS. 30, 1443

[145] MASCHKE U, BENMOUNA M, COQUERET X (2002) MACROMOL. RAPID COMMUN. 23, 159.

[146] ROUSSEL F, BUISINE JM, MASCHKE U, COQUERET X (1997) MOL. CRYST. LIQ. CRYST. 299, 321

[147] VICIOSA MT, NUNES AM, FERNANDES A, ALMEIDA PL, GODINHO MH, DIONISIO MD (2002) LIQ. CRYST. 29, 429

[148] VAN BOXTEL MCW, WÜBBENHORST M, VAN TURNHOUT J, BASTIAANSEN CWM, BROER DJ (2003) LIQ. CRYST. 30, 235.

[149] VAN BOXTEL MCW, WÜBBENHORST M, VAN TURNHOUT J, BASTIAANSEN CWM, BROER DJ (2004) LIQ. CRYST. 31, 1207.

[150] BRAS AR, VICIOSA MT, RODRIGUES C, DIAS CJ, DIONISIO M (2006) PHYS REV E, 73, 061709.

[151] JACOBSEN B, SAUNDERS K, RADZIHOVSKY L, TONER J (1999) PHYS. REV. LETT. 83 1363; RADZIHOVSKY L, TONER J (1999) PHYS. REV. B 60, 206.

[152] RZOSKA SJ, PALUCH M, PAWLUS S, DROZD-RZOSKA A, ZIOLO J, JADZYN J, CZUPRYNSKI K AND DABROWSKI R (2003) PHYS. REV. E 68, 031705; DROZD-RZOSKA A, RZOSKA S J, PALUCH M, PAWLUS S, ZIOLO J, SANTANGELO P G, ROLAND C M, CZUPRYNSKI K, DABROWSKI R (2005) PHYS. REV. E 71, 011508.

[153] KUTNJAK Z, GARLAND CW (1997) PHYS. REV. E 55, 488.

[154] IANNACCHIONE GS, GARLAND CW, MANG JT, RIEKER TP (1998) PHYS. REV. E 58, 5966.

[155] LEHENY RL, PARK S, BIRGENEAU RJ, GALLANI J-L, GARLAND CW, IANNACCHIONE GS (2003) PHYS. REV. E 67, 011708.

[156] JIN T, FINOTELLO D (2004) PHYS. REV. E 69, 041704.

[157] CRAWFORD GP, STEELE LM, ONDRIS-CRAWFORD R, IANNACCHIONE GS, YEAGER CJ, DOANE JW, FINOTELLO D (1992) J. CHEM. PHYS. 96, 7788.

[158] IANNACCHIONE GS, CRAWFORD GP, QIAN S, DOANE JW, FINOTELLO D, ZUMER S (1996) PHYS. REV. E 53, 2402.

[159] ROTUNNO M, BUSCAGLIA M, CHICCOLI C, MANTEGAZZA F, PASINI P, BELLINI T, ZANNONI C (2005) PHYS. REV. LETT. 94, 097802.

[160] LEYS J, SINHA G, GLORIEUX C, THOEN J (2005) PHYS. REV. E 71, 051709.

[161] LEYS J, SINHA G, GLORIEUX C, THOEN J (2008) J. PHYS.: CONDENS. MATTER 20, 244111.

[162] BENGOECHEAM R, ALIEV FM (2005) J. NON-CRYST. SOLIDS 351, 2685; ALIEV FM, BENGOECHEAM R, GAO CY, COCHRAN HD, DAI S (2005) J. NON-CRYST. SOLIDS 351, 2690; SINHA G, LEYS J, GLORIEUX C, THOEN J (2005) PHYS. REV. E72, 051710; LOBO CV, KRISHNA PRASAD S, YELAMAGGAD CV (2006) J. PHYS.: CONDENS. MATTER 18, 767.

[163] SINHA GP, ALIEV FM (1998) PHYS. REV. E 58, 2001.

[164] FRUNZA L, FRUNZA S, KOSSLICK H, SCHÖNHALS A (2008), PHYS. REV. E 78, 051701.

[165] CRAMER CH, CRAMER TH, KREMER F, STANNARIUS R (1997) J. CHEM. PHYS 106 (9).

[166] FRUNZA S, FRUNZA L, TINTARU M, ENACHE I, BEICA T, SCHÖNHALS A (2004) LIQ. CRYST. 31, 7, 913.

[167] FRUNZA L, FRUNZA S, KOSSLICK H, SCHÖNHALS A (2008) PHYS. REV. E 78, 051701.

[168] CRAWFORD GP, ALLENDER DW, DOANE JW (1992) PHYS. REV. A 45, 8693.

[169] IANNACCHIONE GS, CRAWFORD GP, ŽUMER S, DOANE JW, FINOTELLO D (1993) PHYS. REV. LETT. 71, 2595.

[170] KITYK AV, WOLFF M, KNORR K, MORINEAU D, LEFORT R, HUBER P (2008) PHYS. REV. LETT. 101, 187801.

[171] GUÉGAN R, MORINEAU D, LOVERDO C, BÉZIEL W, GUENDOUZ M (2006) PHYS. REV. E 73, 011707.

[172] JOSHI GV, KEVADIYA BD, PATEL HA, BAJAJ HC, JASRA RV (2009) INT. J PHARM. 374, 53.

[173] E RUIZ-HITZKY, K ARIGA, YM LVOV (EDS) (2008), "BIO-INORGANIC HYBRID NANOMATERIALS: STRATEGIES, SYNTHESES, CHARACTERIZATION AND APPLICATIONS" WILEY-VCH.

[174] SALONEN J, KAUKONEN AM, HIRVONEN J, LEHTO VP (2008) JOURNAL OF PHARMACEUTICAL SCIENCES 97, 632.

[175] BECK S, VARTULI JC, ROTH WJ, LOENOWICZ ME, KRESGE CT, SCHMITT KD, CHU CTW, OLSON DH, SHEPPARD EW, MCCULLEN SB, HIGGINS JB, SCHLENKER JL (1992) J. AM. CHEM. SOC. 114, 10834.

[176] FAN J, YU C, GAO F, LEI J, TIAN B, WANG L, LUO Q, TU B, ZHOU W, ZHAO D (2003) ANGEW. CHEM. 115, 3254; FAN J, YU C, GAO F, LEI J, TIAN B, WANG L, LUO Q, TU B, ZHOU W, ZHAO D (2003) ANGEW. CHEM. INT. ED. 42, 3146.

[177] VALLET-REGÍ M, BALAS F, ARCOS D (2007) ANGEW. CHEM. INT. ED. 46, 7548.

[178] VALLET-REGÍ M, RÁMILA A, DEL REAL RP, PÉREZ-PARIENTE J (2001) CHEM. MATER. 13, 308.

[179] MUÑOZ, RÁMILA A, PÉREZ-PARIENTE J, DÍAZ I, VALLET-REGÍ M (2003) CHEM. MATER. 15, 500.

[180] DOADRIO C, SOUSA EMB, IZQUIERDO-BARBA I, DOADRIO AL, PÉREZ-PARIENTE J, VALLET-REGÍ M (2006) J MATER CHEM 16, 462.

[181] ZENG W, QIAN XF, ZHANG YB, YIN J, ZHU ZK (2005) MATER. RES. BULL. 40, 766.

[182] QU F, ZHU G, HUANG S, LI S, SUN J, ZHANG D, QIU S (2006) MICROPOROUS MESOPOROUS MATER. 92, 1.

[183] NUNES CD, VAZ PD, FERNANDES AC, FERREIRA P, ROMÃO CC, CALHORDA MJ (2007) EUROPEAN JOURNAL OF PHARMACEUTICS AND BIOPHARMACEUTICS 66, 357.

[184] IZQUIERDO-BARBA I, MARTÍNEZ A, DOADRIO AL, PÉREZ-PARIENTE J, VALLET-REGÍ M (2005) EUR. J. PHARM. SCI. 26, 365.

[185] MELLAERTS R, JAMMAER JAG, VAN SPEYBROECK M, CHEN H, VAN HUMBEECK J, AUGUSTIJNS P, VAN DEN MOOTER G, MARTENS JA (2008) LANGMUIR 24, 8651.

[186] DOADRIO AL, SOUSA EMB, DOADRIO JC, PÉREZ-PARIENTE J, IZQUIERDO-BARBA I, VALLET-REGÍ M. (2004) J. CONTROLLED RELEASE, 97, 125.

[187] VALLET-REGÍ M, DOADRIO JC, DOADRIO L, IZQUIERDO- BARBA I. PÉREZ-PARIENTE J (2004) SOLID STATE IONICS 172, 435.

[188] TOZUKA Y, WONGMEKIAT A, KIMURA K, MORIBE K, YAMAMURA S, YAMAMOTO K (2005) CHEM. PHARM. BULL. 53, 974.

[189] ZHENG JP, LUAN L, WANG HY, XI LF, YAO KD (2007) APPL. CLAY SCI. 36, 297.

[190] LIN FH, LEE YH, JIAN CH, WONG JM, SHIEH MJ, WANG CW (2002) BIOMATERIALS 23, 1981.

[191] HANCOCK BC, ZOGRAFI G (1997) J. PHARM. SCI. 86, 1; ROBERTS CJ, DEBENEDETTI PG (2002) AICHE J 48, 1140.

[192] HANCOCK BC, PARKS M (2000) PHARM. RES 17, 397; ZHOU D, ZHANG GGZ, GRANT DJW, SCHMITT EA (2002) J. PHARM. SCI. 91, 1863.

[193] AZAIS T, TOURNE-PETEILH C, AUSSENAC F, BACCILE N, COELHO C, DEVOISSELLE JM, BABONNEAU F. (2006) CHEMISTRY OF MATERIALS 18, 6382.

[194] CHARNAY C, BEGU S, TOURNE-PETEILH C, NICOLE L, LERNER DA, DEVOISSELLE JM (2004) EUR. J. PHARM. BIOPHARM. 57, 533.

[195] AZAÏS T, HARTMEYER G, QUIGNARD S, LAURENT G, TOURNE-PETEILH C, DEVOISSELLE JM, BABONNEAU F (2009) PURE APPL. CHEM. 81, 8, 1345.

[196] MUWOZ, RÁMILA A, PÉREZ-PARIENTE J, DÍAZ I, VALLET-REGÍ M (2003) CHEM. MATER. 15, 500.

[197] SONG SW, HIDAJAT K, KAWI S (2005) LANGMUIR, 21, 9568.

[198] BALAS F, MANZANO M, HORCAJADA P, VALLET-REGÍ M (2006) J. AM. CHEM. SOC. 128, 8116.

[199] QU F, ZHU G, HUANG S, LI S, QIU S (2006) CHEMPHYSCHEM 7, 400.

[200] TANG Q, XU Y, WU D, SUN Y (2006) CHEM. LETT. 35, 474.

[201] JOHARI GP (2005) J. CHEM. PHYS. 122, 194504; STROBL G (2006) PROGR POLYM SCI, 31, 398.

[202] SIROTA EB (2007) MACROMOLECULES 40, 1043; RENGARAJAN GT, ENKE D, BEINER M (2007) OPEN PHYS. CHEM. J 1, 18.

[203] STROBL G (2004) "CONDENSED MATTER PHYSICS", SPRINGER-VERLAG, BERLIN.

[204] ZARZYCKI J (1991) "GLASSES AND THE VITREOUS STATE", CAMBRIDGE: CAMBRIDGE UNIVERSITY PRESS.

[205] IVANOV DA, POP T, YOON DY, JONAS AM (2002) MACROMOLECULES 35, 9813.

[206] FORREST JA, DALNOKI-VERESS K, ANCES AD (2001) COLLOID AND INTERFACE SCIENCE 94, 167, 196.

[207] SCHÖNHALS A, GOERING H, SCHICK CH, FRICK B, ZORN R (2005) J. OF NON-CRYST. SOLIDS 351, 2668.

[208] NGAI KL, ROLAND CM (1993) MACROMOLECULES 26, 2688.

[209] MIJOVÍC J, SY JW (2002) MACROMOLECULES 35, 6370.

[210] EZQUERRA TA, MAJSZCZYK J, BALTÀ-CALLEJA FJ, LÓPEZ-CABARCOS E, GARDNER KH, HSIAO BS (1994) PHYS. REV. B 50, 6023.

[211] WILLIAMS G (1979) ADV. POLYM. SCI. 33, 59.

[212] DIONÍSIO M, VICIOSA MT, WANG Y, MANO JF (2005) MACROMOL. RAPID COMMUN. 26, 1423.

[213] LAREDO E, GRAIMAU M, BARRIOLA P, BELLO A, MÜLLER AJ (2005) POLYMER 46, 6532.

[214] BOYD RH, LIU F (1997) "DIELECTRIC SPECTROSCOPY OF POLYMERIC MATERIALS", RUNT JP, FITZGERALD JJ (EDS.) AMERICAN CHEMICAL SOCIETY, WASHINGTON, CH. 4.

[215] KANCHANASOPA M, RUNT J (2004) MACROMOLECULES 37, 863.

[216] EZQUERRA TA, ZOLOTUKHIN M, PRIVALKO VP, BALTA-CCALLEJA FJ, NEQULQUEO, GARCIA C, DE LA CAMPA JG, DE ABAJO J (1999) J. CHEM. PHYS. 22,10, 134.

[217] WANG Y, GOMEZ RIBELLES JL, SALMERON SANCHEZ M, MANO JF (2005) MACROMOLECULES 38(11), 4712.

[218] ALVES NM, MANO JF, BALAGUER E, MESEGUER DUEÑAS JM, GÓMEZ RIBELLES JL (2002) POLYMER 43(15), 4111.

[219] FITZ BD, ANDJELIC´ S (2003) POLYMER 44, 3031.

[220] EZQUERRA TA, BALTÁ-CALLEJA FJ, ZACHMANN HG (1994) POLYMER 35, 2600.

[221] FUKAO K, MIYAMOTO YJ (1997) J. NON-CRYST. SOLIDS 212, 208; FUKAO K, MIYAMOTO YJ. (1998) J. NON-CRYST. SOLIDS 235-237, 534.

[222] SHAFEE EEL (2001) EUR. POLYM. J. 37, 1677.

[223] SOCCIO M, NOGALES A, LOTTI N, MUNARI A, EZQUERRA TA (2007) POLYMER 48, 4742.

[224] SANZ A, NOGALES A, EZQUERRA TA, LOTTI N, MUNARI A, FUNARI SS (2006) POLYMER 47, 1281.

[225] WUNDERLICH B (2005) MACROMOL. RAPID COMMUN. 26, 1521.

[226] CHENG SZD, WUNDERLICH B (1988) MACROMOLECULES 21, 789.

[227] WUNDERLICH B (2003) PROGRESS POLYM. SCI. 28, 383.

[228] THOMSON RC, WAKE MC, YASZEMSKI MJ, MIKOS AG. (1995) ADV. POLYM. SCI. 122, 245; IKADA Y, TSUJI H. (2000) MACROMOL. RAPID COMMUN. 21, 117; SÖDEGARD A, STOLT M (2002) PROG. POLYM. SCI. 27, 1123; KIM HD, BAE EH, KWON IC, PAL RR, NAM JD, LEE DS (2004) BIOMATERIALS 25, 2319.

[229] DI LORENZO ML (2001) POLYMER, 42, 9441; SÁNCHEZ FH; MATEO JM, COLOMER FJR, SÁNCHEZ MS, RIBELLES JLG, MANO JF (2005) BIOMACROMOLECULES 6, 3283; YAMASHITA K, KIKKAWA Y, KUROKAWA Y, DOI Y (2005) BIOMACROMOLECULES 6, 850; MIYATA T, MASUKO T, (1998) POLYMER, 39, 5515.

[230] LUNKENHEIMER P, SCHNEIDER U, BRAND R, LOIDL A (2000) CONTEMPORARY PHYSICS 41, 1.

[231] BLYTHE T, BLOOR D (2005) "ELECTRIC PROPERTIES OF POLYMERS" 2ND EDN, CAMBRIDGE UNIVERSITY PRESS.

[232] MIJOVIC J (2003) "BROADBAND DIELECTRIC RELAXATION" EDS. F KREMER AND A SCHÖNHALS, SPRINGER-VERLAG, BERLIN, CH. 9.

[233] APPLICATION NOTE 1217-1, (1992) "BASICS OF MEASURING THE DIELECTRIC PROPERTIES OF MATERIALS," HEWLETT PACKARD LITERATURE NUMBER 5091-3300E.

[234] KREMER F, SCHÖNHALS A (2003) "BROADBAND DIELECTRIC RELAXATION" EDS. F KREMER AND A SCHÖNHALS, SPRINGER-VERLAG, BERLIN, CH.1.

[235] MCGRUN NG, READ BE, WILLIAMS G (1991) "ANELASTIC AND DIELCTRIC EFFECTS IN POLYMERIC SOLIDS", WILEY, NEW YORK (REPRINTED BY DOVER, NEW YORK).

[236] LANDAU LD, LIFSCHITZ EM (1979) "TEXTBOOK OF THEORETICAL PHYSICS, VOL. V STATISTICAL PHYSICS", BERLIN, AKADEMIE-VERLAG.

[237] BÖTCHER CJF, BORDEWIJK P (1978) "THEORY OF ELECTRIC POLARISATION, VOL.II DIELECTRICS IN TIME DEPENDENT FIELDS" ELSEVIER AMSTERDAM, OXFORD, NEW YORK.

[238] KREMER F, SCHÖNHALS A (2003) "BROADBAND DIELECTRIC RELAXATION" (EDS.) F KREMER AND A SCHÖNHALS, SPRINGER-VERLAG, BERLIN, CH.3.

[239] COLE KS, COLE RH (1941) J. CHEM. PHYS. 9, 341.

[240] FUOSS RM, KIRKWOOD JG (1941) J. AM. CHEM. SOC. 63, 385.

[241] DAVIDSON DW, COLE RH (1950) J. CHEM. PHYS. 18, 1417.

[242] DAVIDSON DW, COLE RH (1950) J. CHEM. PHYS. 19, 1484.

[243] HAVRILIAK S, NEGAMI S (1966) J. POLYM. SCI. C 16, 99; HAVRILIAK S, NEGAMI S (1967) POLYMER C 8, 161.

[244] JONSCHER AK (1983) "DIELECTRIC RELAXATION SOLIDS", CHELSEA DIELECTRICS PRESS, LONDON.

[245] DIAZ-CALLEJA R (2000) MACROMOLECULES 33, 8924.

[246] BOERSEMA A, VAN TURNHOUT J, WÜBBENHÖRST M (1998) MACROMOLECULES 31, 7453.

[247] KOHLRAUSCH R (1847) ANN. PHYS. 12, 393.

[248] WILLIAMS G, WATTS DC (1970) J. CHEM. SOC. FARADAY TRANS. II 68, 1045.

[249] LINDSAY CP, PATTERSON GD (1980) J. CHEM. PHYS. 73, 3348.

[250] ALVAREZ F, ALEGRIA A, COLMENERO J (J1991) PHYS. REV. B, 44, 7306.

[251] NGAI KL (2003) J. PHYS.: CONDENSED MATTER. 15, S1107.

[252] NGAI KL, KAMIŃSKA E, SEKUŁA M, PALUCH M (2005) J. CHEM. PHYS. 123, 204507.

[253] JOHARI GP, GOLDSTEIN MJ (1970) CHEM. PHYS. 53, 2372; (1971) J. CHEM. PHYS. 55, 4245.

[254] KIRKWOOD JG (1939) J. CHEM. PHYS. 7, 911.

[255] ONSAGER L (1936) J. AM. CHEM. SOC. 58, 1486.

[256] DEBYE P (1929) "POLAR MOLECULES", NEW YORK, THE CHEMICAL CATALOUGE COMPANY, DOVER.

[257] FRÖHLICH H (1958) "THEORY OF DIELECTRICS" 2ND EDN, CALDERON PRESS.

[258] STICKEL F, FISCHER EW, RICHERT R (1996) J. CHEM. PHYS. 104, 2043; STICKEL F, KREMER F, FISCHER EW (1993) PHYSICA A, 201, 318.

[259] PATHMANATHAN K, JOHARI GP (1993) J. POLYM. SCI. PART B: POLYM PHYS. 31, 265.

[260] HODGE IM, ANGELL CA (1977), J. CHEM. PHYS. 67, 1647.

[261] MAXWELL JC (1891) "A TREATISE ON ELECTRICITY AND MAGNETISM- VOLUME 1" CLARENDON PRESS, OXFORD, THIRD EDITION, REPRINT BY DOVER, PAGES 450 FF; WAGNER KW (1914) ARCH. ELEKTROTECH. 2, 371; SILLARS RW (1937) J. INST. ELECTR. ENG. 80, 378.

[262] BÖTTCHER CJF (1973) "THEORY OF ELECTRIC POLARIZATION" ELSEVIER, AMSTERDAM.

[263] STEEMAN PA, MAURER FHJ (1992) POLYMER 33, 4236.

[264] KREMER F, SCHÖNHALS A (2003) "BROADBAND DIELECTRIC SPECTROSCOPY" (EDS.) F. KREMER, A. SCHÖNHALS, SPRINGER-VERLAG, BERLIN HEIDELBERG, PAGE 392 FF.

[265] NORDIO PL, RIGATTI G, SERGE U (1973) MOL PHYS. 25, 129.

[266] WILLIAMS G (1994) "THE MOLECULAR DYNAMICS OF LIQUID CRYSTALS" (EDS.) GR LUCKHURST AND CA VERACINI, KLUWER ACADEMIC PRESS, 431.

[267] CAPACCIOLI S, PREVOSTO D, BEST A, HANEWALD A, PAKULA T (2007) J. NON-CRYST. SOLIDS 353, 4267.

CHAPTER 2|EXPERIMENTAL

INDEX

2.1 Introduction

This chapter describes the equipment used to perform the analysis used in the different studies. Special relevance is given to dielectric relaxation spectroscopy (DRS), the main technique employed in this work, which is outlined briefly.

In DRS two impedance analyzers were used:

1) The ALPHA-N from Novocontrol, available both in the Chemical Department of Faculdade de Ciências e Tecnologia from Universidade Nova de Lisboa in Portugal and in BAM Federal Institute of Materials Research and Testing in Berlin, Germany;

2) The HP 4191A available in BAM Federal Institute of Materials Research and Testing in Berlin, Germany.

Also in this chapter, a characterization of both the studied materials and the confinement porous will be done, as well as a description of the impregnation method for the different studied systems.

2.2 Principles of dielectric spectroscopy

Dielectric relaxation spectroscopy comprises an exceptionally wide frequency range [1] not able to be covered by a single apparatus. Thus, a combination of several equipments/methods is used: frequency-response analysis (10^{-4} to 10^{11} Hz), impedance analysis (10^{2} to 10^{7} Hz), radio frequency-reflectometry (10^{6} to 10^{9} Hz) and network analysis (10^{7} to 10^{12} Hz).

In order to obtain the dielectric information of a material, it is used an electric circuit with several components which simulate the response of the material. This model circuit is known as *equivalent circuit*. The loss part of the dielectric response is represented by a resistance R_x, while the introduction of a capacitance C_x plays the role of the storage material, i.e. the ability to store the electric field. In such a way, the overall admittance $Y(\omega)$ and impedance $Z(\omega)$ in a RC circuit is given by the sum of the contributions of both elements:

$$Y(\omega) = \frac{1}{Z(\omega)} = \frac{1}{R_P(\omega)} + i\omega C_P(\omega) = \frac{1}{R_S(\omega) + \frac{1}{i\omega C_S(\omega)}} \qquad \textbf{Equation 2.1}$$

where sub index P and S correspond to parallel and series circuits respectively, i is $\sqrt{-1}$ and ω is the angular frequency (this equivalence does not apply to d.c. step-function experiments [2]). The measured values will depend on the geometry of the sample. As that is localized between a parallel capacitor the factors to be considered are the plate area A and separation d (with $A \gg d$). In order to avoid this influence, the dielectric properties of the material are expressed in terms of dielectric permittivity (eventually, with conductivity) using the relation $\varepsilon^*(\omega) = C^*(\omega)/C_0$. Here, $C_0 = A\varepsilon_0/d$ is the vacuum capacitance of the parallel plate capacitor and C^* is the complex capacitance of the same

capacitor filled with the material under study. If a sinusoidal electric field is applied, the complex permittivity relates to the impedance through:

$$\varepsilon^*(\omega) = \frac{1}{i\omega Z(\omega) C_0} \qquad \textbf{Equation 2.2}$$

When one is in presence of a material with a Debye response, i.e. with a relaxation process with a single relaxation time, the simplest equivalent circuit consists in one resistance R_1 associated in series with the capacitance C_1. For describing the instantaneous polarization due to atomic an electronic contributions, a capacitance, C_∞ associated in parallel with those components must be included [3,4] (see Figure 2. 1.a). For describing this situation, Equation 2.1 (for series elements) must be introduced in Equation 2.2:

$$\varepsilon^*(\omega) = \frac{C_\infty}{C_0} + \frac{1}{i\omega C_0 \left[R_S(\omega) + \frac{1}{i\omega C_S(\omega)}\right]} = \varepsilon_\infty + \frac{1}{i\omega C_0 R_S(\omega) + \frac{C_0}{C_S(\omega)}}$$

$$= \varepsilon_\infty + \frac{\frac{C_S(\omega)}{C_0}}{i\omega C_S(\omega) R_S(\omega) + 1} \qquad \textbf{Equation 2.3}$$

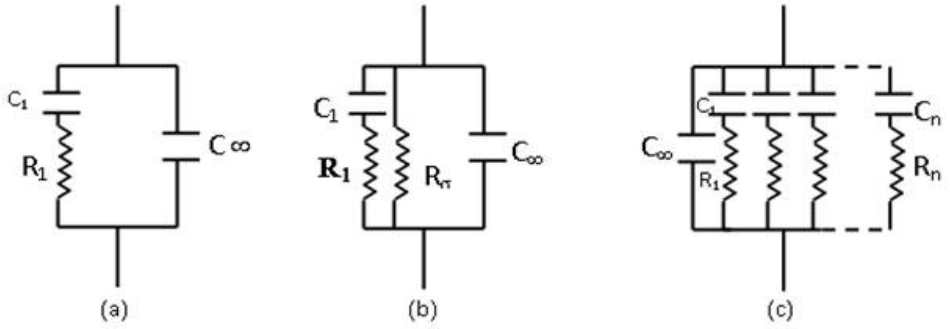

Figure 2. 1- Circuit diagrams for a material exhibiting: (a) a relaxation process with a single relaxation time and induced polarization, (b) a relaxation process with a single relaxation time, conduction and induced polarization and (c) a distribution of relaxation times and induced polarization (reproduced from reference [5]).

where ε_∞ denotes the quotient C_∞/C_0. In the last expression, the relaxation time of the equivalent RC circuit as $\tau_{RC} = R_S C_S$ and $\varepsilon_0 - \varepsilon_\infty$ as the fraction C_∞/C_0 can be identified, Rewriting Equation 2.3, we obtain:

$$\varepsilon^*(\omega) = \varepsilon_\infty + \frac{\varepsilon_0 - \varepsilon_\infty}{1 + i\omega\tau_{RC}} \qquad \textbf{Equation 2.4}$$

which is a typical representation of complex permittivity for a material that responds according the Debye function (see equation 1.29 in chapter I).

Additionally, if translational diffusion of mobile charges occurs, i.e. if the material exhibits conduction, the term $1/R_\sigma$ must be introduced in the overall impedance leading to a complex permittivity as:

$$\varepsilon^*(\omega) = \frac{C_\infty}{C_0} + \frac{1}{i\omega C_0\left[R_S(\omega) + \frac{1}{i\omega C_S(\omega)} + \frac{1}{R_\sigma}\right]} = \varepsilon_\infty + \frac{\varepsilon_0 - \varepsilon_\infty}{1 + i\omega\tau_{RC}} - \frac{i}{\omega C_0 R_\sigma} \qquad \textbf{Equation 2.5}$$

The conduction process appears as a low frequency tail in the plot of ε'', giving a value for $C_0 R_\sigma = \varepsilon_0/\sigma_0$, being σ_0 the frequency independent specific conductivity. The equivalent circuit is presented in Figure 2. 1 (b).

For a substance that presents a non-Debye behavior, i.e. when it is necessary to considerer a distribution of relaxation times, the equivalent circuit results of a combination of several $R_i C_i$'s associated in series, as shown in Figure 2. 1 (c) which also holds the conductivity contribution.

2.3 Impedance Analyzers

Two different equipments are used which are described below. Samples were prepared in parallel plate geometry between two gold-plated electrodes with diameter of: 10 and 20 mm in the frequency range from 10^{-2} Hz to 10^6 Hz. In the range from 10^6 Hz to 10^9 Hz a different geometry is used: the sample holder is an active sample cell for which the diameter of the electrodes is 6 mm.

2.3.1 *Alpha High Resolution impedance analyzer*

The Alpha-N analyzer measures the impedance or complex dielectric function of materials at frequencies between 3 μHz and 10 MHz with high precision. In addition, it can be used in gain phase mode by measurement of two a.c. voltages and their phase relation.

Two major parts are distinguished in this analyzer:

- A frequency response analyzer with a sine wave and two a.c. voltage input channels. Each input channel measures the a.c. voltage amplitude of an applied sine wave. The phase shift between the sine waves applied to the both inputs is also detected.
- A dielectric (or impedance) converter with a wide dynamic range current to voltage converter and a set of precision reference capacitors. This dielectric converter is mounted inside the Alpha analyzer mainframe.

For electric material measurements an additional dielectric sample cell is required. The BDS1200 sample cell from Novocontrol was employed for the measurements. It is suitable for low frequency

range from DC to 10 MHz. It includes PT100 temperature sensor localized inside the inferior electrode. It can work in the temperature range from 113 K to 723 K.

Principles of operation

The frequency response analyzer (FRA) in the ALPHA analyzer is used in combination with the dielectric converter. This component measures the response of a system to a harmonic (sinusoidal) excitation. The excitation and the response signals are voltages. The response signal is analyzed by Fourier transform, being of especial interest the amplitude and phase angle of the sinusoidal base wave with respect to the excitation signal.

The basic principle of measurement of the internal Alpha current to voltage converter used for impedance measurements is shown in Figure 2. 2.

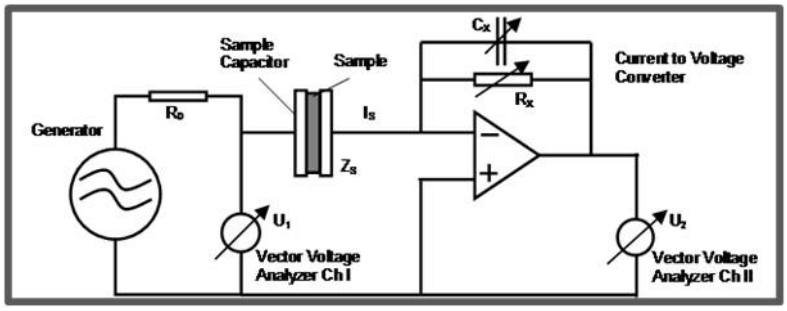

Figure 2. 2- Principle of the impedance measurement (reproduced from reference [6]).

The a.c. voltage from the generator is applied to the sample and measured in amplitude and phase as U_1. The resistor R_0 (50 Ω) limits the sample current if the sample impedance becomes too low. The sample current I_s feeds in the inverting input of an operational amplifier which has the variable capacity C_x (100-470 pF) and the resistor R_x (it switches between 30 Ω, 100 Ω and 1 T Ω) in its feed back loop. The Alpha analyzer selects a combination of R_x and C_x in such a way that the output voltage U_2 is in good measurable range of the voltage input channels (3 V – 30 mV). For ideal components, U_2 is related to the sample current I_S by:

$$I_S = -\frac{U_2}{Z_x} \qquad \textbf{Equation 2.6}$$

where $Z_x = (R_x - 1 + i\omega C_x)^{-1}$ and $\omega = 2\pi f$. For an ideal operational amplifier, the voltage at the input is 0 V with respect to ground and therefore U_1 corresponds to the voltage over the sample capacitor. By this way, the sample impedance Z_S is calculated from:

$$Z_S = \frac{U_1}{I_S} = -\frac{U_1}{U_2} Z_x \qquad \textbf{Equation 2.7}$$

The impedance Z_S relates to the complex dielectric permittivity through the Equation 2.2.

2.3.2 *HP 4191A impedance analyzer*

From 1MHz to 1GHz a coaxial reflectometer was employed based on the impedance analyser HP 4191A. In contrast to the low frequency technique already described, above 10MHz the measurement cables always contribute to the sample impendance. Above 30MHz standing waves arise at the line and a direct measurement of the sample impedance completely fails. This can be avoided by application of microwave techniques taking the measurement line as the main part of the measured impedance account [7,8,9]. Therefore, precision lines with defined propagation constants are required. The principle of measurement is shown in Figure 2. 3.

The sample capacitor is used as the termination of a precision coaxial line. The complex reflection $r(l)$ at the analyzer end of the line depending on the sample with two directional couplers and are phase sensitively measured. r is defined as the ratio of the voltages (or electrical fields) of the reflected wave, U_{Ref}, to the incoming wave, U_{In}, on the line. It depends on the location of the measurement on the line.

$$r(x) = \frac{U_{Ref}(x)}{U_{In}(x)} = -\frac{U_1}{U_2} Z_x \qquad \textbf{Equation 2.8}$$

For an ideal line, $r(l)$ which is measured by the reflectometer can be transformed to the reflection factor $r(l)$ at the sample end of the line by:

$$r(0) = r(l) \cdot e^{2/(\alpha + i \cdot \beta)} \qquad \textbf{Equation 2.9}$$

where α is the damping constant and $\beta = 2\pi l/\lambda$ (λ: wavelength) the propagation constant of the line. From Equation 2.9, the sample impendance is calculated by:

$$Z_S = Z_0 \cdot \frac{1 + r(0)}{1 - r(0)} \qquad \textbf{Equation 2.10}$$

where Z_0 is the wave resistance of the line. As can be seen from Equation 2.10, the measurement range is limited to the sample impedance Z_S being in the range of Z_0. If this is not the case, the reflection $r(0)$ becomes nearly 1 or -1 and the measured $r(l)$ changes only marginally.

In practice, the lines are not ideal and sophisticated calibration procedures have to be applied. Nevertheless, low loss precision lines matching to the output resistance of the reflectometer are required. The line parameters α, β must be homogeneous over the whole line and also independent of temperature, as the calibration generally can only be carried out at room temperature.

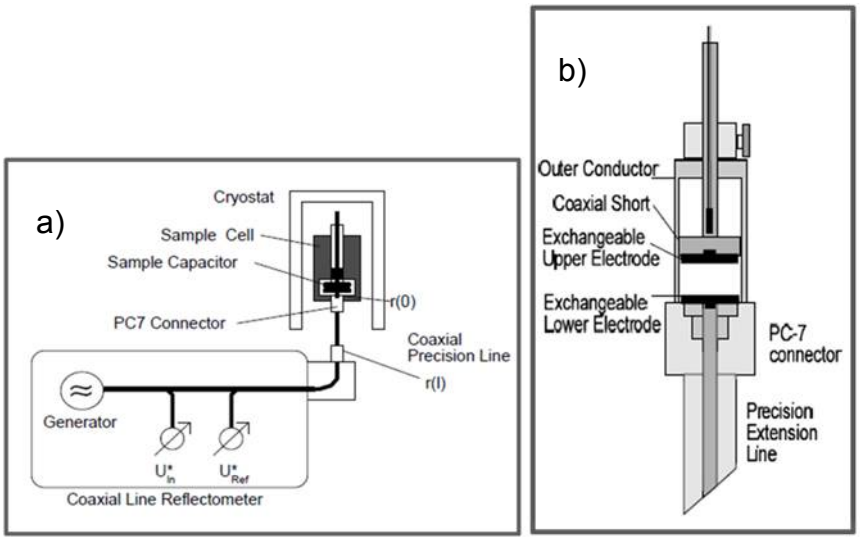

Figure 2. 3- a) Dielectric measurement using coaxial line reflectometry between 1MHz – 10GHz; b) RF sample cell (reproduced from reference [9]).

The same criteria mentioned for the line apply to the sample cell. Therefore an additional calibration which eliminates the influence of internal impedances in the sample cell is required. The sample cell used in the system based on the analyzer HP 4191A, including the coaxial wave guide is shown in Figure 2. 3 b).

In order to keep the wave guide as short as possible, the cryostat with the sample is directly mounted at the front of the analyzer. The system is automatically operated by a computer and all calibrations are done by software.

2.4 Temperature control

The temperature control was made by the QUATRO modulus also from Novocontrol. This temperature controller can be connected to the Alpha-N analyzer and to the HP4191A.

The Quatro controller has four circuits controlling the sample temperature, the gas temperature, the temperature of the liquid nitrogen in the dewar and the pressure in the dewar. The sample temperature is reached by heating the N_2 gas with a precision that can be of $\pm\, 0.01$ K. All the nitrogen passing circuit is isolated by a vacuum chamber whose pressure is measured.

Both the acquisition data and the temperature control are carried out by the software WinDETA also from Novocontrol.

2.5 Data Treatment

For the data treatment the software WinFIT from Novocontrol was always used considering the HN fitting functions for the analysis of the real and imaginary parts of $\varepsilon^*(\omega)$ [10].

2.6 Thermal Analysis

2.6.1 *Differential Scanning Calorimetry (DSC)*

2.6.1.1 E7

The thermal characterization of the bulk liquid crystal $E7$ was carried out in Laboratório de Análises[1] (Departamento de Química da Universidade Nova de Lisboa, Faculdade de Ciências e Tecnologia) by Differential Scanning Calorimetry (DSC). The calorimeter used was a SETARAM DSC 131 calorimeter fitted with a liquid nitrogen cooling accessory. Dry high-purity He gas with a flow rate of 30 $cm^3.min^{-1}$ was purged through the sample. The baseline was calibrated scanning the temperature domain of the experiments with an empty pan. The temperature calibration was performed taking the onset of the endothermic melting peak of Indium.

The sample was cooled down to 153 K and both the transition from glass to the supercooled nematic phase (T_g) and the transition from nematic to the isotropic phase (T_{NI}) were collected in the heating mode, from 173 to 353 K. The T_g for $E7$ was determined by DSC as the temperature of the midpoint, T_{mid} of the glass to the supercooled nematic transition, acquired with a heating rate of 5 $K.min^{-1}$.

2.6.1.2 Ibuprofen

The thermal characterization, using Differential Scanning Calorimetry (DSC), was carried out in Centro de Química-Física (Instituto Superior Técnico)[2] by Dr. Natália Correia. A 2920 MTDSC TA Instruments calorimeter interfaced with a liquid nitrogen cooling accessory (LNCA) was used for the DSC experiments. Dry high-purity He gas with a flow rate of 30 $cm^3.min^{-1}$ was purged through the sample. The baseline was calibrated scanning the temperature range of the experiments with an empty pan. The temperature calibration was performed taking the onset of the endothermic melting peak of several calibration standards (see *Experimental* of ref. [11]). A sample of 4.03 mg was introduced in an aluminum pan and hermetically sealed using an encapsulating press. The DSC runs cover a temperature range from 173 K to 353 K using a heating/cooling rate of 5 $K.min^{-1}$.

2.6.2 *Specific Heat Spectroscopy*

Specific heat spectroscopy was carried out in collaboration with the group of Prof. Dr. Christoph Schick by Dr. Heiko Huth in the Physics Department of the University of Rostock through a combination of Temperature Modulated DSC (TMDSC) and AC calorimetry.

---

[1] The author would like to thank the work done by Dr. Carla Rodrigues.

[2] The author would like to thank Professor Dr. J. J. Moura Ramos and Dr. Hermínio Diogo for the facilities in using the calorimetric equipment.

The temperature profile imposed to the sample is the superposition of some temperature oscillation in the shape of a sinusoidal to the conventional DSC isotherm or heating or cooling ramp. The analysis of the measured heat flow oscillation is performed on the basis of the first harmonic of the Fourier transform of the periodic heat flow curve.

These measurements result in a complex heat capacity $c^*(f) = c'(f) - i\,c''(f)$ (c'- real part, c''- loss part) [12]. $\tan\delta = c''(f) / c'(f)$ is the part of the phase angle which is due to time dependent processes in the sample. It must be corrected for heat transfer processes [13].

At low frequencies TMDSC measurements were carried out by a Perkin Elmer Pyris1 DSC. The frequency f of the temperature oscillation is varied from 10^{-3} Hz to 0.1 Hz. All data were taken from the heating runs where the corresponding rates were chosen between 1 K.min^{-1} and 3 K.h^{-1} to meet stationary conditions. Details can be found elsewhere [14].

The AC calorimetric measurements were done using the new chip sensor X-3974 from Xensor Integrations, NL. Frequency sweeps from 20 Hz to 2000 Hz are performed and the temperature is changed stepwise from 193 K to 293 K in steps of 2 K. The maximum in the phase angle is used to determine the dynamic glass transition temperature at the given frequency. A detailed description of the method and the data evaluation is given in [15].

2.6.3 *Thermo-Gravimetric Analysis (TGA)*

The thermo-gravimetric measurements were carried out in the BAM Federal Institute for Materials Research and Testing in Berlin, Germany[3]. The analyses were performed by a Seiko TG/DTA 220 apparatus, under a dry synthetic air atmosphere using a part of the sample prepared for the dielectric measurements.

In this work, the weight loss due to the burning and decomposition of the organic molecules is measured up to ca. 900 K ($E7$ samples) and 800 K (Ibuprofen samples) while the molecular sieves are thermally stable up to temperatures above 1000 K (its weight is constant by increasing the temperature up to 1073 K).

2.7 High Performance Liquid Chromatography

HPLC was carried out in collaboration with Prof. Dr. João Paulo Noronha and Dr. Alexandra Antunes from the Chemistry Department of Universidade Nova de Lisboa (Faculdade de Ciências e Tecnologia).

The analysis was carried out with a HPLC system (Waters) coupled with a pump and a controller (Waters 600), an in-line degasser (Waters), an autosampler (Waters 717 plus) and a photodiode array

[3] Herrn Neubert möchte ich für die Durchführung der TGA-Messungen danken.

detector (DAD, Waters 996). The HPLC analysis was performed in a reverse phase column (Purosphere RP-18e, 250x4 mm, 5 μm, Merck) with DAD detection from 200 to 600 nm with a flow rate of 1.0 ml.min^{-1}, using a 20 min linear gradient from 15 to 100 % acetonitrile in formic acid (0.1 %), both HPLC grade, followed by a 10 min isocratic elution with acetonitrile. The two analyzed samples (ibuprofen as received and the one obtained after thermal treatment) were dissolved in methanol (HPLC grade).

2.8 Electrospray Ionization Mass Spectrometry

Electrospray Ionization Mass Spectrometry (ESI-MS) was carried out in collaboration with Prof. Dr. João Paulo Noronha and Dr. Alexandra Antunes from the Chemistry Department of Universidade Nova de Lisboa (Faculdade de Ciências e Tecnologia).

The experiments were performed in a quadropole VG Platform (Micromass, UK Ltd) spectrometer equipped with an electrospray ionization source operating in the negative ionization mode. The samples of ibuprofen in methanol (HPLC grade) were infused by a syringe infusion pump (pump 22, Harvard Instruments, USA) with a flow rate of 10 μl.min^{-1}. Capillary temperature was kept constant between 373 K and 393 K. A capillary voltage of 3.5 kV was used. The data were acquired at a constant cone voltage ranging from -20 V to - 100 V (in steps of 10 V).

Nitrogen at room temperature was used as drying and nebulizing gas at 300 ml.min^{-1} and 10 ml.min^{-1}, respectively. The used spectra m/z range was 200-650. The measurement and data handling were accomplished with MassLynx® software version 4.0.

2.9 Infrared Spectroscopy

2.9.1 *E*7

Fourier Transform Infrared (FTIR) spectroscopy was carried out in the BAM Federal Institute for Materials Research and Testing in Berlin, Germany.

The interaction of the $E7$ molecules with the pore surface of molecular sieves is investigated by Fourier Transform Infrared (FTIR) spectroscopy. The infrared spectra of the samples were recorded by a Thermo-Nicolet (Nexus® 670) FTIR spectrometer at room temperature in transmission. The measurements were carried out in the wave number range from 400 to 4000 cm^{-1} accumulating 128 scans having a resolution of 4 cm^{-1}.

2.9.2 *Ibuprofen*

Infrared Spectroscopy (IR) was carried out in the Chemistry Department of Universidade Nova de Lisboa (Faculdade de Ciências e Tecnologia).
Infrared spectra of both *i*) KBr pellet containing an aliquot of ibuprofen recrystallized after being kept 1 hour at 353 K and *ii*) a drop of neat ibuprofen cooled from the melt inserted between NaCl windows, were recorded, at room temperature, using an ATI Mattson Genesis Series Fourier transform infrared spectrometer. Spectra were taken with a resolution of 4 cm^{-1}; 64 scans were averaged.

Attenuated Total Reflection Fourier Transform Infrared (ATR-FTIR) measurements were carried out in BAM Federal Institute for Materials Research and Testing in Berlin, Germany, of both Ibuprofen confined to MCM-41 and SBA-15 were performed, at room temperature. The infrared spectra of the samples were recorded by a Thermo-Nicolet (Nexus® 670) *FTIR* spectrometer at room temperature. The measurements were carried out in the wave number range from 400 to 4000 cm^{-1} with a resolution of 4 cm^{-1}; 64 scans were accumulated.

2.10 Materials

2.10.1 *E7*

$E7$ was purchased from Merck (Darmstadt, Germany) and used without further purification. It is a mixture of four components (4-cyano-4'-pentyl-1,1'-biphenyl ($5CB$) (51 wt-%), 4-n-heptyl-4'-cyanobiphenyl ($7CB$) (25 wt-%) , 4,4'-n-octyloxycyanobiphenyl ($8OCB$) (16 wt-%) and 4'-n-pentyl-4-cyanoterphenyl ($5CT$) (8 wt-%); this composition was determined by some of us by using HPLC [16]; the obtained proportion of constituents showed excellent agreement with data provided by the supplier [17]. The general structure of $E7$ is shown in Figure 2. 4 and their properties listed in Table 2. 1.
$E7$ was selected to be studied because it does not crystallize and shows, besides the isotropic to nematic phase transition at T_{NI} = 331 K, a glass transition phenomenon with a T_g value of 210 K [18], in good agreement with values reported in [17].
The thermogram obtained in the conditions described in section 2.6.1.1 is presented in Figure 2. 5 where these two transitions were clearly detected.

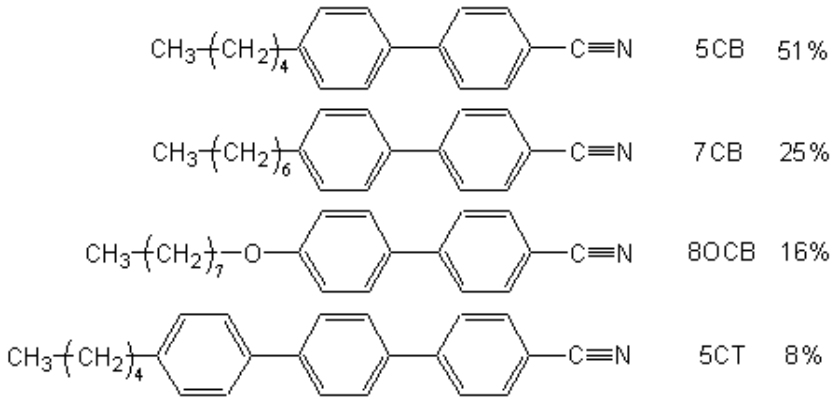

Figure 2. 4- Structures of the components of the nematic liquid crystal *E*7 used in this work.

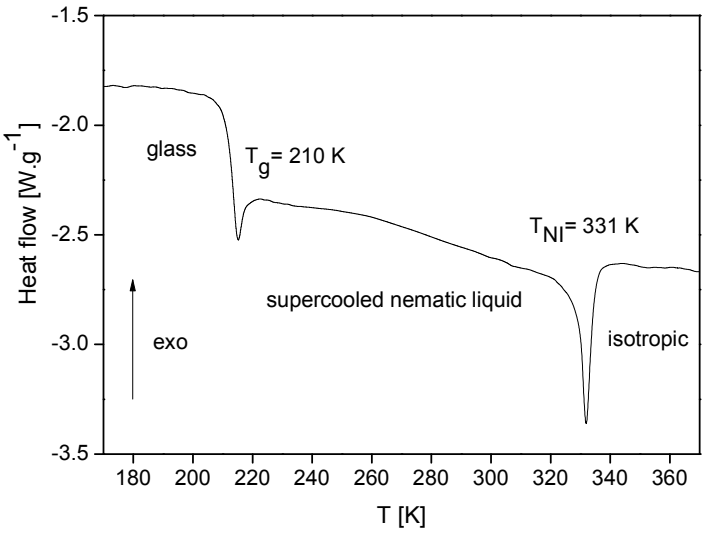

Figure 2. 5- DSC heating curves for *E*7 bulk liquid crystal, obtained at a rate of 5 K.min^{-1}. Data published in reference [18]

The heat capacity jump, ΔC_p, of the calorimetric glass transition is high and well defined being equal to 120±10 J.(K.mol)$^{-1}$. The respective molar enthalpy change at the transition from supercooled nematic to the isotropic phase is 1.2 ± 0.1 kJ.mol^{-1}. Therefore dielectric spectroscopy can be applied in a broad frequency range from 10^{-2} Hz to 10^{9} Hz covering a temperature range of approximately 200 K for the comparison of bulk and confined *E*7. This is not possible for related cyanobiphenyl systems like 7OCB [19] or 8CB [20] because these materials crystallize at lower temperatures.

	*E*7
Mol. Wt. (g.mol^{-1}) [16]	271.75
Density (g.cm^{-3}) [21]	1.0
Supplier	Merck KGaA

Table 2. 1- Properties of the liquid crystal *E*7 used in the studies.

2.10.2 *Ibuprofen*

Ibuprofen is a non-steroidal worldwide used pharmaceutical compound showing analgesic, antipyretic and anti-inflammatory properties [22].

Ibuprofen ((2RS)-2[4-(2-Methylpropyl)phenyl]propanoic acid) with 99.8% GC purity assay was purchased from Sigma (catalogue number I4883), being provided as a racemic mixture of (+)-ibuprofen and (-)-ibuprofen. It was used without further purification. For simplicity, hereinafter the studied (±)-ibuprofen will be referred to as ibuprofen. The general structure is presented in Figure 2. 6 and their properties are shown in Table 2. 2.

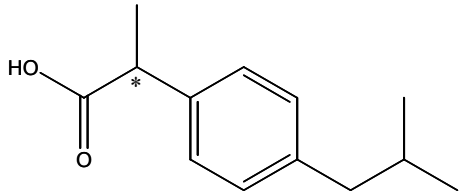

Figure 2. 6- Chemical structure of Ibuprofen molecule; C* is a chiral carbon atom.

It is a crystal at room temperature with a melting point of 350-351 K. The experimental details to achieve the conditions to obtain ibuprofen in the supercooled and glassy state are described in Chapter III.

	Ibuprofen
Mol. Wt. ($g.mol^{-1}$)	206.29
Density ($g.cm^{-3}$) [23,24]	1.077 (crystal)
Supplier	Sigma
CAS number	15687-27-1

Table 2. 2- Properties of Ibuprofen used in the studies. Most properties are given by the suppliers.

2.10.3 *PLLA*

Samples of poly(L-lactic acid) (PLLA) used to characterize PLLA amorphous state and to study PLLA isothermal crystallization at 353 K, as well as the respectively obtained semi-crystalline state, are from Purac Biochem with an inherent viscositiy of 5.87 dl/g.

Figure 2. 7 show an example of the constitutive units of PLLA polymer.

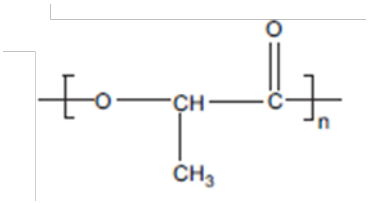

Figure 2. 7- PLLA constitutive units

PLLA films for isothermal crystallization at 353 K, were prepared by melting the materials in a hot plate (at ca. 473 K), compressed between two metallic disks and quenching them in cold water. The PLLA films obtained are amorphous as checked by DSC and X-ray. Number average molecular weight, M_n and weight average molecular weight, M_W, of the polymer, evaluated from gel permeation chromatography (Shimadzu, LC 10A, Japan) using polystyrene as standard and chloroform as solvent, are 269 000 and 301 000, respectively.

The study of amorphous and semi-crystalline PLLA achieved at different crystallization temperatures, T_c ranging from 368 K ≤ T_c ≤ 438 K [25 and references cited therein], employed PLLA of commercial grade (Resomer® L 210), from Boehringer Ingelheim, with molecular weights of $\langle Mn \rangle$ = 180 000 and $\langle Mw \rangle$ = 220 000 also evaluated from gel permeation chromatography (Shimadzu, LC 10A, Japan) using polystyrene as standard and chloroform as solvent.

Isothermally cold-crystallized specimens were prepared by annealing the plates for 12 h in an oven at temperatures, T_c, ranging between 368 and 438 K from the glassy state. After annealing, all the specimens were cooled down to room temperature at about 20 K.min^{-1}. The resulting crystallinity degrees, χ_c, were estimated by WAXS [26] varying between 0.43 (T_c = 368 K) and 0.65 (T_c = 438 K) (see Table 5.2 in Chapter V).

2.11 Confining Porous Hosts

2.11.1 *Anopore membranes*

Anopore inorganic membranes were supplied by Whatman [27] (catalogue number 6809-6002). They consist of a high-purity Al_2O_3 matrix with pores of 20 nm in diameter. The pores are almost cylindrical trough the membrane with a thickness of 60 μm. The properties of the membrane, such as their large porosity (40% volume), high surface-to-volume ratio, well defined pore size (see Figure 2. 8) and a relatively ordered distribution of pores in the matrix make them adequate as host material for confinement studies.

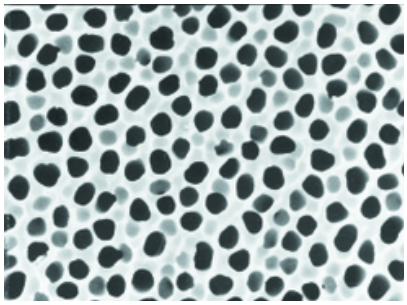

Figure 2. 8- Anodisc pore structure [reproduced from [27])

2.11.2 *Molecular Sieves*

Molecular sieves of MCM-41 and SBA- 15 type, (100% Si composition), provided by the research groups of A. Corma (Instituto de Tecnologia Química (UPV-CSIC), Universidad Politécnica de Valência, Spain) and I.M Fonseca (Faculdade de Ciências e Tecnologia, Universidade Nova de Lisboa) were hydrothermally synthesized and characterized according to the procedures described in the literature [28,29,30,31,32].

Sample	*BET Area* [m^2/g]	*Pore diameter d* [nm]	*Pore volume* V_p [cm^3/g]
MCM-41-28	1238	2.8	1.150
MCM-41-36	884	3.6	0.790
MCM-41-41	411	4.1	0.478
SBA-15-68	593	6.8	1.009

Table 2. 3- Texture properties of the MCM-41 and SBA-15 samples

MCM-41 was synthesized using aerosil as the silica source and alkyltrimethylammonium bromide with different lengths of the alkyl chains as templates allowing to tune the pore sizes.

For the syntheses of SBA-15 the blockpolymer poly(ethylene oxide)-poly(propylene oxide)-poly(ethylene oxide) (PEO-PPO-PEO) was used as a template in acidic conditions and tetraethyl orthosilicate (TEOS) was used as silica source in that case.

For calcination the templates were heated with a rate of 1 $K.min^{-1}$ to 813K for the MCM-41 samples and to 773K for the SBA-15 material, kept there under dry nitrogen for 1 h and after that under dry air for 6 h.

(A)

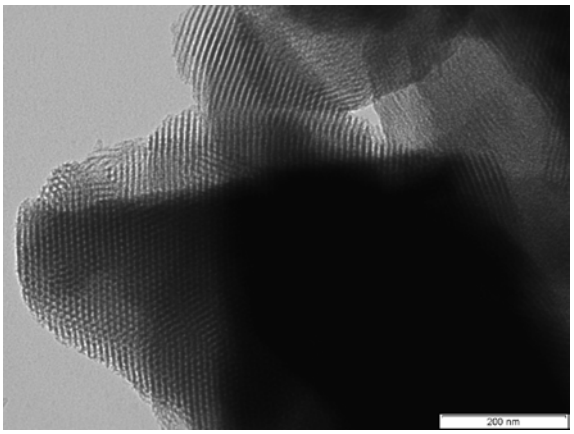

(B)

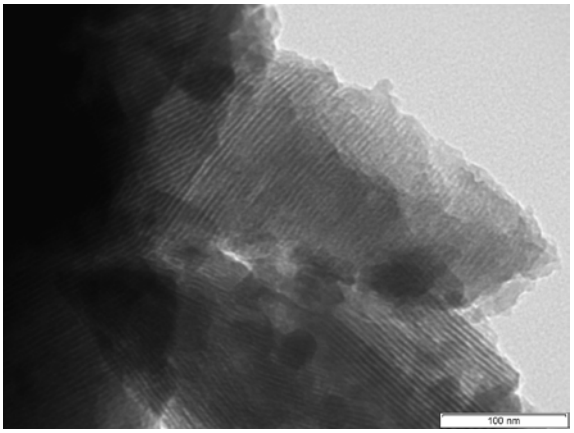

(C)

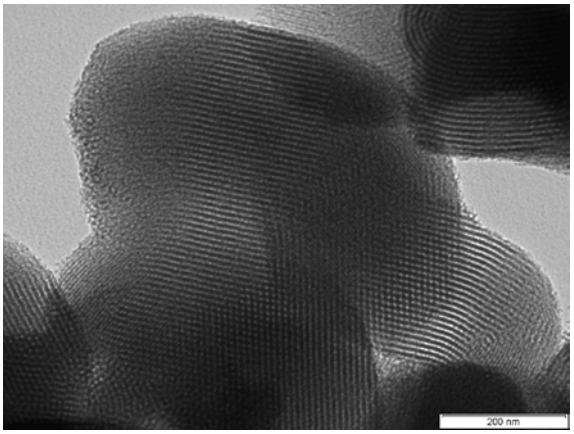

Figure 2. 9- TEM pictures for the MCM-41 material with pore diameter of 3.6 nm (A) and 4.1 nm (B) and the SBA-15 material with a pore diameter of 6.8 nm (C).

The texture features obtained by nitrogen absorption analysis are presented in Table 2. 3. The terminal number in the sample code gives the pore diameter in Å.

The obtained materials were routinely characterized by X-Ray Diffraction (XRD) and Tansmission Electron microscopy (TEM), except for the MCM-41-28 which has already been described in [29]. TEM analyses were performed on a Hitachi S-2400 scanning electron microscope, at a current voltage of 25 kV. The powder X-ray patterns were obtained on a Rigaku D/max III C diffractometer with a Cu Kα (λ = 1.5418 Å) radiation source (50 kV,30 mA). Measurements were performed for 2θ in the 2–40º range.

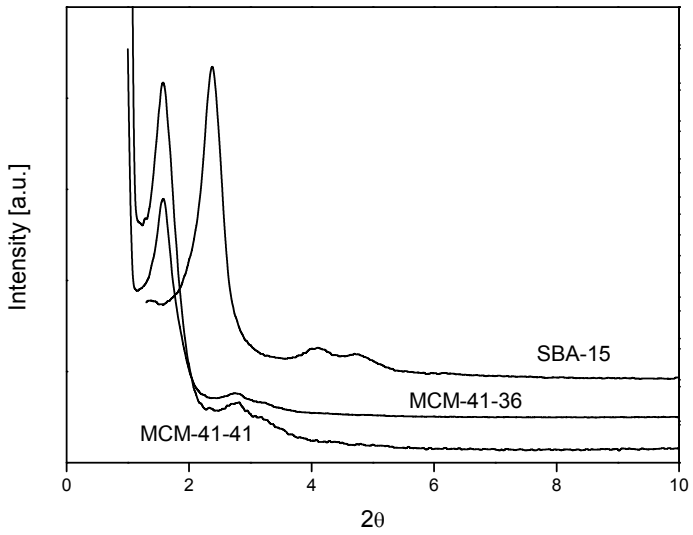

Figure 2. 10- Powder XRD patterns for different studied molecular sieves.

Figure 2. 10 shows XRD patterns of the molecular sieves, exhibiting one similar intense d100 diffraction and two similar weaker reflection peaks for 2θ values between 4º and 5º for the SBA-15 and between 2.5º and 3.5º for both MCM-41 types, indicative of d110 and d200 diffractions, implying that ordered dimensional-hexagonal mesostructure could be well preserved.
TEM images in Figure 2. 9 further confirmed the ordered mesostructure.

2.12 Impregnation Protocol

2.12.1 *E*7

2.12.1.1 Anopore Membranes

The Anopore membrane was cut into disks of about 20 mm in diameter. Each disk was outgassed in vacuum of 10^{-4} mbar at 473 K for 12 h to remove water and other impurities. Then the discs were slowly cooled down to T=343 K under vacuum. Please note that this temperature is above the nematic to isotropic phase transition of bulk *E*7. A solution (20 g.l^{-1}) of *E*7 in n-heptane (PA, Merck) was injected directly into the vacuum chamber. The pores were filled by capillary wetting at that temperature for 72 h. The guest excess and the solvent were removed by a moderate vacuum.
To study the alignment of the liquid crystal and its specific surface interaction under confinement, in a second experiment the pores were treated with a phospholipid from soybean (L-α-lecithin), CAS Number 8002-43-5, obtained by Fluka (Sigma-Aldrich), before filling with *E*7. The chemical structure of lecithin is given in Figure 2. 11. The native Anopore surface is hydrophilic providing a strong adsorption for the polar head group of lecithin.

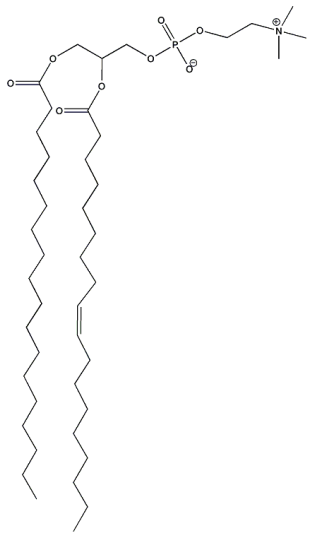

Figure 2. 11- Chemical structure of L-α-lecithin

After the high temperature treatment described above the disks were cooled down to 298 K under vacuum. A solution of 0.6% w/w of lecithin in hexane (PA, Merck) was injected and allowed to adsorb with the surface of the pores for 4h. According to the literature the pore surface should be covered by a monolayer of lecithin molecules by this procedure. Its thickness is estimated to be approximately 2 nm [33]. Then the rest of the solution was manually removed and a low vacuum was employed to evaporate the hexane from the pores for 12 h.

2.12.1.2 Molecular Sieves

Finely grounded powder of these molecular sieves was pressed under a low pressure to self-supported pellets with a thickness of 50 to 100 μm. To remove water and other impurities adsorbed at the pore walls the pellets were evacuated under vacuum (10^{-4} mbar) at 573 K for 7 h. After that the pellets were cooled down to 343 K under vacuum and pores of the molecular sieves were loaded with $E7$ using small excess in isotropic state [34,35]. $E7$ was first outgassed by applying a low vacuum (10^{-2} mbar) at 373 K for 5 min. Then $E7$ was injected directly in the vacuum chamber by a syringe. The pellets were covered by $E7$ in a small excess and kept at 343K for 12 h. After that the excess of $E7$ molecules located on extra pores of the grains and on the outer surface of the molecular sieves were removed as much as possibly by applying a low vacuum (10^{-2} mbar) at 373 K for at least 6 h. The removal of the excess $E7$ was checked optically when the optical state of the sample changes from translucent to opaque. The samples were prepared just before the measurements and handled in a desiccator.

2.12.2 *Ibuprofen*

2.12.2.1 Molecular Sieves

The Ibuprofen confinement procedure was performed in finely grounded powder of the molecular sieves pressed under a low pressure to self-supported pellets with a thickness of 50 to 100 μm. To

remove water and other impurities adsorbed at the pore walls the pellets were evacuated under vacuum (10^{-4} mbar) at 573 K for 7 h. After that the pellets were cooled down to 298 K under vacuum and the pores of the molecular sieves (MCM-41 and SBA-15) were loaded with a solution of Ibuprofen in ethanol (~ 0.05 g·cm^{-3}) according to the procedure adapted from references [36,37].This process consisted of five successive impregnations (during one day) of 0.06 g of molecular sieve with a 400 µl of the solution, which allowed the powder to just be wetted. Note that the first impregnation was still done with the molecular sieves under vacuum atmosphere. Between each impregnation the solvent was removed by heating at 333 K. Finally, after one night at room temperature, the samples were carefully washed with a small amount of ethanol to remove the excess of non-confined Ibuprofen that crystallized in the outer surface of the pellet. To test the influence of the solvent in the impregnation process, a reference sample (MCM-41) was prepared at the same conditions as described below, but instead the pellets were soaked in a solution of Ibuprofen in hexane (0.05 g.cm^{-3}) [36,38].
The samples were prepared just before the measurements and handled in a desiccator.

2.13 References

[1] SCHNEIDER U, LUNKENHEIMER P, BRAND R, LOIDL A (1999) PHYS. REV. E 59(6), 6924.

[2] WILLIAMS G, THOMAS DK (1998) "PHENOMENOLOGICAL AND MOLECULAR THEORIES OF DIELECTRIC AND ELECTRICAL RELAXATION OF MATERIALS", APPLICATION NOTE DIELECTRICS 3, NOVOCONTROL GMBH.

[3] MIJOVIC J, FITZ BD (1998) "DIELECTRIC SPECTROSCOPY OF REACTIVE POLYMERS", APPLICATION NOTE DIELECTRICS 2, NOVOCONTROL GMBH.

[4] KREMER F, BOESE D, MAIER G, FISCHER EW (1989) PROG. COLLOID. POLYM. SCI. 80. 129.

[5] DIONISIO M, MANO J (2008) "HANDBOOK OF THERMAL ANALYSIS AND CALORIMETRY VOL. 5 RECENT ADVANCES, TECHNIQUES AND APPLICATIONS" EDS M BROWN AND P GALLAGHER, ELSEVIER, CH. 7.

[6] (2003) "ALPHA HIGH RESOLUTION DIELECTRIC/IMPEDANCE ANALYZER" NOVOCONTROL.

[7] SLATER JC (1950) "MICROWAVE ELECTRONICS", D. VAN NOSTRAND COMPANY, NEW YORK.

[8] SOMLO PI, HUNTER JD (1985) "MICROWAVE IMPEDANCE MEASUREMENTS", LONDON. PETER PEREGRINUS.

[9] SCHAUMBURG G (1994) "DIELECTRIC NEWSLETTER 1", NOVOCONTROL GMBH.

[10] SCHAUMBURG G (1996) "DIELECTRIC NEWSLETTER 5", NOVOCONTROL GMBH.

[11] MOURA RAMOS JJ, CORREIA NT, DIOGO HP (2004) PHYS. CHEM. CHEM. PHYS. 6, 793.

[12] GOBRECHT H, HAMANN K, WILLERS G (1971) J. PHYS. 4, 21; BIRGE NO, NAGEL SR (1985) PHYS. REV. LETT. 54, 2674; SCHAWE JEK (1995), THERMOCHIM. ACTA 260, 1.

[13] WEYER S, HENSEL A, SCHICK CH (1997) THERMOCHIM. ACTA 304, 267.

[14] SCHICK CH (2002) "HANDBOOK OF THERMAL ANALYSIS AND CALORIMETRY" ED S CHENG, ELSEVIER, P 713. VOL. 3.

[15] HUTH H, MINAKOV A, SCHICK CH (2006) POLYM. SCI. B POLYM. PHYS. 44, 2996.

[16] BRÁS ARE, HENRIQUES S, CASIMIRO T, AGUIAR RICARDO A, SOTOMAYOR J, CALDEIRA J, SANTOS C, DIONÍSIO M (2007) LIQ. CRYST. 34, 591.

[17] MASCHKE U, BENMOUNA M, COQUERET X (2002) MACROMOL. RAPID COMMUN. 23, 159.

[18] BRAS AR, VICIOSA MT, RODRIGUES C, DIAS CJ, DIONISIO M (2006) PHYS REV E 73, 061709.

[19] DIEZ S, LÓPEZ DO, DE LA FUENTE MR, PÉREZ-JUBINDO MA, SALUD J, TAMARIT JL (2005) J. PHYS. CHEM. B 109, 23209.

[20] BENGOECHEA MR, ALIEV FM (2005) J. NON-CRYST. SOLIDS 351, 2685.

[21] EXPERIMENTAL DATA TAKEN DIRECTLY FROM EXPERIMENTAL MEASUREMENTS DONE BY THE AUTHOR.

[22] GOODMAN LS, GILMAN A (1990) "THE PHARMACOLOGICAL BASES OF THERAPEUTICS", 8TH ED PERGAMON PRESS: NEW YORK.

[23] SHANKLAND N, WILSON CC, FLORENCE AJ, COX PJ (1997) ACTA CRYST. C53, 951.

[24] TANIS I, KARATASOS K (2009) J. PHYS. CHEM. B 113, 10984.

[25] ZHANG J, TASHIRO K, TSUJI H, DOMB AJ (2008) MACROMOLECULES 41,1352.

[26] WANG Y, FUNARI SS, MANO JF (2006) MACROMOL. CHEM. PHYS. 207, 1262.

[27] ANOPORE INORGANIC MEMBRANES ARE COMMONLY USED FOR LABORATORY FILTRATION APPLICATIONS. MORE INFORMATION CAN BE OBTAINED IN WWW.WHATMAN.COM.

[28] SERCHELI R, VARGAS RM, SCHELDON RA, SCHUCHARDT V (1999) J MOLECULAR CATALYSIS A: CHEMICAL 148, 173.

[29] OLIVEIRA P, MACHADO A, RAMOS AM, FONSECA IM, BRAZ FERNANDES FM, BOTELHO DO REGO AM, VITAL J (2007) CATALYSIS COMMUNICATIONS 8, 1366.

[30] KRESGE CT, LEONOWICZ ME, ROTH WJ, VARTULLI JC, BECK JS (1992) NATURE 359, 710.

[31] CORMA A (1997) CHEM. REV. 97, 2373.

[32] CORMA A, GRANDE MS, GONZALEZ-ALFARO V, ORCHILLES AV (1996) JOURNALS OF CATALYSTS 159, 375.

[33] JAGADEESH B, PRABHAKAR A, DEMCO DE, BUDA A, BLÜMICH B (2005) CHEM. PHYS. LETT. 404, 177.

[34] A) ZUBOWA H-L, KOSSLICK H, CARIUS E, FRUNZA S, FRUNZA L, LANDMESSER H, RICHTER M, SCHREIER E, FRICKE R (1974) MICROPOR. MESOPOR. MATER. 16, 171; (B) FRUNZA L, KOSSLICK H, FRUNZA S, SCHÖNHALS A (2006) MICROPOR. MESOPOR. MATER. 90, 259.

[35] FRUNZA S, SCHÖNHALS A, FRUNZA L, ZUBOWA H-L, KOSSLICK H, FRICKE R, CARIUS H (1999) CHEM. PHYS. LETT. 307, 167; FRUNZA L, FRUNZA S, SCHÖNHALS A (2004) J. PHYS. IV 10, 121, 11170.

[36] CHARNAY C, BEGU S, TOURNE-PETEILH C, NICOLE L, LERNER DA, DEVOISSELLE J-M (2004) EUR. J. PHARM. BIOPHARM. 57, 533.

[37] AZAIS T, TOURNE-PETEILH C, AUSSENAC F, BACCILE N, COELHO C, DEVOISSELLE J-M, BABONNEAU F (2006) CHEM. MATER. 18, 6382.

[38] VALLET-REGI M, RAMILA A, DEL REAL RP, PEREZ-PARIENTE J (2001) CHEM. MATER. 13, 308.

CHAPTER 3| MOLECULAR MOBILITY OF BULK MATERIALS

INDEX

This subchapter was published in *Physical Review E* **75** (2007) 061708

3.1 Liquid Crystal *E*7

3.1.1 Introduction

In this subchapter a combination of broadband dielectric (10^{-2} Hz – 10^{9} Hz) and specific heat (10^{-3} Hz – 2×10^{3} Hz) spectroscopy was employed to study the molecular dynamics of the glass-forming nematic liquid crystal (LC) *E*7 in the temperature range from 193 to 391 K.

The liquid crystal *E*7 vitrifies upon cooling having a dynamic glass transition relaxation process. Therefore a thermal characterization was also performed by differential scanning calorimetry, allowing the confirmation of *E*7 glass transition and nematic to isotropic transition temperature.

In the region of the nematic phase the dielectric spectra shows the two relaxation processes which are theoretically expected, the δ-relaxation which corresponds to rotational fluctuations around its short axis and the tumbling mode at higher frequencies than the former one. For both processes the temperature dependence of the relaxation times follows the Vogel-Fulcher-Tammann formula which is characteristic for glassy dynamics. In this work the relaxation process responsible for the *E*7 glass transition will be clarified.

The liquid crystal *E*7 was already characterized by the pioneer work of Viciosa et al. [1], however in a narrower frequency range, so the present work updates its dielectric behavior.

3.1.2 Experimental Conditions

The nematic liquid crystal *E*7 previously described in Chapter II was used.

Dielectric spectra were recorded in the frequency range from 10^{-2} Hz to 10^{9} Hz (experimental details see Chapter II).

Two different samples were measured, one with preferential orientation of the nematic director parallel to the electrical field and a second one with a preferential orientation of the nematic director perpendicular to it.

3.1.3 Results and Discussion

3.1.3.1 Specific Heat Spectroscopy

Heat capacity measurements are the most commonly method used to detect the transition from the liquid to a glass. Therefore to study which dielectric active mode corresponds to glassy dynamics, specific heat spectroscopy was carried out. In difference to dielectric spectroscopy this method is

sensitive to enthalpy (entropy) fluctuations and only one relaxation process related to glassy dynamics is expected. Figure 3. 1 gives an example for AC calorimetry data measured at 640 Hz.

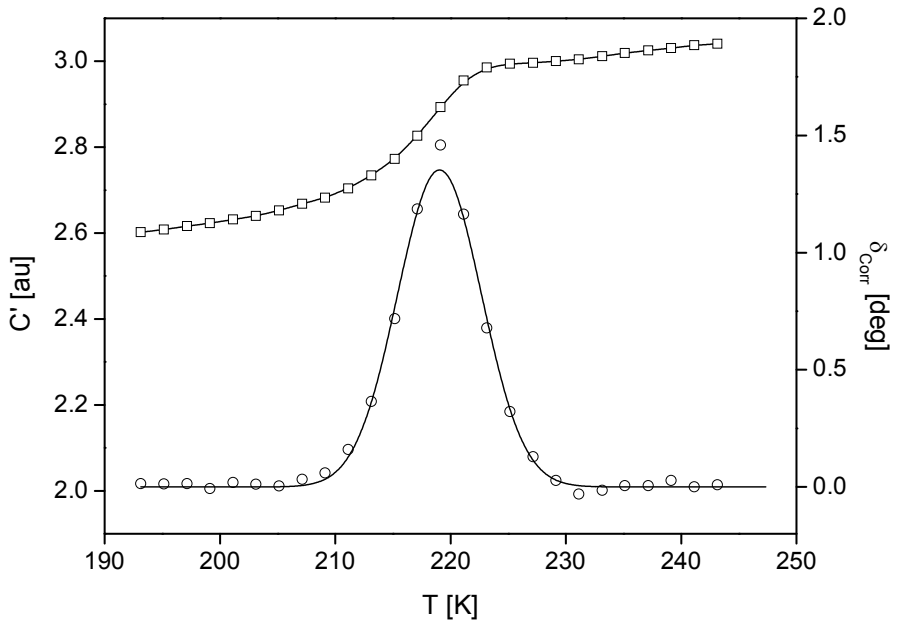

Figure 3. 1- Real part of the complex heat capacity c'(□) and phase angle δ_{Corr} (O) *versus* temperature of an AC calorimetry measurement at 640 Hz. The phase angle is corrected for heat transfer processes. The solid line is a guide for the eyes. The dashed line is a fit of a Gaussian to the data of the phase angle to estimate its maximum position.

The maximum in the phase angle is used to determine the dynamic glass transition temperature at the given frequency. From these measurements the relaxation time related to enthalpy (entropy) fluctuations can be extracted and compared directly to those measured by dielectric spectroscopy.

3.1.4 Dielectric Characterization

The liquid crystal $E7$ phase transformations were also monitored by Dielectric Relaxation Spectroscopy (DRS). Figure 3.3 presents a) the real part of the complex permittivity, ε', at different frequencies ranging from 10^3 to 10^6 Hz, and b) the real, ε', and imaginary, ε'', parts of the complex permittivity at $f = 10^4$ Hz. The assignment of two different transitions is quite clear in Figure 3. 2a), however quite different in nature. A frequency independent steep decrease with a midpoint at 333 K is an indication of a first order thermodynamic transition showing the nematic to isotropic transition (T_{NI}) of $E7$ in good agreement with calorimetric measurements [2,3,4] (331 K); see thermogram in Chapter II. The other transition at lower temperatures is one purely kinetic in nature which in Figure 3. 2b) is accompanied by a corresponding dielectric absorption peak, ε'' curve, and typical for glassy dynamics. Nevertheless looking in more detail to the imaginary curve, two peaks are observed

(indicated by the arrows) which is theoretically expected in the case of liquid crystals (see chapter I). The one responsible for the glass transition will be clarified further on in this subchapter.

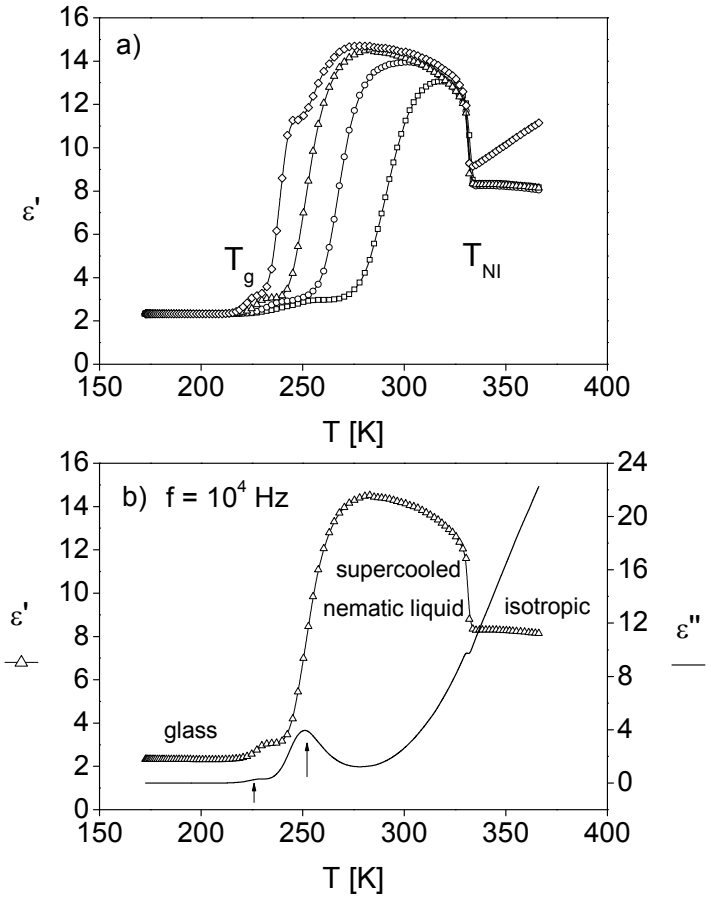

Figure 3. 2- Temperature dependence of a) the real (*ε'*) part of the dielectric function at fixed frequencies ◇- $f = 1 \times 10^3$ Hz, △- $f = 1 \times 10^4$Hz, ○- $f = 1 \times 10^5$Hz, □- $f = 1 \times 10^6$Hz showing the differences between glass transition (T_g) and nematic to isotropic transition (T_{NI}). The step decrease of *ε'* stands clear for the T_{NI}; b) the real (*ε'*) and imaginary (*ε''*) part of the dielectric function at $f = 1 \times 10^4$Hz. The relaxation processes observed on the supercooled nematic liquid phase are identified by the *ε''* peaks and the corresponding *ε'* steps.

It must be emphasized that DRS trace allowed direct comparison with conventional DSC thermogram and proved to be a sensitive tool to monitor phase transitions through either *ε'* and *ε''* curves being easy to interpret even for non-experts in dielectric relaxation. In particular, for the case of *E*7, T_{NI} is almost undetectable in *ε''* though by a very slight step, given that it is masked by conductivity effects, which does not affect the temperature dependence of *ε'*. Therefore, a well defined change is observed in *ε'* curve.

a)

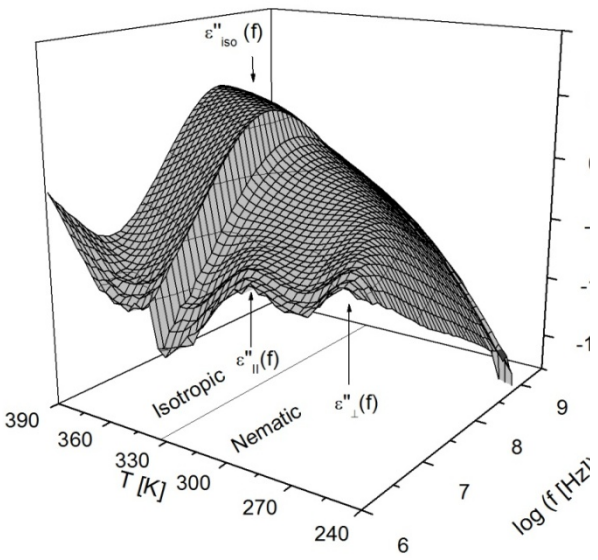

b)

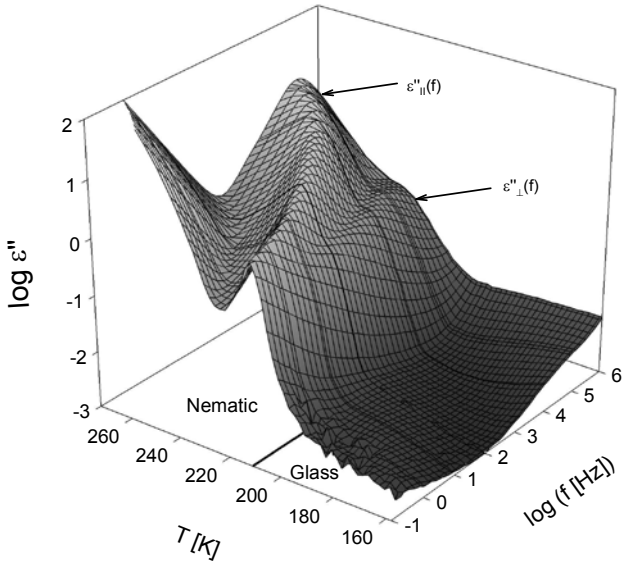

Figure 3. 3- Dielectric loss *versus* frequency and temperature for an unaligned sample of *E*7 in a) high frequency range; b) low frequency range.

To further investigate the dielectric behaviour of the liquid crystal *E*7, data acquisition in both a) high and b) low frequency analyzer was done by cooling the liquid crystal down from room temperature to a) 261 K, and successive frequency sweeps were carried out, isothermally, in increasing temperature steps of 2 K to 391 K; b) 193 K frequency sweeps were performed every 5 K and from 193 K to 303 K in steps of 2 K.

The dielectric loss of an unaligned sample of *E*7 *versus* frequency and temperature in a 3D representation in the both a) high frequency range and b) low frequency range are given in Figure 3. 3. In the nematic state two relaxation processes indicated by peaks in ε'' can be observed which are assigned to the tensorial components of the complex dielectric function parallel and perpendicular to the director. The process at lower frequencies corresponds to the δ-relaxation whereas the peak at higher ones is the tumbling mode. Above the clearing temperature the two processes collapse into one broadened relaxation.

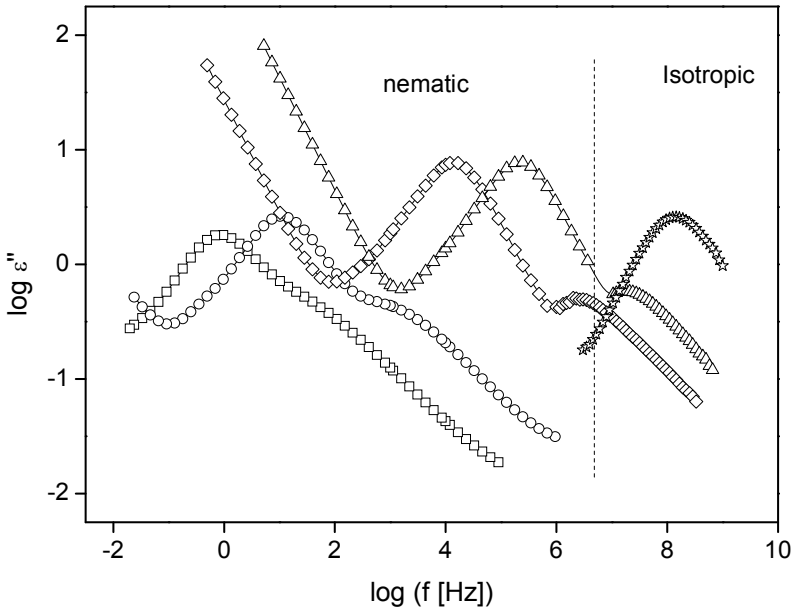

Figure 3. 4- Dielectric loss *versus* frequency for *E*7 at different temperatures and mesophases. Nematic State: □ - *T* = 216.2 K, O - *T* = 222.2 K, ◇ - *T* = 252.2 K, Δ - *T* = 274.2 K. Isotropic state: ☆ - *T* = 363.7 K. Lines are guides to the eyes. Because the dielectric properties in the low and in the high frequency range are measured using different samples their order parameter can be also slightly different.

Figure 3. 4 gives the dielectric loss of *E*7 in the available frequency range at the labelled temperatures. A careful analysis of the measurements shows that there is in addition to the processes discussed above, a third relaxation mode at frequencies lower than that of the δ process. Besides the work from our group [1,2], this process has also been reported by Capaccioli et al [5], giving further evidence of its existence. This process has never been found in any other liquid crystal reported so far and its molecular assignment is still under discussion in the literature.

With increasing temperature the loss peaks shifts to higher frequencies as expected and the dielectric strength of the δ-relaxation increases. According to the relative intensities of the δ- and tumbling mode one has to conclude that this sample has a preferential parallel alignment for frequencies lower than 10^6 Hz (for frequencies higher than 10^6 Hz a different sample cell was used as described in Chapter II).

The dielectric measurements are analysed by fitting the model function of Havriliak-Negami (HN-function) [6] to the data (Equation 1.35). The results of the theory of dielectric relaxation of nematic liquid crystals are summarized in chapter I (Equations 1.48 a) and b) which comprises a sum of different relaxation modes. This proves that the different modes are statistically independent. Therefore if more than one relaxation process is observed in the experimental frequency window a sum of HN functions is fitted to the data.

Figure 3. 5 gives an example of the fit of three HN-functions to the dielectric spectrum at 233 K. From the fit, the relaxation times, τ_{max}, and the dielectric strength were obtained for each relaxation process; these are taken for further discussion.

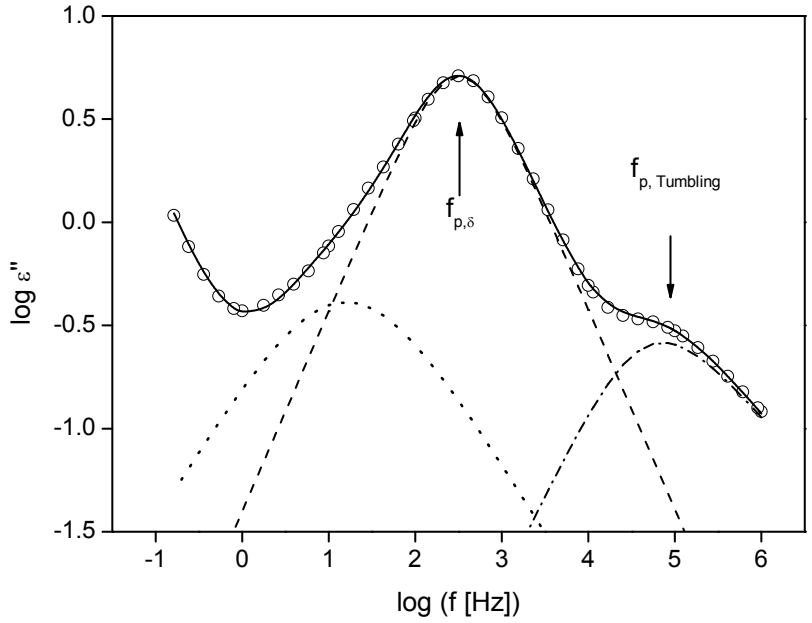

Figure 3. 5- Example of the decomposition of the relaxation spectra at T=233.2 K into the δ- relaxation and the tumbling mode by fitting three HN-functions and one conductivity contribution to the data: solid line – whole fit function; dashed line – contribution δ-relaxation; dashed–dotted line - contribution tumbling-relaxation; dotted line – contribution third relaxation process.

High frequency			
a)	*Isotropic*	δ	*tumbling*
α_{HN}	0.95 ± 0.06	0.96 ± 0.06	0.82 ± 0.10
β_{HN}	0.84 ± 0.08	0.81 ± 0.11	0.80 ± 0.14
$\alpha_{HN}\beta_{HN}$	0.80 ± 0.10	0.78 ± 0.08	0.65 ± 0.09

Low Frequency **b)**		δ	*tumbling*	*slow*
α_{HN}	*Parallel oriented*	0.95 ± 0.07	0.85 ± 0.24	0.73 ± 0.17
β_{HN}		1.0	0.60 ± 0.01	1.0
$\alpha_{HN}\beta_{HN}$		0.95 ± 0.07	0.50	0.73 ± 0.17
α_{HN}	*Perpendicular oriented*	0.89 ± 0.02	0.86 ± 0.21	0.66 ± 0.13
β_{HN}		1.0	0.59 ± 0.05	1.0
$\alpha_{HN}\beta_{HN}$		0.89 ± 0.02	0.50	0.66 ± 0.13

Table 3. 1- Average values of shape parameters taken from HN fitting for all *E*7 relaxation processes for the a) high frequency range: δ-relaxation, tumbling mode and process in the isotropic phase; b) low frequency range in both parallel and perpendicular of the nematic director orientation to the electric field: δ-relaxation, tumbling mode and slow process.

Shape parameters (average values) obtained from the HN fitting procedure are presented in Table 3. 1 for all the observed processes a) in the high frequency range and b) in the low frequency range for both preferential orientations of the nematic director to the electrical field.

Figure 3. 6 shows the relaxation times, τ_{max}, for each relaxation process plotted *versus* reciprocal temperature. The absolute value and the temperature dependence of the relaxation times do not depend on the macroscopic orientation of the sample. This is further confirmed by the data presented in the inset of Figure 3. 6 which agree in the low frequency range with those published in [2]. These data were measured on a different sample having a different order parameter (see inset of Figure 3. 6). This proves that dielectric strengths of the δ-relaxation and the tumbling mode depend on the orientation of the sample but not the relaxation times including its temperature dependence.

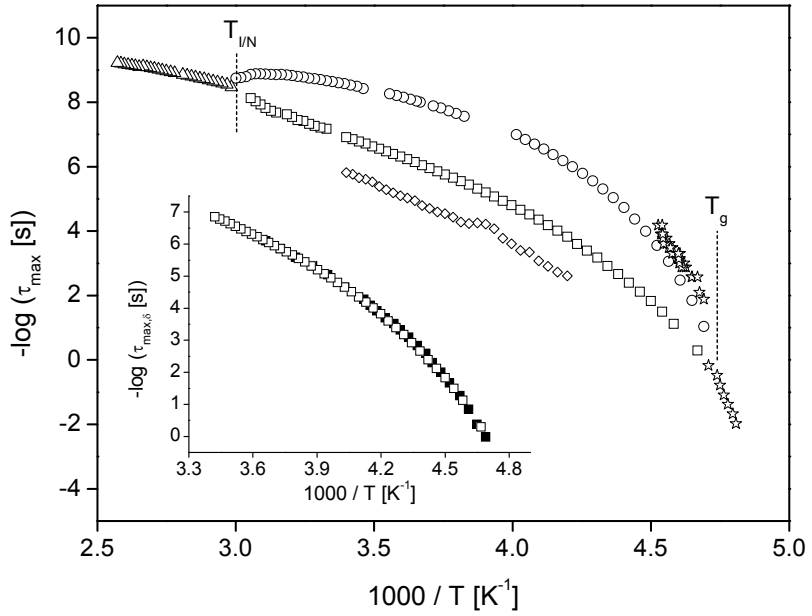

Figure 3. 6- Relaxation times, τ_{max}, *versus* inverse temperature obtained by dielectric spectroscopy for the different processes (□- δ-relaxation; ○ - tumbling mode, △ - isotropic state) and specific heat spectroscopy (☆). The inset compares the temperature dependence of the relaxation times of the δ process reported here (□) with data taken from ref. [2] (■). Note also that the relaxation times measured for both samples with the different orientation collapses into one chart with regard to its absolute values and its temperature dependence for both the δ- and the tumbling mode.

The temperature dependencies of relaxation times for the observed processes are essentially different. This will be discussed in detail now. The third process, placed at the lowest frequencies, seems to follow an Arrhenius behavior. Further discussion can be found in [1,2]. The temperature dependence of τ_{max} of both the δ-relaxation and the tumbling mode is curved in the Arrhenius plot. At high temperatures, close to the phase transition from the nematic to the isotropic state, both modes show a pronounced pre-transition behavior (see Figure 3. 6). At low temperatures, approaching the glass

transition these two modes seem to follow a VFT-dependence. It looks like as if they merge at T_g also clear in Figure 3. 3b).

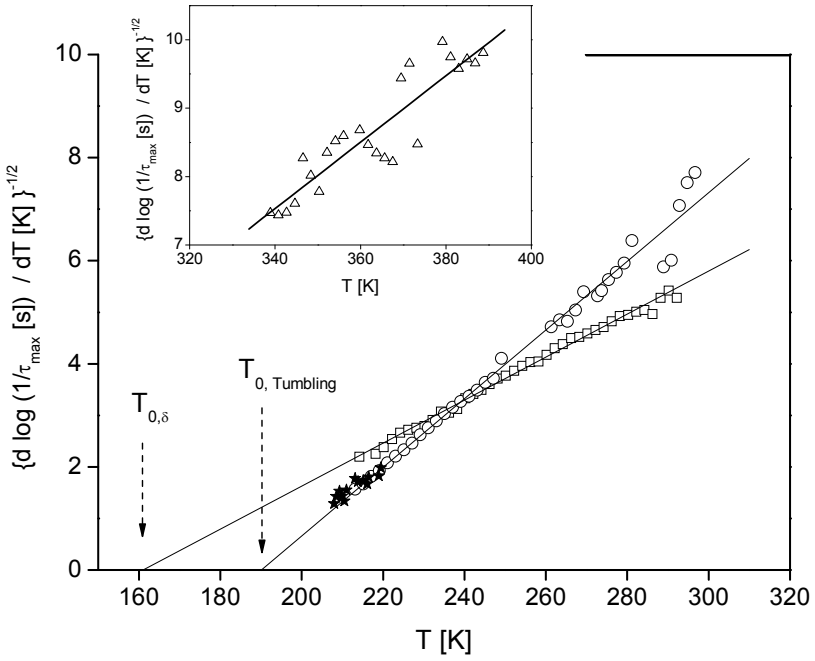

Figure 3. 7- $[d\log(1/\tau_{max})/dT]^{-1/2}$ *versus* temperature for dielectric spectroscopy for the different processes (□ - δ-relaxation; ○ - tumbling mode) and specific heat spectroscopy (★). The lines are linear regressions to the dielectric data for the different processes. The inset shows $[d\log(1/\tau_{max})/dT]^{-1/2}$ *versus* temperature for the dielectric data in the isotropic range at temperatures above the phase transition. The line is a linear regression to the data.

Generally a temperature dependence of the relaxation rates or times according to the VFT-equation (see Equation 1.2) is regarded as a sign of glassy dynamics. For a more detailed analysis of the temperature dependence of the relaxation times a derivative method is used [7,8] (see Equation 1.4).

The plot of $[d\log(1/\tau_{max})/dT]^{-1/2}$ *versus* T is illustrated in Figure 3. 7 showing up as a straight line which confirms a VFT-dependence for the relaxation times of both the δ-relaxation and the tumbling mode. For the first time it is shown that both processes have different Vogel temperatures. The estimated VFT parameters are summarized in Table 3. 2.

Close to T_g the temperature dependence of the tumbling mode is much steeper than that of the δ-relaxation. Consequently, fragility measured by the D parameter (see Equation 1.17) is much smaller for the tumbling mode that that for the δ-relaxation (see Table 3. 2). The difference in the Vogel temperatures is about 30 K.

A similar phenomenon is observed for the α-relaxation and the chain dynamics of polymers [8 and references quoted] and for the α- and δ-relaxation in liquid crystalline side group polymers [7,9,10] To be more general a decoupling of the temperature dependence of the rotational and translatorial

diffusion in low molecular weight glass forming liquids has also been reported [11] and can be regarded as characteristic for glassy dynamics.

Process	$-log\ (\tau_\infty\ [s])$	$T_0\ [K]$	$A\ [K]$	D
δ *- relaxation*	11.2	161.0	576	8.2
Tumbling mode	10.8	190.1	225	2.7
Isotropic	11.3	184.9	424	5.3

Table 3. 2- Estimated VFT-parameters for the different processes. The Vogel temperature and the A parameter were taken from the derivative technique. The prefactors were obtained by a fit of the VFT-equation to the relaxation times keeping T_0 and A fixed. D was calculated according to Equation 1.17.

Both Figure 3. 6 and Figure 3. 7 also present the temperature dependence of the relaxation time related to enthalpy (entropy) fluctuations extracted from both AC and TMDSC already described above. Looking in detail, it is concluded that AC calorimetry data agree with that obtained for the dielectric tumbling mode with regard to both its absolute values and its temperature dependence. This becomes even more convincing, applying the derivative technique also to the thermal data (full stars in Figure 3. 7). The temperature dependence of the relaxation times measured by both AC and TMDSC follow exactly the linear regression obtained using only the dielectric tumbling mode data. Therefore one has to conclude that the molecular process that determines the glassy dynamics in this nematic liquid crystal is the tumbling mode. In other words, the tumbling mode in $E7$ corresponds to the α-relaxation in conventional glass-forming systems. This statement is achieved unambiguously only by the direct combination of broadband dielectric and specific heat spectroscopy without any sophisticated data treatment.

Therefore, one can estimate from the VFT parameters which are presented in Table 3. 2 for the tumbling-mode, now assigned as the dynamic glass transition of E7, the glass transition temperature, T_g, using the criterion $\tau(T_g) = 100$ s [12,13], as T_g = 208 K in good agreement with the detected calorimetric glass transition temperature 210 K as depicted in and from the literature [2]. Also, the fragility index m at T_g (see Equation 1.15) can be determined as $m(T_g) = 146$, showing that $E7$ is a very fragile glass former.

To be complete also the temperature dependence of the relaxation time in the isotropic phase shows a VFT-like behavior (see inset of Figure 3. 7). This is expected because for temperatures above the clearing temperature the system should behave as a normal glass-forming system. The corresponding VFT parameters are also given in Table 3. 2. The fragility D of this relaxation process is in-between the values obtained for the δ process and the tumbling mode.

Finally, the temperature dependence of the dielectric strengths of the δ and tumbling processes will be discussed briefly. The Debye theory of dielectric relaxation generalized by Kirkwood and Fröhlich

[14] (see chapter I) predicts the temperature dependence of the dielectric relaxation strength according to Equation 1.46 (Chapter I).

The relative dielectric strengths of both processes should be dependent on the macroscopic orientation of the sample. This is demonstrated in Figure 3. 8a).

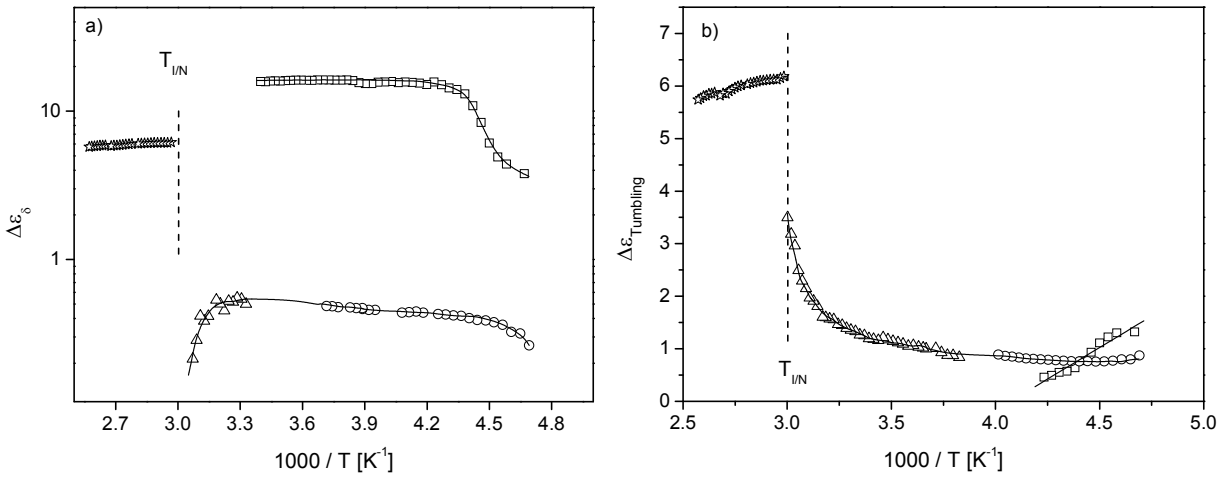

Figure 3. 8- a) Dielectric strength $\Delta\varepsilon_\delta$ in logarithmic scale of the δ-relaxation *versus* reciprocal temperature: □ - parallel oriented sample; ○ - perpendicular oriented sample at low frequencies; △ - perpendicular oriented sample at high frequencies. ☆ - isotropic state. Lines are guides for the eyes. b) Dielectric strength $\Delta\varepsilon_{tumbling}$ of the tumbling-relaxation *vs.* reciprocal temperature: □ - parallel oriented sample; ○ - perpendicular oriented sample at low frequencies, △ - perpendicular oriented sample at high frequencies. ☆ - isotropic state. Lines are guides for the eyes.

Figure 3. 8a) compares the temperature dependence of the dielectric relaxation strength of the δ process, $\Delta\varepsilon_\delta$, for a sample with a preferential parallel orientation of the nematic director (squares) with respect to the electrical field with that one which is preferentially perpendicular oriented (circles). The corresponding dielectric strengths differ by more than one order of magnitude (Figure 3. 8a is in logarithmic scale). As it can be seen already from the raw data (see Figure 3. 4), $\Delta\varepsilon_\delta$ for the δ- relaxation increases with increasing temperature and reaches a plateau for temperatures higher than about 238 K. Moreover there seems to be a slight difference in the temperature dependence of $\Delta\varepsilon_\delta$ for the two different main orientations. Close to the phase transition to the isotropic state, $\Delta\varepsilon_\delta$ drops down. This can be also seen directly from Figure 3. 3. Such a behavior is expected for a liquid crystal with a positive dielectric anisotropy [15]. Near to the phase transition the orientation of the sample is lost.

The reason for this temperature dependence of $\Delta\varepsilon_\delta$ is not clear now and needs further investigation. Because dipole moment is constant using Equation 1.46, this can be understood either by an increase of the number density of fluctuating dipoles or by an increase of the correlation factor g. The latter

explanation seems to be more likely because it is known that the order parameter changes with temperature. This will change the dielectric strength of the δ process (see equation 1.48 in chapter I).
The dielectric strength for the tumbling mode, $\Delta\varepsilon_{tumbling}$, is given in Figure 3. 8b). The difference between the samples with the different orientations seems to be small (circles against squares). At low temperatures, far from the phase transition, $\Delta\varepsilon_{tumbling}$ is approximately constant but increases strongly close to T_{IN}.
Also the relaxation strength of the process in the isotropic state decreases with increasing temperature as expected.
Resuming, the temperature dependence of the dielectric strengths for both δ and tumbling processes present different temperature dependences far from the phase transition T_{IN} and near it. The same behaviour near to the isotropic to nematic transition have already been reported for related cyanobyphenyls [16,17,18,19] and has been discussed in terms of the Mayer-Saupe mean field predictions [16]. In the case of 5CB, due to dipolar antiparallel ordering, calculations deviate from expected. This liquid crystal constitutes more than 50% of $E7$, therefore one can suppose a similar reason for $\Delta\varepsilon$ of $E7$ near T_{IN}.
Moreover, looking closer in Figure 3. 8b) in the parallel oriented sample (squares) far from T_{IN}, a slight decrease of $\Delta\varepsilon$ with increasing temperature can be seen as a further argument for being associated to the glass transition.

3.1.5 Conclusion

It was shown that the nematic liquid crystal $E7$ undergoes a glass transition [1,5,3,4,5] characterized by a glass transition temperature T_g. Up to know the molecular origin of glassy dynamics in constrained systems with partial order and restricted mobility is under strong discussion in the literature. To study the glassy dynamics in $E7$ as model case, broadband specific heat spectroscopy was combined with dielectric spectroscopy. The theory of dielectric relaxation of liquid crystals predicts for the nematic state two relaxation processes, the δ-relaxation and the tumbling mode. The broadband dielectric measurements give that the temperature dependence of the relaxation times of both the δ process and the tumbling mode follows the Vogel-Fulcher-Tammann behavior, which is regarded as a proof of glassy dynamics. By employing a derivative technique it is shown for the first time that Vogel temperatures of both processes are different by about 30 K. Close to T_g, the temperature dependence of the tumbling mode is much steeper having a higher Vogel temperature than the δ-relaxation.
The assignment which dielectric active relaxation process corresponds to the structural α-relaxation was not done using dielectric data alone. By combined DRS data with specific heat spectroscopy
it was concluded that the dielectric tumbling mode has to be linked to the α-relaxation which is responsible for glassy dynamics in the nematic liquid crystal $E7$.

This subchapter was published in *Journal of Physical Chemistry B* **112** (2008) 11087-11099

3.2 Ibuprofen

3.2.1 Introduction

In this subchapter dielectric spectroscopy is applied to get relevant information regarding ibuprofen different molecular fluctuations from the molten down to the glassy state, since studies about the molecular dynamics of ibuprofen are scarce in literature [20]. A better understanding of the mechanisms of molecular mobility which can cause changes during processing or even storage and handling of pharmaceutical substances is given. Both a wide temperature (143 K to 363 K) and frequency range (10^{-1} Hz to 10^{9} Hz) is employed, allowing to provide a complete relaxation map which includes besides the α process already discussed by Johari *et al.*[20] two secondary relaxations (β and γ), and a Debye-type process known for alcohols [21]. The study enables the characterization of ibuprofen without a partial crystallization as it is reported in ref.[20]. The DRS investigations were complemented with Differential Scanning Calorimetry (DSC), High-Performance Liquid Chromatography (HPLC), Electrospray Ionization Mass Spectrometry, Infrared Spectroscopy (IR) experiments and Molecular Dynamics (MD) simulation in order to gain deep insights in the molecular dynamics, molecular structure and the strong tendency of ibuprofen to form hydrogen bonded aggregates such as dimers and trimers either cyclic or linear which seems to control in particular the molecular mobility of ibuprofen.

3.2.2 Experimental Conditions

Dielectric spectra (for more details see Chapter II) were recorded in the frequency range from 10^{-2} Hz to 10^{9} Hz.

In order to investigate the molecular mobility in the melt, the supercooled liquid and the glassy state, the sample was kept ~1 hour at 353 K, slightly above T_m, to ensure a complete melting.

3.2.2.1.1 High-Performance Liquid Chromatography

In order to determine the chemical stability of ibuprofen recrystallized from melt after being kept 1 hour at 353K, High-Performance Liquid Chromatography (HPLC) was performed in comparison with the chromatogram obtained for ibuprofen as received.

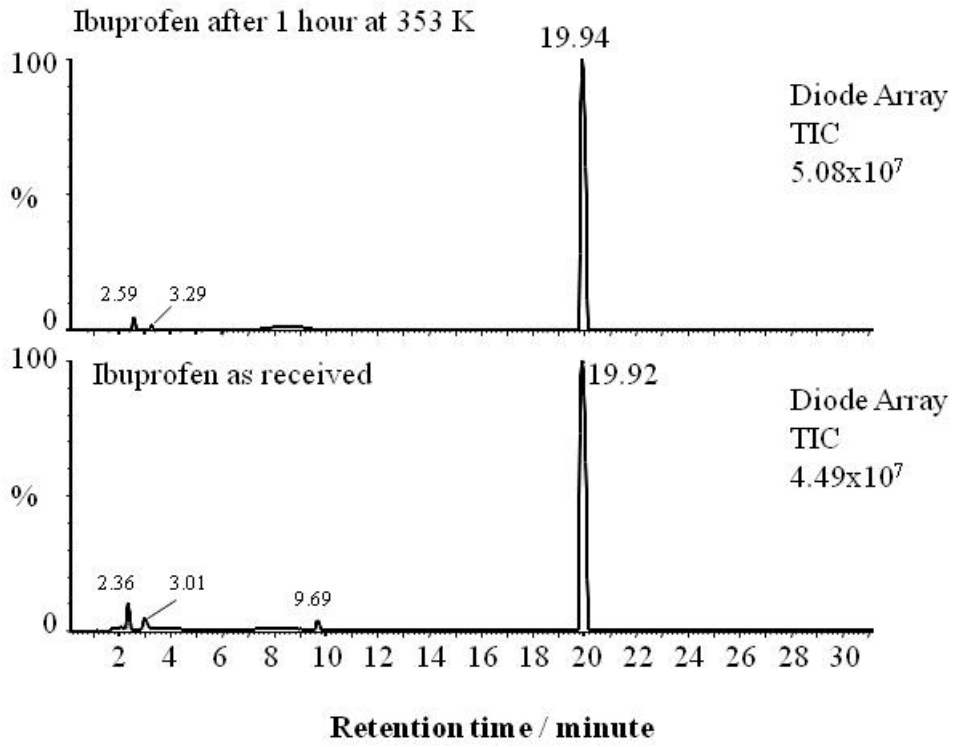

Figure 3. 9- HPLC chromatogram (Total Ion Current (TIC) *versus* Retention time) of ibuprofen dissolved in methanol with a concentration of around 4-5 × 10^{-4} mol/l. Ibuprofen as received – bottom chromatogram; Ibuprofen recrystallized from the melt after annealed at 353 K for 1 hour- top chromatogram.

Only one sharp peak with a retention time of 19.93 ± 0.02 min is detected for both samples of ibuprofen as received and annealed at 353 K during 1 hour (Figure 3. 9). This proves that the thermal treatment does not affect the ibuprofen structure chemically.

3.2.3 Results and Discussion

3.2.3.1 Association of ibuprofen molecules by hydrogen bonding

3.2.3.1.1 Electrospray Ionization Mass Spectrometry

Electrospray Ionization Mass Spectrometry (ESI-MS) was used as a complementary analytical tool in order to investigate the tendency of ibuprofen to form molecular aggregates. Figure 3. 10 shows the mass spectra due to the ionization of ibuprofen (Ibu) obtained for two cone voltages: (a) -20 V and (b) -40 V. The intensities of the peaks depend on the ionization conditions. The most probable ion, under these conditions, are: the deprotonated monomer, $[Ibu–H]^-$, which is the one that presents the highest intensity, a homogenous dimer species, $[2Ibu–H]^-$; and two sodium bridged adducts, $[2Ibu–2H+Na]^-$ and $[3Ibu–2H+Na]^-$, respectively, involving two and three ibuprofen molecules.

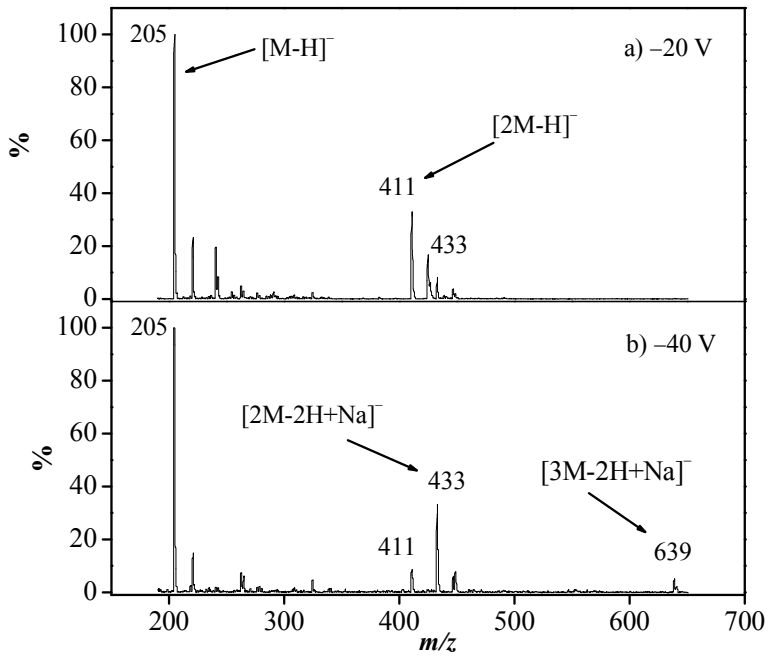

Figure 3. 10- ESI mass spectra, relative intensity (% of spectral intensity with respect to the most intense peak - the deprotonated molecular ion, [Ibu–H]⁻) *vs.* m/z of Ibuprofen in methanol solution, obtained in the negative ionization mode with cone voltages of (a) **-20V and** (b) **-40V. The peaks of interest are: [Ibu–H]⁻, m/z = 205; [2Ibu–H]⁻, m/z = 411; [2Ibu–2H+Na]⁻, m/z = 433 and [3Ibu–2H+Na]⁻ , m/z = 639.**

Due to the soft operating conditions of Electrospray Ionization non-covalent aggregated species in solution are kept intact in the gas-phase being detected in the mass spectrum [22,23]. Therefore, the observed dimer species where two ibuprofen molecules are associated via hydrogen bonding ([2Ibu–H]⁻) is most likely a result of intermolecular interactions in the solution phase, as it was established for other ibuprofen derivatives too [22]. Moreover, this peak detected under the milder conditions of Figure 3. 10a) diminishes for an increased cone voltage (Figure 3. 10b). Additionally, two sodium adducts were also found. The formation of pseudo molecular ions between analytes and background metal ions in solution phase is a well known feature of ESI mass spectra. [24,25] For ibuprofen, besides the sodium bridged dimer ion ([2Ibu–2H+Na]⁻) already reported [22], a trimer sodium adduct was also detected upon increasing cone voltage, which can be regarded as an indication that collisions in gas-phase are responsible for adduct formation due to an increased number of gas-phase collisions. However, the trimer species detected maintains a hydrogen bond between two monomers that could exist previous to sampling. A more detailed discussion is beyond the scope of this work; nevertheless these results confirm the strong tendency of ibuprofen molecules to form non-covalent bonded aggregates. This will be further elucidated by both FTIR measurements and simulation studies.

3.2.3.1.2 Infrared Spectroscopy

Infrared Spectroscopy was used to analyze both crystalline and supercooled (amorphous) ibuprofen at room temperature, in order to probe intermolecular interactions as hydrogen bonded (HB) associations between ibuprofen molecules. The wavenumber regions of particular interest are located around 3000 and 1700 cm^{-1}, due to the absorption bands of O-H and C=O stretching modes, respectively. Free O-H and C=O have characteristic frequencies at approximately 3520 and 1760 cm^{-1} appearing as sharp lines [26]. In the presence of hydrogen bonds these stretching vibrations are perturbed: the C=O band shifts down to lower wavenumbers (1700-1725 cm^{-1}) and the O-H vibration gives rise to a broad band between 3300-2500 cm^{-1} (ref. [26]). The contribution attributed to the free OH and CO groups is rather small in the spectra presented in Figure 3. 11 (nevertheless the corresponding frequencies are indicated by arrows). The characteristic bands are assigned to hydrogen bonded groups in both crystalline and supercooled ibuprofen. Similar features are reported for FTIR studies involving hydrogen-bond interaction in materials that also contain carboxylic groups [27,28]. Thus it can be concluded that the ibuprofen molecules exists almost in the form of hydrogen bonded aggregates in both phases. The major difference between them is the lower intensity and the broader bands in the spectrum of the supercooled liquid due to its less organized structure.

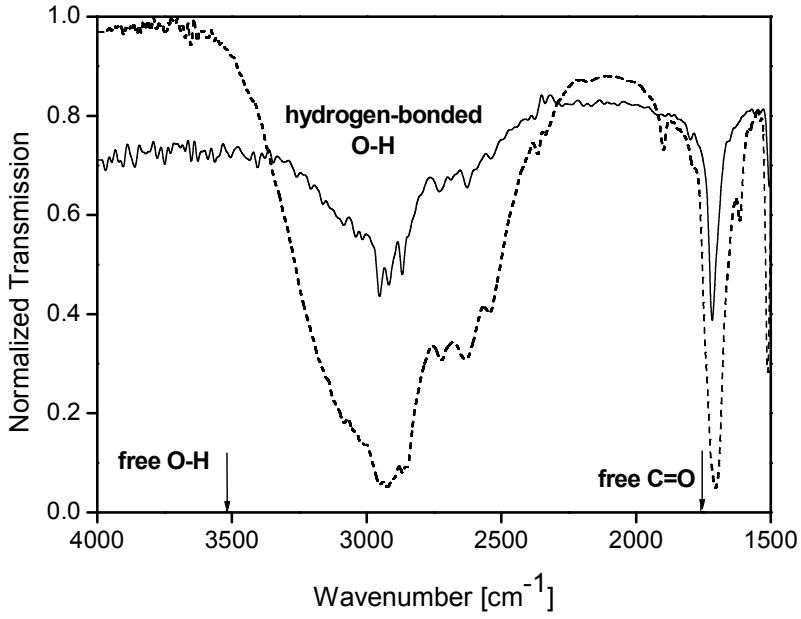

Figure 3. 11- Infrared spectra of crystalline (solid line) and supercooled liquid (dashed line) Ibuprofen at room temperature. The frequencies of the free O-H and C=O stretching vibrations are indicated by arrows, the respective absorption intensities are low in both spectra showing that the ibuprofen molecules form almost hydrogen bonding aggregates.

It is also reported from X-ray diffraction that in racemic crystalline ibuprofen, one R and one S molecules form a cyclic dimer through a strong double-hydrogen bond involving the COOH acid groups, organized in the monoclinic *P*21/*c* space group [29,30]. These IR results corroborate the affinity of ibuprofen molecules to form hydrogen bonded aggregates, such as dimers or trimers, as

concluded from the ESI-MS results. It should be strongly underlined that the combination of experiments reported here verifies the existence of hydrogen bonded aggregates also in the supercooled state. That will strongly affect the dielectric behavior of ibuprofen, as discussed later.

3.2.3.1.3 Computer simulation

Computer simulation as well as the data presented in this subchapter were carried out by Dr. Frederic Affouard from the Laboratoire de Dynamique et Structure des Matériaux Moléculaires of the Université des Sciences et Technologies de Lille (conditions and software used reported in [31]).

A calculation of the average dipole moment yielded to a value of $\simeq$1.64 Debye in agreement with the one reported in the literature for an isolated ibuprofen molecule [32].

The crystalline structure, the melting enthalpy, the position of the first sharp diffraction peak of ibuprofen in the liquid state and its characteristic relaxation time were well reproduced in the simulations validating the assumed model if a density of 0.96 g/cm^3 is considered (an experimental value of the density of liquid ibuprofen is not available in the literature). All data reported in the following have been obtained for liquid ibuprofen at 360 K.

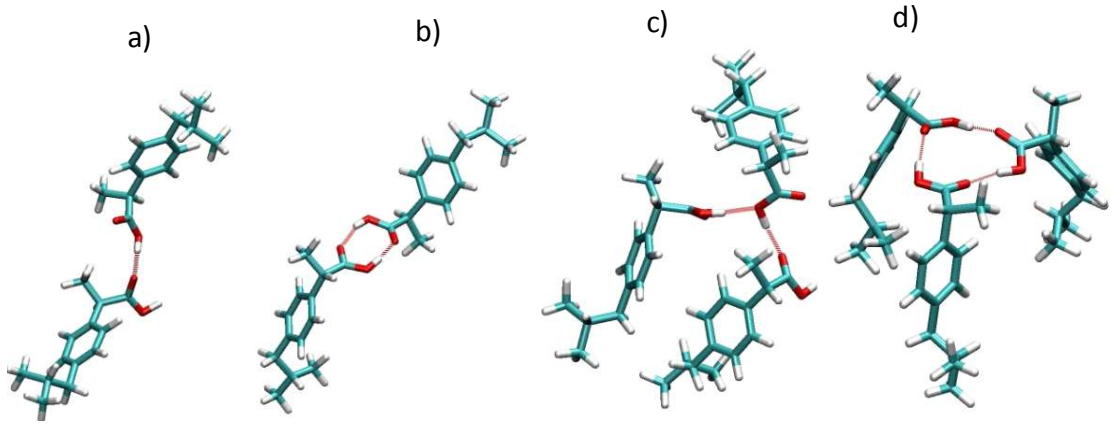

Figure 3. 12- Snapshot of possible hydrogen bonded aggregates of ibuprofen molecules obtained from MD simulations: linear dimer (a)**, cyclic dimer** (b)**, linear trimer** (c) **and cyclic trimer** (d)**.**

Hydrogen bonding statistics was obtained from molecular dynamics (MD) simulation and compared to the experimental results. Especially the population of different HB associated structures can be estimated, which is a useful tool to probe the structure of liquid ibuprofen. Each ibuprofen molecule has two oxygen atoms localized in the carboxylic acid group COOH which can form hydrogen bonds. The carbonyl oxygen site acts as proton acceptor and can only form HB with hydroxyl oxygen sites of other ibuprofen molecules. The hydroxyl oxygen site may act both as acceptor and donor. MD calculations revealed that the fraction of hydroxyl oxygen's forming HBs with other hydroxyl oxygen's is only 0.24 while it is 0.76 with the carbonyl oxygen's. Therefore, cyclic HB associated structures displayed in Figure 3. 12 should be strongly favored.

The fraction of ibuprofen HB hydroxyl oxygen sites forming simultaneously n_s HBs with other neighboring ibuprofen HBs sites either carbonyl or hydroxyl sites is 0.28, 0.63 and 0.09 for n_s = 0, 1 and 2 respectively. The number of sites participating in more than n_s = 2 HBs is negligible. Results for the HB carbonyl oxygen sites are 0.41, 0.57 and 0.02. This result indicates that the structure of ibuprofen is not dominated by long chains of open double hydrogen bonded molecules corresponding to n_s = 2 (see Figure 3. 12c) as usually seen for alcohols [33]. Instead, liquid ibuprofen mainly consists of single HB molecules (n_s = 1) (Figure 3. 12a, b and d). Therefore, fundamental differences are likely to exist between ibuprofen and alcohols in their dielectric properties as discussed below. Moreover, the n_s = 0 fraction can be compared with the intensity of the bands characteristic for free OH and free C=O observed in the IR spectra. At T = 360 K in the simulation, the fraction of non-hydrogen bonded sites is large compared to the IR results shown in Figure 3. 11 for a lower temperature of T = 300 K. This spectra point to a low amount of free OH and free CO. However, additional MD simulations performed at higher temperatures indicate a clear decrease of the value of the n_s = 0 fractions with decreasing temperature. Linear extrapolations to T = 300 K leads to 0.18 for the fraction of free OH and 0.30 for the fraction of free CO which seems still too high. Probably the simulation procedure overestimates the number of non aggregated ibuprofen molecules. But it should be underlined that it gives clear cut evidence for hydrogen bonded aggregates and their structures. The fraction of multimers composed of n ibuprofen molecules detected on average during the MD simulation is displayed in Figure 3. 13. A large variety of aggregates are theoretical possible as also suggested by the electrospray ionization mass spectroscopy and the broad adsorption peaks in the FTIR spectra.

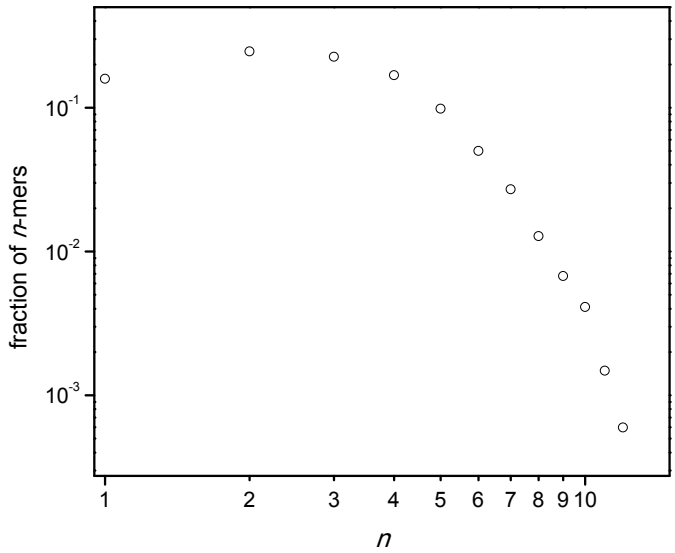

Figure 3. 13- Fraction of ibuprofen inter-molecular hydrogen bonded structures (*n*-mers) as function of the number of molecules *n* involved in the different multimers as obtained from MD simulation for *T* = 360 K. See Figure 3. 12 for snapshots of some examples of hydrogen bonded aggregates.

The fraction of isolated molecules (n = 1) is found to be lower than those of dimers (n = 2), trimers (n = 3) and tetramers (n = 4) which are expected to be the most probable structures from the simulations. Additional larger associated structures are also observed but their fraction is small at this temperature. Most important is the contribution of linear and cyclic geometries to the total number of dimers and trimers structures which is summarized in Table 3. 3. Cyclic tetramers are not considered in the following since their fraction is negligible (below 1 %) in the MD simulations. Oppositely, Table 3. 3 reveals a significant contribution of cyclic structures to the total number of dimers and trimers (see also Figure 3. 13): 43 % and 31 % for the dimers and the trimers respectively. This result is consistent with the reported by potential energy calculations and crystallography for the structures of racemic and non-racemic crystalline ibuprofen in which the molecules form hydrogen-bonded cyclic dimmers [34,35]. Moreover, these cyclic structures are found to be extremely stable compared to the linear ones. Estimated lifetimes of dimers and trimers either cyclic or linear are reported in Table 3. 3. This shows that the estimated lifetimes of cyclic geometries are about one decade longer than that of the linear ones.

T = 360 K	*Dimers*		*trimers*	
	cyclic	*linear*	*cyclic*	*linear*
fraction %	43	57	31	69
lifetime (ps)	346	33	226	13.6
μ (Debye)	1.29	2.15	1.68	2.50
g_K	0.32	0.89	0.38	0.83

Table 3. 3- Fraction, lifetimes, average dipole moments (μ) and Kirkwood correlation factors ($\boldsymbol{g_K}$) of cyclic and linear geometries of the dimers and trimers structures as obtained from the MD simulations.

3.2.3.2 Thermal Characterization

3.2.3.2.1 Differential Scanning Calorimetry

To achieve the conditions to obtain ibuprofen in the supercooled and glassy state differential scanning calorimetry is carried out in three successive scans as shown in Figure 3. 14:

In the first scan ibuprofen was heated to 353 K. An endothermic peak, with an onset at 347 K, identifies the melting of the sample at the melting temperature T_m which is typical for the racemic mixture [36,37]. The enthalpy of fusion is 25.5 kJ.mol^{-1} in agreement with the value reported in ref. [38]. In the subsequent cooling scan (run 2) crystallization is avoided, there is no exothermic peak close to T_m. Continuous cooling leads to the glass transition around 228 K. The subsequent heating scan, run 3, from the glassy state, shows in the heat flow the characteristic signature for the glass transition with an onset at T_g = 228 K, along with an enthalpy overshoot. The heat capacity step at the glass transition is ΔC_P = 0.37 J.K^{-1}.g^{-1} = 76 J.K^{-1}.mol^{-1}. The sample does not re-crystallize during heating to 353 K.

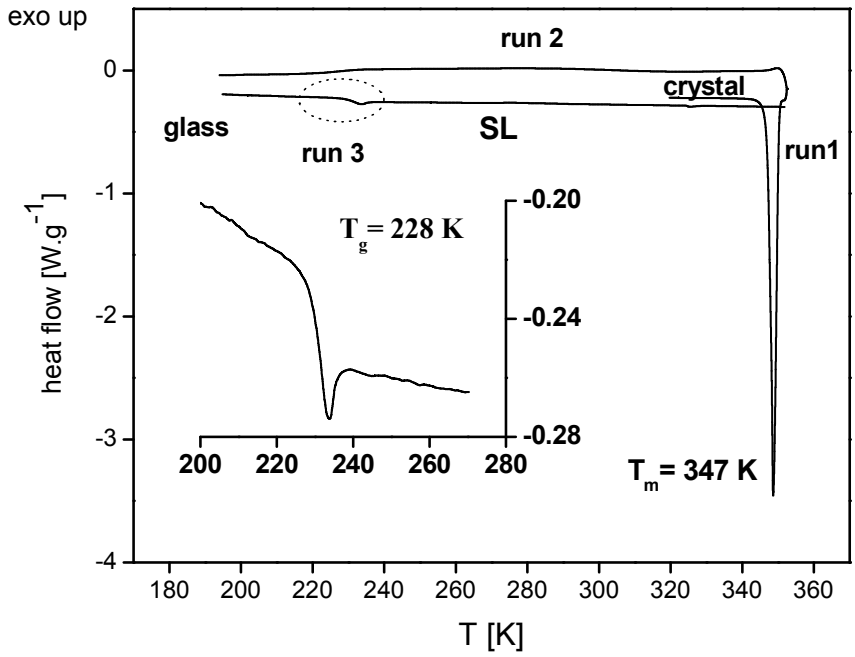

Figure 3. 14- DSC thermograms of ibuprofen obtained during heating/cooling with 5 K/min.

3.2.3.3 Dielectric characterization of the molecular mobility of ibuprofen

3.2.3.3.1 Dielectric Relaxation Spectroscopy

The melting of ibuprofen can be also monitored by Dielectric Relaxation Spectroscopy (DRS) by measuring $\varepsilon^*(\omega)$ from room temperature up to 353 K with a heating rate of 1 K/min, using a compressed disk sample. The measurements using a powder sample (without compressing) give highly scattering data approaching the melting temperature. The real part of the complex permittivity, ε', at a frequency of 10^5 Hz, is plotted in Figure 3. 15a), *versus* temperature. ε' shows a steep increase with a midpoint at 345 K in good agreement with calorimetric measurements. Absolute values for ε' are omitted due to the fact that both thickness and volume of the sample changes during melting.

During subsequent cooling with a rate of 10 K.min^{-1}, after the sample being kept at 353 K, no discontinuity occurs around T_m indicating that crystallization does not take place and a supercooled liquid is obtained (SCL in Figure 3. 15b). ε' remains constant down to 273 K followed by a step indicating the dynamic glass transition (α-relaxation) accompanied by the corresponding dielectric loss peak in ε''.

Like it was already shown in the previous subchapter ε' is a useful property to probe melting and crystallization transitions, with the advantage of being affected neither by conductivity nor implying any data modeling. Thus, ε' has a practical importance to monitor phase transitions in pharmaceutical compounds.

In order to investigate the molecular mobility in the melt, the supercooled liquid and the glassy state, dielectric spectra in the low frequency range were collected isothermally from T = 353 K to T = 143 K decreasing the temperature in different steps: in the range 353 K ≥ T ≥ 283 K in steps of 5 K; from

283 K to 223 K in steps of 1 K and in the remaining temperature range (223 K ≥ T ≥ 143 K) in steps of 2 K. In addition isothermal frequency scans in the high frequency range were carried out from 363 K down to 243 K, in steps of 2 K.

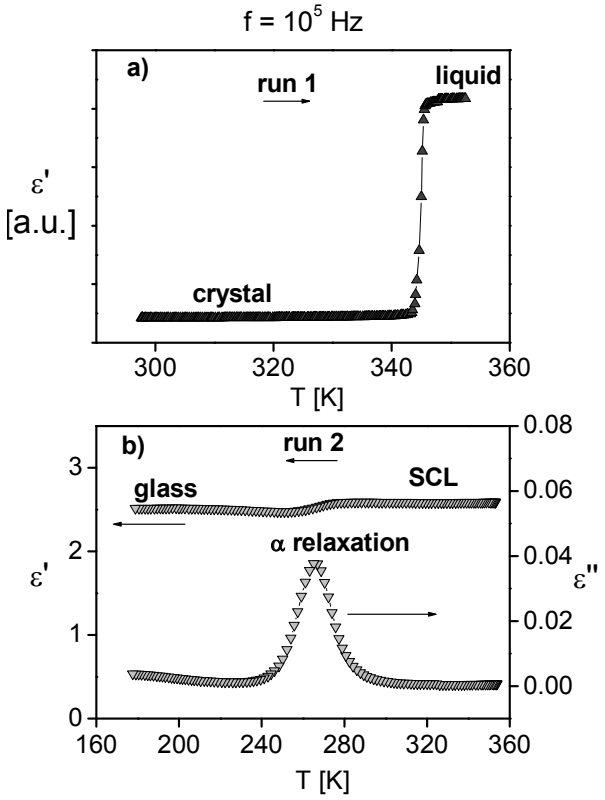

Figure 3. 15- Temperature dependence of the real, ε′ (circles) and imaginary, ε′′ (triangles) part of the complex dielectric function for a frequency $f = 10^5$ Hz. a) Run 1: DRS result obtained on heating at 1 K/min of a compressed disk of the as received crystalline ibuprofen. The observed step increase of ε′ (gray filled circles) is the melting transition, however cannot be taken quantitatively since thickness changes occurred; b) Run 2: DRS result recorded on cooling with 10K/min, after annealing at 353 K for 1 h, evidencing the bypass of crystallization and further occurrence of glass transition. The ε′ scale is only valid for run 2 (see text for details).

The ε´ trace at 10^5 Hz obtained under these experimental conditions is similar to that of Figure 3. 15b). The experimental procedure is equivalent to cooling rates less than 1 K/min (~ 0.6 K/min in the temperature range from 353 K to 273 K and ~0.2 K/min from 273 K to 143 K). So ibuprofen easily supercools with no need of high cooling rates. However, crystallization can occur during the cooling when the time spent previously in the molten state is too short to eliminate all crystallization nuclei. Therefore the sample is kept for 1 hour in the molten state at T = 353 K prior to the measurement. Moreover, it was also observed that if the supercooled liquid is stored at room temperature for several hours, or even days, without any external perturbation, crystallization does not occur.

From the molten state at 353 K down to 277 K, the dielectric measurements are dominated by conductivity, which can be due to ionic impurities that migrate over extended trajectories between the

electrodes [39] and/or proton diffusion along hydrogen bonds [20]. The charge transport takes place due to hopping conduction accompanied by electrical relaxation whose contribution increases with decreasing frequency [40]. Figure 3. 16 gives information on this low frequency/high temperature effect which was obtained from the real part of conductivity, $\sigma'(\omega)$.

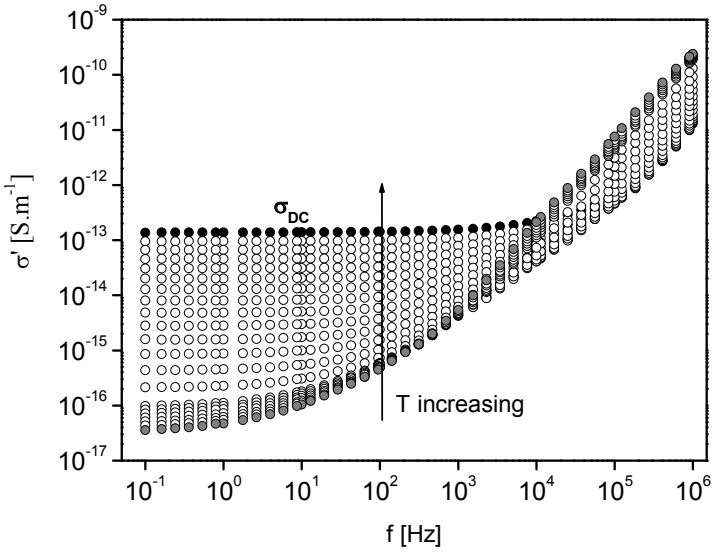

Figure 3. 16- Log-log plot of the real part, $\sigma'(\omega)$, of the conductivity of liquid and supercooled liquid ibuprofen *versus* frequency, in the temperature range from 277 K (closed circles) up to 353 K (closed stars). It exhibits the typical behaviour for ionically conducting systems: the plateau region at low frequencies corresponds to pure dc conductivity, σ_{DC}, that increases with temperature, while at higher frequencies after bending is due to ac conductivity

The $\sigma'(\omega)$ plot is common to a variety of ionically conductive systems [40,41,42,43] showing a transition from a plateau, due to pure d.c. conductivity at low frequencies, bending to a frequency dependent conductivity (a.c. conductivity) at higher frequencies, which follows a power law $\sigma'(\omega) = \sigma_{DC} + A\omega^s$ as proposed by Jonscher [39]. The conductivity values at the plateau increase with the temperature increase. These values are commonly considered accurate values of d.c. conductivity (σ_{DC}). The relaxation time for ionic conductivity can be estimated from d.c. conductivity and will be taken for discussion later in the text.

While dielectric data were presented as $\sigma'(\omega)$ in the region near the melting point, where the imaginary part of the complex permittivity is dramatically affected by σ, upon further cooling the conductivity markedly decreases allowing to extract information from $\varepsilon''(\omega)$.

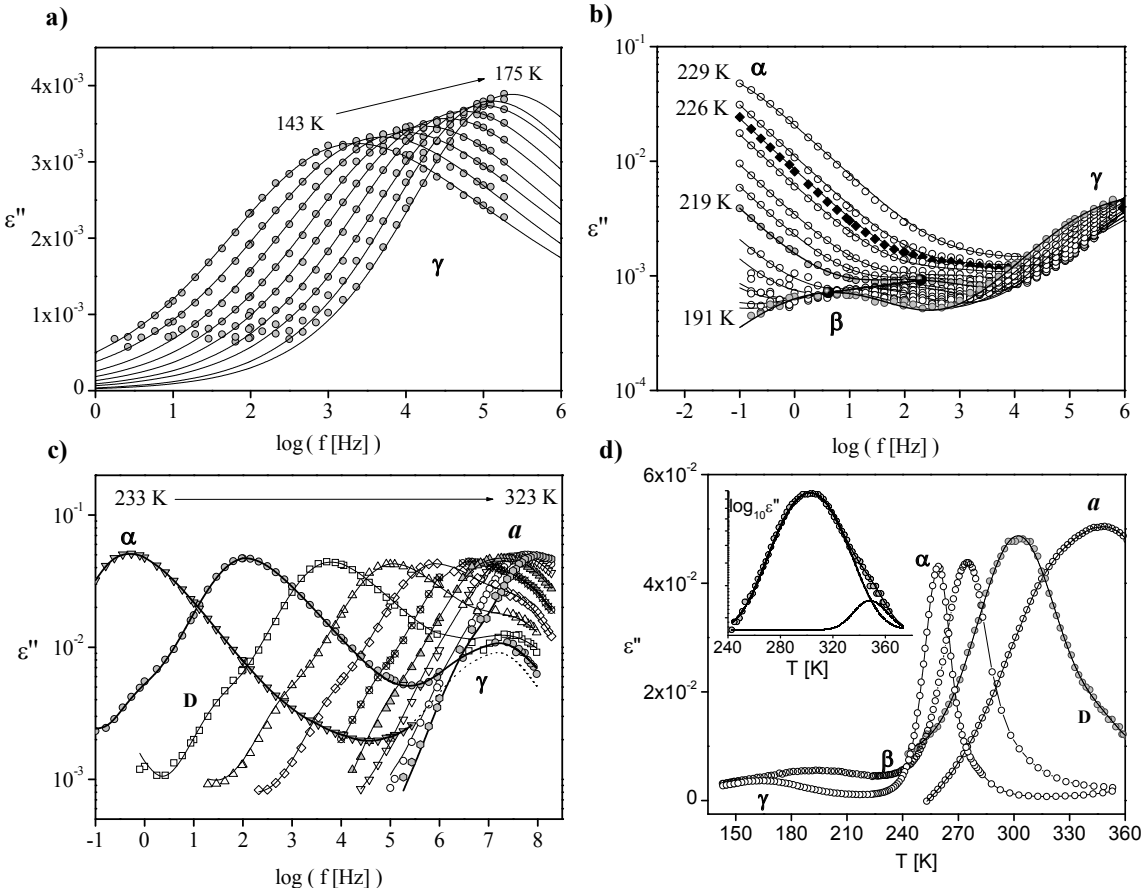

Figure 3. 17- a) Dielectric loss *versus* frequency in the glassy state, in steps of 4 K from T = 143 K to T = 175 K. b) Dielectric loss *versus* frequency from 191 K to T = 229 K in steps of 2 K. Filled black circles are due to the detected β process in the glassy state, whose relaxation rate follows an Arrhenius temperature dependence (Table 3. 4). Filled diamonds represent the isothermal data taken at 226 K which corresponds to $T_{g,diel}(\tau = 100\,s)$. c) Dielectric loss spectra above the glass transition temperature between 233 K and 323 K, in steps of 10 K. In figures a)-c), the solid lines are the overall HN fitting curves to data. d) Dielectric loss ε'' *vs.* temperature T at fixed frequencies: 3.75×10^4, 1×10^6, 2.75×10^7 and 3.31×10^8 Hz, taken from the isothermal data. Solid lines are overall fits to data by a sum of two Gaussians. The inset illustrates at 2.75×10^7 Hz the decomposition of the global fit into two Gaussian peaks.

Illustrative isotherms of the dielectric loss spectra acquired in the available frequency range covering a wide temperature interval from the glass to the supercooled state are shown in Figure 3. 17a) to c). Some isochronal dielectric loss spectra taken from the isothermal data are also shown in Figure 3. 17d) which represent an additional piece of information of the dynamics of ibuprofen from the glassy to the molten state. Multiple relaxation processes take place in ibuprofen. In the glassy state at the lowest temperatures, a well defined broad secondary process with a weak intensity is observed, here designated as γ (Figure 3. 17a). At temperatures between 191 K and 228 K, a further secondary relaxation process, with even lower intensity moves in the frequency window with increasing temperature, labeled as β in Figure 3. 18b). In the supercooled state this process becomes submerged

under the main relaxation process (α-relaxation) associated with cooperative motions responsible for the dynamic glass transition (Figure 3. 17c). In the mega to gigahertz frequency region it is possible to observe the high frequency part of the α process and the secondary γ-relaxation that shifts out from the low frequency window. At higher temperatures, the intensity of the secondary γ process becomes comparable to the magnitude of the main α process and both merge to a single process (for T > 311 K), here named a (Figure 3. 17c and d). Moreover, at frequencies lower or temperatures higher than for the α process (Figure 3. 17c and d), a less intense process named D is observed which persists active in the whole studied temperature range, even for temperatures higher than the overlapping of the α and γ processes.

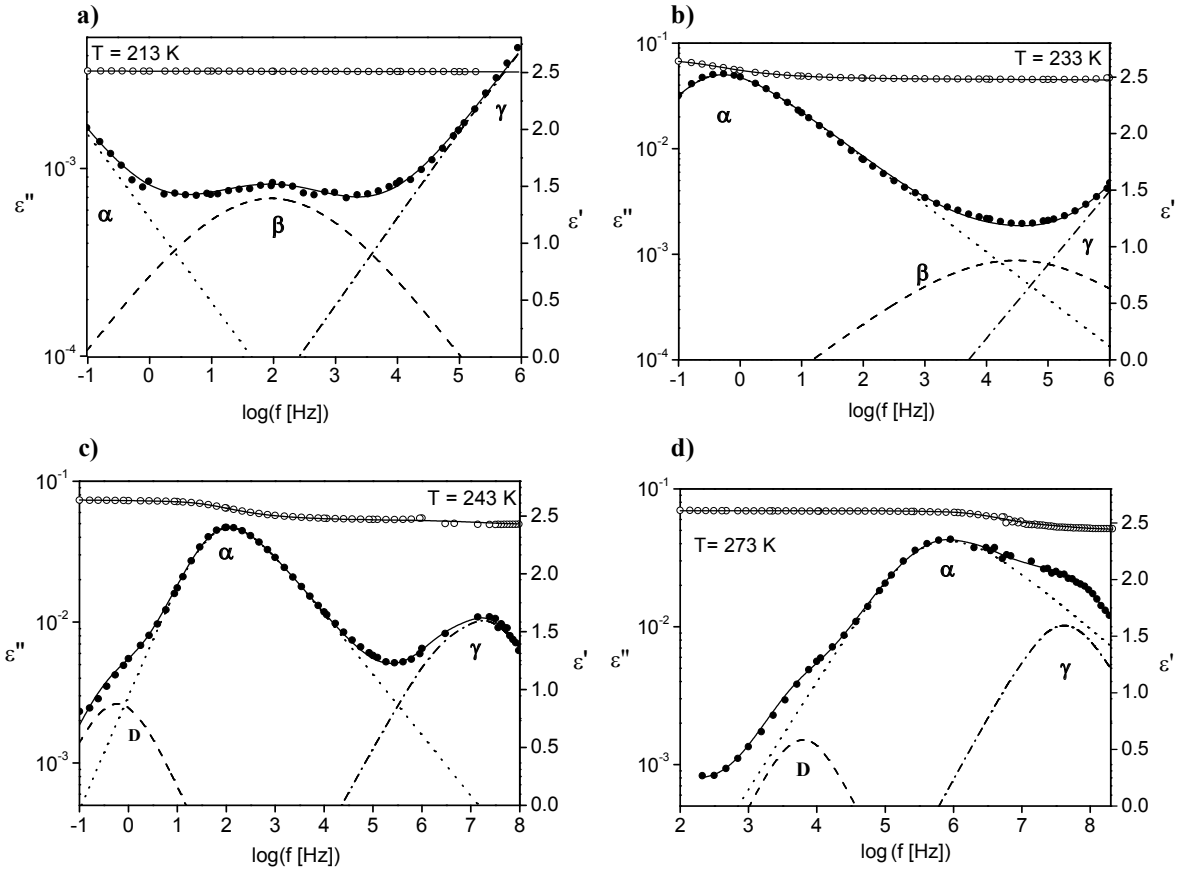

Figure 3. 18- Four examples of the fitting procedure where an additive contribution of three HN-functions is assumed: both the real (filled circles) and the imaginary (open circles) part of complex permittivity were included at a) 213 K, b) 233 K, c) 243 K and d) 273 K. The solid lines represent the overall fit and the dashed lines the individual HN-functions.

The dielectric spectra collected over the entire broadband frequency window were analyzed by fitting a sum of Havriliak-Negami model functions (Equation 1.35) [6].

Conductivity effects were taken into account for temperatures higher than 258 K by adding a contribution $\left({}^{\sigma_{DC}}/_{\varepsilon_0 \omega}\right)$ to the imaginary part of the fit function if this is necessary (see Equation 1.47).

Figure 3. 18 gives four representative examples for this procedure where both the real and the imaginary parts were used during the fits. The spectral shape (α_{HN} and β_{HN}), the dielectric strength ($\Delta\varepsilon$) and the mean relaxation time (τ_{HN}) for each process extracted from the fitting procedure are discussed in the following in detail.

i) Spectral shape

Both secondary relaxation processes show a pronounced non-Debye behavior. The peak of the γ-relaxation (for $T < T_g$) is broad ($\alpha_{HN} \sim 0.5$) and asymmetric ($\alpha_{HN} \cdot \beta_{HN} = 0.2$). For temperatures higher than T_g the shape parameters of the γ-relaxation changes significantly (β_{HN} = 1 and $\alpha_{HN} \sim 0.6–0.8$). The β process, in the subglass region, can be well described by a symmetrical Cole-Cole function (*i.e.*, β_{HN}= 1) with α_{HN}~ 0.45; these parameters were kept constant in the narrow temperature range above T_g where it was still possible to follow the β-trace.

The shape of the α-relaxation has a weak temperature dependence ($\alpha_{HN,\alpha} \approx 0.81$; $\beta_{HN,\alpha} \approx 0.52$), allowing to construct a master curve.

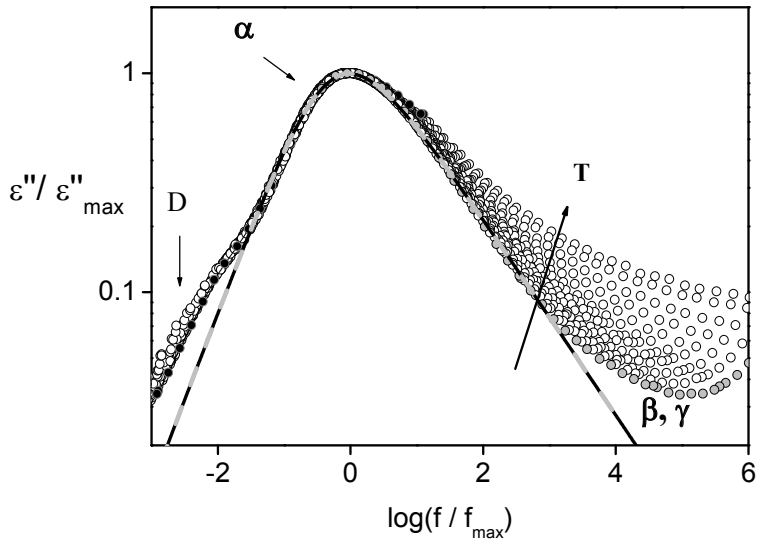

Figure 3. 19- Normalized dielectric loss curves (open circles) in the frequency domain 10^{-1}–10^{6} Hz, illustrating the invariant shape of the α-relaxation. The solid line represents the individual HN function used to fit the α process with α_{HN} = 0.81 and β_{HN} = 0.56. The non-superposition between experimental data and the fitting curve in both low and high frequency sides is due to the overlapping of the indicated processes. The dashed line is the corresponding fit of the one-sided Fourier transform of the KWW function with β_{KWW}= 0.52.

Figure 3. 19 presents the reduced plots of $\varepsilon'' / \varepsilon''_{max}$, where ε''_{max} is the maximum loss of the α-peak, against $log(f / f_{max})$, obtained between 232 and 262 K. The D process that shows up in the low frequency flank is characterized by a Debye-like behavior (α_{HN} = 1; β_{HN} = 1). The high frequency

flank ($(log(f / f_{max}) > 1.5)$ is influenced by the submerged secondary relaxations. In the reaming frequency range all curves superimpose.

To describe the data for T > 262 K, where the experimental frequency range was extended up to 10^9 Hz, the shape parameters of the main relaxation were constrained to vary within the range of values found for lower temperatures ($\alpha_{HN,\alpha}$= 0.81 ± 0.02; $\beta_{HN,\alpha}$ = 0.54 ± 0.02). For the D process a Debye character is assumed in accordance with the experimental data.

The non-Debye nature of the relaxation response in supercooled liquids can also be described in the time domain, by the well-known Kohlrausch-Williams-Watts (KWW) function (see Equation 1.37) [44,45]. Fitting the normalized HN function that describes the α-loss peak (solid line in Figure 3. 19) by the one-side Fourier transformation of the stretched exponential function, a β_{KWW} value of 0.52 is obtained. This value matches the value estimated from the empirical correlation proposed by Alegria *et al*. [46] (see Equation 1.39) and is similar to the value reported in ref. [20] (β_{KWW}= 0.54). The estimated KWW-parameters will be later used for a quantitative discussion.

ii)-Dielectric strength

The temperature dependence of the dielectric strength, $\Delta\varepsilon$, for the different processes is shown in Figure 3. 20.

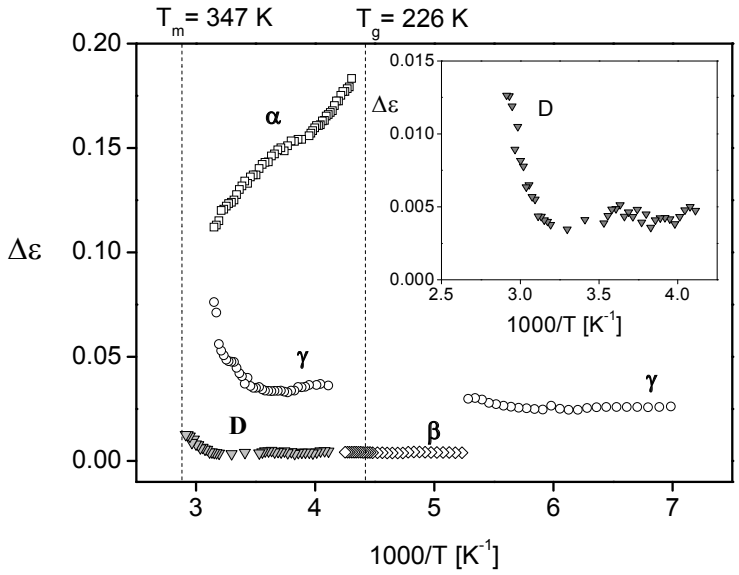

Figure 3. 20- . Dielectric strength, $\Delta\varepsilon$, for the α, β, γ and D process *versus* $1/T$. The inset enlarges $\Delta\varepsilon$ *vs.* $1/T$ plot for the D-process.

Considering the polar carboxylic moiety (see structure in Chapter II) and the dipole moment of 1.64 Debye as found for an isolated molecule by MD simulations, the estimated dielectric strength is rather low, even for the α process. The starting point for the analysis of $\Delta\varepsilon$ is the extension of the Debye theory by Onsager, Fröhlich and Kirkwood (see Equation 1.46) [47].

The small values of $\Delta\varepsilon$ agree with that of Johari *et al.*[20], which conclude that hydrogen-bonding in ibuprofen favors an anti-parallel correlation of the dipole vectors. In order to get an insight in the origin of the low dielectric strength from the molecular point of view, average dipole moments and Kirkwood correlation factors for cyclic and linear geometries of the dimers and trimers structures were calculated from the MD simulations. The corresponding values are summarized in Table 3. 3. The calculated Kirkwood factors g_K < 1 verify the anti-parallel correlation of the dipoles. This is specifically true for cyclic dimers and trimers which are present in larger fractions (see Table 3. 3). Moreover the dipole moments are found to be smaller for the cyclic aggregates than for the linear ones. Both results are consistent with the low measured dielectric strength. Moreover, it should be mentioned that the average dipole moment of the cyclic dimers is even smaller than that of the isolated molecule (1.64 Debye). This result is consistent with the estimation of a weak dipole moment from the *ab-initio* calculations [48] of the isolated racemic (0.00 Debye) and non-racemic (0.54 Debye) cyclic dimers as found in crystalline ibuprofen [29,34,35]. However, the values of the dipole moment of the cyclic dimers obtained in the disordered phase (50:50 mixture of racemic/non-racemic) are significantly higher than that for crystalline one since the structures might have distorted geometries.

Concerning the temperature dependence of the dielectric strength, for a localized process like the β-relaxation, $\Delta\varepsilon$ generally increases with temperature due to an increase of the number of fluctuating dipoles and/or the fluctuation angle of the dipole vector with temperature [49,50]. This is the case for both secondary relaxation processes found for ibuprofen. The intensity of the γ-relaxation increases strongly in the temperature range close to the merging with the α-relaxation (see Figure 3. 20). The same behavior was observed in other systems [51,52,53,54]. For an epoxy resin it was argued that local motions couple with diffusive motions dominating at temperatures above T_g [55]. For ibuprofen the molecular reason of the γ-relaxation are probably fluctuations of carboxylic groups. For temperatures above T_g the number of hydrogen bonded carboxylic decreases with increasing temperature which is also confirmed by molecular simulations. Therefore, the $\Delta\varepsilon$ increase of the γ process should be related to the increasing number of free carboxylic groups which can contributes now to the process.

For the α process, the $\Delta\varepsilon$ decreases with increasing temperature as it is well know for conventional glass formers and polymers. It should be noted that the corresponding temperature dependencies are much stronger than predicted by Equation 1.46. This particular behavior can be recognized as a characteristic of the α-relaxation. It can be explained by the cooperative character of the underlying molecular motions responsible for glassy dynamics [14].

A different pattern is observed for the Debye process. While at the lowest temperatures its dielectric strength is almost temperature independent, at temperatures above the merging of the α and γ processes, $\Delta\varepsilon_D$ increases with increasing temperature (see inset of Figure 3. 20) which can be seen directly in the raw data (compare Figure 3. 17c and d). This behavior will be discussed later.

iii)-Relaxation map

Figure 3. 21 shows the temperature dependence of the relaxation time, τ, for all relaxation processes. Additionally the corresponding values of τ obtained from the isochronal representation of the dielectric loss, *i.e.*, ε'' *versus* temperature at constant frequencies ($\varepsilon''(T; f = const)$) as in Figure 3. 17d) are given. A superposition of k Gaussians [56] was fitted to the isochronal representation of ε'' to obtain the maximum temperature of peaks, $T_{max,k}$, for each measured frequency, like in the example given in the inset of figure 3.19d). The two data sets coincide well. The agreement between the two methods validates the use of isochronal data especially when the respective loss peaks maxima are poorly defined in the frequency domain or out of the accessible frequency range. This method has also been proved to be advantageous in distinguishing multiple processes [56,57,58].

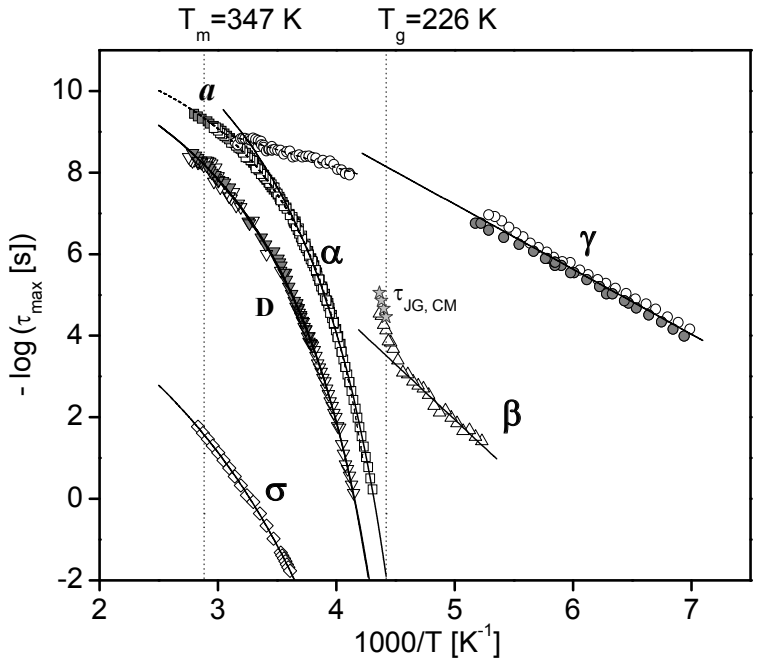

Figure 3. 21- Relaxation times, τ_{max}, *versus* 1/ T for all processes: Open symbols - isothermal loss data collected during cooling; Gray filled symbols - τ obtained from the isochronal plots for all studied frequencies f ($\tau = 1/(2\pi f), 1/T_{max}$). The γ process runs out from the low-frequency window at ~193 K becoming again detectable in the high frequency range where measurements were only performed for temperatures above 243 K (reason for the gap of data close to T_g). Lines are fits of the Arrhenius and VFTH formulas to the corresponding data: in the α, a trace the solid line is the $VFTH_1$ fit and the dashed line is the $VFTH_2$ fit to the data (see text and parameters in Table 3. 4 and Table 3. 5). Light gray stars indicate the JG relaxation time, τ_{JG}, estimated from Coupling Model (Equation 1.40 in Chapter I). Vertical dashed lines are the dielectric glass transition temperature T_g^{diel} ($\tau = 100\ s$) = 226 K and T_m = 347 K.

Since several relaxation processes were found in ibuprofen, for the sake of clarity the relaxation map will be analyzed in order of increasing temperature, with exception to the process found at the highest

temperatures (open losanges). It concerns to the conductivity. The respective relaxation times, τ_σ were estimated according to $^1/_{\tau_\sigma} = \sigma_{DC}/\varepsilon_0\varepsilon_\infty$ [59]. The solid line is the respective VFT-fit obtained with following parameters τ_∞ = 1.1 × 10^{-7} s, B = 985 K and T_0 = 164 K. The same VFT-law behavior has been found for different systems both polymers [41,43], and low molecular weight materials [60,61]. The temperature dependence similarity on relaxation times of ionic conductivity and α-relaxation, supports the point of view of some authors [59] claiming a joint approach to describe ion translation and rotational relaxation.

γ and β process

In the glassy state the relaxation time for the two secondary processes (γ and β) follow a linear temperature dependence of $\log(\tau_{max})$ *vs.* $1/T$ as expected for relaxation processes related to localized molecular mobility. From the Arrhenius equation (see Equation 1.5) values of the activation energy E_A of 31 and 52 kJ·mol^{-1} were estimated for the γ- and the β- relaxation respectively (see Table 3. 4) for temperatures below T_g. For the γ process the two sets of data, isothermal and isochronal, were included in the analysis. Above T_g, the temperature dependence of the relaxation time of the γ process bents towards that of the α process; the corresponding apparent activation energy is lower than that found in the glassy state. A similar behavior is reported for hydrogen-bonded monosaccharides [62] and glass forming epoxy resins [63]. For ibuprofen, the α and the γ process are well separated in this temperature range by several decades (see Figure 3. 17c) so that the bend in the temperature dependence seems to be not a fitting artifact. As discussed above the γ-relaxation is due to molecular fluctuations of the carboxylic groups which are involved in hydrogen bonds at low temperatures. For higher temperatures the number of non hydrogen bonded carboxylic groups firstly increases and secondly the energy barriers for molecular fluctuations are lower for non bonded groups. This is coherent with the bend in the apparent activation energy seen in the experimental data.

The temperature dependence of the relaxation time of the β process shows also a strong change around T_g, *i.e.*, the Arrhenius-like temperature dependence of τ_B below T_g cannot be extrapolated to temperatures above T_g. This crossover of the τ_B trace below the glass transition to stronger temperature dependence above T_g has been observed directly in the raw data for different systems [64,65,66]. This behavior can be discussed in the framework of the Coupling Model (CM) [67].

Using β_{KWW} = 0.52, Equation 1.40 (Chapter I) gives a value of τ_{JG} at T_g of 4 × 10^{-5} s in good agreement with the experimental τ_B value at this temperature (see stars in Figure 3. 21). Also for higher temperatures a good agreement with τ_B is observed. This shows that the changed temperature dependence of τ_B above T_g is consistent with the CM [64]. Furthermore, below T_g the activation energy of the β process estimated from the Arrhenius equation (see Table 3. 4) gives for the ratio E_A/RT_g a value of 28 in accordance with values found for that ratio obtained for genuine JG relaxation processes observed for several glass formers [68] (this is a slightly higher than the value of 24 as proposed by Kudlik *et al.*, [69] $E_{A,JG} = 24RT_g$). Additionally, the Cole-Cole type of the detected

β process is consistent with the usually found profile of the Johari-Goldstein β-relaxation [70]. All these features points to the direction that the detected β-relaxation is a "genuine" Johari-Goldstein process as also found in other pharmaceutical glass formers such as indomethacin [71], sorbitol [72] and aspirin [73,74].

A different way to rationalize the change in activation energy of the β process at T_g is to assume that the actual relaxation rate is free volume dependent [75]. Since the free volume significantly increases upon passing the glass transition this will accelerates the relaxation rate that results in a corresponding increase in the apparent activation energy.

γ process ($T < T_g$)		β process ($T < T_g$)	
E_A [kJ·mol^{-1}]	τ_∞ [s]	E_A [kJ·mol^{-1}]	τ_∞ [s]
30.5±0.7	$(6 \pm 4) \times 10^{-16}$	52±2	$(3 \pm 4) \times 10^{-16}$

Table 3. 4- Estimated parameters of the Arrhenius fit (Equation 1.5) to the secondary $\gamma-$ and β-relaxation times.

The α- and α- relaxation

For the α-relaxation the temperature dependence of the relaxation times is curved when plotted *versus* 1/T (see Figure 3. 21). Close to T_g this dependency is often described by the empirical Vogel- Fulcher- Tammann-Hesse (VFTH) equation (see Equation 1.2).

For conventional glass formers and polymers it is known that a single VFTH-law describes the temperature dependence of the relaxation times only up to a temperature $T_B \approx (1.2 - 1.3)\, T_g$. At T_B the temperature dependence of τ changes from a low temperature VFTH-behavior to a high temperature one. This is regarded as the onset of cooperative fluctuations [76,77]. For a detailed analysis of the temperature dependency of the α-relaxation of ibuprofen a derivative method is applied (see Equation 1.4) [63,77,78,79]. In the following this type of analysis is applied to the dynamic glass transition. Figure 3. 22a) shows that for ibuprofen at least two VFT equations (one at high $VFTH_2$ and one at low temperatures $VFTH_1$) have to be used to describe the data in the whole temperature range. This is shown for ibuprofen for the first time.

The derivative analysis shows that $VFTH_1$ and $VFTH_2$ have distinct Vogel temperatures that differ about 20 K, with $T_{0,1} < T_{0,2}$ indicating a different dynamical behavior in the low and high temperature regime. The intersection of the two VFTH lines gives a crossover temperature T_B = 265 K. These fits are shown respectively as solid ($VFTH_1$) and dashed ($VFTH_2$) lines in the relaxation map (Figure 3. 22) and the characteristics parameters are presented in Table 3. 5.

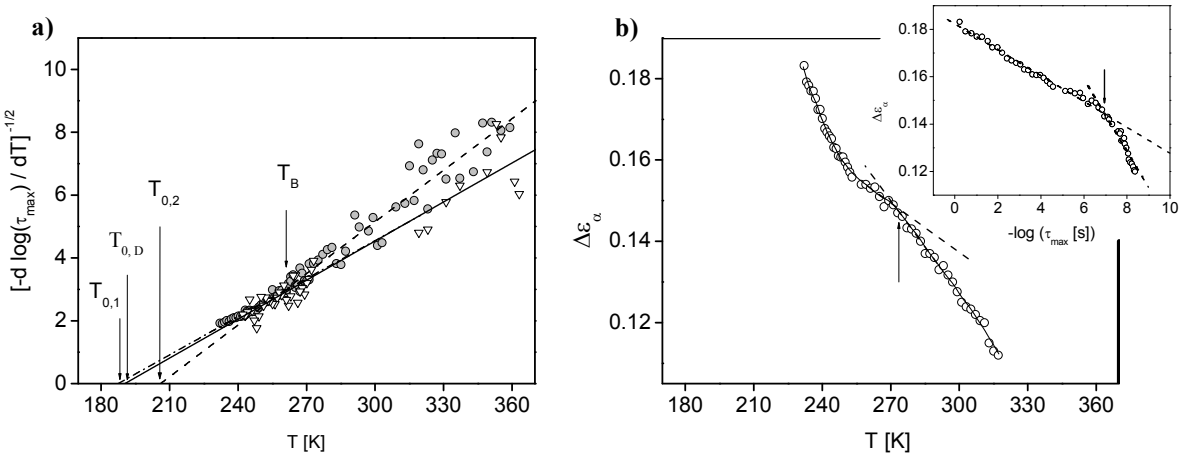

Figure 3. 22- a) $[d\log(1/\tau_{max})/dT]^{-1/2}$ ***vs.*** **temperature for the relaxation times of the α, a (circles) and the Debye (triangles) processes. The dash-dotted line is a linear regression to the low-temperature α- relaxation data where VFTH$_1$ regime holds with a Vogel temperature $T_{0,1}$, while the dashed line is the linear fit to the high temperature data characterized by VFTH$_2$ with $T_{0,2}$. The intersection of the two lines defines the crossover temperature T_B = 265 K. The solid line is the linear fit to the Debye data characterized by a VFTH law with $T_{0,D}$. b) Temperature dependence of the α-relaxation dielectric strength, $\Delta\varepsilon_\alpha$. Lines are guides for the eyes. The arrow indicates a crossover temperature separating the high and low temperature region in agreement with the T_B value calculated from the intersection of the VFTH$_1$ and VFTH$_2$ law. The inset gives $\Delta\varepsilon_\alpha$ *versus* $-log(\tau_{max})$. The intersection of the two temperatures regimes is indicated by the arrow which gives a relaxation time corresponding to the crossover temperature of the $\Delta\varepsilon_\alpha$ *vs.* temperature plot.**

	α, a processes			D process		
	B[K]	τ_∞ [s]	T_0 [K]	B[K]	τ_∞ [s]	T_0 [K]
VFTH$_1$	1426±50	$(1.2 \pm 0.6) \times 10^{-14}$	187±1	1379±49	$(0.9 \pm 036) \times 10^{-12}$	191±1
VFTH2$_1$	792±13	$(1.7 \pm 0.1) \times 10^{-12}$	205.6±0.6			

Table 3. 5- Estimated parameters of the VFTH fit (equation 1. 2) to the $\alpha-, a-$ and D-relaxation times.

Moreover, the Arrhenius temperature dependence of τ_β (the JG- relaxation) that holds below T_g can be extrapolated to temperatures above T_g which intersects the α-trace at a temperature T_β = 256 K. This is the conventional way to estimate the merging of the α and β processes at a temperature T_β, even when a deviation from the Arrhenius temperature dependence occurs at T_g [80]. T_β is found to be close to T_B for a variety of systems [81] and also here for ibuprofen.

The existence of a crossover in the temperature dependence of the α- relaxation can be revealed also by its dielectric relaxation strength, which is re-plotted as a function of temperature in Figure 3. 22b).

Besides its strong increase with decreasing temperature (see also Figure 3. 20), two well separated regions are observed which can be approximated by two different dependences of $\Delta\varepsilon_\alpha$ *versus* temperature. From the high temperature regime the temperature of the α- relaxation onset, T_{on}, can be estimated by the linear extrapolation of $\Delta\varepsilon_0$ to zero ($\Delta\varepsilon_\alpha \rightarrow 0$) as $T_{on} \approx 463\ K$. The change from the low temperature behavior to the high temperature dependence takes place close to T_B. Having in mind that the crossover phenomenon was estimated from two different properties, the static quantity dielectric strength and the dynamic relaxation time, a correlation between both is expected as emphasized in ref. [77]. The plot of $\Delta\varepsilon_\alpha$ *versus* $\log(1/\tau_{max})$ shown in the inset of Figure 3. 22b, illustrates the predicted correlation where two regions with different dependencies are observed. Their intersection defines a model-free crossover time corresponding to the temperature T_B.

While τ_B is close to T_B proving the interrelationship of the β and the α process, there is no indication of a change in the α-trace when the γ-relaxation overlaps with the latter (T_γ = 313 K). This is confirmed by the absence of a bend around this T_γ temperature in the derivative plot.

Additionally, the curvature of the $log(\tau_\alpha)$ *vs.* $1/T$ plot, *i.e.*, the degree of deviation from Arrhenius-type temperature dependence near T_g, allows to quantitative measure the fragility as the steepness index m according to Equation 1.15.

Taking the B and T_0 values of the $VFTH_1$ fit to the α-relaxation (Table 3. 5), a fragility index of $m = 93$ is estimated for ibuprofen. Analogous values are found for sorbitol ($m = 93$) [82] and other non-pharmaceutical glass formers [82], allowing to classify ibuprofen as a fragile glass former.

Böhmer *et al*. [82], using data for 55 glass formers, proposed a correlation between m and β_{KWW}: $m = 250(\pm 30) - 320\beta_{KWW}$. For $m = 93$, it gives $\beta_{KWW} = 0.49$, in reasonable agreement with the value *0.52*, obtained by fitting the dielectric α- relaxation.

The Debye- type- relaxation

The D-relaxation has similar features to the process found in many hydrogen-bonding liquids reported as Debye-like, observed at lower frequencies side of than the α process and lacking off a calorimetric signature (see ref. [21] and references therein). The reported studies concerning to mainly alcohols, where this process is the prominent. In those cases its dielectric strength exceeds the value expected on the basis of the molecular dipole moments [21,83]. For ibuprofen the D process has a rather low dielectric strength, the most intense dielectric process is the α-relaxation. An assignment to specific molecular motions in this class of liquids cannot be made unambiguously but correlated dipole orientations through hydrogen bonding are discussed to be in its origin.

From the MD simulations it is concluded that the cyclic structures are characterized by longer lifetimes, smaller dipole moments and Kirkwood correlation factors (see Table 3. 3). This might imply that the hydrogen bonded cyclic structures may be associated with this Debye peak. In fact, the increase of the dielectric strength with temperature observed for the D process (see inset of Figure 3. 20), can be explained by an increase of g_K and consequently of the effective dipole moment with increasing temperature, which is expected since the anti-parallel alignment of the cyclic

aggregates will be increasingly less favorable causing an increase of the effective dipole moment. Additional MD simulations are needed in order to validate this conjecture.

Moreover the hydrogen bonded aggregates can form liquid crystalline mesophases due to a supramolecular arrangement induced by hydrogen bonding interactions [84] that persists in the supercooled state. For example, some of *p*-alkoxybenzoic acids [85] exhibit liquid crystalline properties attributed to their ability to form hydrogen-bonded dimers. The same tendency is observed in salicylsalicylic acid where it is proposed that dimers act as mesogenic units, being in the origin of a nematic phase [86]. Since ibuprofen molecules exist as hydrogen bonded aggregates it is reasonable to assume that specific arrangements of aggregates can give rise to the formation of mesophases. This point needs also further investigation.

Figure 3. 21 shows that the temperature dependence of the relaxation times for the D process is curved when plotted *versus* $1/T$. The derivative analysis was also applied to this set of data (Figure 3. 22a). A straight line is obtained which proves that the relaxation times of the D process follow the VFTH-equation. The value of the obtained Vogel temperature of 191 K by the derivative plot is similar to that of the low temperature regime of the α-relaxation. Therefore it is concluded that some correlation seems to exist between both processes. Besides the agreement in the low temperature limit revealed by comparable Vogel temperatures, also a convergence is found in the relaxation time at infinite temperature as seen by the resemblance of τ_∞ of $VFTH_D$ and $VFTH_2$ (see Table 3.4). Assuming that the D process is associated to hydrogen bonding, the similarity of its temperature dependence with that of the main relaxation could be an indication that the dynamics of the former is governed by the dynamics of the α-relaxation.

3.2.4 Conclusion

The crystallization of the pharmaceutical ibuprofen can be easily avoided. Therefore amorphous ibuprofen which may have advantageous therapeutic properties is studied from the melt down to the glassy state by a combination of different experimental techniques and molecular simulations.

The existence of intermolecular hydrogen bonded associations was verified in the supercooled liquid by IR spectroscopy, Electrospray ionization mass spectrometry and predicted by MD simulations. From the molecular point of view especially ESI and the MD simulations reveals the strong tendency of ibuprofen to form non-covalent molecular aggregates such as dimers and trimers either cyclic or linear. The hydrogen bonded cyclic structures were found to have the longer lifetime, smaller dipole moment and smaller Kirkwood correlation factor.

An almost complete dielectric characterization of ibuprofen in the glassy, supercooled and molten states is provided covering a broad frequency range. The results show that ibuprofen has a complex relaxation map including two secondary relaxations, γ and β, a main α process associated with the dynamic glass transition and a Debye-like process (D-relaxation).

In the glassy state, the relaxation times of the two secondary relaxation processes have an Arrhenius temperature dependence that changes at T_g. For the γ process located at the highest frequencies is probably related to fluctuations of the carboxylic group. A decrease of the apparent activation energy is observed at higher temperatures than T_g where its dielectric strengths gains in intensity. These peculiarities are discussed in terms of the decreasing tendency for hydrogen bonding at higher temperatures. The γ process seems to merge with the dynamic glass transition at high temperatures.

The β-relaxation is interpreted as "genuine" Johari-Goldstein (JG) process which is a fundamental characteristic of glass formation. Its apparent activation energy changes at T_g to higher values which can be described by the coupling model.

The temperature dependence of the relaxation times of the α process is curved in a plot *versus* $1/T$. A more detailed analysis of this dependence by a derivative technique shows that the α-relaxation has a low and a high temperature branch separated by a crossover temperature T_B = 265 K. In both ranges the temperature dependence of the relaxation times, τ, follows the Vogel-Fulcher-Tammann-Hesse formula. The crossover pattern is also reflected in the temperature dependence of the dielectric strength $\Delta\varepsilon$. This is more pronounced in a plot of $\Delta\varepsilon$ *versus* $-log\ \tau$ which shows sharp defined crossover behaviour. So two dynamical different regions of the α-relaxation can be distinguished non-ambiguously. A steepness or fragility index m of 93 was estimated which shows that ibuprofen is a fragile glass former.

At lower frequencies than the α process an additional relaxation process is observed with a weak intensity compared to the dynamical glass transition. It has similar peculiarities to the Debye process found in a large class of hydrogen bonded liquids like alcohols. The temperature dependence of its relaxation times follows a VFTH law, with a Vogel temperature close to the value found for the low temperature branch of the α-relaxation. This point to a correlation between both processes.

From MD simulations, it is concluded that hydrogen-bonded cyclic structures might be associated with this D process. This hypothesis is supported by the temperature dependence of the dielectric strength. The similarity of the temperature dependence of relaxation times of the D-process with that of the main relaxation is an indication that the dynamics of the hydrogen bond dynamics is governed by the dynamic glass transition.

At even lower frequencies and higher temperatures, a high conductivity contribution shows up, which relaxation time obey to a VFT-law temperature dependence. Although no trivial interrelation between the relaxation times of ionic conductivity and α-relaxation exists, the similarity of their temperature dependence should encourage studies to describe ion translation and orientational relaxation in a joint approach.

3.3 References

[1] VICIOSA MT., NUNES AM, FERNANDES A, ALMEIDA PL, GODINHO MH, DIONISIO M (2002) LIQ. CRYST. 29, 429.

[2] BRAS AR, VICIOSA MT, RODRIGUES C, DIAS CJ, DIONISIO M (2006) PHYS. VER. E 73, 061709.

[3] ZHONG ZZ, SCHUELE DE, GORDON WL, ADAMIC KJ, AKINS RB (1992) J. POLYM. SCI. B: POLYM. PHYS. 30, 1443.

[4] ROUSSEL F, BUISINE JM, MASCCHKE U, COQUERET X (1998) LIQ. CRYST. 24, 555.

[5] CAPACCIOLI S, PREVOSTO D, BETS A, HANEWALD A, PAKULA T (2007) J. NON-CRYST. SOLIDS 353, 4267.

[6] HAVRILIAK S, NEGAMI S. (1967) POLYMER, 8, 161; (1966) J. POLYM. SCI. C, 16, 99; RECENTLY REVISED IN HAVRILIAK SJR, HAVRILIAK S (1997) "DIELECTRIC AND MECHANICAL RELAXATION IN MATERIAL" HANSER: MUNICH.

[7] SCHÖNHALS A, KREMER F (2003) "BROADBAND DIELECTRIC SPECTROSCOPY" (EDS) F. KREMER, A. SCHÖNHALS, SPRINGER VERLAG, PP. 392 FF.

[8] SCHÖNHALS A, KREMER F (2003) "BROADBAND DIELECTRIC SPECTROSCOPY" (EDS) F. KREMER, A. SCHÖNHALS, SPRINGER VERLAG, PP. 99 FF.

[9] SCHICK CH, SUKHORUKOV D, SCHÖNHALS A (2001) MACROMOL. RAPID COMMUN. 202, 1398.

[10] SCHÖNHALS A, WOLFF D, SPRINGER J (1998) MACROMOLECULES 31, 9019.

[11] SILLESCU H (1999) J. NON-CRYST. SOLIDS 243, 8; EDIGER MD (2000) ANNU. REV. PHYS. CHEM. 51, 99.

[12] BÖHMER R, NGAI KL, ANGELL CA, PLAZEK DJ (1993) J. CHEM. PHYS. 99, 4201.

[13]. MOYNIHAN CT, MACEBO PB, MONTROSE CJ ET AL. (1976) ANN. N. Y. ACAD. SCI. 279, 15.

[14] SCHÖNHALS A, KREMER F (2003) "BROADBAND DIELECTRIC SPECTROSCOPY" (EDS) F. KREMER, A. SCHÖNHALS, SPRINGER VERLAG, CH.1.

[15] SCHÖNHALS A, KREMER F (2003) "BROADBAND DIELECTRIC SPECTROSCOPY" (EDS) KREMER F, SCHÖNHALS A, SPRINGER VERLAG, PAGE 59.

[16] ROZANSKI SA, KREMER F, GROOTHUES H, STANNARIUS R (1997) MOL. CRYST. LIQ. CRYST. 303, 319.

[17] CRAMER CH, CARMER TH, KREMER F, STANNARIUS R (1997) J. CHEM. PHYS. 106 (9), 3730.

[18]ROZANSKI SA, STANNARIUS R, GROOTHUES H, KREMER F (1996) LIQ. CRYST. 20 (1), 59.

[19] SINHA G, LEYS J, GLORIEUX C, THOEN J (2005) PHYS. REV. E 72, 051710.

[20] JOHARI GP, KIM S, SHANKER RM (2007) J. PHARM. SCI. 96, 1159.

[21] HUTH H, WANG L-M, SCHICK C, RICHERT R (2007) J. CHEM. PHYS. 126, 104503-1.

[22] SCHUG K, MCNAIR HM (2002) J. SEP. SCI. 25, 760.

[23] LOO JA (1997) MASS SPECTROM. REV. 16, 1.

[24] KOSHY KM, BOGGS JM (1996) J BIOL CHEM, 271, 3496.

[25] SCHUG K, MCNAIR HM (2003) J. CHROMATOGR. A, 985, 531.

[26] SILVERSTEIN RM, BASSLER GC, MORRIL TC (1991) SPECTROMETRIC IDENTIFICATION OF ORGANIC COMPOUNDS, 5TH ED.; JOHN WILEY & SONS: NEW YORK.

[27] DONG J, OZAKI Y, NAKASHIMA K (1997) MACROMOLECULES, 30, 1111.

[28] SETOGUCHI Y, MONOBE H, WAN W, TERASAWA N, KIYOHARA K, NAKAMURA N, SHIMIZU Y (2004) MOL. CRYST. LIQ. CRYST. 412, 9.

[29] SHANKLAND N, WILSON CC, FLORENCE AJ, COX PC (1997) ACTA CRYST. C53, 951.

[30] MCCONNELL JF (1974) CRYST. STRUCT. COMM. 3, 73-75.

[31] BRAS AR, NORONHA JP, ANTUNES AMM, CARDOSO MM, SCHONHALS A, AFFOUARD F, DIONISIO M, CORREIA NT (2008) J. PHYS. CHEM. B 112, 11087.

[32] VUEBA ML, PINA ME, DE CARVALHO LAEB (2007) J. PHARM. SCI., 97, 834.

[33] SAIZ L, PADRO JA, GUARDIA E (1999) MOL. PHYS. 97, 897.

[34] HANSEN LK, PERLOVICH GL, BAUER-BRANDL A (2003) ACTA CRYST. E59, O1357.

[35] HANSEN LK, PERLOVICH GL, BAUER-BRANDL A (2006) ACTA CRYST. E62, E17.

[36] LERDKANCHANAPORN S, DOLLIMORE D (1997) J. THERM. ANAL. 49, 879.

[37] ROMERO AJ, SAVASTANO L, RHODES CT (1993) INT. J. PHARM. 99, 125.

[38] XU F, SUN L-X, TAN Z-C, LIANG J-G, LI R-L (2004) THERMOCHIM. ACTA 412, 33.

[39] JONSCHER AK (1999) J. PHYS. D: APPL. PHYS. 32: R57-R70.

40. F. KREMER AND S. A. RÓŻAŃSKI, (2003) "BROADBAND DIELECTRIC SPECTROSCOPY" (EDS.) F. KREMER, A. SCHÖNHALS, SPRINGER, CH.12.

[41] NEAGU E, PISSIS P, APEKIS L, GOMEZ RIBELLES JL (1997) J. PHYS. D: APPL. PHYS. 30, 1551.

[42] SUN M, PEJANOVIĆ S, MIJOVIĆ J (2005) MACROMOLECULES 38, 9854.

[43] LU H, ZHANG X, ZHANG H (2006) J. APPL. PHYS. 100:054104-1 - 054104-7.

[44] KOHLRAUSCH R (1847) POGG. ANN. PHYS (III) 12, 393.

[45] WILLIAMS G, WATTS DC (1966) TRANS. FARADAY. SOC. 66, 80.

[46] ALVAREZ F, ALEGRÍA A, COLMENERO J (1991) PHYS. REV. B, 44, 7306.

[47] BÖTTCHER CJF (1973) "THEORY OF DIELECTRIC POLARIZATION", ELSEVIER: AMSTERDAM, VOL. 1; BÖTTCHER CJF, BORDEWIJK P (1978) THEORY OF DIELECTRIC POLARIZATION, ELSEVIER: AMSTERDAM, VOL. 2.

[48] FRISCH MJ, TRUCKS GW, SCHLEGEL HB, SCUSERIA GE, ROBB MA, CHEESEMAN JR, ZAKRZEWSKI VG, MONTGOMERY JA, STRATMANN RE, BURANT JC, DAPPRICH S, MILLAM J M, DANIELS A, KUDIN KN, STRAIN MC, FARKAS O, TOMASI J, BARONE V, COSSI M, CAMMI R, MENNUCCI B, POMELLI C, ADAMO C, CLIFFORD S, OCHTERSKI J, PETERSSON GA, AYALA PY, CUI Q, MOROKUMA K, MALICK DK, RABUCK AD, RAGHAVACHARI K, FORESMAN JB, CIOSLOWSKI J, ORTIZ JV, STEFANOV BB, LIU G, LIASHENKO A, PISKORZ P, KOMAROMI I, GOMPERTS R, MARTIN RL, FOX DJ, KEITH T, AL-LAHAM MA, PENG CY, NANAYAKKARA A, GONZALEZ C, CHALLACOMBE M, GILL PMW, JOHNSON B, CHEN W, WONG MW, ANDRES JL, HEAD-GORDON M, REPLOGLE ES, POPLE JA (1998) GAUSSIAN98, REVISION A.7. GAUSSIAN, INC.: PITTSBURG, PA.

[49] SCHÖNHALS A (1997) "DIELECTRIC SPECTROSCOPY OF POLYMERIC MATERIALS" (EDS.) RUNT J, FITZGERALD J, ACS BOOKS: WASHINGTON.

[50 SCHÖNHALS A (2003) "BROADBAND DIELECTRIC SPECTROSCOPY" (EDS.) KREMER F, SCHÖNHALS A, SPRINGER VERLAG: BERLIN, CH. 7.

[51] HANSEN C, STICKEL F, BERGER T, RICHERT R, FISCHER EW (1997) J. CHEM. PHYS. 107, 1086.

[52] NGAI KL, PALUCH M (2004) J. CHEM. PHYS. 120, 857.

[53] WAGNER H, RICHERT R (1999) J. PHYS. CHEM. B 103, 4071.

[54] DÖSS A, PALUCH M, SILLESCU H, HINZE G (2002) PHYS. REV. LETT. 88, 095701.

[55] CASALINI R, FIORETTO D, LIVI A, LUCCHESI M, ROLLA PA (1997) PHYS. REV. B 56, 3016.

[56] HARTMANN L, KREMER F, POURET P, LÉGER L (2003) J. CHEM. PHYS. 118, 6052.

[57] SMITH IK, ANDREWS SR, WILLIAMS G, HOLMESB PA (1997) J. MATER. CHEM. 7, 203.

[58] VICIOSA MT, RODRIGUES C, FERNÁNDEZ S, MATOS I, MARQUES MM, DUARTE MT, MANO JF, DIONÍSIO M (2007) J. POLYM. SC.: PART B: POLYM. PHYS. 45, 2802.

[59] SCHÖNHALS A, KREMER F (2003) "BROADBAND DIELECTRIC SPECTROSCOPY" (EDS.) KREMER F, SCHÖNHALS A, SPRINGER VERLAG: BERLIN, CH. 3.

[60] STICKEL F, FISCHER EW, RICHERT R (1996) J. CHEM. PHYS. 104, 2043.

[61] RIVERA A, RÖSSLER EA (2006) PHYS. REV. B 73, 212201-1.

[62] KAMINSKI K, KAMINSKA E, PALUCH M, ZIOLO J, NGAI KL (2006) J. PHYS. CHEM. B 110, 25045.

[63] COREZZI S, BEINER M, HUTH H, SCHRÖTER K, CAPACCIOLI S, CASALINI R, FIORETTO D, DONTH E (2002) J. CHEM. PHYS. 117, 2435.

[64] PALUCH M, ROLAND CM, PAWLUS S, ZIOLO J, NGAI KL (2003) PHYS. REV. LETT. 91, 115701.

[65] CAPACCIOLI S, KESSAIRI K, PREVOSTO D, LUCCHESI M, NGAI KL (2006) J. NON-CRYST. SOLIDS 352, 4643.

[66] CAPACCIOLI S, KESSAIRI K, PREVOSTO D, LUCCHESI M, ROLLA PA (2007) J. PHYS.: CONDENS. MATTER, 19, 205133.

[67] NGAI KL (2003) J. PHYS.: CONDENS. MATTER 15, S1107.

[68] NGAI KL, CAPACCIOLI S (2004) PHYS. REV. E 69, 031051.

[69] KUDLIK A, TSCHIRWITZ C, BLOCHOWICZ T, BENKHOF S, RÖSSLER E (1998) J. NON-CRYST. SOLIDS 235-237, 406.

[70] WANG L-M, RICHERT R (2007) PHYS. REV. B 76, 064201.

[71] CARPENTIER L, DECRESSAIN R, DESPREZ S, DESCAMPS M (2006) J. PHYS. CHEM. B 110, 457.

[72] NOZAKI R, ZENITANI H, MINOGUCHI A, KITAI K (2002) J. NON-CRYST. SOLIDS 307-310, 349.

[73] NATH R, EL GORESY T, GEIL B, ZIMMERMANN H, BÖHMER R (2006) PHYS. REV. E. 74, 021506.

[74] NATH R, NOWACZYK A, GEIL B, BÖHMER R (2007) J. NON-CRYST. SOLIDS 353, 3788.

[75] BERG OVD, WÜBBENHORST M, PICKEN SJ, JAGER WF (2005) J. NON-CRYST. SOLIDS 351, 2694.

[76] DONTH E, "THE GLASS TRANSITION" (2001), SPRINGER VERLAG, BERLIN.

[77] SCHÖNHALS A., KREMER F "BROADBAND DIELECTRIC SPECTROSCOPY" (2003) (EDS.) KREMER F, SCHÖNHALS A, SPRINGER VERLAG: BERLIN, CH. 4 AND REFERENCES THEREIN.

[78] STICKEL F, FISCHER EW, RICHERT RJ (1996) CHEM. PHYS. 104, 2043.

[79] SCHÖNHALS A, SCHICK CH, HUTH H, FRICK B, MAYOROVA M, ZORN R (2007) J. NON-CRYST. SOLIDS 353, 3853.

[80] NGAI KL, LUNKENHEIMER P, LEÓN C, SCHNEIDER U, BRAND R, LOIDL A (2001) J. CHEM. PHYS. 115, 1405.

[81] BEINER M, (2001) MACROMOL. RAPID COMMUN. 22, 869.

[82] BÖHMER R, NGAI KL, ANGELL CA, PLAZEK DJ (1993) J. CHEM. PHYS. 99, 4201.

[83] WANG L-M, RICHERT R (2005) J. PHYS CHEM. B LETT. 109, 1091.

[84] PALEOS C, TSIOURVAS D (2001) LIQ. CRYST. 28, 1127.

[85] CHEN W, WUNDERLICH B (1999) MACROMOL. CHEM. PHYS. 200, 283.

[86] MOURA RAMOS JJ, DIOGO HP, GODINHO MH, CRUZ C, MERKEL K (2004) J PHYS. CHEM. B 108, 7955.

CHAPTER 4| MOLECULAR DYNAMICS IN CONFINED SPACE

INDEX

This subchapter was published in *Journal of Physical Chemistry B* (2008) **112** 8227-8235

4.1 E7 Confined in Untreated and Treated Anopore Membranes

4.1.1 Introduction

Broadband dielectric spectroscopy (10^{-2} to 10^{9} Hz) was employed to investigate the molecular dynamics of the liquid crystalline mixture $E7$ confined in both untreated and lecithin treated 20 nm Anopore membranes. Because $E7$ does not crystallize it was possible to cover a temperature range of more than 200 K providing an exhaustive dielectric characterization of a liquid crystal (LC) confined to Anopore membranes for the first time. In the nematic state the tumbling (α-) and the δ-relaxations are observed also under confinement conditions. The analysis of their relative intensities give that the orientation of the $E7$ molecules is preferentially axial in untreated but opposite radial in lecithin treated pores. The radial alignment of the LC in the modified membrane is understood as a tail-to-tail conformation of $E7$ molecules imposed by the adsorbed lecithin molecules.

The relaxation times of the α process is lower for $E7$ confined in native Anopore compared with the bulk and $E7$ in treated pores. This is interpreted as resulting from a less dense molecular packing of $E7$ in the middle of the pore compared to the bulk. In both untreated and treated membranes, the relaxation times of the δ process is lower than in the bulk and the values of the respective Vogel-Fulcher-Tammann temperatures depend on the actual surface treatment. Additionally, a surface process was detected due to molecular fluctuations of molecules within an adsorbed layer at the pore wall.

4.1.2 Experimental Conditions

The experimental procedure is described in Chapter II.

The degree of filling was estimated by weighing. For E7 confined in untreated membrane, assuming that the density of the LC within the pores is the same as in the bulk state, the amount of the molecules within the pores can be calculated from the porosity (given by the manufacturer) and compared with the experimental data. Each single disk contained 0.7 mg of $E7$ which supposes an estimated average filling degree of about 96.5%, similar to that obtained by other authors for different liquid crystals (LC's) [1,2]. Two different membranes were prepared with lecithin treated pore surfaces. The first one serves as blank sample to study only the behavior of the lecithin layer. In the second one $E7$ was also injected (see Chapter II). The filling degree was estimated to 92.8%. This calculus is based on the assumption that the lecithin amount in the blank sample is the same than for that specimen filled with $E7$. So the volume available for $E7$ inside the pores was recalculated subtracting a layer of 2 nm thickness from the pore radius due to the adsorbed lecithin. The filling degree seems to be a bit lower

for treated pores but is comparable to the value found for native ones. Finally, a cleaned but empty Anopore membrane is measured for comparison as well.

Dielectric spectra (for more details see Chapter II) were recorded by varying the temperature from 153 to 411 K, in steps of 2 K, in order to cover both isotropic and nematic phases down to the glass transition temperature of $E7$.

4.1.3 Results and Discussion

Figure 4. 1 presents some isothermal dielectric loss spectra of $E7$ confined in an untreated Anopore membrane in the available frequency range at temperatures from 215 to 411 K. That figure includes measurements in both the nematic and the isotropic phase. As a first observation, in the nematic state two peaks are detected where the most prominent is associated to $\varepsilon_{\parallel}^{*}(\omega)$, the δ process. The process mainly associated with $\varepsilon_{\perp}^{*}(\omega)$, ($\alpha$ process), has a much lower intensity and is located at higher frequencies compared to the δ-relaxation as discussed in Chapter III.

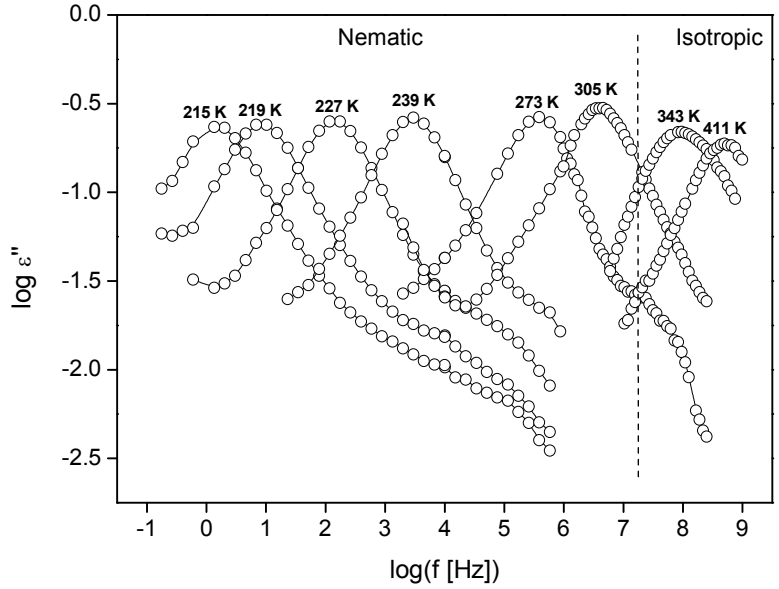

Figure 4. 1- Isothermal dielectric loss spectra for an unaligned sample of $E7$ confined in untreated Anopore over all the frequency range studied and cover both nematic and isotropic states. Lines are guides to the eyes.

Both processes merge in a broadened peak for temperatures higher than $T_{NI} = 333\,K$ (loss curves presented in Figure 4. 1, at 343 and 411 K). The relative intensities of the δ- and α- relaxations in the nematic range, indicate that $E7$ is mainly axially oriented in the pores, *i.e.*, molecules are aligned more or less parallel to the cylindrical pore axis. This means that the nematic director is aligned parallel to the applied electrical field as already observed for bulk $E7$ on a gold substrate (Chapter III and references [3,4]).

The complete dielectric spectra of *E*7 confined to treated pores is given in Figure 4. 2a) in a 3D representation *versus* frequency and temperature. At low temperatures (high frequencies) the already discussed α- and δ-relaxations are observed. At lowest frequencies and highest temperature an electrode polarization phenomenon takes place. In-between the electrode polarization and the two above mentioned loss peaks, an additional dielectric process can be identified as a maximum in the dielectric loss. It is assigned to the fluctuations of an adsorbed surface layer as will be discussed in detail below. Therefore this process will be called surface process.

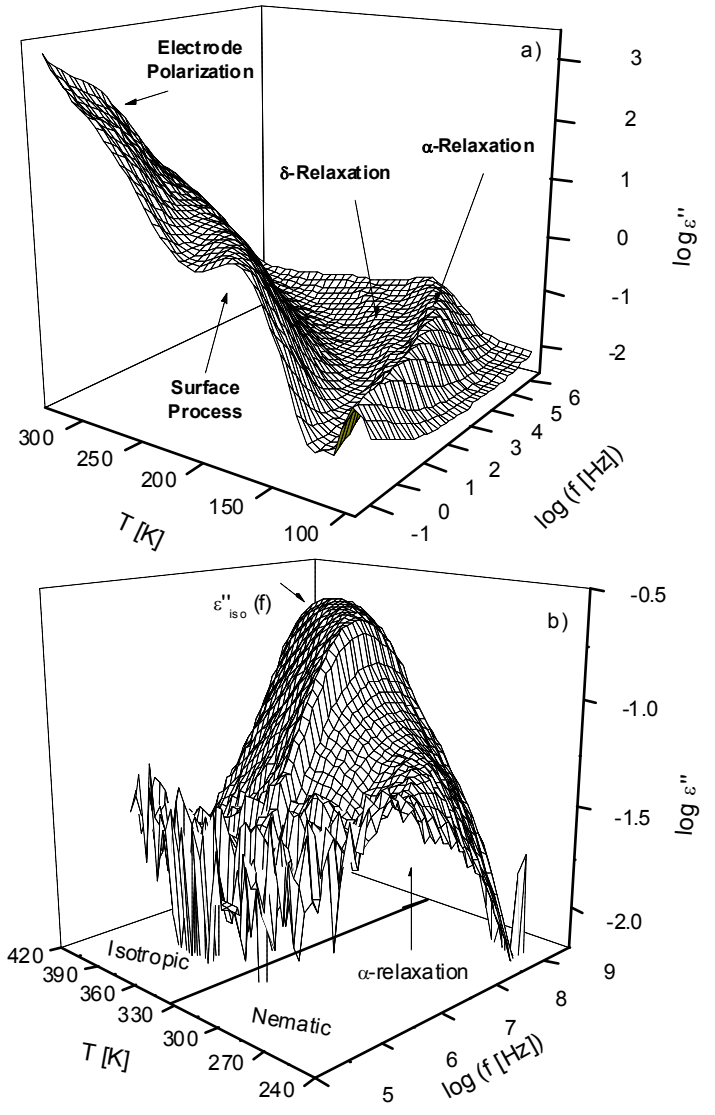

Figure 4. 2- Dielectric loss *versus* frequency and temperature for *E*7 confined in a lecithin treated Anopore membrane a) in the low frequency range and b) in the high frequency range.

To demonstrate that *E*7 undergoes also in the pores the phase transition from the nematic to the isotropic state, Figure 4. 2b) presents the 3D plot of the loss spectra collected in the high frequency region for *E*7 embedded into the lecithin treated Anopore membrane. At the phase transition, the dielectric loss changes dramatically in its frequency and temperature dependence. In the temperature

range of the isotropic phase a single process is observed as mentioned above. But also for temperatures lower than T_{NI} only one peak instead of the expected two is detected. Its frequency position seems to be a bit higher than that in the isotropic phase which might indicate that the process is the α-relaxation.

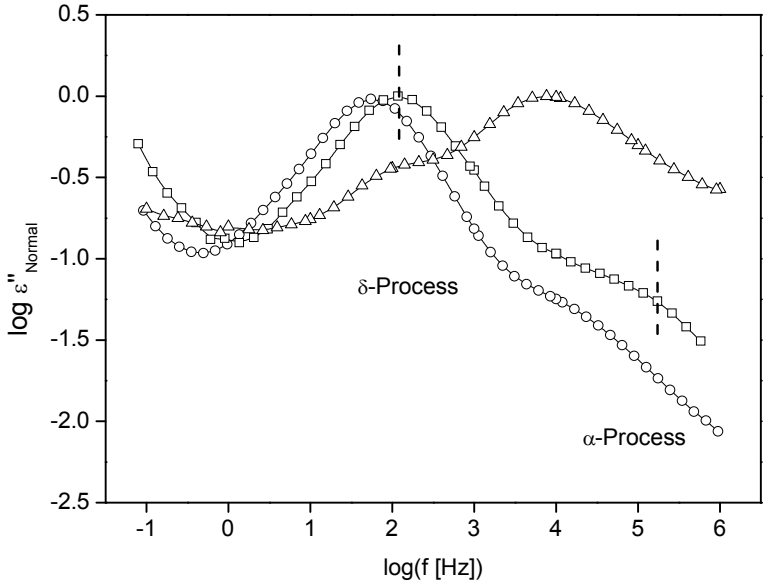

Figure 4. 3- Dielectric loss *versus* frequency at T=227 K for $E7$ in the bulk (○), confined to untreated (□) and lecithin treated (△) Anopore membrane. For each sample the dielectric loss is normalized to its maximum value. Lines are guide to the eyes.

That leads to the conclusion that the orientation of the molecules is changed in the treated pores compared to the untreated ones as discussed also in [5,6,7]. To demonstrate this in more detail Figure 4. 3 compares the dielectric loss *versus* frequency for $E7$ confined to untreated and treated pores at same temperatures together with data for the bulk LC. Because the dielectric losses are quite different in their absolute values, the data are normalized with regard to the corresponding maximum value. The relative dielectric strengths of δ- and α-relaxations are quite similar for bulk $E7$ and confined to untreated pores. This means - as discussed before - that the dipole moment of the molecules is oriented preferentially parallel to the axes of the untreated pores. This is different for $E7$ embedded in treated Anopore. In that case the α-relaxation is much stronger in intensity than the δ process. This leads to the conclusion that for treated pores the nematic director is preferentially oriented radial to the direction of the pore axis. The induction of a radial orientation of single component cyanobiphenyl based LC confined in lecithin treated pore walls is reported also in [8,9,10,11]. But for $E7$ in lecithin treated Anopore membranes this is reported here for the first time.
The change of the orientation of $E7$ molecules can be rationalized by a simple model. The lecithin molecules are anchored to the pore surface by the polar head group. So the apolar tails (see Figure 2.11 in Chapter II) are preferentially directed to the pore center. The whole native pore surface

is so decorated with alkyl chains. When the molecules of *E*7 are embedded in the modified pores their apolar tails are forced to orient in a tail-to-tail conformation. Figure 4. 4 illustrated it schematically:

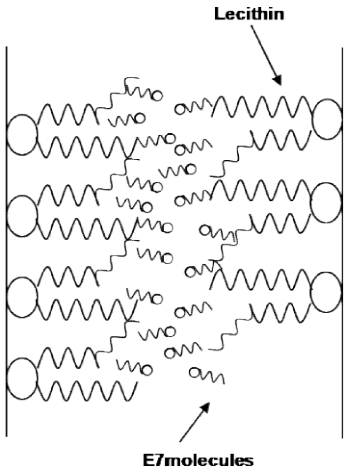

Figure 4. 4- Schematic picture of the *E*7 molecular arrangement in a lecithin treated pore; molecules adopt preferentially a radial orientation assuming a tail-to-tail conformation with the hydrophobic lecithin moiety.

A closer inspection of Figure 4. 3 shows that also the frequency position of the relaxation processes for confined *E*7 is shifted in comparison to the bulk. This shift depends on the treatment of the pore surfaces. To analyze these findings in more detail, the model function of Havriliak and Negami [12] (HN-function) is fitted to the dielectric spectra (Equation 1.35 in Chapter I). For details see [13] and Chapter I.

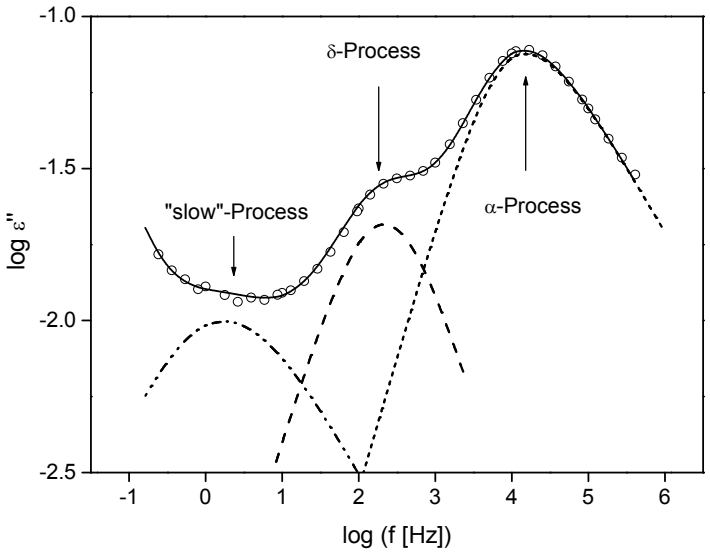

Figure 4. 5- Dielectric loss *versus* frequency at T=229 K for *E*7 confined in lecithin treated Anopore. The solid line is a fit of a sum of three HN-function to the experimental data. The other lines give the contributions of the individual processes to the dielectric loss: dashed-dotted-dotted: slow process; dashed: *δ*-relaxation; short dashed: *α*-relaxation

Figure 4. 5 gives an example of the fitting procedure of three HN-functions to the dielectric spectrum of $E7$ confined in the lecithin treated membrane at 229 K. The "slow process" detected at the lowest frequencies in addition to the δ- and the α-relaxations was also observed for bulk $E7$ (see Chapter III and refs [3,4,14,15]) and therefore cannot be assigned as originating from a surface layer in confinement (see also [16,17 ,18,19]). Its molecular origin is not clear up to now for the bulk as well.
The shape parameters are almost independent of temperature and pore treatment. For the δ- relaxation a Debye-like behavior ($\alpha_{HN} \approx 1$; $\beta_{HN} \approx 1$) is found for both natural and treated pores as it is already known for the bulk. The α process has an asymmetric broadened relaxation function ($\alpha_{HN} \approx 0.7$; $\alpha_{HN} \cdot \beta_{HN} \approx 0.4$).

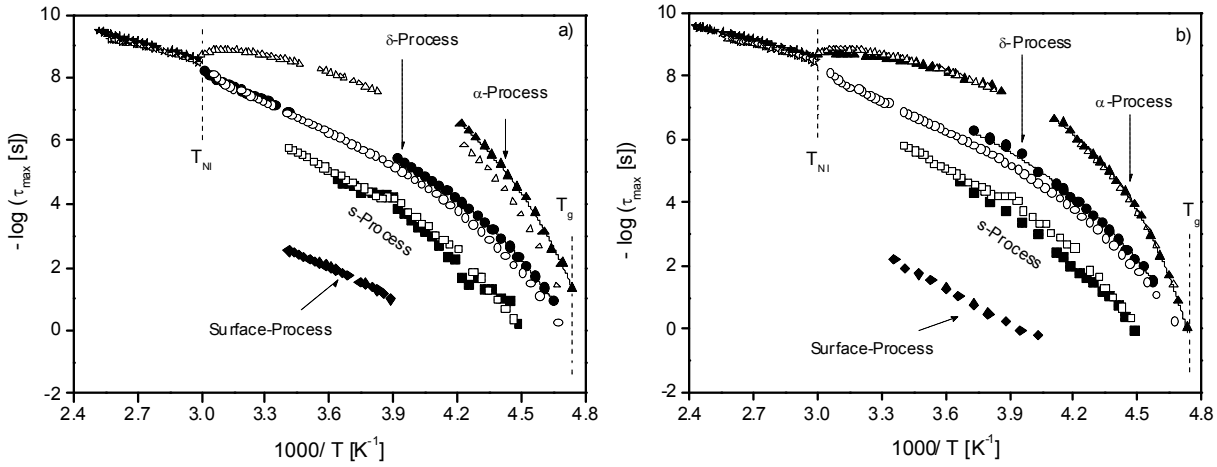

Figure 4. 6- Relaxation times, τ_{max}, *versus* $1/T$ for the different processes for $E7$ embedded in different pores. The solid symbols correspond to confined $E7$ where the open ones are data for the bulk: Triangles- α-relaxation; circles - δ-relaxation; squares – slow process; diamonds- surface process. The lines are fits of the VFT-equation to the data as described in the text.

(a) $E7$ confined in native pores of the Anopore membrane.

(b) $E7$ confined embedded in lecithin coated pores of the Anopore membrane.

The , times τ_{max}, obtained from the fits for the different relaxation processes are plotted *versus* the inverse of temperature in Figure 4. 6a) for $E7$ confined in untreated and in Figure 4. 6b) for $E7$ confined in lecithin treated Anopore membranes. The data for bulk $E7$ are included for comparison (open symbols).
The temperature dependence of the relaxation times of the slow-process seems to be nearly activated and no influence due to the confinement could be detected. Because the molecular origin of this process is not clear up to now it is not further discussed here.
As it is known for the bulk $E7$ the temperature dependence of both the α and the δ processes are curved *versus* $1/T$ and can be described close to T_g by the VFT-equation (Equation 1.2 in Chapter I) also in confinement. For bulk $E7$ it was found that both dependencies seem to merge close to the glass

transition temperature and have quite different Vogel temperatures T_0 (Chapter III and ref. [3]). The same is true for $E7$ confined to native and treated Anopore membranes.

Before analysing the temperature dependence of the relaxation times in more detail, it is worth to point out that when the LC is confined in the untreated membrane, the absolute values of the relaxation times for both the $\alpha-$ and the $\delta-$ relaxations are lower than in the bulk. This means that the confined $E7$ molecules fluctuate faster compared to the bulk. This is already seen in the raw data (see Figure 4. 3) by the shift of both loss peaks to higher frequencies for confined $E7$ with respect to the bulk. The magnitude of the discussed effects is within one decade. When $E7$ is embedded in lecithin treated Anopore, the δ process also shifts to higher frequencies. Nevertheless, no changes seem to occur with regard to the α-relaxation. This will be discussed later on. Also in the isotropic state the relaxation time is only barely influenced by the confinement (see Figure 4. 6 a and b). Similar findings are reported for different LC's embedded in porous membranes (see [22] and references therein).

Table 4. 1- Estimated VFT-parameters for the different processes and samples. The Vogel temperature and the A parameter were taken from the derivative technique. The prefactors were obtained by a fit of the VFT-equation to the relaxation times keeping T_0 and A fixed. D was calculated according to Equation 1.17 in Chapter I.

Process	*Sample*	$-log_{10}(\tau_\infty\,[Hz])$	$T_0[K]$	$A\,[K]$	D
α- *relaxation*	Bulk	11.2	190.1	225	2.7
	untreated	12.8	179.1	366	4.7
	treated	11.1	190.0	236	2.8
δ- *relaxation*	Bulk	11.2	161.0	576	8.2
	untreated	11.0	165.0	498	6.9
	treated	10.7	171.1	436	5.9

In the following the derivative method [20,21] is applied to both the α- relaxation (Figure 4. 7a) and the δ process (Figure 4. 7b) where the data for the different confined $E7$ were compared with the corresponding bulk close to T_g. First, it is concluded that indeed for all considered processes the temperature dependence of the relaxation times follow the VFT law. All experimental data can be well described by straight lines. But as a second result it is obtained that the Vogel temperature T_0 is influenced by the confinement. To estimate the parameters of the VFT-equation and the fragility parameter D for a quantitative comparison, the following procedure was applied. T_0 and the A parameter were taken from the derivative technique by linear regression. The pre-factors were obtained by a fit of the VFT-equation to the relaxation times keeping T_0 and A fixed. All parameters are collected in Table 4. 1.

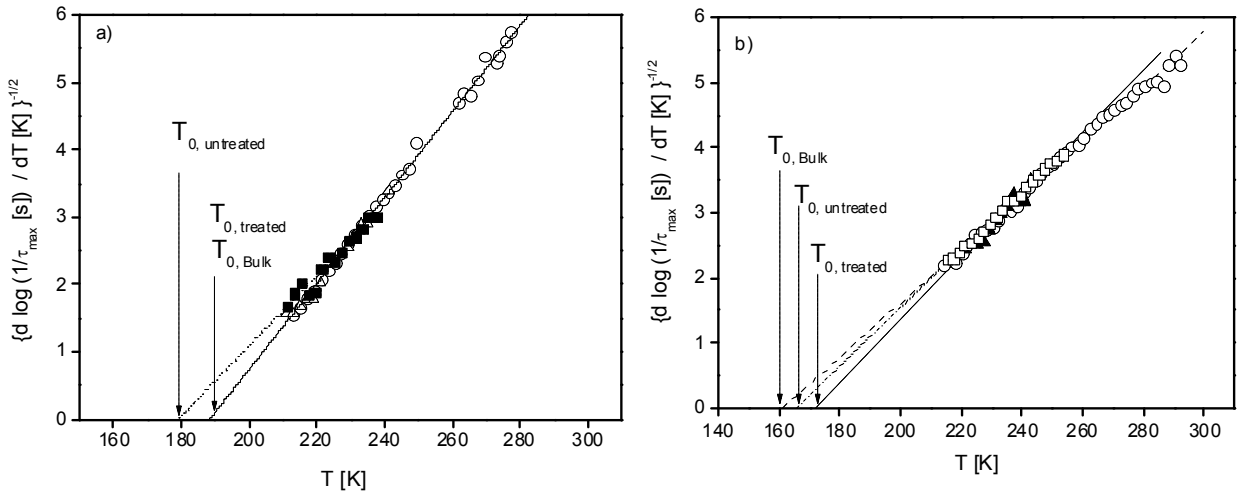

Figure 4. 7- $[d\log(1/\tau_{max})/dT]^{-1/2}$ *versus* temperature for the a) α process: ○ - Bulk; ■ -untreated pores; Δ - lecithin treated pores. Lines are linear regressions to the data: dashed – untreated; solid – bulk and treated; b) δ process: ○ - Bulk; □ -untreated pores; ▲ - lecithin treated pores. Lines are linear regressions to the data: dashed line – bulk; dashed doted – untreated; solid line – treated.

Next, the influence of the confinement on the different processes will be discussed:

α- Relaxation: It becomes evident (also from the raw spectra, see Figure 4. 3) that for $E7$ confined to untreated pores the relaxation time is lower than in the bulk state and for treated pores (see Figure 4. 6a). The data of the latter ones collapse into one chart (see Figure 4. 6b)–and the corresponding derivative analysis (see Figure 4. 7a) shows that the Vogel or ideal glass transition temperatures are the same, 190 K. T_0 for the α-relaxation of $E7$ embedded in native pores is by 11 K lower. This is a significant effect (see Table 4. 1). Also the fragility is higher for the α-relaxation in untreated pores. At the first glance that might be interpreted as confinement effect as discussed in Chapter I. But taking this interpretation, also the data obtained for the treated pores should be affected in a similar way which is not the case. Moreover a pore size of 20 nm seems to be too large to cause considerable effects on the α- relaxation [22,23]. Therefore the origin of the lowered T_0 for the α- relaxation in untreated pores should be of different nature. For native pores the polar groups of the molecules of $E7$ will interact with the pore surface. This increases the densities of molecules in a layer close to the surface leading to a lower dense packing in the middle of the pore than in the bulk $E7$. In consequence the mobility is enhanced and a lowered T_0 is observed. For treated pores the guest molecules do not interact directly with the surface and therefore a behaviour similar than in the bulk is observed.

δ-Relaxation: The relaxation times of the δ process in both native and lecithin treated pores are lower than in the bulk (see Figure 4. 7a). The respective derivative plot (see Figure 4. 7b) gives that also the Vogel temperature and fragility varies systematically with the treatment of the pores. The lowest

Vogel temperature is found for bulk $E7$, followed by that of $E7$ in untreated pores. For the δ −relaxation of $E7$ confined to treated pores a 10 K higher value of T_0 is obtained compared to the bulk (see Table 4. 1). This is again a significant effect. The origin of the δ-relaxation are rotational fluctuations of the molecules around its short axis. The length scale of the involved molecular fluctuations should be larger than that of the α process. Therefore this relaxation process is more sensitive to surface interaction than the former one.

Dielectric relaxation strength

The absolute values of the dielectric relaxation strengths for the α- and δ-relaxations depend on the orientation of the molecules. For the confined $E7$ the orientation of the molecules cannot be quantified. Therefore here only the dielectric strengths, $\Delta\varepsilon$, in the isotropic range which do not depend on the orientation are compared. The values are normalized with respect to the pore volume fraction (Figure 4. 8). The Debye theory of dielectric relaxation generalized by Kirkwood and Fröhlich [24] predicts the temperature dependence of the dielectric relaxation strength according to Equation 1.46 in Chapter I.

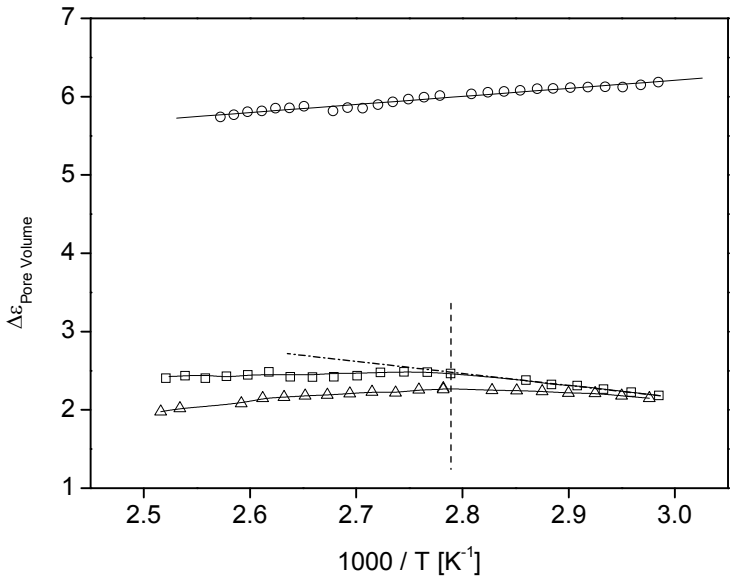

Figure 4. 8- Δε normalized to the pore fraction *versus* inverse temperature for temperatures higher than $T_{N/I}$.: ○ - Bulk; □ -untreated pores; △ - lecithin treated pores. Lines are guides for the eyes. The dashed dotted line indicates the increase of $\Delta\varepsilon$ at lower temperatures for $E7$ confined to untreated pores.

The dielectric strength for bulk $E7$ is by a factor of approximately 3 times higher than that for confined $E7$. According to Equation 1.46 of Kirkwood and Fröhlich this means that a large fraction of molecules do not contribute to that relaxation process at these temperatures and frequencies. These molecules strongly interact with the surface and are slowed down in their mobility or become completely immobilized which will be discussed later. Moreover the temperature dependency for

confined $E7$ is different in confinement that in the bulk. For the latter, $\Delta\varepsilon$ decreases with $1/T$ as expected. For confined $E7$, $\Delta\varepsilon$ first increases slightly up to a certain temperature and than decreases with further increase of temperature. This can be understood assuming two competing effects. On the one hand thermal energy kT increases with increasing temperature. This would lead to decrease of $\Delta\varepsilon$ according to Equation 1.46. On the other hand, due to a reduced interaction the adsorbed molecules become more mobile with increasing temperatures. This can be expressed by a growing number density of contributing dipoles. So for lower temperatures the increase of the dipole density overcompensate the influence of the thermal energy. At higher temperatures, the thermal energy wins although the decrease in $\Delta\varepsilon$ is still smaller than in the bulk.

There are also differences between the temperature dependencies of $\Delta\varepsilon$ for $E7$ confined to native and treated pores. For $E7$ confined to native pores $\Delta\varepsilon$ is more or less constant whereas $\Delta\varepsilon$ for $E7$ confined to treated pores decreases. To understand this, one has to keep in mind that for native pore the $E7$ molecules – which are monitored by dielectric spectroscopy – directly interact with the surface (hard interface) whereas for treated pores the lecithin molecules are in between the hard pore walls and the $E7$ (soft interface). For that reason the increase in the dipole density with temperature is stronger for $E7$ embedded in native pores than for treated pores because in the latter case the $E7$ molecules are already more decoupled/less anchored from the surface. This results in a stronger decrease of $\Delta\varepsilon$ with increasing temperature for lecithin treated pores.

Surface Relaxation: Figure 4. 2 shows that there is an additional process located at essential lower frequencies than the α and δ processes. At a first glance that might be due to a Maxwell/Wagner/Sillars polarization. Such a phenomenon is related to the blocking of charge carriers at interfaces as observed for nanoporous hosts [25]. But in the experiment presented here the cylindrical pores are perfectly oriented in the direction of the electrical field which drives the charge carriers. Therefore the probability of the blocking of charge carriers is low. But the analysis of the relaxation strength gives that a considerably amount of molecules are in close interaction with the surface. As a consequence the molecular mobility of these molecules is slowed down. So the fluctuations of a part of these molecules should be observed by dielectric spectroscopy at higher temperatures and lower frequencies. Therefore the relaxation process observed at lower frequencies than the α and δ processes is assigned to molecules which are slowed down due to the interaction with the surface.

To confirm this interpretation measurements for an empty and a lecithin coated Anopore membrane are carried out. For T = 298 K the dielectric loss is compared for the empty, the blank lecithin coated and $E7$ in treated pores in the inset of Figure 4. 9. For the empty Anopore besides an electrode polarization no dielectric active process is observed. In difference to the empty membrane, a further relaxation process is observed for the lecithin modified membrane. Because the only difference to the empty membrane is the lecithin layer this process is assigned to fluctuations of the adsorbed lecithin molecules in that surface layer. NMR studies confirm the existence of molecular motions in close

packed adsorbed lechitin like reorientational fluctuations whit the polar head group fixed at the pore surface [26]. For the *E7* filled lecithin treated membrane, nearly at the same frequency position, the surface process discussed above is observed. This coincidence gives further evidence that this assignment seems to be correct.

The processes are also analyzed by fitting the HN-function to the data. Due to the electrode polarization phenomena only the relaxation time can be estimated (see Figure 4. 9). Their temperature dependencies seem to be linear *versus* $1/T$ and an apparent activation E_A can be estimated. For the membrane coated only with the lecithin layer a rather high value of 166 kJ/mol is obtained. This point to a strong adsorption of the lecithin molecules on the pore walls of the Anopore membrane. For *E7* confined to the Anopore membrane lower values are obtained which depend on the surface treatment: 70 kJ/mol for lecithin treated pores and 59 kJ/mol for native pores. It is worth to note that the value estimated for treated pores is in between that calculated for native and the single lecithin coated pores. Obviously the strongly adsorbed lecithin molecules have a considerable impact on the molecular fluctuations of the near surface *E7* molecules. This is also in agreement with the observation that for treated pores the highest value of the Vogel temperature is observed.

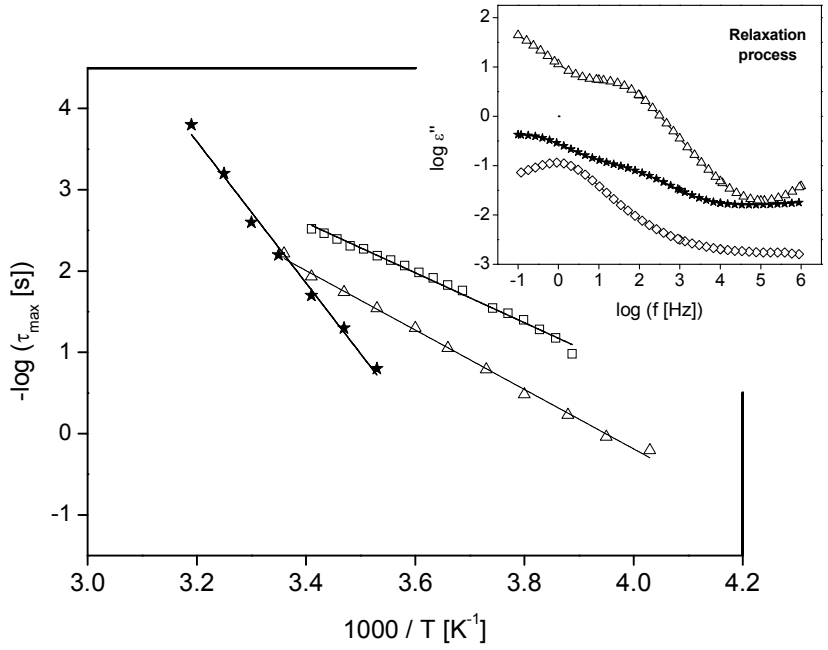

Figure 4. 9- Relaxation times, τ_{max}, *versus* $1/T$ for the surface process: ★ - lecithin layer; △ - *E7* in lecithin coated pores; □- *E7* in native pores. Lines are fits of the Arrhenius equation to the data. The inset gives the dielectric loss *versus* frequency at T = 303 K for an empty Anopore membrane (◇), pores coated with a lecithin layer (★) and *E7* in lecithin treated pores (△). Lines are guides for the eyes.

4.1.4 Conclusions

Broadband dielectric relaxation spectroscopy was employed for the first time to investigate the molecular dynamics of a nematic liquid crystal, $E7$, confined to both native and lecithin treated pores of Anopore membranes. A wide temperature range was used to cover the isotropic to nematic phase transition down to the glass transition temperature.

Besides the relaxation peak characteristic for the isotropic state (above 333 K), two main relaxation processes were detected in the nematic range, labelled as α- and δ-relaxations in order of decreasing frequency. The former process is related to molecular tumbling modes where the latter is due to rotational fluctuations around the molecular short axis of the molecules. The relative intensities of both relaxation processes are directly related to the orientation of the nematic director with respect to the measuring electrical field. Both the alignment and the molecular mobility of $E7$ are influenced by the confinement and the treatment of the pore surfaces. In the first case when the liquid crystal is confined to the native pores of the membrane, the dominating relaxation process is the δ-relaxation, which corresponds to a preferential alignment of the nematic director aligned parallel to the electric field. Because the pores are also parallel to the field this is an indication that $E7$ molecules are mainly orientated with their long axis tangential to the pore axis. In the other case, when $E7$ is confined to the modified membrane, the prominent peak is due to the α-relaxation, corresponding to a perpendicular alignment of the nematic director with respect to the outer field. This means that the long axis of the molecules is arranged in a radial orientation perpendicular to the pore axis. The change in orientation was rationalized by a special arrangement of the $E7$ molecules as embedded in the modified pores with their apolar tails forced to adopt a tail-to-tail conformation with the hydrophobic lecithin alkyl groups.

The temperature dependence of the relaxation times of both the α and δ processes follows the VFT-equation. The relaxation time of the latter is lower by around 1 decade when $E7$ is confined to untreated pores of the Anopore membrane. A derivative method was applied to estimate the VFT-parameters especially the Vogel temperature T_0. For the α-relaxation, a T_0 value 11 K lower than for the bulk was found. This is a significant effect which however cannot be attributed to a confinement effect in that sense as discussed in the introduction chapter. A more reasonable explanation assumes a different dynamical nature of the α- relaxation, which is also supported by a change in the fragility index. The lower relaxation time can be interpreted in terms of a lower density of $E7$ in the pore centre relative to the pore wall where the molecules are anchored in a dense packing arrangement. In the treated pores of the Anopore membrane, a lecithin layer is already settled at the pore wall and the $E7$ molecules behave similar to the bulk state with regard to the α-relaxation, leaving its relaxation time unaffected.

For confined $E7$, either in native or modified pores of the Anopore membrane, the relaxation time is lower about 1 decade for the δ process and T_0 decreases with surface treatment. The higher length

scale involved in this process relatively to that of the α one makes it more sensitive to surface interactions.

The temperature dependence of the relaxation times of the relaxation process observed in the isotropic state is only barely influenced by the confinement. The main effect is considerable reduction of the dielectric relaxation strength which is explained by a relatively high amount of molecules which are immobilized at the pore walls or slowed down in their molecular mobility.

Additional to the α- and the δ-relaxations at lower frequencies, a so-called surface relaxation process is observed. This relaxation process is assigned to molecules which are in close or even strong interaction with the pore surface. The temperature dependence of the corresponding relaxation times can be described by an Arrhenius law with apparent activation energy E_A. The highest value of E_A is found for the lecithin treated in unfilled pores, followed by that of $E7$ in treated pores. The lowest E_A is found for the LC confined native pores. This is discussed in terms of the different interaction of the molecules with the pore wall.

This subchapter was submitted for publication

4.2 E7 Confined to Molecular Sieves with a Low Filling Degree

4.2.1 Introduction

The nematic liquid crystalline mixture $E7$ was confined to molecular sieves (MCM-41 and SBA-15) with constant composition (100% Si) and similar filling degrees (50-60%) but differing in their pore diameter (from 2.8 to 6.8 nm). FTIR analysis proved that the $E7$ molecules interact *via* the cyano group with the molecular sieves most probably inside the pores.

The molecular dynamics was investigated by broadband dielectric spectroscopy (10^{-2} -10^{9} Hz) covering a wide temperature range of ca. 200K from temperatures well above the isotropic-nematic transition (T_{NI} = 333 K) down to the glass transition (T_g = 211 K) of bulk $E7$. Besides a Maxwell / Wagner / Sillars polarization a variety of relaxation processes are observed including two modes which are located close to the bulk behavior. The temperature dependence of the relaxation times for these bulk-like processes coincides well with that observed for the bulk, for both the isotropic and the nematic state.

For confined $E7$ for all samples two relaxation processes, at frequencies lower than the processes observed for the bulk, were detected. At lower temperatures their relaxation times have different temperature dependencies whereas at higher temperatures they seem to collapse in one chart.

The temperature dependence of the slowest process, designated S process, obeys the Vogel-Fulcher-Tammann (VFT) law being attributed to the glass transition of the LC anchored to the inner pore surface. The pore size dependence of both the Vogel temperature and fragility index revealed a step-like transition around 4 nm with increasing pore size which can be taken as an indication of a transition from a strong to fragile behavior of adsorbed $E7$ at this confining length scale.

The process with a value of the relaxation time in between the bulk-like and the S process, named I process, shows no dependence on the pore size. The agreement of the I process with the dynamic behavior of a $5CB$ surface layer adsorbed on nonporous silica spheres leads to the assignment of the I-process to $E7$ molecules anchored at the outer surface of the micro crystals of the molecular sieves.

The simultaneous detection of two surface processes due to molecules adsorbed at outer and inner confining surfaces of molecular sieves is to our knowledge reported for the first time.

4.2.2 Experimental Conditions

Thermogravimetric (TG) measurements were carried out to estimate the $E7$ content inside the pores as already described for other composites [27]. The thermogravimetric measurements were performed by a Seiko TG/DTA 220 apparatus, under a dry synthetic air atmosphere using a part of the sample prepared for the dielectric measurements. Examples for TG curves are shown in Figure 4. 10 giving

the mass loss processes that occur during heating at 10 K/min. The content of $E7$ loaded within the system m_{E7} was determined from these measurements and the filling degree Θ was defined as the ratio

$$\Theta = \frac{mass\ measured}{maximal\ mass\ for\ complete\ pore\ filling} = \frac{m_{E7}}{m_{MCM} \cdot V_P \cdot \rho_{E7}^{Con}} \qquad \textbf{Equation 4. 1}$$

where ρ_{E7}^{Con} is the density of $E7$ in confinement and m_{MCM} the mass of the empty molecular sieve. Assuming that $\rho_{E7}^{Con} \approx \rho_{E7}^{Bulk} = 1\mathrm{g} \cdot \mathrm{cm}^{-1}$ the filling degree Θ can be calculated. The estimated filling degrees are given in Table 4. 2. All samples have similar filling degrees of about 50 to 60 wt-% and can be therefore compared directly. These relatively low filling degree values were chosen to study the molecular mobility of the $E7$ molecules adsorbed in a surface layer at the pore walls independently from bulk-like $E7$ located in the centre of the pores.

Sample	Θ (wt %)	$A_{Bulk-like}$	$A_{Surface}$	κ
$E7$/MCM-41-28	51	5.57	10.04	1.8
$E7$/MCM-41-36	60	17.38	21.68	1.247
$E7$/MCM-41-41	63	0.389	0.273	0.702
$E7$/SBA-15	63	14.3	11.75	0.821

Table 4. 2- Filling degree of $E7$ within the molecular sieves. $A_{Bulk-like}$ and $A_{Surface}$ denote contributions of the bulk-like and interacting $E7$ molecules taken from the FTIR spectra. k is the interaction parameter (see Equation 4. 2).

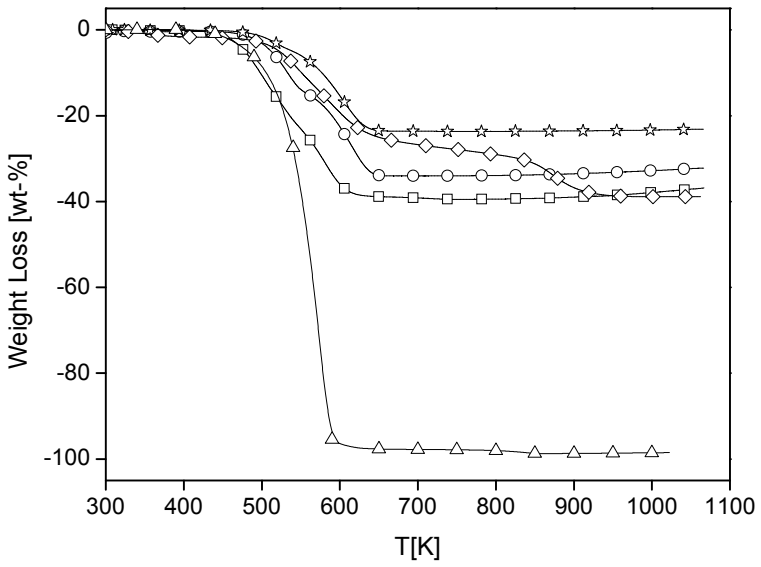

Figure 4. 10- TG curves for the different samples: □ - $E7$/MCM-41-28, ○ - $E7$/MCM-41-36, ☆ - $E7$/MCM-41-41, ◇ - $E7$/SBA-15. The behavior of bulk $E7$ (△) was given for comparison.

Dielectric spectra (for more details see Chapter II) were recorded by varying the temperature which was decreased stepwise: a) $E7$/MCM-41-28, from 373 K to 203 K, in steps of 2 K, and, from 198 K to 173 K, in steps of 5 K; b) $E7$/MCM-41-36, from 373 K to 237 K, in steps of 2 K; c) $E7$/MCM-41-41, from 373 K to 225 K, in steps of 2 K and d) $E7$/SBA-15 from 373 K to 173 K in steps of 2 K.

4.2.3 Results and Discussion

FTIR-Spectroscopy

To analyze interactions of $E7$ with the pore wall, FTIR measurements were carried out. All components of $E7$ are terminated by the cyano group. Therefore this group is used for further analysis. Figure 4. 11 a) gives the FTIR spectra for bulk $E7$ for the main CN-stretching vibration. This band can be well described by a Gaussian centered at 2226.2 cm^{-1} and a band width of 8.6 cm^{-1}. A more detailed discussion of the CN-stretching vibration and its separation into a contribution of monomers and dimers can be found for related cynanobiphenyls elsewhere [28,29]. Such a detailed analysis is out of the scope of this contribution and therefore the CN-stretching vibration is approximated here by one Gaussian.

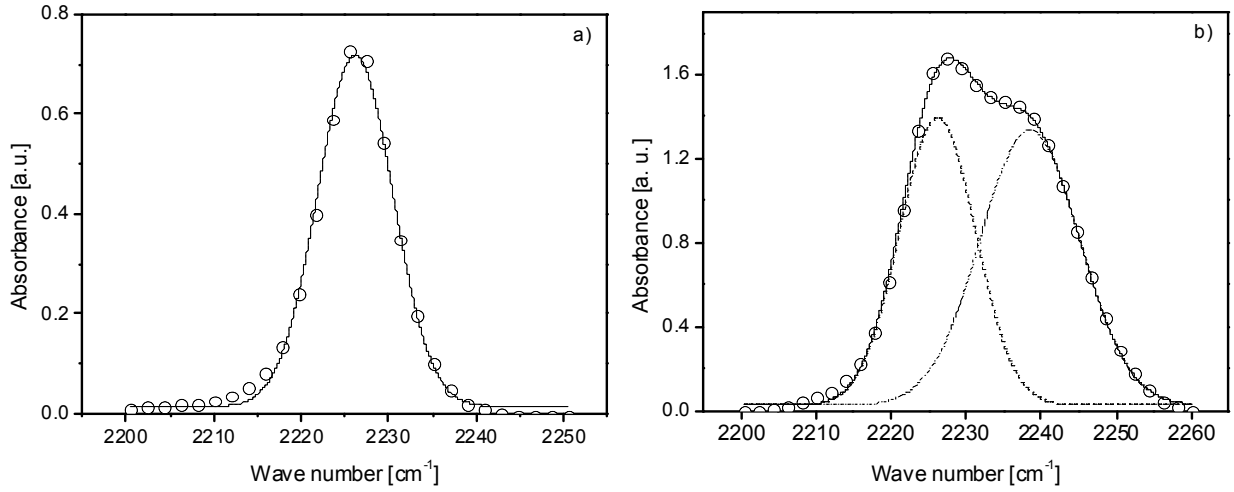

Figure 4. 11- a) FTIR spectrum for the CN-stretching vibration (O). The line is a fit of a Gaussian to the data. The regression coefficient is r=0.996; b) FTIR spectrum for the CN-stretching vibration (O) of $E7$ confined to the molecular sieve MCM-41-36. The solid line is a fit of two Gaussians to the data. The dashed line represents the bulk-like contribution whereas the dashed dotted line gives the contribution of the molecules interacting with the surface of the pores The regression coefficient is r = 0.998.

Figure 4. 11 b) gives the corresponding FTIR spectrum for $E7$ confined to the molecular sieve MCM-41-36 (sample $E7$/MCM-41-36). The data show two well separated regions for the CN-stretching vibration. One is located in the wave number range characteristic for bulk $E7$. The second region is shifted to higher wave numbers compared to the bulk and is related to $E7$ molecules which interact

with the surfaces of the pores by hydrogen bonding via the CN group of $E7$ and the hydroxyl groups of the molecular sieves. The position of the band is located at 2237 cm^{-1} as it is already known for a related cyanobiphenyl system [30]. The involvement of the hydroxyl groups is confirmed by the FTIR spectrum in the wave number region of the OH stretching.

For a quantitative discussion of the FTIR spectra of confined $E7$ one has to keep in mind that unfortunately the molar absorptivities of the bond and free CN groups can be different, so that a direct comparison of the integrated intensities can bear some errors. In principle this problem can be solved considering different filling degrees. Nevertheless to analyze the FTIR spectra of the CN stretching vibration two Gaussians were fitted to the data. To reduce the number of the fit parameters the position of the bulk-like contribution was fixed to 2226.2 cm^{-1}. The data are well described by this procedure. For the confinement the width broadens slightly by ca. 11 cm^{-1}. The width of the second contribution is approximately constant for all molecular sieves and it is between 13.5 cm^{-1} and 14.1 cm^{-1}. From the fits to the areas under the band for the bulk-like contribution $A_{Bulk-like}$ and for the strongly interacting $E7$ molecules $A_{Surface}$ are obtained and an interaction parameter k is defined by

$$\kappa = \frac{A_{Surface}}{A_{Bulk-Like}} \qquad \textbf{Equation 4. 2}$$

k is proportional to the number of molecules (mol fraction) which are interacting with pore surface. The corresponding values are given in Table 4. 2.

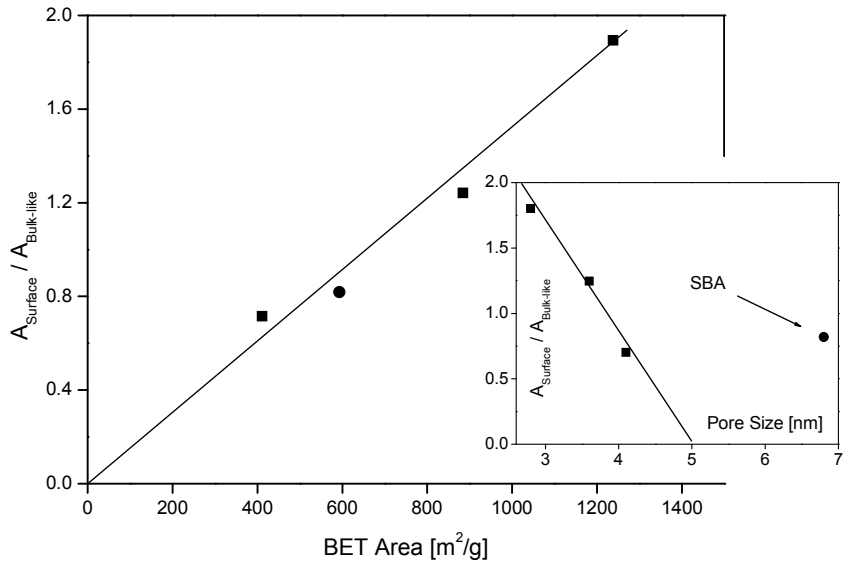

Figure 4. 12- Interaction parameter *k versus* the BET area: ■ - MCM-41; ● - SBA-15. The line is a guide for the eyes. The inset gives *k versus* pore size: ■ - MCM-41; ● - SBA-15. The line is a guide for the eyes.

Firstly one has to note that an important part of the $E7$ molecules is interacting with the surface. Secondly, although the filling degree of the pores is only between 51 wt-% and 63 wt-% the FTIR spectra indicate also a relative large amount of $E7$ molecules which behaves bulk-like in difference to a related system [30]. The molecular sieve used in that case as host is an Al-MCM-41 material ($Si/Al = 14.7$). It is known that the aluminum provides stronger interaction centers than Si. This might be a reason for the different behavior. A more refined discussion together with the dielectric data will be given during the course of this sub-chapter. A closer inspection of Table 4. 2 shows that the interaction parameter k depends on the pores size. The inset of Figure 4. 12 gives the interaction parameter *versus* pore size.

For the MCM-41 type materials k correlates well with the pore size but the value for the molecular sieve SBA-15 is located far away from this correlation line. At the first glance this seems to indicate that both sets of materials behave differently. However, for the interaction of the molecules with the pore walls not only the pore size is the relevant but also the available surface area. Therefore Figure 4. 12 displays the interaction parameter *versus* the BET area (see Table 2.3 in Chapter II). The data for both types of materials follow well a single correlation line. This correlation line goes through the origin which is reasonable because if no surface is available for the interaction, the interaction parameter should be zero.

Dielectric Spectroscopy

The dielectric relaxation behavior of bulk $E7$ was discussed in detail in Chapter III.

A thorough analysis of the temperature dependence of the relaxation times, τ_{max}, shows that both the $\alpha-$ and δ- relaxations are described by the Vogel-Fulcher-Tamman (VFT-) law (Equation 1.2 in Chapter I) [31,32,33].

Close to T_g the temperature dependence of the relaxation times of the tumbling mode is much stronger than that of the δ process and $T_{0,tumb} >> T_{0,\delta}$ is found where $T_{0,tumb}$ and $T_{0,\delta}$ are the corresponding Vogel temperatures of the tumbling and δ processes respectively [34]. According to Equation 1.17 (Chapter I) the fragility parameter D can be estimated. For bulk $E7$ it is found that the D parameter for δ process is much higher than for the tumbling mode.

Due to experimental reasons the unloaded molecular sieves could not be investigated in the fully dehydrated state. However it was already shown for related materials e.g. of AlMCM-41 [35], porous glass [36] or Anopore membranes [37] that the contribution of the pore wall material is negligibly small compared to that observed for the (liquid) filled samples [35]. On the other hand, the dielectric behavior of the water adsorbed into the pores of identical molecular sieves was previously investigated in detail [38]. A saddle-like temperature dependence of the relaxation time of water for the low and high frequency processes in AlSBA-15 was found [39].

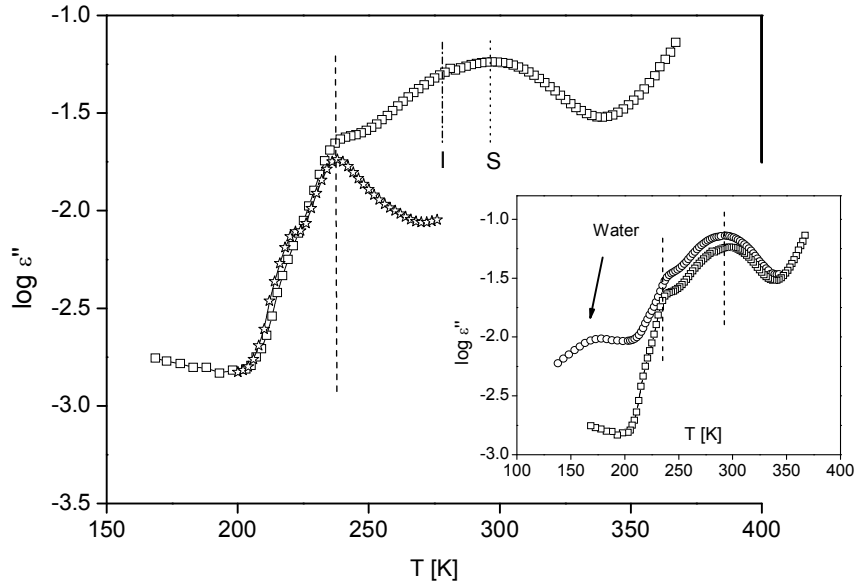

Figure 4. 13- Dielectric loss of *E*7 *versus* temperature at a frequency of 1 kHz confined to the molecular sieve MCM-41-28 during cooling (□) in comparison to the bulk (☆). The dielectric loss of bulk *E*7 was scaled in order to match the values of the confined material. The inset gives the dielectric loss *vs*. temperature at a frequency of 1 kHz for *E*7 confined to the molecular sieve MCM-41-28 during heating (O) and cooling (□).

Figure 4. 13 compares the dielectric loss for $E7$ in the bulk and confined to the pores of the molecular sieve MCM-41-28 (sample $E7$/MCM-41-28) *versus* temperature at fixed frequency (isochronal plot). As already discussed for bulk $E7$ two relaxation process indicated by peaks in the dielectric loss are observed. The process located at lower temperatures corresponds to the α- relaxation (tumbling mode) whereas the mode observed at higher temperatures is the δ- relaxation. The dielectric loss of $E7$ embedded to the molecular sieve with 2.8 nm show several dielectrically active relaxation processes. Although the filling degree is low, in the temperature range where the processes for bulk $E7$ are observed, two modes with a weak dielectric strength are visible (note that the y-scale is logarithmic). These processes are assigned to $E7$ molecules which behave bulk-like probably located in the center of the pores. At higher temperatures a broad and rather intensive peak (compared to the bulk-like modes) is observed. A closer inspection of this broad mode indicates that it consists of two relaxation processes labeled by I and S in order of increasing temperature. These two processes are assigned to $E7$ molecules which interact with different surfaces of the molecular sieves. These relaxation processes will be discussed in detail in their pore size dependence during the course of this sub-chapter.

The inset of Figure 4. 13 compares the dielectric loss of $E7$ confined to the pores of the molecular sieve MCM-41-28 during heating and cooling. During heating a relaxation process at quite low temperatures below 200 K takes places. Because both the cleaning and the filling of the pores was done in high vacuum this process is assigned to water molecules (no bulk water) adsorbed at the outer surface of the crystalline silica particles or at the extra pores after taking out the sample of the

preparation apparatus where the pores are filled. Moreover considering the huge dipole moment of water in comparison to $E7$ the amount of adsorbed water is small. During cooling this relaxation process disappears because the water molecules are easily desorbed under the influence of the dry nitrogen atmosphere used for the temperature control. For these reasons the "water process" is not discussed further during the course of this sub-chapter. Despite a small decrease of intensity the relaxation processes due to $E7$ remain unchanged especially in their temperature position.

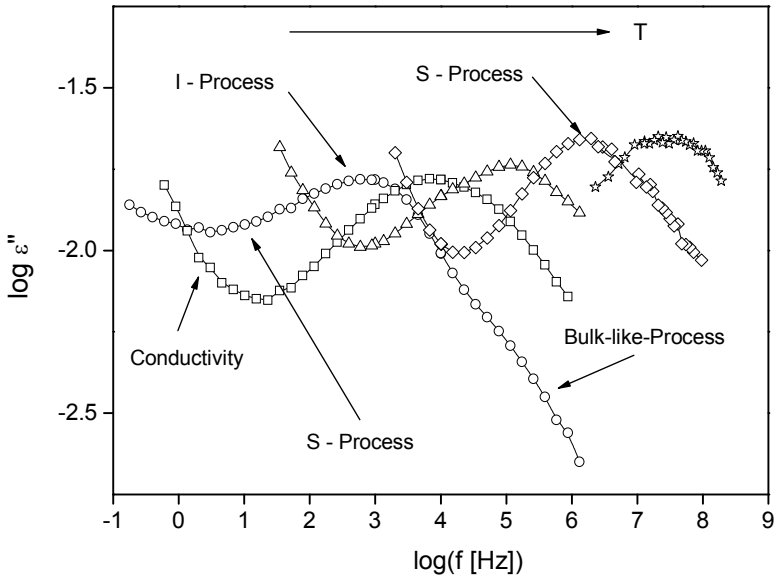

Figure 4. 14- Dielectric loss of $E7$ *versus* frequency for different temperatures confined to the molecular sieve MCM-41-36: O - T=295.2 K; □ - 315.2 K; △ - 335.2 K; ◇ - 373.2 K; ☆ - 413.2 K. The lines are guides to the eyes.

Figure 4. 14 gives the dielectric loss of $E7$ embedded in the pores of the molecular sieve MCM-41-36 (sample $E7$/MCM-41-36) for different temperatures for the available frequency range. As already discussed, the dielectric spectra show a multimode behavior. Besides a weak contribution of $E7$ molecules which behave bulk-like and a conductivity contribution at low frequencies, the I process is observed followed by the S-mode (consider the spectra at T = 295.2 K). With increasing temperature the S process gains in its dielectric strength and becomes the dominating process. The I-mode is assigned to molecules which are adsorbed at the outer surfaces of the silica particles or at the surfaces of the extra pores. The S process is related to $E7$ molecules confined inside the pores which are in interaction with the pore surface (Surface process). For the different molecular sieves discussed here as confining hosts, a similar behavior is found.

The model-function of Havriliak-Negami (HN-function) is used to analyze and to separate the different relaxation processes (details can be found in Chapter I and [24,40])

The results obtained for bulk $E7$ were compared with those of $E7$ confined to the molecular sieves using mainly the temperature dependence of the relaxation times, τ_{max}, and partly that of the dielectric strength $\Delta\varepsilon$.

Figure 4. 15 gives two examples for the used fitting procedure. Figure 4. 15 a) provides data for $E7$ confined to the molecular sieve MCM-41-41 (Sample $E7$/MCM-41-41). The spectra show two relaxation processes related to the S process at lower and to the I-Mode at higher frequencies. Figure 4. 15 b) shows a dielectric spectra of $E7$ confined to SBA-15 (Sample $E7$/SBA-15). Again the the S and I Process can be identified. In addition to these processes, bulk like modes of $E7$ are observed.

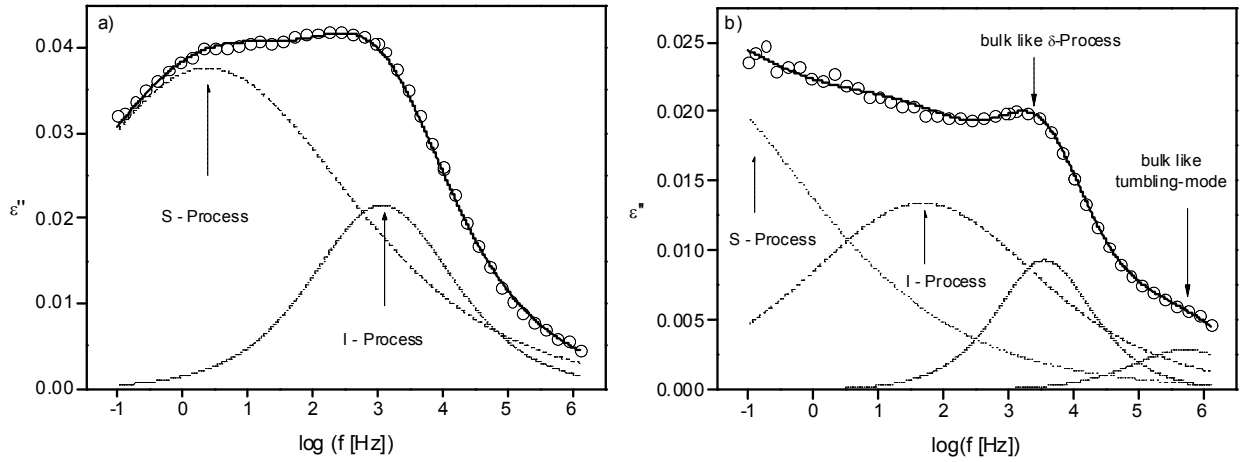

Figure 4. 15- a) Dielectric loss for the sample $E7$/MCM-41-41 at a temperature of T=257.2 K. The solid line is the overall fit function. The dashed line is the contribution of the S- and the dashed dotted line that of the I process; b) Dielectric loss for the sample $E7$/SBA-15 at a temperature of T=243.2 K. The solid line is the overall fit function: dotted line – contribution S process; dashed line contribution I process; dashed –dotted line – bulk like δ process; dashed-dotted-dotted line – bulk like tumbling mode.

In Figure 4. 16 the relaxation times, τ_{max}, for each relaxation process are plotted *versus* reciprocal temperature for the sample $E7$/MCM-41-28. In addition, the data for bulk $E7$ were included. The relaxation times for each process observed for confined $E7$ have different temperature dependencies. Therefore in the following the influence of the confinement on the different relaxation processes is discussed separately.

Bulk-like relaxation processes

The quantitative analysis of these relaxation processes is difficult because its dielectric strengths are low. Moreover, in the temperature range of the nematic phase the relative dielectric strength depends on the orientation of the molecules with respect to the outer electrical field which can be different for the different pore sizes. This means also that not all bulk-like relaxation processes can be observed for each sample.

The temperature dependence of the relaxation times for the bulk-like processes observed for $E7$ in confinement coincide well with that observed for the bulk. This concerns both the isotropic and the nematic state. The molecules which behave bulk-like inside pores undergo also a phase transition from

the isotropic to the nematic state. Unfortunately due to the weak intensity of the bulk-like processes the phase transition temperatures cannot be identified directly by dielectric spectroscopy and discussed in this pore size dependence.

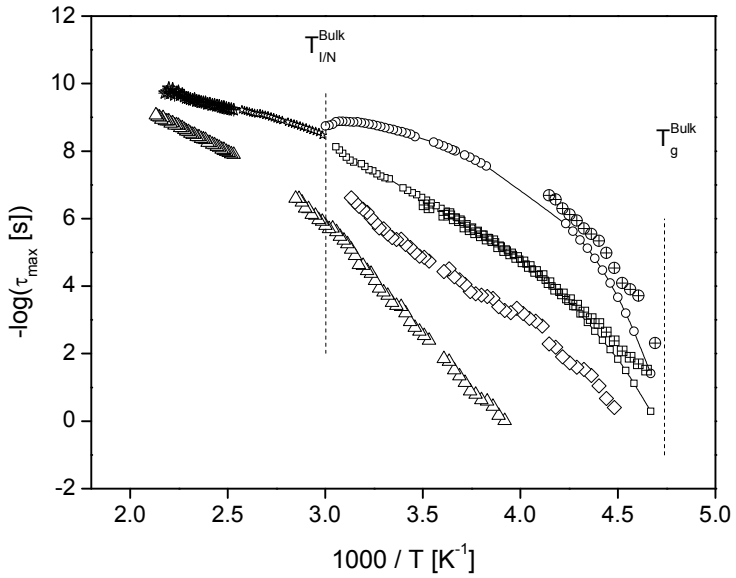

Figure 4. 16- Relaxation times, τ_{max}, *vs.* $1/T$ for $E7$ embedded in the molecular sieve MCM-41-28 (sample $E7$/MCM-41-28) in comparison to the bulk: O - tumbling mode bulk; □ - δ- relaxation bulk; ☆ - relaxation process isotropic phase bulk; ⊕ - bulk-like tumbling mode; ⊞ - bulk-like δ- relaxation; ✯ - bulk-like relaxation process in the isotropic phase; ◇ - *I* process; △ - *S* process. The lines are guides for the eyes.

A closer inspection of the data in the nematic state reveals that close to the glass transition temperature for both the bulk-like δ- and the bulk-like tumbling mode the temperature dependencies are weaker than that of the corresponding bulk (see Figure 4. 17). This effect is similar to the confinement effect observed for conventional glass forming systems in confinement [41,42,43,44]. Because the tumbling mode is related to glassy dynamics this indicates that the glass transition temperature of the bulk-like $E7$ molecules in confinement is lower than in the bulk itself. This effect can be discussed in two directions. On the one hand side the weaker temperature dependence of both the tumbling and the δ-mode in confinement are due to a real confinement effect. This means that the length scale of the cooperative molecular fluctuations related to the glassy dynamics are interfering with that of the confining host which leads to a weaker temperature dependence and a faster dynamics compared to the bulk. On the other hand because the filling degrees are low and so the pores are not completely filled the density of the bulk-like molecules in confinement is lower than in the bulk which would also lead to a faster molecular dynamics. To discriminate between these two possibilities on systems with different filling degrees are necessary which are in preparation.

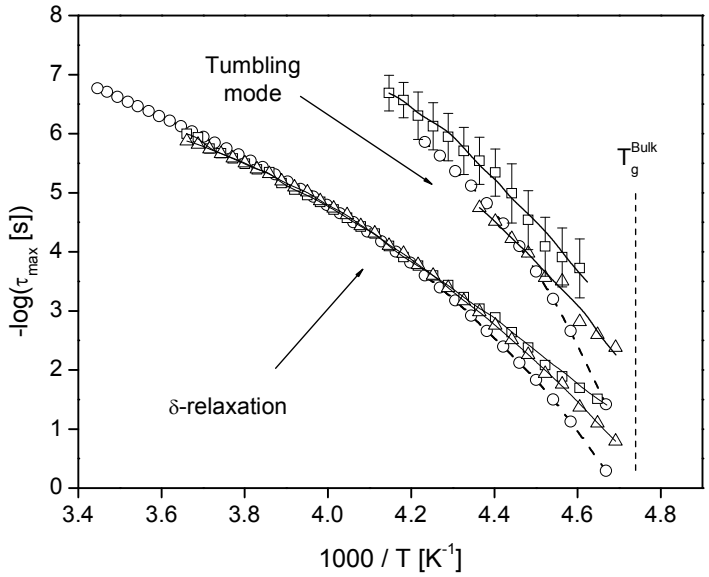

Figure 4. 17- Comparison of the temperature dependence relaxation times of the bulk-like processes with that of the bulk: O -bulk; △ - *E*7/SBA-15; □ - *E*7/MCM-41-28. Lines are guides for the eyes. Especially for small pore sizes the dielectric strength of the tumbling mode is small. This means the estimation of the relaxation bears some uncertainties. The error bars to the tumbling mode of *E*7/MCM-41-28 might be some estimates for these uncertainties.

Surface process (S process)

Figure 4. 16 shows that the S process is much slower than the processes observed for the bulk. At T=285 K the difference of its relaxation time to the δ-relaxation is approximately 4 decades, to the tumbling more than 5.5 decades. For all samples a similar behavior is observed. As discussed above the S process is assigned to confined $E7$ molecules which are adsorbed at the internal wall of the pores via hydrogen bonding. The FTIR measurements discussed above proof that a part of the molecules interacts with the pore wall. It is well known that these interactions will slow its molecular dynamics.

The inset of Figure 4. 18 compare the temperature dependence of the relaxation time of the surface layer for the discussed samples. For all pore sizes $\tau_{max}(T)$ is curved in a plot *versus* $1/T$ and the data do not follow the Arrhenius law. Moreover this figure indicates also that the temperature dependence of τ_{max} for the surface layer depends on the pore size. For larger pore sizes the $\tau_{max}(T)$ seems to be more curved than for smaller ones. For high temperatures the curves for the different pore sizes seem to collapse more or less into one chart.

The inset of Figure 4. 18 shows that the absolute value of the relaxation time of the surface layer at a given finite temperature seems to decrease with decreasing pore size. To analyse the temperature dependence of the surface layer in more detail a derivative method is applied (Chapter I). The obtained linear dependence indicates that indeed the temperature dependence of the relaxation times follows a VFT-dependence with a $T_0 \gg 0$ (see Figure 4. 18). It is believed that a dependence according to the VFT-law it is a sign of glassy dynamics. Therefore the S process is assigned to the dynamic glass transition of the $E7$ molecules which are adsorbed at the pore wall.

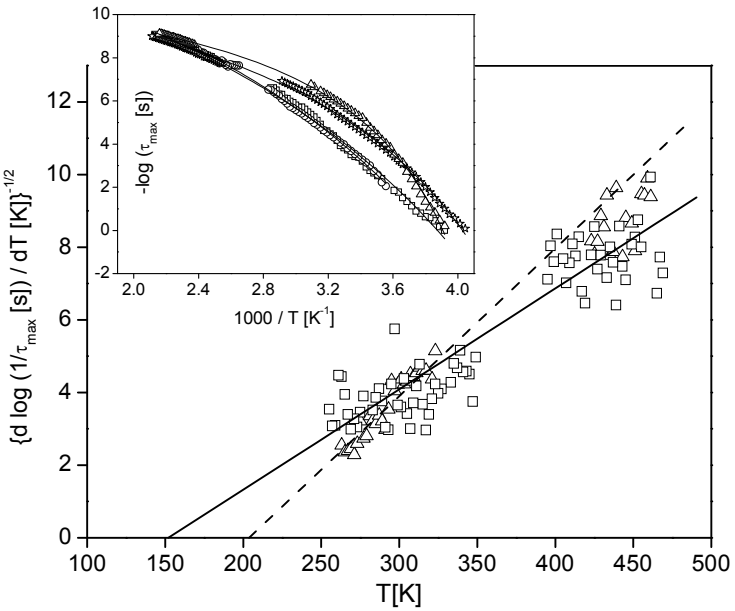

Figure 4. 18- $[d\log(1/\tau_{max})/dT]^{-1/2}$ *vs.* temperature for the samples $E7$/MCM-41-28 (□) and $E7$/SBA-15 (△). The lines are linear regressions to the corresponding data. The inset is the comparison of the temperature dependence relaxation times for the S process: □ - $E7$/MCM-41-28; ○ - $E7$/MCM-41-36; ☆ - $E7$/MCM-41-41; △ - $E7$/SBA-15. The lines are fits of the VFT-equation to the data.

The observation of two glass transitions for conventional glass-forming liquids confined in nanopores, was already reported and being found to depend on the interaction between the wall of the pore and the confined liquid. Whereas one of the detected T_g's is close to the bulk, the second one is found to be lower than that for the bulk when guest host interactions are weak while for strong interactions the second T_g is higher [45 and references therein]. The latter is verified for the present study where the strong interaction with the pore wall was proved by FTIR.

The VFT-equation was fitted to the data (see Figure 4. 18) where the obtained VFT-parameters are given in Table 4. 3. In Figure 4. 19 the Vogel temperature T_0 for the *S* process is plotted *versus* the pore size. With decreasing pore size T_0 decreases strongly. Within the frame of the experimental errors the pore size dependence of T_0 might be described by a straight line (see dashed line in Figure 4. 19). But a closer inspection of the data indicate that there is a kind of transition between large pore sizes and smaller ones. This becomes more evident considering the fragility D (see inset of Figure 4. 19). With increasing pore size the fragility parameter D decreases with a step-like change around 4 nm. This might indicate a transition from a strong to fragile behavior of adsorbed $E7$ at this confining length scale.

In general the pore size dependence of the Vogel temperature of the *S* process should be due to two effects: the strength of the interaction of the molecule with the pore wall and the pore size. Because the molecular sieve used here as host have the same composition (100 % silica) the strength of the interaction of the molecules and the pore wall does not change with the pore size. Moreover the FTIR

measurements show that the interaction parameter k is proportional to the BET area. This means that the ratio between the number of interacting molecules per available interaction area is constant. Therefore the observed decrease of T_0 with decreasing pore size and the transition at ca. 4 nm is considered as a special kind of a confinement effect. Probably for smaller pore sizes the molecular order and/or the density of the $E7$ molecules forming the surface layer is less than for larger pore sizes resulting in a decreased T_0. This issue is further discussed below considering the temperature dependence of the dielectric relaxation strength.

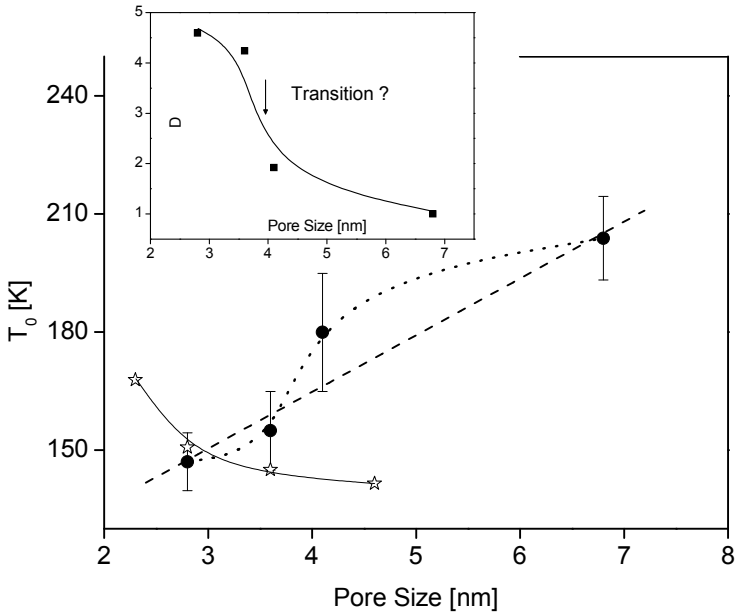

Figure 4. 19- T_0 for the surface process *versus* pore size for $E7$ confined to the described hosts (●). The line is a linear regression to the data. The dotted line is a guide for the eyes. ☆ - are data for 8CB confined to the pores of Al-MCM [30]. The solid line is a guide for the eyes. The inset gives the fragility *D versus* pore size for E7 confined to the described hosts. The line is a guide for the eyes.

In addition Figure 4. 19 compares the pore size dependence of T_0 of molecules adsorbed in a surface layer for the related system $8CB$ confined to Al-MCM-41 ($Si/Al = 14.7$) with the data obtained here. The absolute values obtained for both systems agree witch each other but the pore size dependence is different. As discussed above Al provides stronger interaction centers than Si. Moreover the relative concentration of Al close to the pore walls is higher for lower than for larger pore size [30]. This means in difference to the system discussed here the strength of the interaction of the molecules with the walls increases with decreasing pore size. This might be the reason for the different behavior.
The Debye theory of dielectric relaxation generalized by Kirkwood and Fröhlich [24,46] predicts the temperature dependence of the dielectric relaxation strength according to Equation 1.46.

Sample	$-\log(\tau_\infty\,[s])$	$A\,[K]$	$T_0\,[K]$	D
$E7$/MCM-41-28	12.4	1556	147	4.59
$E7$/MCM-41-36	12.5	1512	154.9	4.24
$E7$/MCM-41-41	10.0	794	179.9	1.92
$E7$/SBA-15	9.3	480	203.8	1.0

Table 4. 3- VFT-parameters characterizing temperature dependence of the relaxation time of the surface layer obtained by fitting of Equation 1.2 to the data.

Figure 4. 20compares the temperature dependence of $\Delta\varepsilon$ of the surface layer for two pore sizes. For all pore sizes a similar behavior is obtained. For low temperatures $\Delta\varepsilon$ increases with increasing temperature up to a maximum value. For higher temperatures the dielectric strength decreases with increasing temperature.

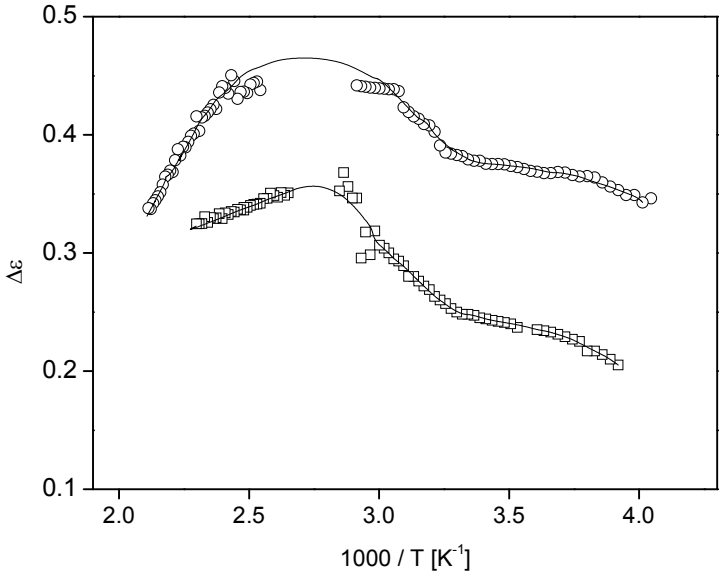

Figure 4. 20- Dielectric strength of the surface layer Δε *versus* inverse temperature: □ - *E*7/MCM-41-28; O - *E*7/MCM-41-41.

This temperature dependence of the relaxation strength can be understood by a counterbalance of two effects. According to Equation 1.46 (Chapter I) $\Delta\varepsilon$ should decrease with increasing the temperature. Because the involved dipole moment is constant an increase of $\Delta\varepsilon$ can be explained by an increase of the number density of fluctuating dipoles in the surface layer. In general, the strength of the interaction of the $E7$ molecules with the surfaces of the pores depends on temperature. For higher temperatures the strength of this interaction is weaker than for lower ones. Because the strength of the interaction is a key parameter for molecular mobility of the molecules at higher temperatures the number of molecules contributing to the surface process is higher than at low temperatures, which explains the increase of $\Delta\varepsilon$ at low temperatures which overbalance the $1/T$ dependence. At higher temperatures the Boltzmann term $1/T$ wins and $\Delta\varepsilon$ decreases with T. This line of argumentation is in agreement with

the discussion of the pore size dependence above. In this framework it could be interesting to analyze the pore size dependence of the dielectric strength of the surface process. Unfortunately this cannot be done because the samples for the dielectric measurements are prepared by pressing a powder and so no absolute values could be provided.

Interaction process (I process)

The frequency position of the *I* process is located in between the bulk-like processes and the surface process. Therefore the corresponding relaxation time is lower than that of the *S* process (see Figure 4. 16). The quantitative analysis of the *I* process is difficult because compared to the *S* process its intensity is low and both processes overlap strongly at least at higher temperatures. Therefore the data have a larger scatter than for the *S* process.

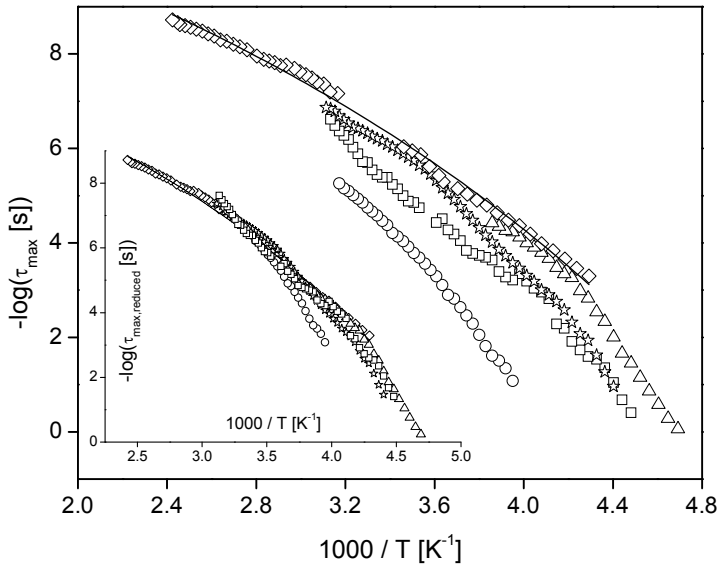

Figure 4. 21- Comparison of the temperature dependence relaxation times for the *I* process: □ - *E*7/MCM-41-28; ○ - *E*7/MCM-41-36; ☆ - *E*7/MCM-41-41; △ - *E*7/SBA-15. ◇ - are the relaxation time of $5CB$ adsorbed in a monolayer at the outer surface of silica particles [19]. The line is a fit of the VFT equation to the latter data. The inset compares the temperature dependence of relaxation times of the *I* process shifted in the direction of the $y-scale$ to mach the data of $5CB$. The symbols are the same than in the main figure.

Figure 4. 21 compares the temperature dependence of the relaxation times of the surface process for the different samples. For all pore sizes a similar behavior is obtained. There seems to be no dependence of the relaxation on the pore size. In addition, the temperature dependence of the relaxation time of $5CB$ adsorbed nearly as a monolayer on silica is given [47]. This system is selected because $5CB$ is the main component of $E7$ (see Chapter II). The data for the *I* process observed for the system discussed here are close to that of the $5CB$ molecules adsorbed at the outer surface of the silica particles. This concerns both its absolute values and its temperature dependence. For the latter reason

the data for the I process are vertically shifted to match the temperature dependence of the relaxation time of $5CB$ adsorbed onto the outer surface of silica (see inset of Figure 4. 21). The data for all systems collapse approximately into one chart. Therefore it is concluded that the I process observed is due to $E7$ molecules adsorbed at the outer surfaces of the microcrystals of the molecular sieves and/or at its inter grains.

4.2.4 Conclusions

The molecular mobility of $E7$ confined in MCM-41 and SBA-15 molecular sieves with identical composition (100% Si) but a different pore size was investigated by broadband dielectric spectroscopy. Since crystallization in $E7$ is easily avoided it was possible to cover a temperature range of more than 200 K providing an exhaustive dielectric characterization of confined liquid crystal (LC). TGA measurements allowed to obtain the respective filling degrees which are low and between 50 to 60%. Moreover FTIR spectra confirmed the strong anchoring of the LC molecules to the silica surface. For the deconvolution of the absorption band in the nitrile stretching region (2226 cm^{-1}), two overlapping Gaussians were considered: one related to bulk like LC and a second one broader and shifted to higher wave numbers compared to the bulk, which is related to $E7$ molecules interacting with the surfaces of the pores by hydrogen bonding via the CN group of $E7$ and the hydroxyl groups of the molecular sieves. An interaction parameter k was estimated by the ratio of the area of the second Gaussian and the one bulk related, revealing a good linear correlation with the BET area for all samples.

Dielectric relaxation spectroscopy detected the processes similar to the bulk, both in the isotropic and nematic state. It was also shown that inside pores the molecules undergo the phase transition from the isotropic to the nematic state.

Besides the bulk processes, two additional relaxation processes were observed with a single temperature dependence at high temperatures. However at low temperatures it splits into two independent traces in the relaxation map. The comparison with the dynamical behaviour of homologous cyanobiphenyl molecules allowed to assign the detected processes. The one with higher relaxation times, S process, obeys a Vogel-Fulcher-Tamman (VFT) law, as shown by the analysis using a derivative technique, indicating that this process is related to the glassy dynamics of the LC molecules interacting with the inner surface of the pores. The pore size dependence of the fragility index revealed a transition around 4 nm, which seems to indicate a strong to fragile behavior of adsorbed $E7$ at this confining length scale. This step-like pore size dependence was also felt by Vogel temperature dependence and can be seen as a special confinement effect.

At intermediate relaxation times between the S process and the bulk-like a relaxation was detected, I process, attributed to the $E7$ molecules adsorbed at the outer surfaces of the microcrystals of the molecular sieves and/or at its inter grains, having a faster dynamics at low temperatures than inside the pores.

This subchapter will be submitted for publication

4.3 Ibuprofen Confined to Molecular Sieves with a Low Filling Degree

4.3.1 Introduction

The effect of nanometer confinement on the molecular dynamics of Ibuprofen confined to MCM-41 and SBA-15 (pore sized 3.6 and 6.8 nm) is investigated by dielectric relaxation spectroscopy. A complex relaxation map including two secondary relaxations, γ and β, a main bulk-like α process associated with the dynamic glass transition, a S-process assigned to the Ibuprofen molecules weakly adsorbed at the internal pore wall and a related Debye-like process (D_S -relaxation) is given for the first time. The dynamics of secondary processes do not depend on the pore size and is essentially discussed the same as in the bulk Ibuprofen. The β-relaxation is also identified as the genuine Johari-Goldstein process. For both systems the temperature dependence of the relaxation times of the bulk-like α-relaxation changes from a Vogel-Fulcher-Tamman (VFT) like to an apparent Arrhenius behavior where the activation energy depends on the pore size. Thus the glassy dynamics of the bulk-like α process is faster than for the bulk which originates from an inherent length scale of the underlying molecular motions, eventhough the minimal length is not yet reached for 3.6 nm. For Ibuprofen confined to the 3.6 and 6.8 nm pores the molecular dynamics is determined by a counterbalance of an adsorption and confinement effect, where the temperature dependence of the S process relaxation times follows the VFT-equation, being attributed to the glass transition of the Ibuprofen molecules linked via weak hydrogen bonding to the inner pore surface. This effect slows down the molecular dynamics of the surface process. The D_S process has a Debye-like relaxation function and seems to be governed by the S process.

4.3.2 Experimental Conditions

Ibuprofen ((2RS)-2[4-(2-methylpropyl)phenyl]propanoic acid), $C_{13}H_{18}O_2$ previously described in Chapter II was used.

Molecular sieves of MCM-41-36 and SBA-15 types (100% Si composition) were employed as hosts for the confinement porous (see Chapter II). The MCM-41-36 ibuprofen-loaded samples will be referred in the forthcoming text as Ibu/MCM-41.

The molecular sieves pellets were prepared by loading Ibuprofen in a solution of ethanol (Chapter II). To test the influence of the solvent in the impregnation process, the pellets of a reference sample (MCM-41) were soaked in a solution of Ibuprofen in hexane (more details in Chapter II).

Estimation of the Filling Degree

Thermogravimetric (TG) measurements were carried out to estimate the Ibuprofen content inside the pores as previously described for E7.

Examples for TG curves of SBA-15 Ibuprofen loaded, bulk Ibuprofen and empty SBA-15 are shown in Figure 4. 22 giving the mass loss processes that occur during heating with a rate of 10 K/min. The analysis of the empty molecular sieves mass loss shown in Figure 4. 22c) revealed a water content of about ~1.5%. Concerning bulk Ibuprofen it starts decomposition about 473 K. Thus in the confined Ibuprofen the first small step until 423 K is related to solvent mass loss (~1% for Ibu/MCM-41 and ~ 3 % for Ibu/SBA-15) and it was not considered for the filling degree determination of Ibuprofen.

The content of Ibuprofen loaded within the host matrices was determined from these measurements and the filling degree Θ was defined for Ibuprofen according to Equation 4. 1. For this calculation, the density of liquid Ibuprofen at 298 K (1.00 g·cm^{-3}) was obtained from NPT Molecular Dynamic Simulations [48,49] since no experimental value was found.

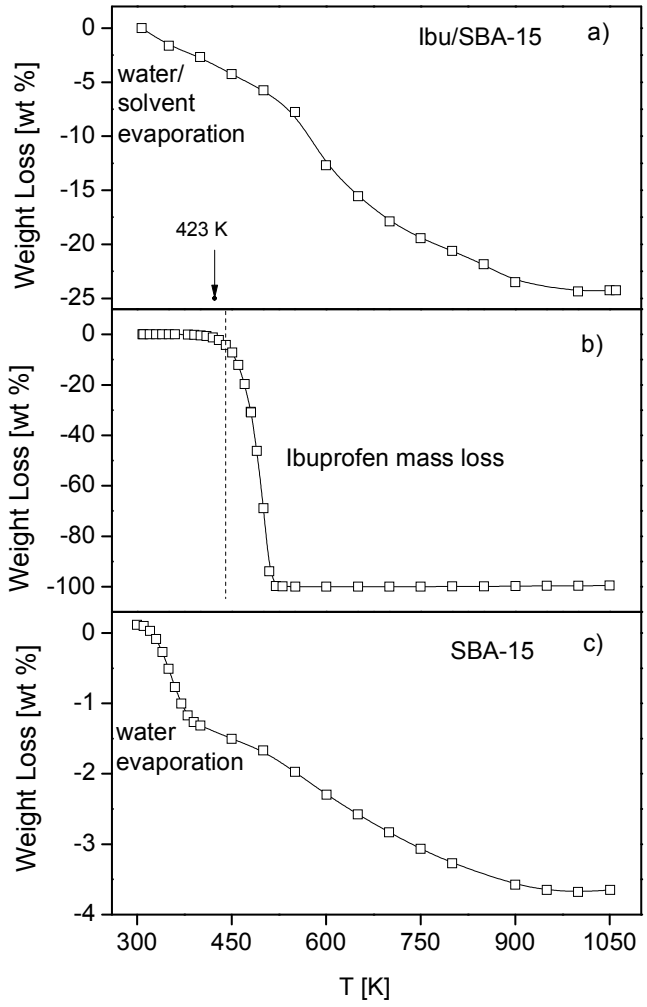

Figure 4. 22- TG curves for: a) Ibu/SBA-15; b) bulk Ibuprofen and c) empty SBA-15. The arrow indicates the temperature after which the Ibuprofen mass loss was considered for the filling degree calculation.

The estimated filling degrees are given in Table 4. 4. All samples obtained from ethanolic solution have similar filling degrees of about 30 wt-% and can be therefore compared directly. These relatively low values of the filling degree are in accordance to other published data of Ibuprofen confined in the same molecular sieve types [50,51]. Eventhough these values are lower than for Ibuprofen impregnated from an hexane solution, as also reported by Charnay et al. [52], the chosen solvent to continue the studies was ethanol since it is convenient and non-toxic.

Sample	Ibu/MCM-41 (ethanol solution)	Ibu/SBA-15 (ethanol solution)	Ibu/MCM-41 (hexane solution)
$\Theta\ wt-\%$	32	27	52

Table 4. 4- Filling degree of Ibuprofen within the molecular sieves MCM-41 and SBA-15 (impregnation from a ethanol solution). Data for Ibuprofen loaded from a hexane solution (see above) is given for comparison.

Dielectric Spectroscopy

The samples were cooled down to 153 K with a rate of 10 K/min and dielectric spectra were collected isothermally from 153 K to 373 K in increasing steps of 2 K. Then the temperature was decreased in steps of 2 K in the range a) 373 K ≥ T ≥ 153 K for Ibu/MCM-41and b) 373 K ≥ T ≥ 159 K for Ibu/SBA-15.

4.3.3 Results and Discussion

ATR-FTIR Spectroscopy

ATR-FTIR was used to analyze intermolecular interactions as hydrogen bonded (HB) associations between Ibuprofen molecules. The wavenumber regions of particular interest are located around 3000 and 1700 cm^{-1}, due to the absorption bands of O-H and C=O stretching modes, respectively. Free O-H and C=O have characteristic frequencies at approximately 3520 and 1760 cm^{-1} appearing as sharp peaks [53]. In the presence of hydrogen bonds these stretching vibrations are perturbed: the C=O band shifts down to lower wavenumbers (1700-1725 cm^{-1}) and the O-H vibration gives rise to a broad band between 3300-2500 cm^{-1} [53].

In Figure 4. 23 spectra for Ibu/MCM-41 and Ibu/SBA-15 are compared with both the crystalline Ibuprofen and the empty MCM-41. Figure 4. 23a) shows the spectra range characteristic for the O-H stretching mode and Figure 4. 23b) the spectral region typical for C=O group. It is observed that similar to what was seen previously for amorphous bulk Ibuprofen, the contribution attributed to both free OH and CO groups is also absent in the spectra of Ibuprofen confined to the molecular sieves. The characteristic bands are assigned to hydrogen bonded groups and thus it can be concluded that the Ibuprofen molecules exist almost in the form of hydrogen bonded aggregates in both samples.

In addition, Figure 4. 23a) also shows for empty MCM-41 as well as for confined Ibuprofen a broad band around 3400 cm^{-1} which is attributed to –OH stretching of water [54]. Related to this feature the bending mode of water is also observed at 1626 cm^{-1} in Figure 4. 23b). These bands do not appear in bulk crystalline Ibuprofen. Moreover Figure 4. 23b) presents the absorption band observed at 1721 cm^{-1} (not seen for empty MCM-41 and SBA-15) for crystalline Ibuprofen, corresponding to the carbonyl-stretching vibration in hydrogen-bonded dimmers which for confined Ibuprofen show a shift down to 1709 cm^{-1}, indicating a weakening of the C=O bond. The same trend is also observed for bulk supercooled Ibuprofen when compared to the crystalline one (see Figure 3.11 in chapter III). Therefore, this can be taken as an indication that confined Ibuprofen is in an amorphous state at room temperature, in accordance with NMR results which have evidenced a high mobility of Ibuprofen molecules confined in MCM-41 [55] and SBA-15 [56,57], that is not characteristic for crystallized molecules.

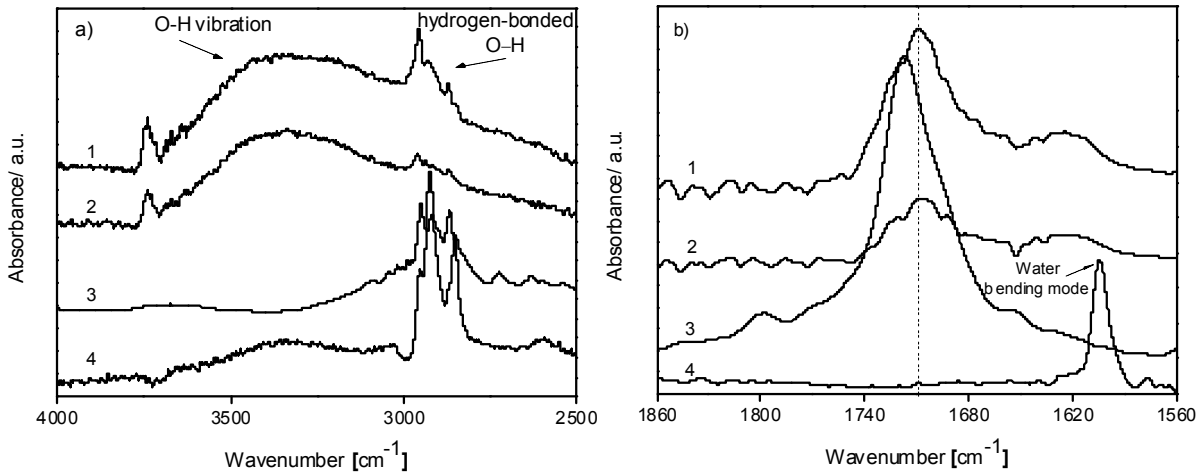

Figure 4. 23- Infrared spectra of (1)-Ibu/SBA-15, (2)-Ibu/MCM-41, (3)-crystalline Ibuprofen and (4)- empty MCM-41 at room temperature, in the frequency region of a) free O-H stretching (~3520 cm^{-1}) and b) free C=O vibrations (~1760 cm^{-1}). The ATR-FTIR spectra were vertically shifted for sake of clarity.

Dielectric Spectroscopy

Thermal Behaviour

The ε´ trace for a frequency of 10^5 Hz obtained for Ibu/SBA-15 is shown in Figure 4. 24. After a first cooling to 159 K (not shown) dielectric spectra were measured with increasing temperature to 373 K (run1). By comparison with the ε' trace (triangles in Figure 4. 24) obtained on heating of bulk Ibuprofen in the crystalline state (see Chapter III), it can be observed that around the bulk melting temperature (T_m) no discontinuity occurs for Ibu/SBA-15. This can be taken as an indication that, at least within the DRS detection limits, residual Ibuprofen crystallized outside the mesoporous was efficiently removed by the washing step. Besides that, also in this first run, the ε' trace shows a small decreasing after 300 K which can be related to evaporation of water or residual solvent which will be

discussed later. On subsequent cooling scan (run 2) a step-like decreasing is observed which is dependent of the measurement frequency, contrary to what happens for a first-order transition, and thus it is probably associated to a dynamic glass transition. Similar behavior is observed for IBU/MCM-41 as will be shown later (Figure 4. 25a). Also, having in mind the ATR-FTIR results discussed above, it can be concluded that Ibuprofen inside the pores is in an amorphous state as well as reported in the literature either for MCM-41 [52,50,58,59,60] and SBA-15 [56,61]. In fact X-ray diffraction studies of Ibuprofen confined in MCM-41 (3.4 nm), at room temperature, evidenced a pattern which is consistent with an amorphous state [52]. Moreover, for the same type of mesoporous matrices (MCM and SBA), Babonneau et al. showed by NMR studies [50,51,58,59,60,56] that the Ibuprofen molecules exhibit high mobility at room temperature, agreeing with a liquid-like behavior inside the pores. In particular, it was concluded that probably due to steric considerations, nucleation of crystallites inside a 3.5 nm pore diameter (MCM-41) is not possible and a vitrification process occurs when temperature is decreased down to 223 K [50]. Looking in detail to the DRS results obtained on cooling for Ibu/SBA-15 (Figure 4. 24) and for Ibu/MCM-41 (see Figure 4. 25 below) a similar interpretation can be done, since there is no evidence of crystallization when the temperature is decreased down to ~160 K.

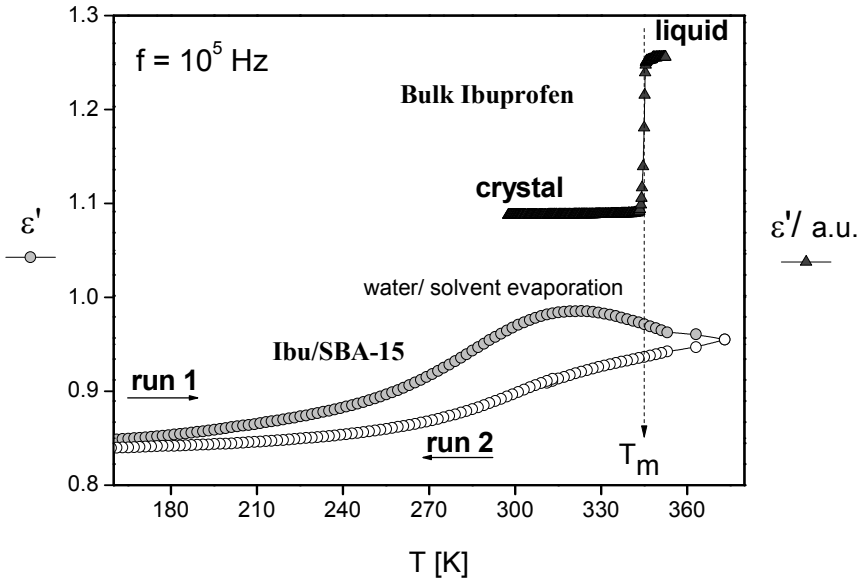

Figure 4. 24- Temperature dependence of the real part of the complex dielectric function, ε′, for a frequency at 10^5 Hz. In the lower part (circles): Run 1-heating of Ibu/SBA-15 sample (there is no evidence of melting) from 153 to 373 K (light gray circles); Run 2- Subsequent cooling of the confined sample (open circles). For comparison purposes in the upper part (triangles) is shown data for the as received crystal obtained on heating; T_m = 347 K is the extrapolated onset melting temperature.

Figure 4. 25 compares the temperature dependence of the real, ε' and imaginary, ε'' part of the complex dielectric function for both Ibuprofen confined to MCM-41 prepared from an ethanol and

from a hexane solution. It can be seen that during heating the ε′ trace of both samples (squares in Figure 4. 25a) shows the same kind of decreasing after 300 K (indicated by the vertical solid line). From these results, it can be concluded that, as hexane is non-polar solvent, the observed decreasing in the ε' trace can be only attributed to water release, whose presence in confined materials was already detected in the ATR-FTIR spectra (Figure 4. 23). It must be noted that in the ε' spectra obtained on the subsequent cooling (triangles in Figure 4. 25a), there is no evidence of a decrease associated to water evaporation, instead a step-like decrease associated to a kind of dynamic glass transition is observed, as already discussed for Ibu/SBA-15 (Figure 4. 24).

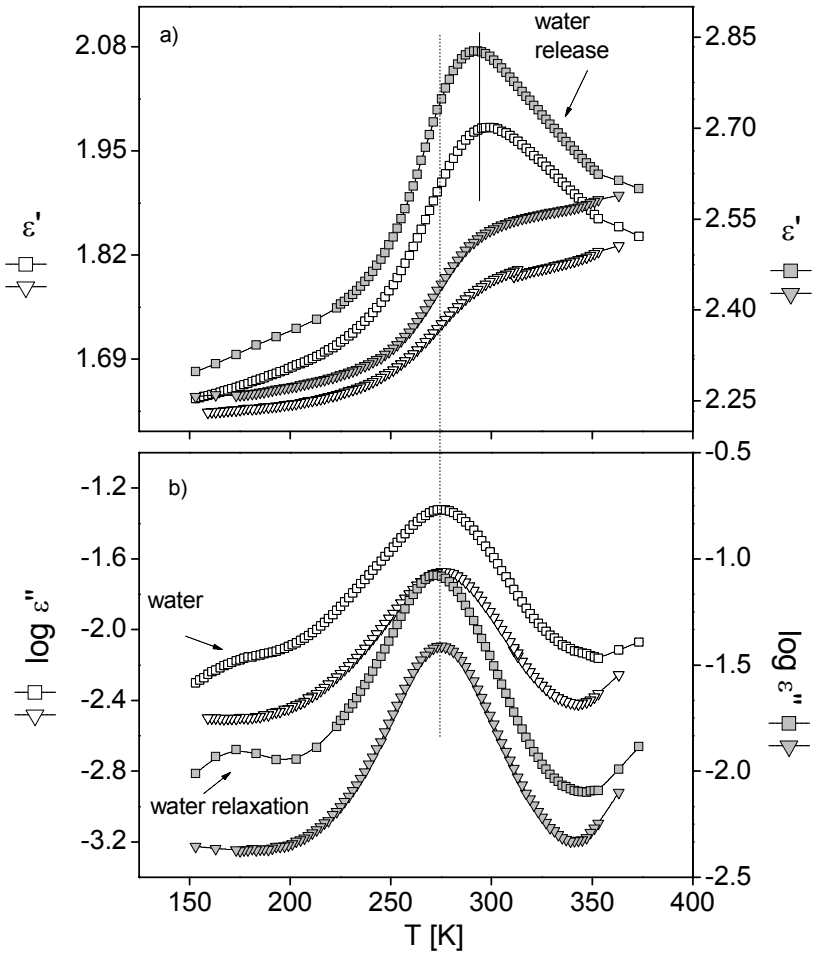

Figure 4. 25- Isochronal curves of ε'-a) and ε''-b) taken from the isothermal data at 10^3 Hz for Ibu/MCM-41 (ethanol solution)-open symbols and Ibu/MCM-41 (hexane solution)- light gray full symbols. Comparison between the heating (squares) and subsequent cooling (down triangles) is given. The dashed line indicates the temperature position of the detected peaks and the solid line gives an indication of the temperature where water release is observed.

In Figure 4. 25b) it can be seen that on heating a relaxation process appears for Ibu/MCM-41 at quite low temperatures below 200 K like the one observed for E7. This process which takes place on both samples prepared from ethanol and hexane solutions (indicated by the arrows in the figure), is assigned to water molecules (no bulk water) adsorbed at the outer surface of the silica particles or at

the extra pores once the sample is taken out from the vacuum chamber, after the first impregnation step (remember drug loading procedure). Moreover considering the huge dipole moment of water in comparison to Ibuprofen, the amount of adsorbed water is small, as calculated from TGA measurements (1-3%). During cooling there is no evidence of this relaxation process since in the previous heating scan the water molecules easily desorbed under the influence of the dry nitrogen atmosphere used for the temperature control. For these reasons the "water process" is not discussed further during the course of this contribution. In addition it must be noted that although a small decrease of intensity of the Ibuprofen relaxation processes is observed, its temperature position remains unchanged, as exemplified by the dashed line in Figure 4.26b). Only the spectra obtained on cooling will be taken for further analysis.

Molecular Mobility

Figure 4. 26 gives the dielectric loss of Ibuprofen confined to the pores of MCM-41 for different temperatures for the available frequency range. The dielectric loss of Ibuprofen embedded to the MCM-41 molecular sieve shows several dielectric active relaxation processes as already discussed for bulk Ibuprofen. At the lowest temperatures (Figure 4. 26a) a secondary process with a weak intensity is observed, pursued with increasing temperature by a further secondary relaxation process which have similar features to the bulk local γ and β processes therefore the same label will be applied. Besides the two local relaxations, at higher temperatures three processes, labeled I, II and III in order of increasing temperature are observed (Figure 4. 26b). With increasing temperature the process labeled II gains in its dielectric strength and becomes the dominating process.

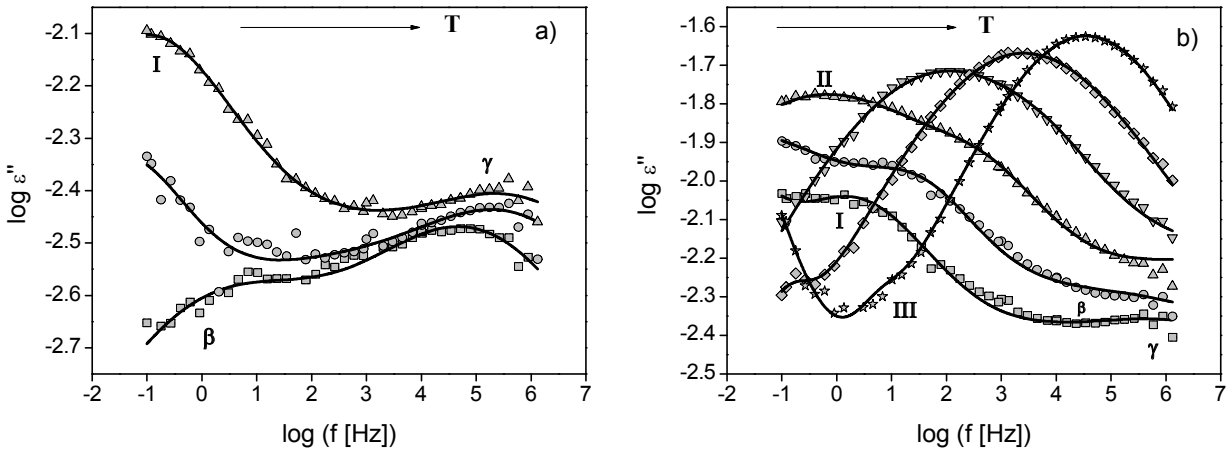

Figure 4. 26- (a) Dielectric loss *versus* frequency for Ibu/MCM-41 at □ - *T* = 159 K, O- *T* = 183 K and △- *T* = 203 K; (b) Dielectric loss *versus* frequency for Ibu/MCM-41 at □- *T* = 219 K, O- T= 233 K, △- *T* = 247 K, ▽- T = 263 K, ◇- *T* = 277 K and ☆- *T* = 293 K. The solid lines are the overall HN fitting curves to the data.

Figure 4. 27 compares the dielectric loss for Ibuprofen in the bulk and confined to the pores of both molecular sieves *versus* temperature at fixed frequency (isochronal plot), also illustrating the multi-

modal character of the spectra. Process II shows up for Ibuprofen confined in both matrices as a broad and rather intensive peak as compared to the other modes. In spite of the low filling degree, the plots confirm the existence of secondary relaxations in the confined systems. One can see that Ibuprofen has a different mobility in confinement; moreover the molecular mobility seems to be sensitive to the pore size.

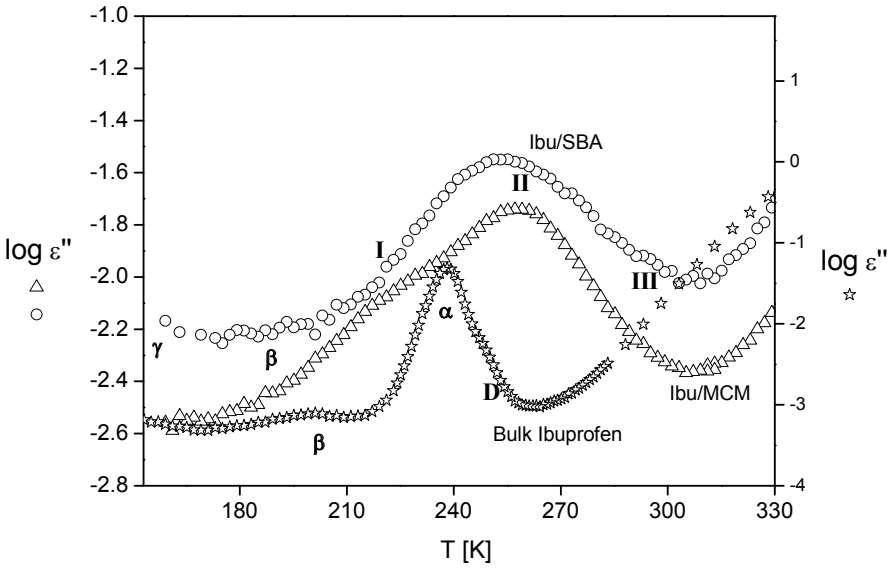

Figure 4. 27- Dielectric loss of Ibuprofen *versus* temperature at a frequency of 10 Hz confined to the MCM-41 and SBA-15 molecular sieves during cooling in comparison to the bulk.

The model-function of Havriliak-Negami (HN-function) is used to analyze the dielectric data and to resolve the different relaxation processes (details can be found in Chapter I and [24,40]).
Figure 4. 28 gives four examples for the used fitting procedure. The spectral shape (α_{HN} and β_{HN}), the dielectric strength ($\Delta\varepsilon$) and the relaxation time (τ) for each process extracted from the fitting procedure are discussed in the following in detail.

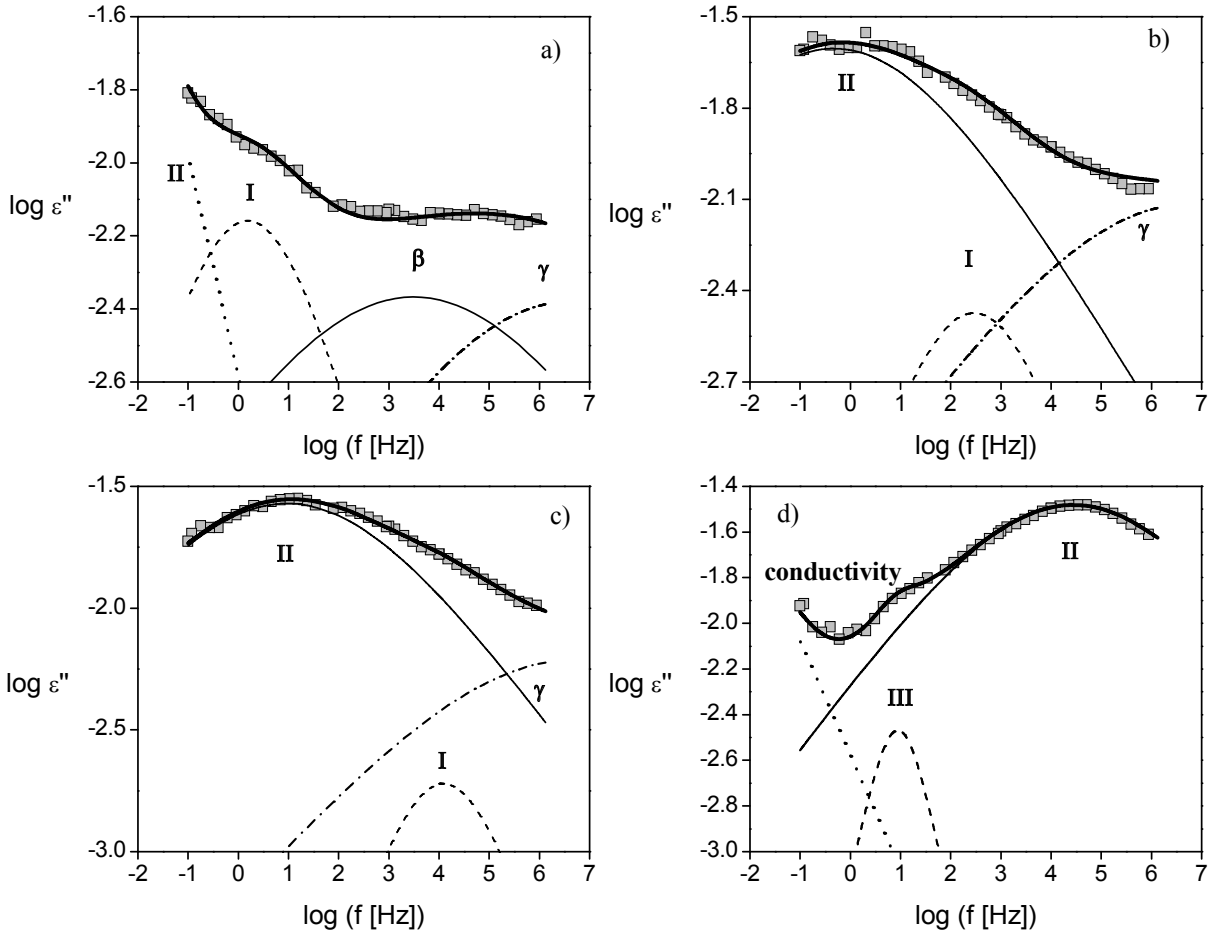

Figure 4. 28- Four examples of the fitting procedure for Ibu/SBA-15 where an additive contribution of three HN-functions is assumed at a) 219 K, (b) 243 K, (c) 253 K and (d) 287 K. The solid lines represent the overall fit and the dashed lines the individual HN-functions.

i) Spectral shape

Both secondary relaxation processes show a pronounced non Debye behavior for the different confined samples. The peak of the γ-relaxation is broad ($\alpha_{HN} \sim 0.3$) and almost symmetric ($\alpha_{HN} \cdot \beta_{HN} = 0.27$). The β process can be well described by a symmetrical Cole-Cole function (*i.e.*, β_{HN}= 1) with $\alpha_{HN}\sim 0.25$; these parameters were kept constant in the narrow temperature range where it was possible to follow the β-trace.

The peak of relaxation I is symmetric for both samples, with $\alpha_{HN}= 0.50 \pm 0.08$ for Ibu/MCM-41 and $\alpha_{HN}= 0.50 \pm 0.05$ for Ibu/SBA-15, slightly increasing with the temperature. The same is observed for process II with $\alpha_{HN}= 0.33 \pm 0.05$ for the different confined systems. Process III is characterized by a Debye-like behavior (α_{HN} = 1; β_{HN} = 1).

ii)-Dielectric strength

The temperature dependence of the dielectric strength, $\Delta\varepsilon$, for the different processes in both confined samples, is shown in Figure 4. 29.

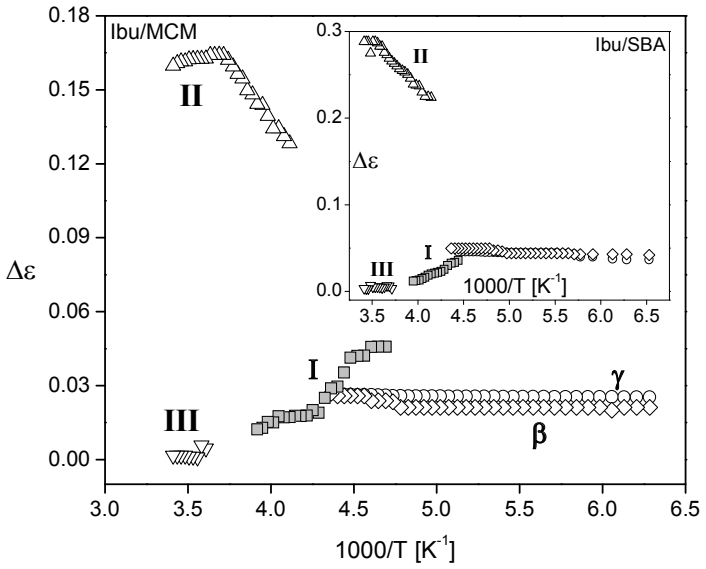

Figure 4. 29- Dielectric strength, $\Delta\varepsilon$, for the γ (circles), β (losanges), processes I (squares), II (triangles) and III (down triangles) *versus* 1/T for Ibu/MCM-41. The inset shows $\triangle\varepsilon$ *vs.* 1/T plot for the Ibu/SBA-15.

Concerning the temperature dependence of the dielectric strength, for localized processes like the γ- and the β-relaxation, $\Delta\varepsilon$ generally increases with temperature due to an increase of the number of fluctuating dipoles and/or the fluctuation angle of the dipole vector with temperature [62,63]. In the case of both secondary relaxation processes found for Ibuprofen confined to the different molecular sieves only a slight increase is observed, like for bulk Ibuprofen.

For process I, $\Delta\varepsilon$ decreases with increasing temperature. This particular behavior can be recognized as a characteristic sign of the α-relaxation, as it is well known for conventional glass formers and polymers [64].

A different pattern is observed for the process II. $\Delta\varepsilon_{II}$ increases with increasing temperature which has been already seen in the raw data (Figure 4. 26b). However, it increases up to a maximum value. This will be discussed later on.

Taking into consideration that process I has the features of the dynamic glass transition as also seen by the closeness in temperature location to the α process detected in the bulk and that process II is a rather broad and intense process, localized at higher temperatures compared to the bulk processes (remember Figure 4. 27), it can be assumed that the process I is assigned to Ibuprofen molecules confined inside the pores which behave bulk-like probably located in the center of the pores and the latter is related to the Ibuprofen molecules confined inside the pores which are in interaction with the pore surface. In fact, recent multinuclear solid-state NMR studies of Ibu/SBA-15 by Izquierda-Barba et al. [56] suggested the existence of two families of molecules, with different mobilities: one which does not interact with the surface, and another that could interact with the Si-OH present at the pore wall. The weak hydrogen bonds between the carboxylic moiety groups of Ibuprofen monomers and the silanol groups are exemplified in Figure 4. 30.

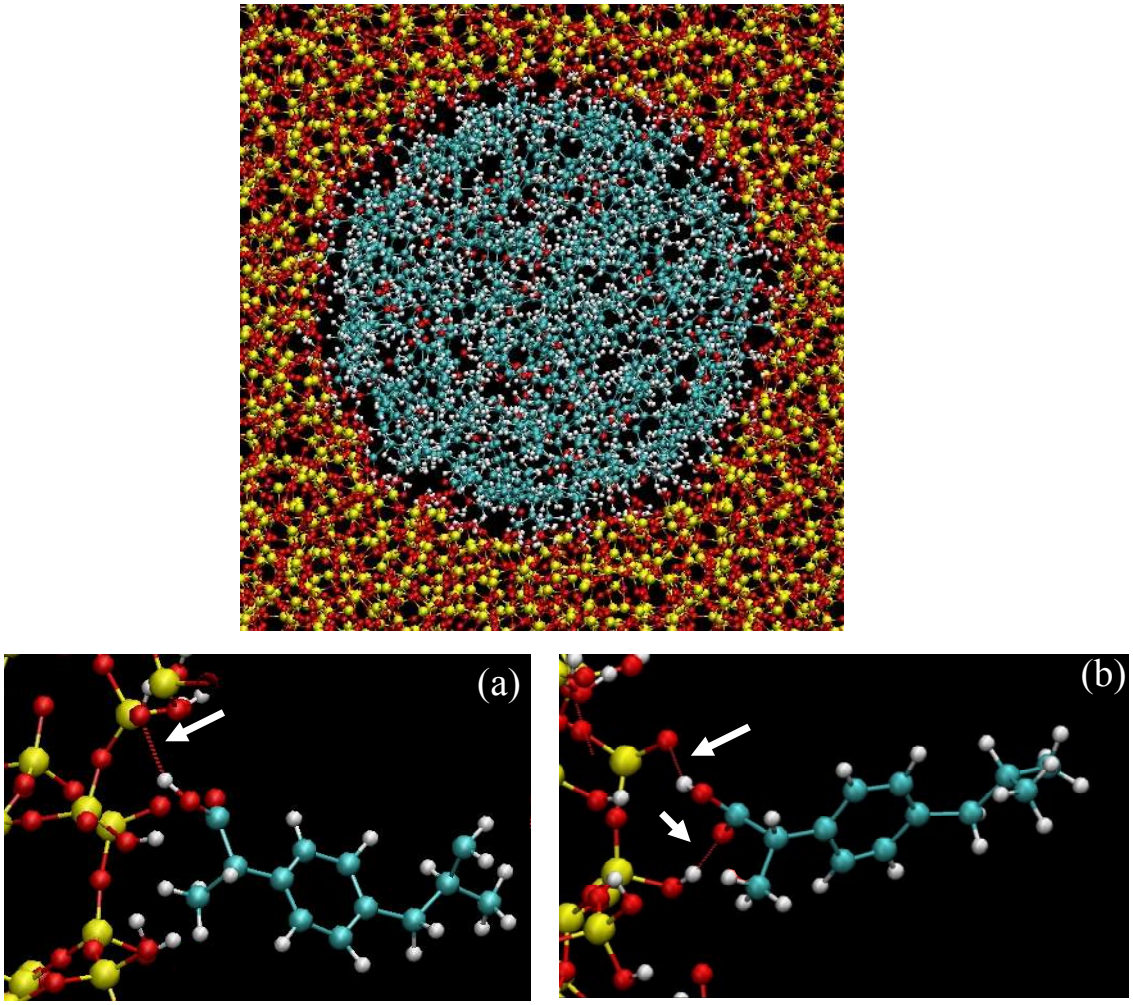

Figure 4. 30- The upper part shows the top view of a simulation cell obtained by MD simulations of ibuprofen confined in a completely filled cylindrical pore of 3.6 nm diameter that mimics MCM-41 mesoporous materials [65] (courtesy of F. Affouard, LDSMM, Univ. Lille); The lower part represents a zoom of the simulation cell illustrating the interaction of ibuprofen group carboxylic with the silanol groups through: (a) one hydrogen bond and (b) two hydrogen bonds identified by the white arrows.

Thus process II could be related to Ibuprofen molecules weakly linked to the silanol groups of the pore wall via the carboxyl groups as shown in Figure 4. 30 and/or as physisorbed dimmers [66].

A different hypothesis for explaining the origin of process I is that it can be due to Ibuprofen molecules attached to the outer pore surface as was detected for *E*7 confined in the same kind of hosts. However, in the latter the two surface processes (inner and outer) merge into a single one at high temperatures which does not seem to be the case for processes I and II. Also a completely different guest-host interactions is observed between the two systems: *E*7 strongly interacts with the silanol groups (see previous sub-chapter) while Ibuprofen will link to the silanol via weak OH-interactions. Moreover, the detection of the secondary processes already weak in the bulk Ibuprofen make it reasonable that a process associated to the dynamic glass transition should also take place.

Concerning process II, it has an abnormally broad shape and a high intensity, similarly to the surface processes detected in other confined systems, like confined $E7$ as seen previously [19,30]. Although the studies on bulk amorphous Ibuprofen point to a majority of molecules associated as hydrogen bonded aggregates predominantly cyclic (Chapter III), this result can be an indication that Ibuprofen molecules are linked preferentially as monomers (see Figure 4. 30) or linear dimers to the matrix surface. In fact, having in mind that the dipole moment of linear dimers, estimated from molecular dynamics simulation results, for bulk Ibuprofen [67] are higher than the respective cyclic ones, it is expected that a process involving monomers or linear aggregates would result in a more intense dielectric response.

For the above reasons, process I will be designated α-relaxation and process II as S process.

Regarding process III, its dielectric strength is almost temperature independent and it is a Debye-type relaxation (α_{HN} = β_{HN}= 1) similarly to the D process observed in the supercooled and liquid states of bulk Ibuprofen. As process III shows up in the low frequency flank of the S process (remember Figure 4. 26 b) and Figure 4. 28 d), it will be labeled from now on as D_S in order to distinguish from the bulk-like D process. This attribution will be clarified further on.

iii)-Relaxation map

Figure 4. 31 shows the temperature dependence of the relaxation times, τ_{max}, for all relaxation processes in comparison with the bulk. Additionally the corresponding values of τ obtained from the isochronal representation of the dielectric loss, *i.e.*, ε'' *versus* temperature at constant frequencies ($\varepsilon''(T; f = const)$) are given for Ibu/SBA-15. A superposition of 3 Gaussians [68] was fitted to the isochronal representation of ε'' to obtain the maximum temperature of peaks, $T_{max,k}$, for each measured frequency, like in the example given in Figure 3.17 in Chapter III. The two data sets coincide very well. The agreement between the two methods validates the use of isochronal data especially when the respective loss peaks maxima are poorly defined in the frequency domain or out of the accessible frequency range. This method has also been proved to be advantageous in distinguishing multiple processes [68,69,70]

Due to the multiple relaxation processes found in Ibuprofen, for the sake of clarity the relaxation map will be analyzed in order of increasing temperature.

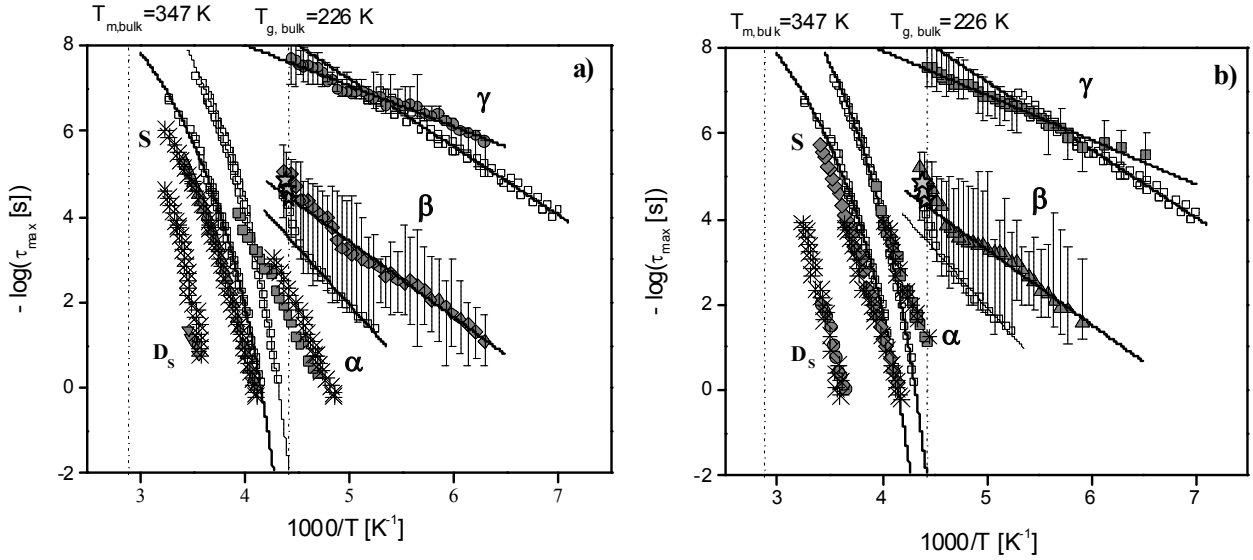

Figure 4. 31- Relaxation time, τ_{max}, *versus* $1/T$ for all processes: Open symbols – bulk isothermal loss data collected during cooling; Gray filled symbols - τ obtained from isothermal loss data collected during cooling for the confined samples: a) Ibu/MCM-41, b) Ibu/SBA-15; Asterisks - τ obtained from the isochronal plots for all studied frequencies f ($\tau = 1/(2\pi f), 1/T_{max}$). Lines are fits of the Arrhenius and VFTH formulas to the corresponding data. Light gray stars indicate the JG relaxation time, τ_{JG}, estimated from Coupling Model (Equation 1.40 in Chapter I) for the bulk Ibuprofen. Vertical dashed lines are the dielectric bulk glass transition temperature T_g^{diel} ($\tau = 100\ s$) = 226 K and the bulk crystal melting temperature T_m = 347 K. The dielectric strength of γ and β processes is small. This means the estimation of the relaxation bears some uncertainties. The error bars in these relaxations might be some estimates for these uncertainties.

γ and β process

In the glassy state the relaxation times for the two secondary processes (γ and β) follow a linear dependence of $-log(\tau_{max})$ *vs.* $1/T$ as expected for relaxation processes related to localized fluctuations. The activation energy E_A and the τ_∞ parameters calculated for Ibuprofen confined in 3.6 and 6.8 nm pores are included in Table 4. 5. It can be seen that these values are similar, appearing not to be dependent on the pore size.

The values of the activation energy (pre-exponential factor) of both samples for the γ- and the β-relaxations are relatively lower (higher) than the corresponding values for the bulk (Chapter III).

One has to keep in mind that the analysis of the γ and β processes, due to a very low dielectric strength presents some uncertainties and therefore error bars of the corresponding times were integrated in the relaxation map.

Normally, localized processes are not commonly observed in confined systems [30,34] but here the presented results show the presence of two secondary relaxations as revealed in Figure 4. 26, Figure 4. 27 and Figure 4. 28 in agreement with Bergman *et al.* who have already reported secondary

processes for two glass-formers confined to Na-vermiculate clay, namely the dipropylene glycol and the 3-fluoroaniline [71].

	$\gamma - process$		$\beta - process$	
$Samples$	E_A [kJ·mol^{-1}]	τ_∞ [s]	E_A [kJ·mol^{-1}]	τ_∞ [s]
Ibu/MCM-41	18.2 ± 0.6	(2 ± 1) × 10^{-12}	34 ± 1	(5 ± 3) × 10^{-13}
Ibu/SBA-15	20.0 ± 0.6	(8 ± 5) × 10^{-13}	34 ± 1	(9 ± 4) × 10^{-13}

Table 4. 5- Activation energy and pre-exponential factor for the secondary γ- and β- relaxation times for Ibuprofen confined to the both molecular sieves estimated from the Arrhenius equation (Equation 1.5).

The temperature dependence of the relaxation time of the β process for both systems can be discussed in the framework of the Coupling Model (CM) [72]. The bulk Ibuprofen dielectric data have been analyzed before by the CM indicating that the β process of bulk Ibuprofen is a "genuine" Johari-Goldstein relaxation (Chapter III). The corresponding relaxation time value of $\tau_{JG} \approx \tau_0$ at bulk T_g is 4x10^{-5} s (Chapter III), in good agreement with the experimental τ_β of 2 × 10^{-5} s and 1.26 × 10^{-5} s for 3.6 nm and 6.8 nm pores, respectively, at the same temperature. Therefore one can assign the β process observed for both confined samples as also a JG- relaxation [73]. Under extreme confinement the α- relaxation becomes indistinguishable from the JG or the primitive relaxation [74]. In this case the primitive relaxation time at bulk T_g is too high for the τ_α values found for these confined systems suggesting that it will probably be reached on further decrease of the pore size.

The α −relaxation

Figure 4. 32 presents the data of τ_α for both Ibuprofen confined to 3.6 and 6.8 nm pores collected over slightly more than 3 decades in comparison with bulk Ibuprofen data. The first interesting observation is that both confined systems follow an Arrhenius-like behaviour, contrary to what was observed for bulk Ibuprofen, that presents a pronounced VFT-law dependence. Close to T_g the dynamics is much faster than that in the bulk. In the literature this is the so called confinement effect [75], which points to an inherent length scale [76,77,78] for glassy dynamics of Ibuprofen in MCM-41 and SBA-15. Moreover the temperature dependence of τ_α for Ibu/MCM-41 seems to cross that of the bulk. A similar effect was clearly observed by Schönhals et al. [78,79,80] for poly (methyl siloxane) (PMPS) confined to nanoporous glasses smaller than 7.5 nm pore sizes. The authors suggested that this points to the fact that the thermodynamical state of the confined polymer is different to that of the bulk [77]. However for a more detailed discussion further studies are needed.

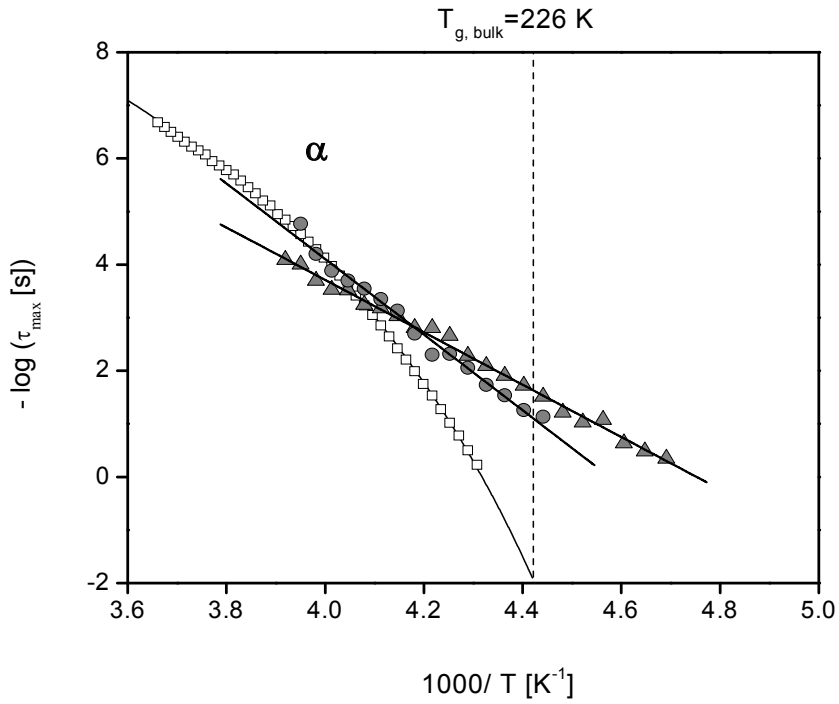

Figure 4. 32- Comparison of the temperature dependence relaxation times of the α processes for both 3.6 and 6.8 nm pores with that of the bulk: □ -bulk; gray filled △ - Ibu/MCM-41; gray filled O - Ibu/SBA-15. Lines are fits of the Arrhenius and VFTH formulas to the corresponding data.

The values estimated for the parameters E_A, $\tau_\infty$and T_g ($\tau = 100s$) obtained by fitting the Arrhenius equation (Equation 1.5- Chapter I) to the data are summarized in Table 4. 6. It can be seen that the activation energy decreases with decreasing pore size, indicating that the glassy dynamics of Ibuprofen in MCM-41 is faster than in SBA-15. Concerning the prefactor τ_∞ the obtained values are unphysically low and unacceptable as also reported for example, for poly(dimethyl siloxane) (PDMS) confined to 5.0 nm silica-based nanoporous glasses [77]. In fact, typical values of the prefactor τ_∞ for simple Arrhenius processes are around 10^{-12} - 10^{-14}s and lower values imply an activation entropy greater than zero according to the Eyring formalism [81], which are associated with complex mechanisms. Thus, the results obtained suggest that some degree of cooperativity of the α- relaxation is still remaining in both Ibuprofen confined to 3.6 and 6.8 nm pores. In other words, the temperature dependence of τ_α is probably still VFTH-like [74], although it is much weaker than that of bulk Ibuprofen. These results are in agreement with the temperature dependence of the relaxation strength shown above which according to Kirkwood and Fröhlich should decrease with increasing the temperature for VFT-like temperature dependence of the relaxation time τ.

As already mentioned under extreme confinement the α- relaxation becomes indistinguishable from the JG or the primitive relaxation [74]. Nevertheless, the results here presented for the α- relaxation show that the activation energy (pre-exponential factor) for confined Ibuprofen (Table 4. 6) is higher (lower) than the corresponding values of the secondary β_{JG} (Table 4. 5). This is an indication that a minimal length scale relevant for the glassy dynamics in Ibuprofen is not yet reached at 3.6 nm.

Figure 4. 33 shows the glass transition temperature as a function of the inverse of pore diameter $1/d$. It is seen in the figure that a decrease in T_g for Ibuprofen in the studied molecular sieves is observed with decreasing pore size [82]. The experimental data show a linear relationship between T_g and $1/d$ over the range of pore diameters investigated (correlation coefficient of 0.98).

Samples	Ibu/MCM-41	Ibu/SBA-15
E_A [kJ·mol^{-1}]	95 ± 2	136 ± 4
τ_∞ [s]	(8 ± 2) × 10^{-24}	(2.6 ± 0.3) × 10^{-33}
T_g ($\tau = 100\ s$)[K]	194	206

Table 4. 6- Activation energy and pre-exponential factor for the α-relaxation times for both 3.6 and 6.8 nm pores estimated from the Arrhenius equation (Equation 1.5). The glass transition temperature T_g was also estimated at τ=100s.

This effect is similar to the effect observed for conventional glass forming systems in confinement [83,84,85,86]. As noted previously, the cause of the glass transition depression at the nanometre scale size is unknown despite the fact that considerable effort has been made to gain insight into this topic. Nevertheless, this can be discussed in two directions. On the one hand, the weaker temperature dependence of the α- relaxation under confinement in both the 3.6 and 6.8 nm are due to a real confinement effect. This means that the length scale of the cooperative molecular fluctuations related to the glassy dynamics are interfering with that of the confining host which leads to a weaker temperature dependence and a faster dynamics compared to the bulk. On the other hand because the filling degrees are low and so the pores are not completely filled the density of the bulk-like molecules in confinement is lower than in the bulk which would also lead to a faster molecular dynamics.

A closer inspection to Figure 4. 25b) which compares isochronal curves at 10^3 Hz for both Ibuprofen confined to MCM-41 with different filling degrees seems to reveal however that the mobility does not change significantly even if the filling degree has increased. Nonetheless further analysis is necessary which is in preparation.

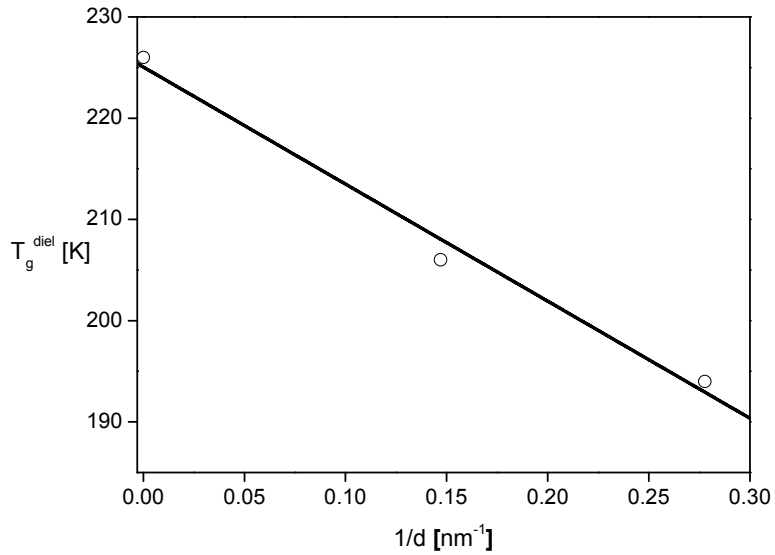

Figure 4. 33- Glass transition temperature determined from the DRS results *versus* pore diameter for Ibuprofen in 3.6 and 6.8 nm pores. The T_g value for bulk liquid ibuprofen is also included (1/ d = 0). The solid line is a linear regression to the data ($r^2 = 0.98$).

The S process

Figure 4. 31 shows that the S process is slower than the bulk-like α- relaxation. As already discussed above and taking into account the NMR results in MCM-41 [60] and SBA-15 [56], the S process is assigned to confined Ibuprofen molecules which are weakly adsorbed at the internal wall of the pores via hydrogen bonding. Therefore these molecules are slowed down in their mobility.

Figure 4. 34 compares the temperature dependence of the relaxation times of the S process for Ibu/MCM-41 and Ibu/SBA-15. For all pore sizes $\tau_{max}(T)$ is curved in a plot *versus* $1/T$ and the data do not follow the Arrhenius law. Moreover this figure indicates also that the temperature dependence of τ_{max} for the surface layer depends on the pore size. For smaller pore sizes the $\tau_{max}(T)$ seems to be more curved than for larger ones: the value of the relaxation time of the surface layer at a given finite temperature seems to decrease with decreasing pore size.

To analyse the temperature dependence of the surface layer in more detail the derivative method is applied (Chapter I). The obtained linear dependence indicates that indeed the temperature dependence of the relaxation times of the S process follows a VFT-dependence with a $T_0 \gg 0$ (see inset of Figure 4. 34). Generally it is believed that VFT-like temperature dependence reflects the cooperative character of the underlying motional process. Hence this can be taken as a hint for the dynamic glass transition of the Ibuprofen molecules which are adsorbed at the pore wall.

The observation of two glass transitions for conventional glass-forming liquids confined in nanopores, was already reported and being found to depend on the interaction between the wall of the pore and the confined liquid. Whereas one of the detected T_g's is close to the bulk, the second one is found to be lower than that for the bulk when guest host interactions are weak while for strong interactions the second T_g is higher [87 and references therein]. The first example seems to be the case for the present study.

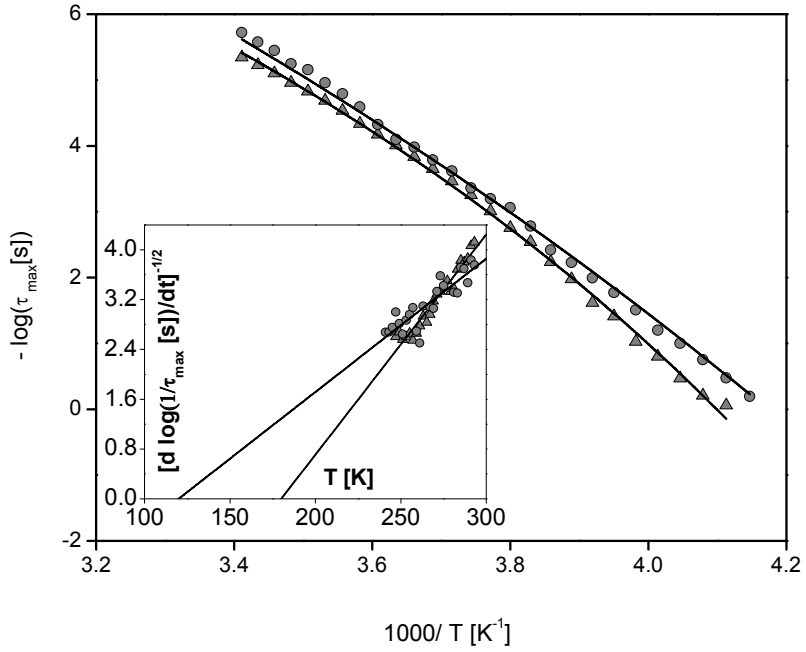

Figure 4. 34- Comparison of the temperature dependence relaxation times for the S process: gray filled △ -Ibu/MCM-41; gray filled O - Ibu/SBA-15. The lines are fits of the VFT-equation to the data. The inset gives $[d\log(1/\tau_{max})/dT]^{-1/2}$ *vs.* temperature for the samples: gray filled △ - Ibu/MCM-41; gray filled O -Ibu$E7$/SBA-15. The lines are linear regressions to the corresponding data.

The VFT-equation was fitted to the data (see Figure 4. 34) where the obtained VFT-parameters are given in Table 4. 7. This analysis shows that the Vogel temperature T_0 related to the dynamics of the surface layer increase systematically with decreasing pore size. This increase in T_0 reflects in addition to the interaction of the molecules with the surface, the influence of the confining geometry on the molecular dynamics of the surface layer. With decreasing pore size due to the geometrical constraint the molecular fluctuations of the molecules becomes more complicated reflected by an increase of T_0. This behavior is different from the one found for $E7$, nevertheless it was already observed for another glass formers under confinement [30,86].

Sample	$-log\ (\tau_\infty[s])$	$A\ [K]$	$T_0\ [K]$
Ibu/MCM-41	14.1	1173	162.4
Ibu/SBA-15	18.2	2177	119.9

Table 4. 7- VFT-parameters characterizing the temperature dependence of the relaxation times of the surface layer obtained by fitting of Equation 1.2 to the data.

This issue is further discussed below considering the temperature dependence of the dielectric relaxation strength.

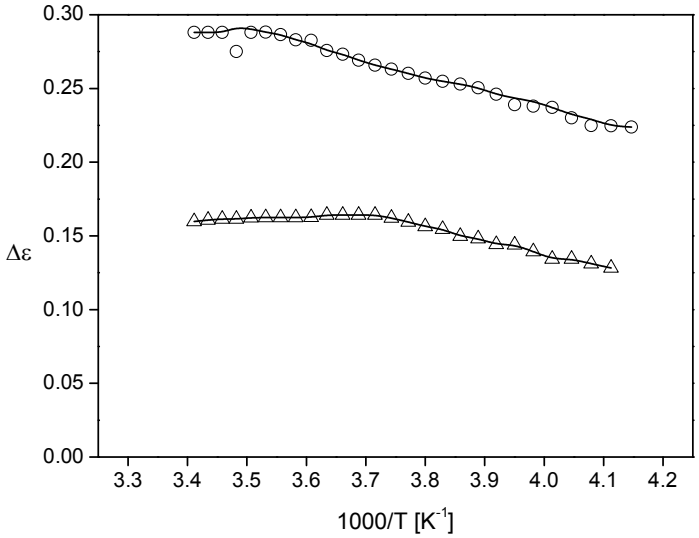

Figure 4. 35- Dielectric strength of the surface layer $\Delta\varepsilon$ *versus* inverse temperature: △ - Ibu/MCM-41; O - Ibu/SBA-15.

Like for the S process of $E7$ confined to the same type of molecular sieves, the temperature dependence of the relaxation strength of the Ibuprofen S process can be understood by a counterbalance of two effects. According to Equation 1.46 by Kirkwood and Fröhlich [24,46] (Chapter I) $\Delta\varepsilon$ should decrease with increasing temperature. Because the involved dipole moment is constant an increase of $\Delta\varepsilon$ can be explained by an increase of the number density of fluctuating dipoles in the surface layer. In general, the strength of the interaction of the Ibuprofen molecules with the surfaces of the pores depends on temperature. For higher temperatures the strength of this interaction is weaker than for lower ones. Because the strength of the interaction is a key parameter for molecular mobility of the molecules at higher temperatures the number of molecules contributing to the surface process is higher than at low temperatures, which explains the increase of $\Delta\varepsilon$ at low temperatures which overbalance the $1/T$ dependence. At higher temperatures the Boltzmann term $1/T$ wins and $\Delta\varepsilon$ decreases with T.

The Debye-type relaxation

Figure 4. 36 shows the temperature dependence of the relaxation times for the D_S process found in the 3.6 and 6.8 nm pores compared with the Debye-like process in the bulk.

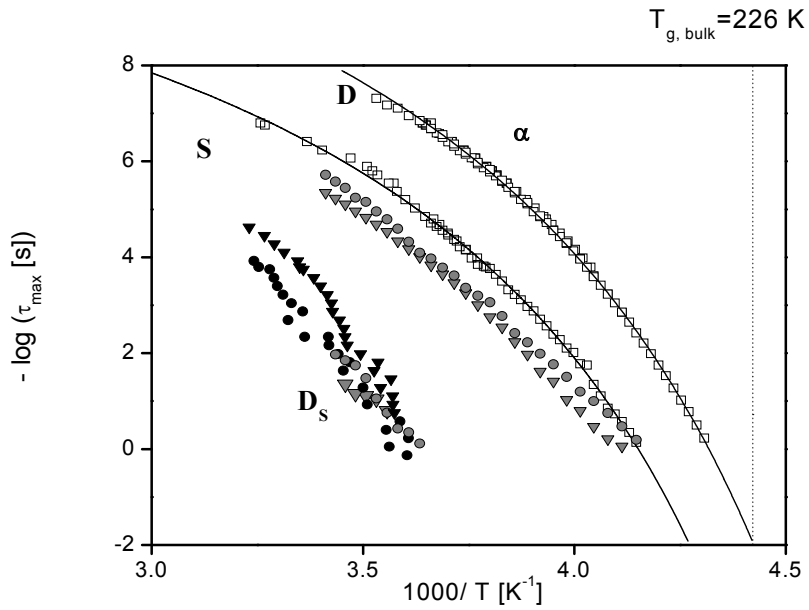

Figure 4. 36- Comparison of the temperature dependence relaxation times for the D_S process for the 3.6 and 6.8 nm pores with that of the bulk: gray filled ▽ - Ibu/MCM-41; gray filled O - Ibu/SBA-15 and □- bulk. Full symbols - τ obtained from the isochronal plots for all studied frequencies f ($\tau = 1/(2\pi f), 1/T_{max}$). The lines are fits of the VFT equation to the bulk data.

As already discussed (chapter III, ref [67]) in bulk ibuprofen a small amplitude Debye-type process appears in the low frequency site of the α-relaxation, presenting some features analogous to the Debye process found in a large class of associating liquids like monohydroxy alcohols, related to hydrogen bonding dynamics. The temperature dependence of its relaxation times (also shown in Figure 4. 36) follows a non-Arrhenius law. Some similarities where found between the VFTH parameters (T_0 and τ_∞) of the D- and the bulk α-relaxation suggesting that the dynamics of the Debye process is governed by the molecular mobility associated to the faster α- relaxation. It was also proposed that the particular molecular mobility of ibuprofen is related to its strong tendency to form a rich distribution of hydrogen bonded aggregates in the liquid and supercooled states (dimers and trimers, either cyclic or linear).

Parallel to bulk ibuprofen, preliminary MD simulations results (not shown here) point to the existence of a distribution of hydrogen bonded aggregates in addition to monomers, in the liquid ibuprofen confined to MCM-41 pores, also suggesting a peculiar dynamical behavior. Consequently, it is not surprising the detection of the slower Debye-like process in confined Ibuprofen (D_S) which is mainly resolved in the isochronal plots of the dielectric loss, located at higher temperatures (lower frequencies) than the most intense S process. The later was attributed in this work to the glass transition of the ibuprofen molecules (*e.g.* monomers, linear dimers) possibly localized close to the pore walls and interacting with the surface silanol groups via weak hydrogen bonds. Given that the D_S-relaxation is localized much closer to the S process than to the bulk-like α-relaxation (remember Figure 4. 31) and it presents a temperature dependence of its relaxation times seemingly parallel to the temperature dependence of τ_S (Figure 4. 36), it may be hypothesized that the dynamics of the D_S

process is controlled by the S process. Additional studies are needed in order to clarify the origin of the Debye process.

4.3.4 Conclusions

Dielectric relaxation spectroscopy was applied to study the molecular mobility of Ibuprofen confined to MCM-41 and SBA-15 molecular sieves with identical composition (100% Si) but different pore sizes, 3.6 and 6.8 nm respectively. TGA measurements allowed obtaining the respective filling degrees which are around 30%, in the same range as the values found in the literature. Moreover, ATR-FTIR confirmed the existence of intermolecular hydrogen bonded associations for both confined samples. A shift to lower wavenumbers of the carbonyl-stretching vibration band, as also detected for supercooled bulk Ibuprofen when compared to the crystalline one, indicated that confined Ibuprofen may be amorphous at room temperature in accordance with previous NMR results.

A complex relaxation map including two secondary relaxations, γ and β, a main bulk-like α process associated with the dynamic glass transition, a S process assigned to the Ibuprofen molecules weakly adsorbed at the internal pore wall and a related Debye-like process (D_S-relaxation) was obtained by the dielectric analysis.

The γ- and β-relaxations have essentially the same dynamics than the secondary processes found in the bulk, and have no dependence on the pore size. Like in the bulk, the β-relaxation for Ibu/MCM-41 and Ibu/SBA-15 are interpreted as "genuine" Johari-Goldstein (JG) process which is a fundamental characteristic of glass formation.

The temperature dependence of the relaxation time of the α process for both Ibu/MCM-41 and Ibu/SBA-15 changed from a VFT- to an Arrhenius-like behavior. Thus, an acceleration of the molecular dynamics compared to the bulk state is observed, which is interpreted as a confinement effect. This points to a dramatic change in the character of the underlying motions processes and thus an inherent length scale relevant to the glassy dynamics was achieved. Moreover, the calculated activation energy values decrease with decreasing pore size, indicating that the glassy dynamics of Ibuprofen in MCM-41 is faster than in SBA-15. However, the values estimated for the pre-exponential factor suggested that some degree of cooperativity of the α-relaxation is still remaining in both Ibuprofen confined to 3.6 and 6.8 nm pores, so a minimal length scale relevant for the glassy dynamics in Ibuprofen is not yet reached at 3.6 nm. This is in agreement with the fact that the τ_α values found for these confined systems are still lower than the primitive relaxation time at bulk T_g since under extreme confinement the bulk-like α-relaxation becomes indistinguishable from the JG or the primitive relaxation.

The S process results revealed that for both systems an interfacial layer via weak hydrogen bonding is formed close to the pore walls which have an essentially lower molecular mobility than the molecular mobility in the bulk. Furthermore it obeys a Vogel-Fulcher-Tamman (VFT) law, as shown by the analysis using a derivative technique. Therefore, a glassy dynamics of the Ibuprofen molecules linked

to the pores surface is given by the S process. The corresponding Vogel temperature increases with decreasing pore size, which can be explained by the interaction of the Ibuprofen molecules with the pore walls and the geometrical restriction due to the confinement.

At lower frequencies than the S process an additional weak intensity relaxation process, with characteristics of a Debye-type relaxation, is observed and designated D_S –relaxation to distinguish from the bulk D process. In parallel to what was found for the D process with the α- relaxation in bulk Ibuprofen, the dynamics of this process seems to be governed by the surface process.

4.4 References

[1] IANNACCHIONE GS, FINOTELLO D (1992) PHYS. REV. LETT. 69, 2094.

[2] IANNACCHIONE GS, FINOTELLO D (1994) PHYS. REV.E 50, 4780.

[3] BRÁS AR, DIONÍSIO M, HUTH H, SCHICK CH, SCHÖNHALS A (2007) PHYS. REV. E 75, 061708.

[4] BRÁS AR, VICIOSA MT, RODRIGUES C, DIAS CJ, DIONISIO M (2006) PHYS REV E 73, 061709.

(5) RÓZANSKI, S. A.; STANNARIUS, R.; GROOTHUES, H.; KREMER, F. LIQ. CRYST. 1996, 20, 59.

[6] RÓZANSKI SA, KREMER F, GROOTHUES H, STANNARIUS R (1997) MOL. CRYST. LIQ. CRYST. 303, 319.

[7] BENGOECHEA MR, ALIEV FM (2005) J. NON-CRYST. SOLIDS 351, 2685.

[8] SINHA G, LEYS J, GLORIEUX C, THOEN (2005) J. PHYS. REV. E 72, 051710.

[9] BENGOECHEA MR, ALIEV FM (2005) J. NON-CRYST. SOLIDS 351, 2685.

[10] VRBANCIC N, VILFAN M, BLINC R, DOLINSEK J, CRAWFORD GP, DOANE JW (1993) J. CHEM. PHYS. 98, 3540.

[11] ZENG H, FINOTELLO D (1992) PHYS. REV. LETT. 69, 2094.

[12] HAVRILIAK S, NEGAMI S (1967) POLYMER 8, 161; HAVRILIAK S, NEGAMI S (1966) J. POLYM. SCI. C 16, 99.

[13] SCHÖNHALS A, KREMER F (2003) "BROADBAND DIELECTRIC SPECTROSCOPY" (EDS.) KREMER F, SCHÖNHALS A, SPRINGER-VERLAG, BERLIN HEIDELBERG, PAGE 59.

[14] VICIOSA MT, NUNES AM, FERNANDES A, ALMEIDA PL, GODINHO MH, DIONISIO M (2002) LIQ. CRYST. 29, 429.

[15] CAPACCIOLI S, PREVOSTO D, BEST A, HANEWALD A, PAKULA T (2007) J. NON-CRYST. SOLIDS 353, 4267.

[16] SINHA G, ALIEV F (1998) PHYS. REV. E 58, 2001.

[17] FRUNZA S, FRUNZA L, SCHÖNHALS A, ZUBOWA HL, KOSSLICK H, CARIUS HE, FRICK R (1999) CHEM. PHYS. LETT. 307, 167.

[18] HOURRI A, BOSE TK, THOEN J (2001) PHYS. REV. E 63, 051702.

[19] FRUNZA S, FRUNZA L, SCHÖNHALS A, TINTARU M, ENACHE I, BEICA T (2004) LIQ. CRYST. 31, 913.

[20] SCHÖNHALS A, KREMER F (2003) "BROADBAND DIELECTRIC SPECTROSCOPY" (EDS.) KREMER F, SCHÖNHALS A, SPRINGER-VERLAG, BERLIN HEIDELBERG, PAGE 99.

[21] SCHÖNHALS A, KREMER F (2003) "BROADBAND DIELECTRIC SPECTROSCOPY" (EDS.) KREMER F, SCHÖNHALS A, SPRINGER-VERLAG, BERLIN HEIDELBERG, PAGE 392 FF.

[22] KREMER F, HUWE A, SCHÖNHALS A, RÓŻAŃSKI SA (2003) "BROADBAND DIELECTRIC SPECTROSCOPY" (EDS.) KREMER F, SCHÖNHALS A, SPRINGER-VERLAG, BERLIN HEIDELBERG, PAGE 212.

[23] LOBO CV, PRASAD SK, RAO DSS (2004) PHYS. REV. E 69, 051706.

[24] SCHÖNHALS A, KREMER F (2003) "BROADBAND DIELECTRIC SPECTROSCOPY" (EDS.) KREMER F, SCHÖNHALS A, SPRINGER-VERLAG, BERLIN HEIDELBERG, PAGE 1.

[25] STEEMAN PAM, VAN TURNHOUT J (2003) "BROADBAND DIELECTRIC SPECTROSCOPY" (EDS.) KREMER F, SCHÖNHALS A, SPRINGER-VERLAG, BERLIN HEIDELBERG.

[26] JAGADEESH B, PRABHAKAR A, DEMCO DE, BUDA A, BLÜMICH B (2005) CHEM. PHYS. LETT. 404, 177.

[27] FRUNZA S, KOSSLICK H, SCHÖNHALS A, FRUNZA L, ENACHE I, BEICA T (2003) J. NON-CRYST. SOLIDS 325, 103.

[28] GNATYUK I, PUCHKOVSKAYA G, YAROSHCHUK O, GOLTSOV Y, MATKOVSKAYA L, BARAN J, MORAWSKA-KOWAL T, RATAJCZAK H (1999) J. MOL. STRUCT. 189, 511.

[29] FRUNZA L, FRUNZA S, POTERASU M, BEICA T, KOSSLICK H, STOENESCU D (2009) SPECTROCHIMICA ACTA PART A, 72 , 248.

[30] FRUNZA L, FRUNZA S, KOSSLICK H, SCHÖNHALS A (2008) PHYS. REV. E 78, 051701.

[31] VOGEL H (1921) PHYS. ZEIT., 22, 645.

[32] FULCHER GS (1925) J. AM. CERAM. SOC. 8, 339.

[33] TAMMANN G, HESSE G (1926) ANORG. ALLGEM. CHEM. 156, 245.

[34] BRAS AR, DIONÍSIO M, SCHÖNHALS A (2008) J. PHYS. CHEM. B 112, 8227.

[35] FRUNZA S, SCHÖNHALS A, FRUNZA L, ZUBOWA H-L, KOSSLICK H, FRICKE R, CARIUS H (1999) CHEM. PHYS. LETT. 307, 167; FRUNZA L, FRUNZA S, SCHÖNHALS A (2004) J. PHYS. IV 10, 121, 11170.

[36] (A) CRAMER CH, CRAMER TH, ARNDT M, KREMER F, NAJI L, STANNARIUS R (1997) MOL. CRYST. LIQ. CRYST. 303, 209; (B) ALIEV FM, SINHA G (1996) MATER. RES. SOC. PROC. 411, 125.

[37] RÓZANSKI SA, KREMER F, GROOTHUES H, STANNARIUS R (1997) MOL. CRYST. LIQ. CRYST. 303, 319.

[38] FRUNZA L, KOSSLICK H, PITSCH I, FRUNZA S, SCHÖNHALS A (2005) J. PHYS. CHEM. B 109, 9154.

[39] RYABOV YA, GUTINA A, ARKHIPOV V, FELDMAN YU (2001) J. PHYS. CHEM. B 105, 1845; RYABOV YE, PUZENKO A, FELDMAN YU (2004) PHYS. REV. B 69, 014204.

[40] KREMER F, SCHÖNHALS A (EDS.) (2003) "BROADBAND DIELECTRIC SPECTROSCOPY", SPRINGER-VERLAG, BERLIN HEIDELBERG, PAGE 35 FF AND 59FF.

[41] ARNDT M, STANNARIUS R, GORBATSCHOW W, KREMER F (1996) PHYS. REV. E 54, 5377.

[42] KREMER F, HUWE A, ARNDT M, BEHRENS P, SCHWIEGER W (1999) J. PHYS.: CONDENS. MATTER, 11, A175.

[43] ARNDT M, STANNARIUS R, GROOTHUES H, HEMPEL E, KREMER F (1997) PHYS. REV. LETT. 79, 2077.

[44] ALIEV FM (1996) "COMPLEX GEOMETRIES" (EDS.) CRAWFORD GP, ŽUMER S, LONDON, TAYLOR AND FRANCIS, CH. 17.

[45] ALCOUTLABI M, MCKENNA GB (2005) J. PHYS.: CONDENS. MATTER 17, R461.

[46] BÖTTCHER CJF (1973) THEORY OF DIELECTRIC POLARIZATION, 2ND ED., ELSEVIER, AMSTERDAM.

[47] FRUNZA S, FRUNZA L, TINTARU M, ENACHE I, BEICA T, SCHÖNHALS A (2004) LIQ. CRYST 31, 7, 913.

[48] PRIVATE COMMUNICATION BY DR. FREDERIC AFFOUARD, DSMM, UNIV. LILLE, FRANCE.

[49] TANIS I, KARATASOS K (2009) J. PHYS. CHEM. B 113, 10984.

[50] AZAIS T, TOURNE-PETEILH C, AUSSENAC F, BACCILE N, COELHO C, DEVOISSELLE J-M, BABONNEAU F (2006) CHEM. MATER. 18, 6382.

[51] VALLET-REGI M, RAMILA A, DEL REAL RP, PEREZ-PARIENTE J (2001) CHEM. MATER. 13, 308.

[52] CHARNAY C, BEGU S, TOURNE-PETEILH C, NICOLE L, LERNER DA, DEVOISSELLE J-M (2004) EUR. J. PHARM. BIOPHARM. 57, 533.

[53] SILVERSTEIN RM, BASSLER GC, MORRIL TC (1991) SPECTROMETRIC IDENTIFICATION OF ORGANIC COMPOUNDS, 5TH ED.; JOHN WILEY & SONS: NEW YORK.

[54] BHAGIYALAKSHMI M, YUN LJ, ANURADHA R, JANG HT J POROUS MATER DOI 10.1007/S10934-009-9310-7

[55] MUÑOZ, RÁMILA A, PÉREZ-PARIENTE J, DÍAZ I, VALLET-REGÍ M (2003) CHEM. MATER. 15, 500.

[56] SONG SW, HIDAJAT K, KAWI S (2005) LANGMUIR 21, 9568.

[57] IZQUIERDO-BARBA I, SOUSA E, DOADRIO JC, DOADRIO AL, PÉREZ-PARIENTE J, MARTÍNEZ A, BABONNEAU F, VALLET-REGI M (2009) J. SOL-GEL SCI. TECHNOL. 50,421.

[58] BABONNEAU F, YEUNG L, STEUNOU N, GERVAIS C, RAMILA A, VALLET-REGI M (2004) J. SOL-GEL SCI. TECHNOL., 31, 219.

[59] BABONNEAU F, CAMUS L, STEUNOU N, RAMILA A, VALLET-REGI M (2003) MATER. RES. SOC. 775, 3261.

[60] AZAÏS T, HARTMEYER G, QUIGNARD S, LAURENT G, TOURNE-PETEILH C, DEVOISSELLE JM, BABONNEAU F (2009) PURE APPL. CHEM. 81, 8, 1345.

[61] MELLAERTS R, JAMMAER JAG, VAN SPEYBROECK M, CHEN H, VAN HUMBEECK J, AUGUSTIJNS P, VAN DEN MOOTER G, MARTENS JA (2008) LANGMUIR, 24, 8651.

[62] SCHÖNHALS A (1997) "DIELECTRIC SPECTROSCOPY OF POLYMERIC MATERIALS" (EDS.) RUNT J, FITZGERALD J, ACS BOOKS: WASHINGTON.

[63] SCHÖNHALS A (2003) "BROADBAND DIELECTRIC SPECTROSCOPY" (EDS.) KREMER F, SCHÖNHALS A, SPRINGER VERLAG: BERLIN, CH. 7.

[64] KREMER F, HUWE A, SCHÖNHALS A, RÓŻAŃSKI SA (2003) "BROADBAND DIELECTRIC SPECTROSCOPY" (EDS.) SCHÖNHALS A, KREMER F, SPRINGER-VERLAG, BERLIN HEIDELBERG, CHP.4.

[65] BUSSELEZ R, LEFORT R, JI Q, AFFOUARD F, MORINEAU D PHYS. CHEM. CHEM PHYS. IN PRESS. DOI: 10.1039.

[66] VALLET-REGI M, BALAS F, ARCOS D. (2007) ANGEW. CHEM. INT. ED. 46, 7548.

[67] BRAS AR, NORONHA JP, ANTUNES AMM, CARDOSO MM, SCHONHALS A, AFFOUARD F, DIONISIO M, CORREIA NT (2008) J. PHYS. CHEM. B 112, 11087.

[68] HARTMANN L, KREMER F, POURET P, LÉGER L (2003) J. CHEM. PHYS. 118, 6052.

[69] SMITH IK, ANDREWS SR, WILLIAMS G, HOLMESB PA (1997) J. MATER. CHEM., 7, 203.

[70] VICIOSA MT, RODRIGUES C, FERNÁNDEZ S, MATOS I, MARQUES MM, DUARTE MT, MANO JF, DIONÍSIO M (2007) J. POLYM. SC.: PART B: POLYM. PHYS. 45, 2802.

[71] BERGMAN R, MATTSON J, SVANBERG C, SCHWARTZ GA, SWENSON J (2003) EUROPHYS. LETT. 64 (5), 675.

[72] NGAI KL (2003) J. PHYS.: CONDENS. MATTER 15, S1107.

[73] NGAI KL (2006) J. POLYM. SC.: PART B: POLYM. PHYS. 44, 2980.

[74] NGAI KL, KAMIŃSKA E, SEKUŁA M, PALUCH M (2005) J. CHEM. PHYS. 123, 204507.

[75] KREMER F, HUWE A, SCHÖNHALS A, RÓŻAŃSKI SA "BROADBAND DIELECTRIC SPECTROSCOPY" SCHÖNHALS A, KREMER F (EDS) SPRINGER-VERLAG, BERLIN HEIDELBERG, 2003, CHP.6.

[76] JOHARI GP, GOLDSTEIN MJ (1970) CHEM. PHYS. 53, 2372; (1971) J. CHEM. PHYS. 55, 4245.

[77] SCHÖNHALS A, GOERING H, SCHICK CH, FRICK B, MAYOROVA M, ZORN R (2007) EUR. PHYS. J. SPECIAL TOPICS 141, 255.

[78] SCHÖNHALS A, GOERING H, SCHICK C, FRICK B, ZORN R (2004) COLLOID POLYM. SCI. 282, 882.

[79] SCHÖNHALS A, GOERING H, SCHICK C, FRICK B, ZORN R (2003) EUR. PHYS. J. E 12, 173.

[80] SCHÖNHALS A, GOERING H, SCHICK C, FRICK B, ZORN R (2005) J. NON-CRYST. SOLIDS 351, 2668.

[81] EYRING H (1936) J. CHEM. PHYS. 4 183.

[82] JACKSON CL, MCKENNA GB (1991) J. NON-CRYST. SOLIDS 131–133, 221.

[83] ARNDT M, STANNARIUS R, GORBATSCHOW W, KREMER F (1996) PHYS. REV. E, 54, 5377.

[84] KREMER F, HUWE A, ARNDT M, BEHRENS P, SCHWIEGER W (1999) J. PHYS.: CONDENS. MATTER. 11, A175.

[85] ARNDT M, STANNARIUS R, GROOTHUES H, HEMPEL E, KREMER F (1997) PHYS. REV. LETT. 79, 2077.

[86] ALIEV FM (1996) "COMPLEX GEOMETRIES" (EDS.) CRAWFORD GP, ŽUMER S, LONDON, TAYLOR AND FRANCIS, CH. 17.

[87] ALCOUTLABI M, MCKENNA GB (2005) J. PHYS.: CONDENS. MATTER. 17, R461.

CHAPTER 5| CHANGES IN POLY(L-LACTIC ACID) MOLECULAR MOBILITY UPON CONSTRAINING

INDEX

Sections of this chapter were published in *Macromolecules* (2006) **39** 6513-6520, and *Macromolecules* (2008) **41** 6419-6430

5.1 Introduction

In this work, dielectric relaxation spectroscopy was used to monitor isothermal crystallization in poly(L-lactic acid) (PLLA) by probing the evolution of the loss peak with crystallization time. It was found, by crystallization either from the glassy or melt states, that the data could be given by a linear combination of three loss processes, where just their intensities vary: the α process of the amorphous material, the constrained α process presented in the fully crystallized material, corresponding to the segmental motions of the amorphous phase confined by the crystalline lamellae, and the sub-glass β-relaxation. The appearance of the confined process was detected in the earlier stages of the crystallization, suggesting that the confinement effects are effective during primary crystallization. It was observed that the isothermal crystallization is slower as compared with a lower molecular weight PLLA and evolves faster for the material undergoing cold-crystallization as compared with crystallization from the melt. Nevertheless, the confined dynamics is not very dependent on the thermal history prior to the crystallization step.

Moreover, specimens with $0.43 \leq \chi_C \leq 0.65$ were also dielectric characterized. By changing the temperature of crystallization, T_C, distinct crystalline forms were obtained. The dynamic glass transition relaxation process shifts to higher frequencies/lower temperatures with the increase of crystallinity. From the VFT temperature dependence of relaxation times, the glass transition and Vogel temperatures were estimated decreasing with increasing χ_C. The semi-crystalline morphology of PLLA was analyzed in terms of a three phase model consisting of crystalline, mobile amorphous and rigid amorphous phases, MAP and RAP, respectively [1]. The mobility enhancement in specimens with higher χ_C was rationalized in terms of both i) thicker rigid amorphous phase that decreases the influence of the rigid crystalline wall on the cooperative motions of the main relaxation process and ii) less dense mobile amorphous phase.

A multi-component character was found for the secondary relaxation process, being the sum of three components with weighted contributions that vary with crystallinity, each presenting Arrhenius temperature dependence. These processes tend to converge at high temperatures in a single broad process identical to the one found in amorphous PLLA.

5.2 Experimental Conditions

PLLA Non-isothermal and Isothermal Crystallization at 353 K

Amorphous samples were evacuated at about 323 K for 48h to remove absorbed water [2]. The cooling down to room temperature was accomplished under vacuum.

Two samples were used: sample 1) was employed to characterize amorphous PLLA, tempting non-isothermal crystallization ($\langle Mn \rangle$= 180 000), and sample 2) to induce isothermal crystallization ($\langle M_n \rangle = 269\,000$). Both were cooled down to 153 K.

Sample 1)- The dielectric spectra were collected in increasing temperature steps from 153 up to 413 K: in the temperature range 168 K ≤ T ≤ 203 K and 333 K ≤ T ≤ 373 K the dielectric spectra were recorded every 2 K; in the remaining temperature region the spectra were recorded every 5 K.

Sample 2)- The dielectric spectra were gathered in increasing temperature steps from 153 K up to 298 K: in the temperature range 168 K ≤ T ≤ 203 K the dielectric spectra were recorded every 2 K; in the remaining temperature region the spectra were recorded every 5 K.

After this procedure, dielectric spectra of sample 2) were acquired, isothermally (T = 353 K) every 2 min, during 6 h; the crystallization achieved in these conditions will be designated as *cold crystallization*. Next, the sample was cooled down to 153 K and the dielectric spectra were collected up to 413 K; in the temperature range 168 K ≤ T ≤ 203 K and 333 K < T ≤ 373 K, the dielectric spectra were recorded every 2 K; in the remaining temperature region the spectra were recorded every 5 K. Then sample 2) was kept two minutes at 473 K to assure melting and immediately cooled down to

353 K. At this temperature, the crystallization was monitored according to the same procedure followed during cold crystallization; the crystallization achieved in these conditions will be designated as *melt crystallization.*

Finally, sample 2) was refrigerated to 153 K and dielectric spectra were collected in increasing steps from 153 K up to 413 K, according to the same preset as followed after the cold crystallization procedure.

During both types of crystallization, the complex permittivity was measured within the range from 100 Hz to 1 MHz, in such a way that each spectrum was collected in a time that did not exceed 1 min. This warranted that during any frequency scan the change in crystallinity was significantly small. In the remaining experiments data were acquired in an enlarged frequency range, from 10^{-1} to 1 MHz.

Semi-Crystalline PLLA achieved at different crystallization temperatures T_c >353 K.

The samples ($\langle Mn \rangle$ = 180 000) used for this study were previously vacuum dried at 343 K during 2 days. It was found that this drying period was not enough for specimens crystallized at 368 and 383 K, since the respective dielectric spectra still revealed the presence of water through the additional process like reported in [2]. The disappearance of this dielectric water signature in these PLLA specimens was achieved after 3 more days under vacuum drying at 343 K.

The samples were cooled down to 153 K and the dielectric spectra were collected in increasing temperature steps from 153 K up to 443 K: in the temperature range 153 K ≤ T ≤ 333 K and 373 K ≤ T ≤ 443 K the dielectric spectra were recorded every 5 K; in the remaining temperature region from 333 K ≤ T ≤ 373 K the spectra were recorded every 2 K.

5.3 Amorphous state

5.3.1 Dielectric Relaxation Spectroscopy

The dielectric loss ε'' curves for the α-relaxation in the amorphous PLLA between 337 K and 357 K are shown in Figure 5. 1.

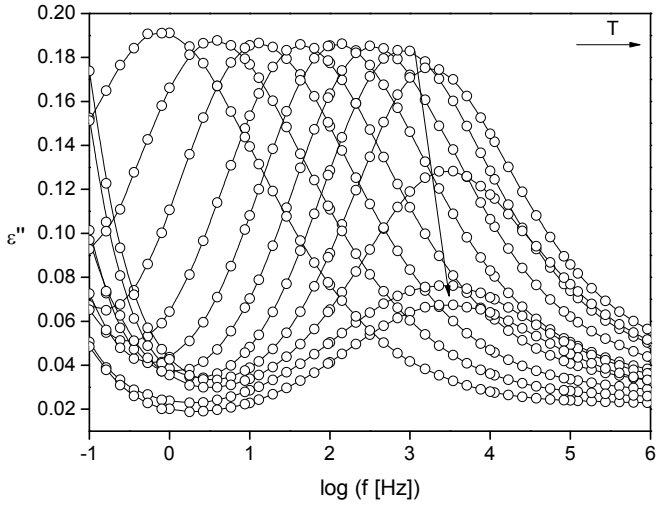

Figure 5. 1- Dielectric loss spectra for amorphous PLLA between 341 K and 357 K in steps of 2 K.

The spectra show a strong relaxation process, associated with the dynamic glass transition. For temperatures higher than 351 K the main relaxation peak decreases abruptly due to crystallization, more specifically in this case, since crystallization is occurring as temperature is changing, *non-isothermal cold-crystallization*. This behavior will be further commented in the text.

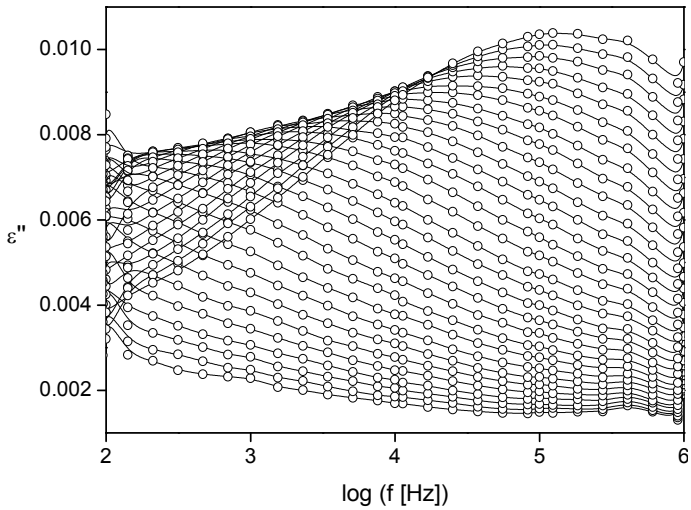

Figure 5. 2- Dielectric loss spectra of the secondary relaxation process detected in the amorphous PLLA sample, within the temperature range from 153 K to 298 K, in steps of 5 K.

At lower temperatures, the dielectric loss spectra obtained for PLLA amorphous state also revealed the existence of a broad secondary β-relaxation (see Figure 5. 2).

The loss curves of the main and secondary processes were fitted by the well known Havriliak-Negami (HN) function [3], as described in Chapter I.

5.3.1.1 The α process

The α process can be fitted by the HN function with the following shape parameters: α_{HN} = 0.53±0.05 and β_{HN} = 0.88 ±0.12. The fact that the shape parameters remain almost invariant with temperature allow drawing a master curve in a normalized plot (see Figure 5. 3).

During the non-isothermal cold-crystallization process, besides a decrease of the dielectric strength $\Delta\varepsilon$, also the shape parameters associated to the α-peak undergo some changes. This can be an indication that the distribution of the relaxation times of the conformational large scale motions associated to the glass transition is affected by the restrictions imposed by crystallization (further in text this will be proved as compared with isothermal cold-crystallization).

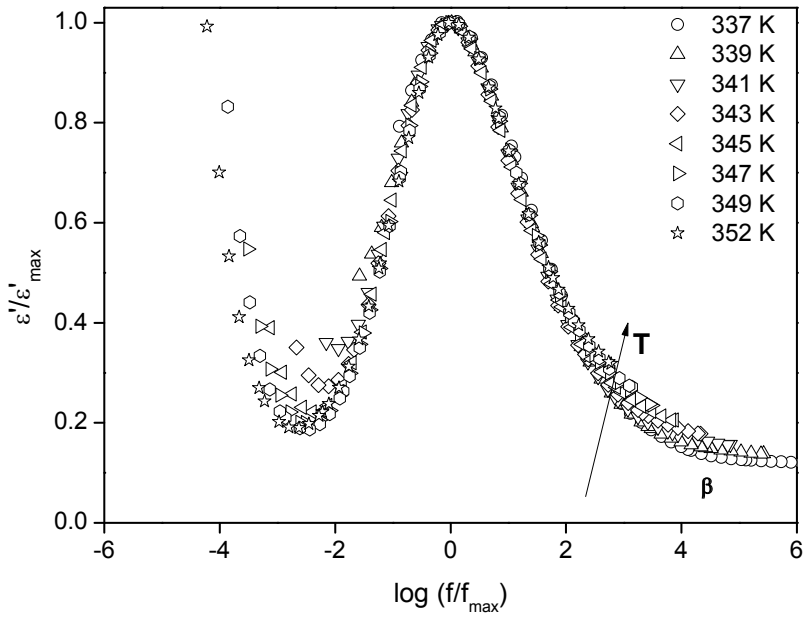

Figure 5. 3- Master curve constructed for amorphous PLLA narrow temperature range (see legend indicated in the figure).

The temperature dependence of the characteristic relaxation time for the α process is presented in Figure 5. 4. It shows a characteristic curvature and the Vogel-Fulcher-Tamman-Hesse equation [4,5,6]] (see Equation 1.2) was fitted to the data.

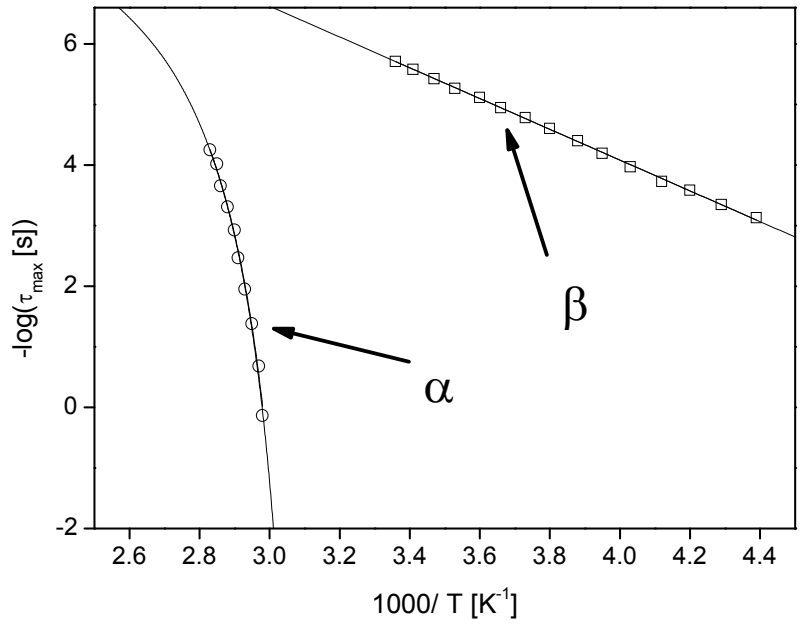

Figure 5. 4- Relaxation map for amorphous PLLA. The solid lines are fits of the VFT-equation and Arrhenius-equation to the data.

The respective parameters are summarized in Table 5.1 that also includes the glass transition temperature, apparent activation energy and fragility index estimated according Equations 1.2 and 1.15, respectively.

τ_∞[s]	B [K]	T_0 [K]	T_g [K]	m
(8±1)×10^{-10}	425±56	315±4	332	221

Table 5. 1- VFTH fitting parameters for the main relaxation process of amorphous PLLA, glass transition (T_g) at 100 s, activation energy energy at T_g and fragility index, m.

The dielectric glass transition value determined is in close agreement with calorimetric data as reported in ref [7] (T_g= 332 K).

5.3.1.2 The β process

The secondary relaxation, as already mentioned, was detected since the very beginning of the measurements at the lowest temperatures (153 K).

The α_{HN} and β_{HN} shape parameters were found to be 0.28±0.02 and 0.79±0.03, respectively. From the linear temperature dependence of the relaxation time, included above in Figure 5. 4, an activation energy of 50 kJ·mol^{-1} was estimated. The low value of α_{HN} indicates that the β-relaxation is characterized by a broad distribution of relaxation times, typically attributed to the existence of a large variety of environments felts by the relaxing species [8]. Due to the inexistence of polar side groups in the PLLA chain, this secondary process has been assigned to twisting motions in the main chains.

Combining dielectric and dipolar moment calculations, Ren *et al.* estimated that the amplitude of such motions in poly(*d,l*-lactic acid) could be characterized by an average twisting angle of around 11º [9]. Its dielectric strength increases with temperature from 0.08 at 223 K to 0.1 at 278 K as usual in localized molecular mechanisms.

5.4 Isothermal crystallization at 353 K

The sample described in the section 5.2 as 2) (see *Experimental Condition* above) was afterwards heated up to 353 K and isothermal loss spectra were collected during 6 hours (*cold crystallization* process). Figure 5. 5a) presents the dielectric loss curves each 10 minutes during the first 4 hours; the last 2 curves were collected after, respectively, 5 and 6 hours.

A similar trend was obtained from melt crystallization at 353 K with a lower molecular weight PLLA, (M_n= 86000, M_w= 151000) [10], here designated as $PLLA_{86kD}$. In that case, besides the expected decrease in the intensity, the main loss peak shifts continuously towards lower frequencies almost one decade, being able to be fitted as a sum of three relaxation processes: (i) the secondary process in the high frequency flank, an α process of the bulk-like (non-restricted) amorphous phase, similar to the one found in nearly amorphous material (α_{NA}) and (iii) an α process of the amorphous fraction influenced by the crystalline structure, similar to the one found in fully transformed material (α_{SC}), each keeping both shape and relaxation time unaltered. The initial ($t = 0$) and the final scans ($t = 6$ h) are considered, respectively, as the nearly amorphous (NA) and fully semi-crystalline (SC) PLLA. It is assumed that these two situations correspond to the two extremes in the segmental dynamics that occur within the amorphous chains: in the former one, all the conformational motions take place in the bulk-like amorphous phase whereas in SC-PLLA all the amorphous phase exists within the spherulites, constrained between the crystalline lamellae or lamellar stacks. The data here obtained were analyzed following the same criterion as in $PLLA_{86kD}$: only three parameters, $\Delta\varepsilon$ of each HN relaxation function, were allowed to change. Therefore, a linear combination of the intensities of the pure loss peaks of the three relaxation processes was fit to the data:

$$\boldsymbol{\varepsilon''_{(t_C,\omega)} = \Delta\varepsilon_{\alpha NA}(t_C)\varepsilon''_{\alpha NA}(\omega) + \Delta\varepsilon_{\alpha SC}(t_C)\varepsilon''_{\alpha SC}(\omega) + \Delta\varepsilon_{\beta}(t_C)\varepsilon''_{\beta}(\omega)} \qquad \textbf{Equation 5. 1}$$

where $\varepsilon''_{\alpha NA}$, $\varepsilon''_{\alpha SC}$ and ε''_{β}, are the loss peaks of the pure α_{NA} (from the results at t_c=0), pure α_{SC} (obtained from the results after complete crystallization, at t_c= 6h) and for β it was found to be irrelevant to pick the parameters of the initial or final states since it almost does not vary.

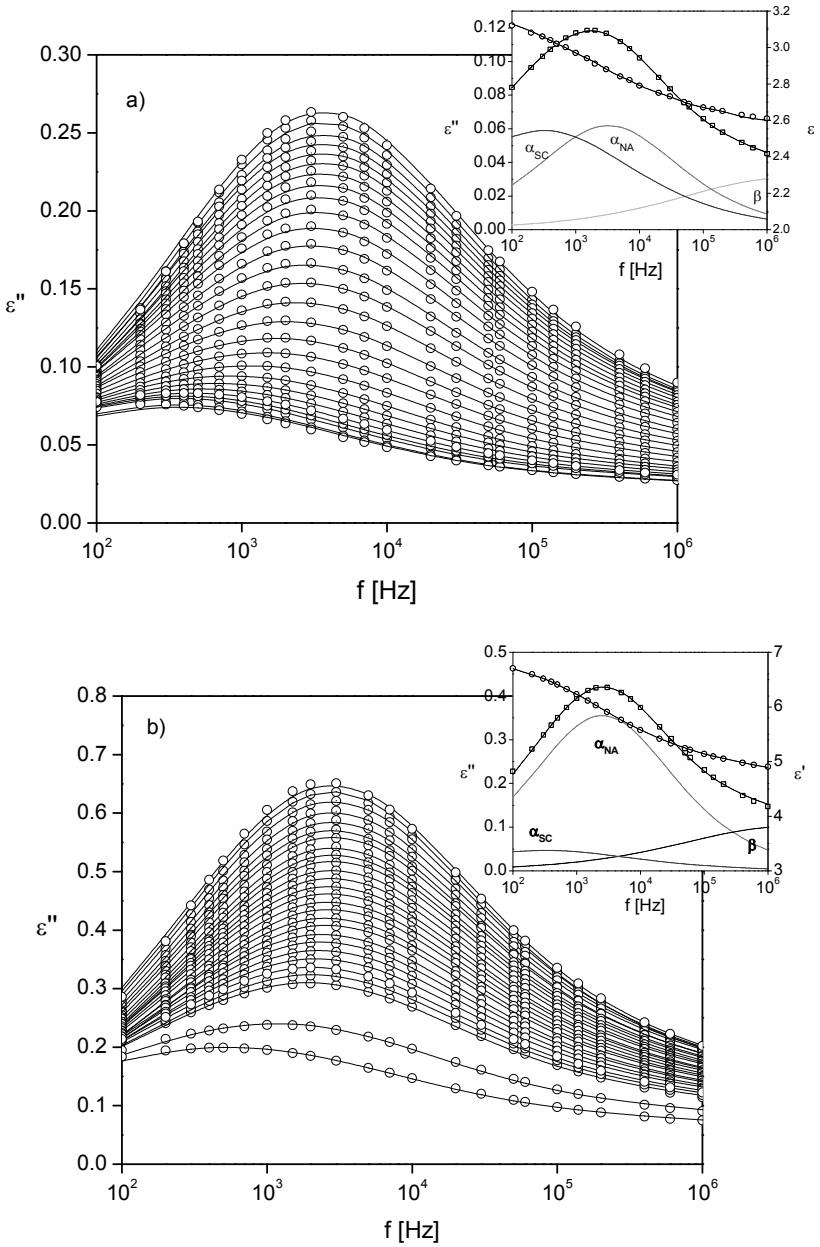

Figure 5. 5- Dielectric loss spectra (circles) at 353 K during a) cold crystallization and b) melt crystallization. The solid lines are the fitting obtained using the sum of three Havriliak-Negami (HN) functions. Only the loss curves collected each 10 minutes are shown for the first 4 hours, and the last two curves were collected at, respectively, 5 and 6 hours. The inset graphics shows the experimental results at 160 minutes (squares for ε'' and circles for ε') and the corresponding fitting taking into account three HN individual curves (solid lines).

The solid lines in Figure 5. 5a) correspond to the overall fitting assuming Equation 5. 1. The inset shows the loss spectrum obtained after 160 min, the obtained fit and the correspondent three individual HN functions. The following parameters were used to fit the different relaxations: for the α_{NA} loss peak, the α shape parameter (α_{HN}) and relaxation time (τ) were 0.53, and 4.80x10^{-5}s respectively, whereas for the α_{SC} loss peak, the correspondent α_{HN} and τ values were 0.43 and 5.06x10^{-4} s; both β shape parameters (β_{HN}) were found to be unit. The β-relaxation was fitted with α_{HN}=0.38, β_{HN}=0.82,

and τ =1.4x10^{-7} s, obtained by the extrapolation of the activation plot of the secondary relaxation process detectable at lower temperatures.

The evolution of the normalized dielectric strength for all processes upon cold crystallization is presented in Figure 5. 6. The data were normalized by the maximum value obtained for the nearly amorphous α process for comparison purposes.

The maximum transformation degree was reached after 200 minutes with the dielectric strength of the bulk-like relaxation process becoming zero and the constrained glass transition relaxation process attaining a steady value.

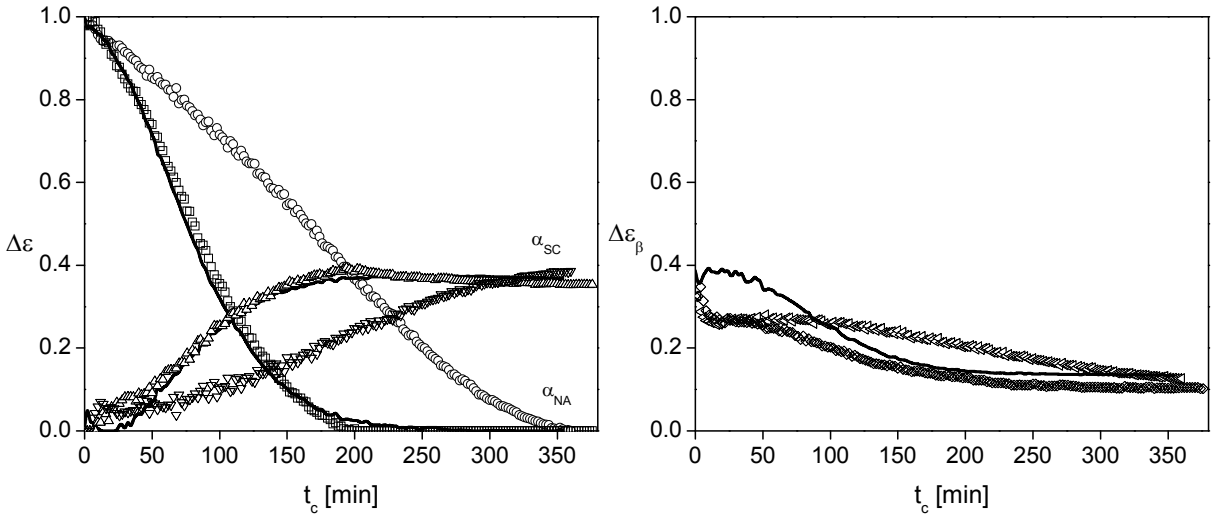

Figure 5. 6- Evolution of the dielectric strength during PLLA cold crystallization and melt crystallization of the three relaxations detected: a) α-relaxation for the nearly amorphous phase (α_{NA}), (□)- cold crystallization and (O)- melt crystallization; α-relaxation for the semi-crystalline phase (α_{SC}), (△)-cold crystallization and (▽)-melt crystallization; b) β-relaxation, (◇)- cold crystallization and (◁)-melt crystallization. Results for a lower molecular weight PLLA, PLLA$_{86kD}$, during cold crystallization were included as solids lines for comparison. Dielectric strength values were normalized by the maximum value obtained for the nearly amorphous α process.

As described in the *Experimental Conditions* section, the same sample was further crystallized isothermally at 353 K after melting at 473 K (melt crystallization process). Dielectric loss spectra were collected as previously during 6 hours and, once again, data were able to be fitted as a sum of exactly the three same HN functions, having only different dielectric strengths (see Figure 5. 5b). Figure 5. 6 includes the variation of the normalized dielectric strength thus obtained. There is a less abrupt decay of the relaxation strength for the bulk-like glass transition relaxation process only vanishing for t_c=350 min, i.e., 150 minutes later than for the cold crystallization process. The same happens with the emerging of the constrained α process, i.e., the respective dielectric strength increases more gradually during melt crystallization meaning that this crystallization process develops slower relative to cold crystallization. This is not surprising since the number of crystal nuclei that are produced during

quenching should be considerable, as the nucleation rate increases with the distance to the equilibrium melting temperature. Therefore, during cold crystallization a greater number of spherulites will grow at a given crystallization temperature with respect to the crystallization at the same conditions with the material coming from the melt. Such difference in the spherulitic development were observed by optical microscopy (see ref. [11]).

Also included in Figure 5. 6 are the normalized dielectric strength values for $PLLA_{86kD}$ obtained during melt-crystallization at 353 K. This plot allows evaluating the influence of molecular weight, where the solid lines, for $PLLA_{86kD}$, should be compared with the circle symbols (higher molecular weight PLLA studied in this work) evidencing that for the low molecular weight the crystallization progress is accelerated. Although the general trends are similar, the evolution of the crystalline process, as monitored through the changes occurring within the amorphous fraction, is much faster for $PLLA_{86kD}$. Such difference was already observed during non-isothermal cold crystallization of the same two polymers, observed by simultaneous SAXS and WAXS and DSC [12].

Figure 5. 5 and Figure 5. 6 demonstrate that the assumptions used to treat dielectric data are valid for two different molecular weights and are independent whenever we consider cold or melt crystallization. This provides new support to state that, at least for PLLA, the development of crystallinity leads to the formation of a more restricted amorphous phase, that increases in magnitude during crystallization, with a concomitant vanishing of the initial bulk-like amorphous phase. This process seems to occur since the very initial stages of crystalline evolution, i.e., the effect of lamellar confinement in the amorphous phase is observed as the total dielectric strength of the loss modulus is decreasing. In fact, Figure 5. 6 shows an increase of $\Delta\varepsilon_{\alpha SC}$ in the very initial stages of the crystallizations, when a decrease in $\Delta\varepsilon_{\alpha NA}$ is also observed. It is hypothesized that the origin of the α_{SC}-relaxation should be a result of the confined mobile amorphous phase placed between the crystalline lamellae, which start to be formed in the primary crystallization step. Besides the mobile amorphous phase, there is also the formation of a rigid amorphous phase placed between the mobile amorphous layer and the crystalline lamellae [13]. The appearance of this phase does not contribute for the increase of $\Delta\varepsilon_{\alpha SC}$, but contributes for the decrease of $\Delta\varepsilon_{\alpha NA}$, because no segmental motions take place in such regions. Therefore the much more notorious decrease in $\Delta\varepsilon_{\alpha NA}$ is explained by the consumption of bulk segments in the amorphous phase giving rise to crystalline material and rigid amorphous phase. This loss of response highly overcomes the simultaneous build up of a confined mobile amorphous phase, which gives rise to lower increase of $\Delta\varepsilon_{\alpha SC}$.

The α_{SC}-relaxation is broader than the α_{NA} process (the α_{HN} parameter is 0.43 and 0.53, respectively). This is consistent with the general observation that the loss peak of the $\alpha-$relaxation for semi-crystalline polymers is broader than that for the corresponding amorphous material [15]. When confined within the crystalline structure the mobile polymeric segments will experiment a wider variety of environments, as they can site more or less apart from the stiff walls, leading to a broadening of the distribution of relaxation times.

Some authors studying different polymers under isothermal crystallization, decided to fit the global loss peaks by using a single HN function (see, for example, refs. [14,15]). In such cases a broadening was continuously observed since the very initial stages of crystallization, as perceived by a decrease in the α_{HN} parameter. Such observations strengths the suggestion that the influence of the confinement caused by the crystalline fraction starts to be effective during primary crystallization. During isothermal crystallization it was seen, from small-angle X-ray scattering, that the thickness of the amorphous layer is kept approximately constant, around 5 nm [16]. Therefore one should not expect a notorious variation of the features, such as the shape parameters and frequency position, of segmental dynamics of the confined amorphous layer during isothermal crystallization. This information is implicit in the proposed model where the loss peak should be given by a linear combination of two "pure" loss processes. Therefore the widening of the global loss peak observed during crystallization has two origins: the fact that the α_{SC} loss peak is intrinsically broader than the α_{NA} and the fact that at intermediate crystallization times we have the influence of both processes.

5.5 Semi-crystalline state

After each crystallization process, PLLA was measured from 153 K up to 413 K, in an enlarged frequency range to detect the influence of crystallization on the secondary β-relaxation and to characterize the restricted glass transition relaxation process that remains.

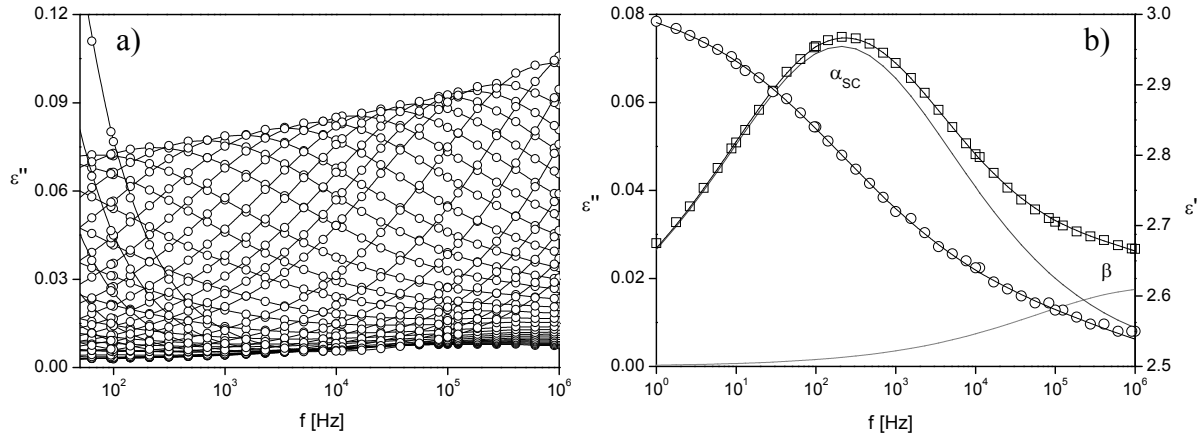

Figure 5. 7- a) Isothermal dielectric loss spectra for the constrained α process detected after cold crystallization within the temperature range from 298 K to 413 K; b) Isothermal loss spectrum at 353 K and the two individual contributions of the α_{SC} and β process.

Figure 5. 7 presents the dielectric loss spectra obtained after complete cold crystallization from 298 K up to 413 K, where mainly the α_{SC} is observable. Nevertheless the β-relaxation is felt in the high frequency side as shown in Figure 5. 7b) obtained at 353 K. Both β and α_{SC} processes were fitted by the Havriliak-Negami equation. The resulting shape parameters and dielectric strength are presented in Figure 5. 8a) for the β process and b) for the α_{SC}-relaxation process.

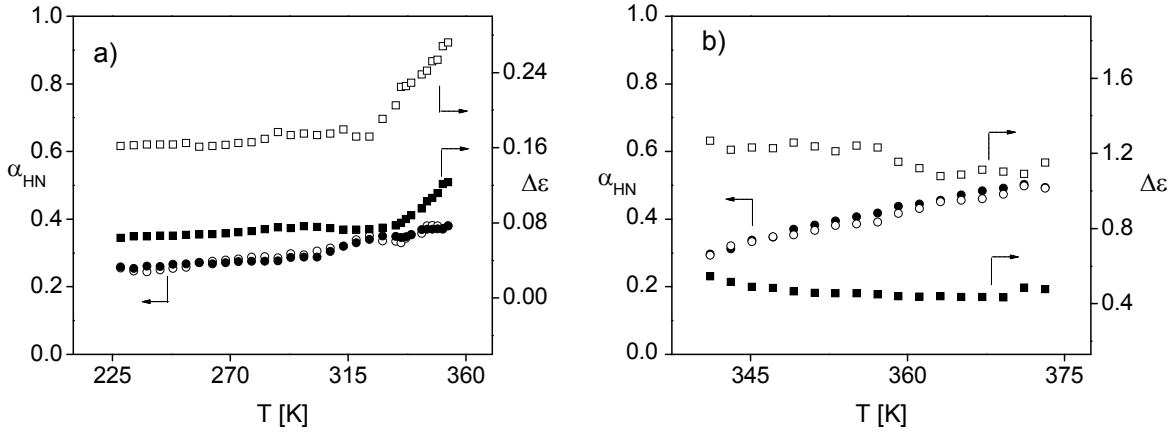

Figure 5. 8- Temperature dependence of α_{HN} shape parameter (circles) and dielectric strength, Δε, (squares) estimated through fitting for the a) β-relaxation and the b) constrained α process detected after cold (full symbols) and melt (open symbols) crystallizations.

The β_{HN} parameter was found to be 0.79 ± 0.03 for the secondary relaxation detected, being equal to the value found for the relaxation detected in the amorphous state.

The respective α_{HN} shape parameters (circles) increase with the temperature increase revealing the narrowness of the distribution of relaxation times with simultaneous symmetry increase (β_{HN} = 1).

The temperature dependence of the obtained relaxation times is shown in Figure 5. 9 for all processes detected.

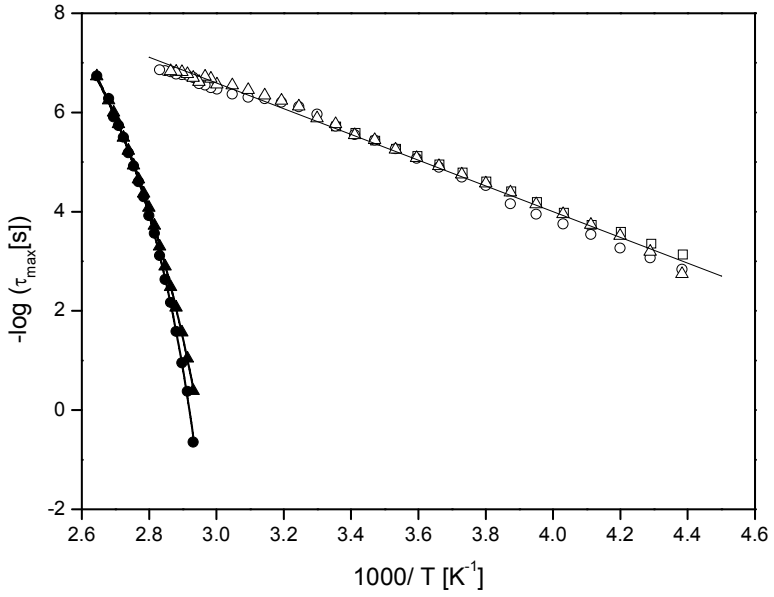

Figure 5. 9- Relaxation map for the secondary process (open symbols) and α constrained relaxation (full symbols) detected after cold crystallization (circles) and after melt crystallization (triangles); the temperature dependence for the β-relaxation detected in the amorphous sample prior to crystallization is also included (squares).

The secondary relaxation process (open symbols) shows the expected linear dependence while the α constrained relaxation process (full symbols) exhibits the usual curvature of cooperative processes.

Additionally, in what concerns the β process, a superposition with the process detected in the amorphous state (squares) is observed, thus, the mobility responsible for this secondary process is not affected by crystallization at T_C = 353 K. The effect of crystallinity in the β-relaxation has been analyzed before. Typically, for flexible polymers, the features of this process are not sensitive to the presence of crystallinity [17]. However, for more stiff materials, a different behavior can be found. For example, for poly(ether ether ketone) is was seen that the isochronal loss maxima of crystallized material were shift towards higher temperatures as compared with the amorphous polymer, indicating that the extent of the motions assigned to this secondary process is greater than would be expected for typically sub-glass relaxations [18]. For the PLLA it may be concluded that the dipole fluctuations assigned to the β-relaxation cover volumes that should be substantially smaller than the geometrical confinement imposed by the crystalline structures, developed from both cold and melt crystallization.

From the Arrhenius equation fit to the data of the three secondary processes a mean activation energy of 50 ± 3 kJ·mol^{-1} was estimated. This value is higher than the activation energies of 36 kJ.mol^{-1} found by other author for PLLA [19,20] or in the range of 36-46 kJ.mol^{-1} for a series of L-lactide/meso-lactide copolymers [19].

In what concerns the temperature dependence of both α constrained relaxation processes, the VFTH- equation (solid lines in Figure 5. 9) was fitted to the data with the following parameters: α_{SC} after cold crystallization, α_0=(0.8 ± 0.8) × 10^{-15} s, B = 1029 ± 64 K and T_0 = 308 ± 1K; α_{SC} after melt crystallization, α_0 = (1.0 ± 0.8) × 10^{-15} s, B = 1631 ± 76 K and T_0 = 292 ± 1K. Considering that the temperature obtained by replacing τ in Equation 5. 1 by 100 s is a good estimate of the glass transition temperature [21] the so obtained values are 338 and 334 K, for the α_{SC} after, respectively, cold and melt crystallizations. Complementary DSC experiments on the same PLLA crystallized at 353 K from the glassy and melt states were performed, and the calorimetric T_g were found to be 343.0 and 342.3 K, respectively. Therefore, also by DSC, the glass transition upon cold crystallization is higher than the one after melt crystallization.

Comparison between the temperature dependence of the relaxation times for the semi-crystalline PLLA attained after isothermal and non-isothermal cold- crystallization is shown in Figure 5. 10. The isochronal plots at 10 kHz taken from isothermal measurements for the same samples are presented as inset in logarithmic scale.

For PLLA non-isothermal cold crystallization the α process is clearly seen, followed by a sharp decrease of ε'' curve that takes place around 353 K, due to crystallization. The new constrained α-relaxation, α_{SC}, appears evidencing a peak with a comparable position to the isothermal crystallization. This is confirmed when looking to the relaxation map where the temperature dependence of the relaxation times for the α_{SC} after non-isothermal crystallization is the same as for the cold-crystallized PLLA.

Moreover, both the different crystallization paths show a superposition of one broad β-relaxation as illustrated in the inset.

It can be concluded that no significant differences of the mobility associated to the α_{SC} relatively to the crystallization method, either isothermal at T_C= 353 K or non-isothermal, are observed.

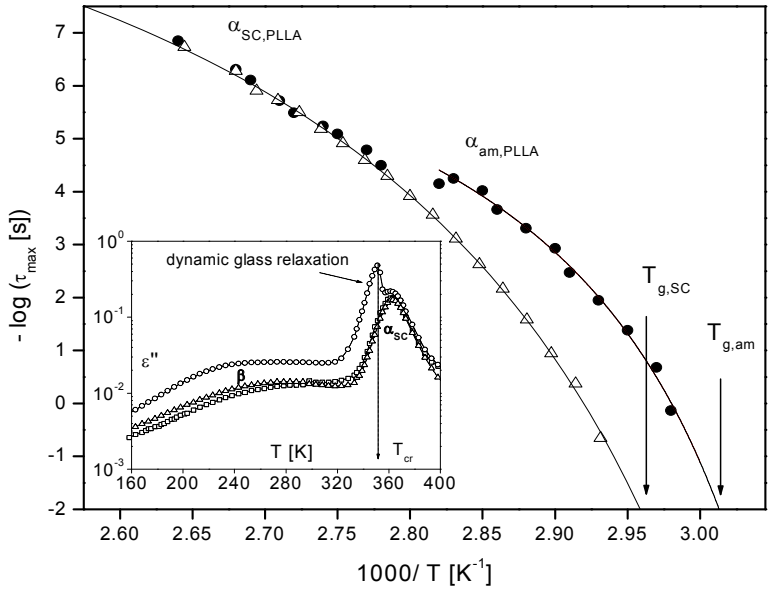

Figure 5. 10- Relaxation map for α constrained relaxation (full circles) detected after non-isothermal cold crystallization and after isothermal cold crystallization (triangles); the temperature dependence for the α-relaxation detected in the amorphous sample prior to crystallization is also included (full circles). The inset shows isochronal plots of ε'' for PLLA non-isothermal crystallization (O), isothermal melt- crystallization (□) and isothermal cold.-crystallization (△). For non-isothermal PLLA crystallization the sharp step at crystallization (T_{cr}) is indicated by the arrow.

5.6 Influence of crystallization at temperatures higher than 353 K

In this section, isothermally cold-crystallized specimens prepared by annealing in an oven for 12 h at temperatures, T_c, ranging between 368 K and 438 K from the glassy state were dielectric characterized (see Chapter II for more details).

The resulting crystallinity degrees, were estimated by WAXS [22] varying between 0.43 (T_c=368 K) and 0.65 (T_c= 438 K) (see Table 5. 2 in the text).

The dielectric loss spectra of semi-crystalline PLLA recorded in the available frequency range at temperatures from 153 K to 373 K is presented in a logarithmic plot in Figure 5. 11 A dominant relaxation process is visible being associated to the dynamic glass transition (α-relaxation) and, at the lowest temperature regions, a secondary process is detected.

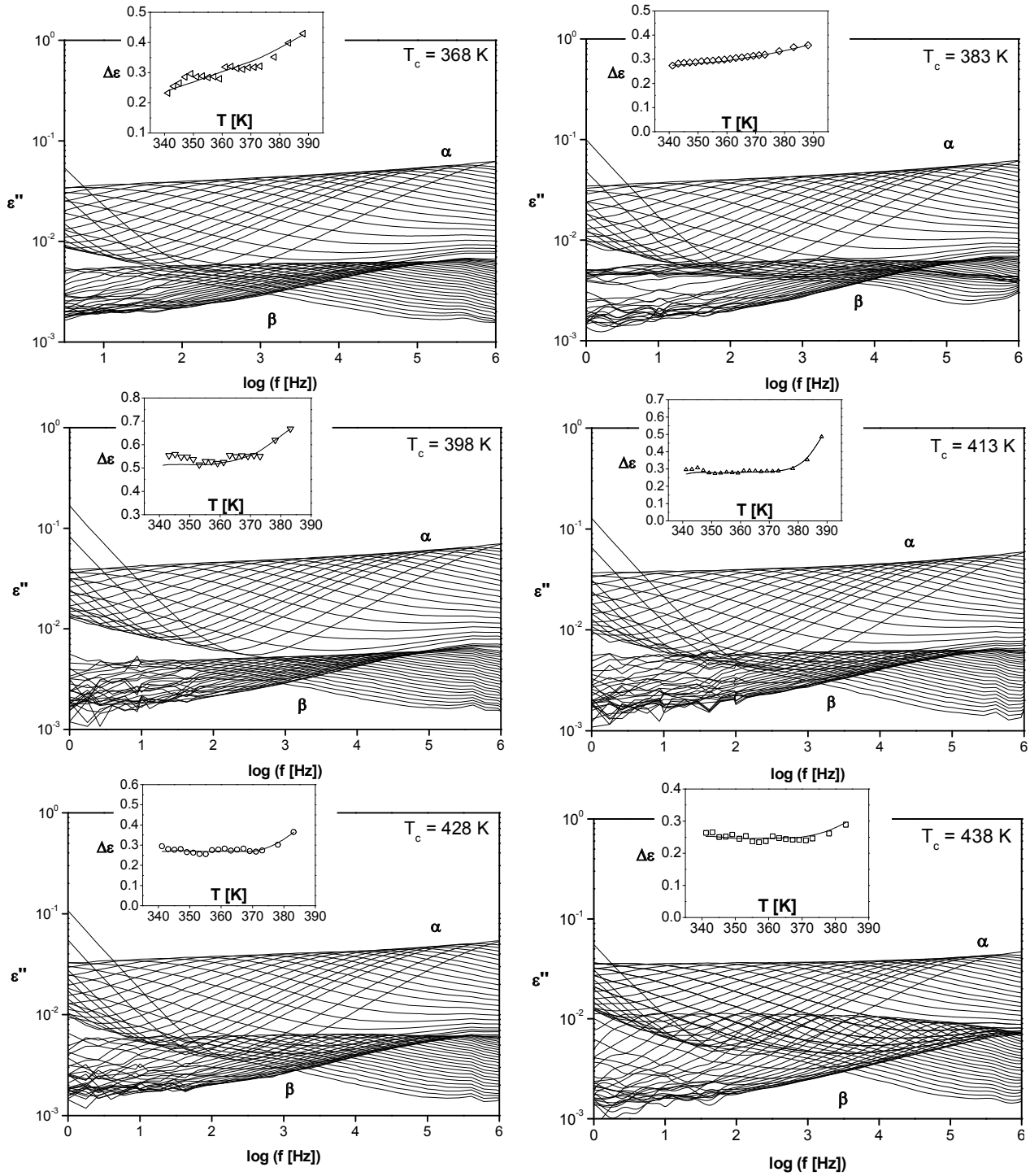

Figure 5. 11- Isothermal dielectric loss spectra for semi-crystalline PLLA from 333 K to 373 K in steps of 2 K in a logarithmic plot. The insets present the temperature dependence of the respective dielectric strength ($\Delta\varepsilon_\alpha$) obtained from the HN fit. Lines are guides to the eyes.

5.6.1 The α-Relaxation

Similar dielectric loss spectra were obtained for the α process of all semi-crystalline PLLA samples. However, a shift in the frequency of the maximum dielectric loss is observed, decreasing with the increase of T_c.

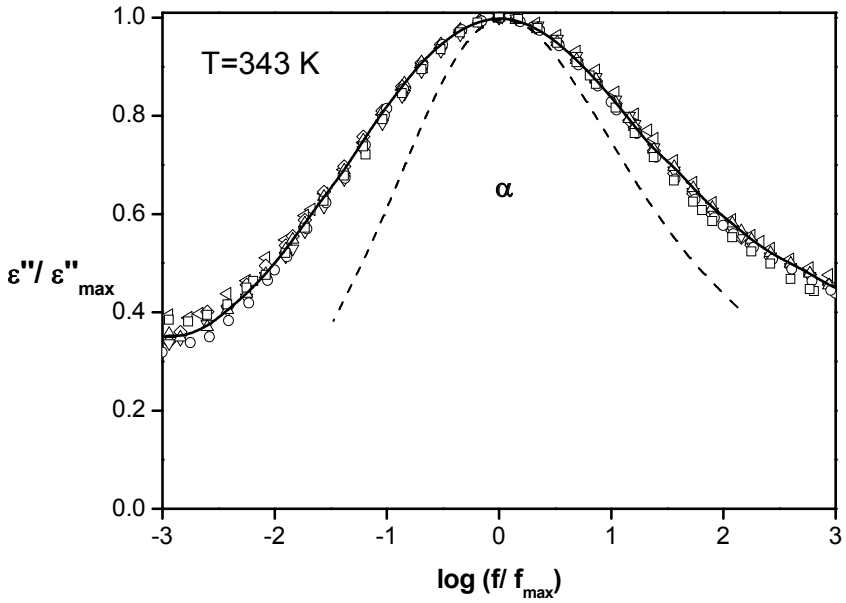

Figure 5. 12- Normalized dielectric loss curves illustrating the invariant shape of the main α-relaxation for all semi-crystalline PLLA specimens at T=343 K: (◁) T_c=368 K, (◇) T_c=383 K, (▽) T_c=398 K, (△) T_c=413 K, (○) T_c=428 K, (□) T_c=438 K, The respective normalized α-peak for the amorphous sample is shown as dashed line. The solid line represents the individual HN function used to fit the semi-crystalline α process.

The estimated α_{HN} shape parameter increases with temperatures from 0.30 (343 K) to 0.42 (383 K) while the β_{HN} fit parameter equals unity. Small variations were found while comparing shape parameters of different specimens. In Figure 5. 12 it is well demonstrated that the normalized α-peak of all specimens at 353 K maintain the same shape as a single curve is defined. The plot includes the normalized α peak for the amorphous sample (dashed line) evidencing a narrower distribution of relaxation times in the latter.

Both α_{HN} and β_{HN} parameters characterizing the present systems, are in good agreement with the values previously found for the constrained α-relaxation detected in PLLA after crystallization at a lower temperature, T_c = 343 K; therefore, it is reasonable to assume that the α-relaxation now detected in the fully transformed semi-crystalline materials is mainly the constrained α_{sc} process previously characterized.

Another parameter obtainable from the HN fit is the dielectric strength, presented in the insets of Figure 5. 11. As can be seen, $\Delta\varepsilon$ generally increases with the temperature increase. This is also evident from the evolution of the peaks height in the raw data; the same trend is observed for all specimens.

Finally, the characteristic relaxation times obtained by the HN fit to the data, which equal τ_{max} given that β_{HN} = 1, are plotted *versus* the inverse of temperature in Figure 5. 13 for all the PLLA samples cold-crystallized at different T_c. The plots exhibit the usual curvature of cooperative processes. However these plots do not lie on the same curve. Instead, as T_c increases the plots deviate to lower

relaxation times as expected from the above mentioned shift of the isotherms to higher frequencies with T_c increasing.

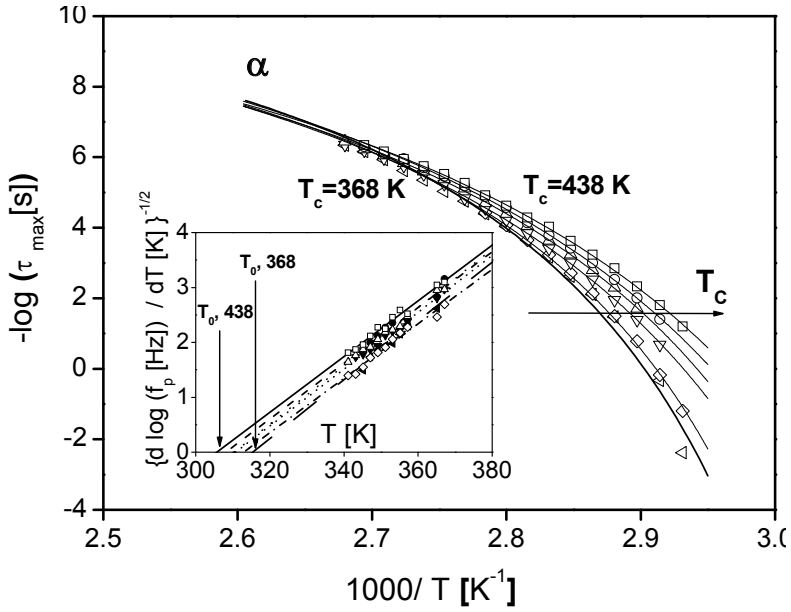

Figure 5. 13- Temperature dependence of the relaxation times for the α- relaxation processes for all PLLA specimens: (◁) T_c=368 K, (◇) T_c=383 K, (▽) T_c=398 K, (△) T_c=413 K, (○) T_c=428 K, (□) T_c=438 K, solid lines are the VFT fit (fitting parameters presented in Table 5. 2). The inset shows $[d\log(1/\tau_{max})/dT]^{-1/2}$ *versus* temperature for PLLA at different T_c: (◁) 368 K, (◇) 383 K, (▼) 398 K, (△) 413 K, (●) 428 K, (□) 438 K. The lines are linear regressions to the dielectric data.

In what concerns the temperature dependence of the α constrained relaxation processes for all the specimens, the VFTH- equation were fitted to the data and the respective parameters are presented in Table 5. 2.

T_c [K]	χ_c	B [K]	τ_∞[s]	$T_{0,VFT}$ [K]	$T_{0,der}$ [K]	T [K] (τ = 100 s)	E_g [kJ·mol^{-1}]	m
368	0.43	577	7×10^{-12}	320	317	339	1513	233
383	0.48	775	10×10^{-13}	312	312	337	1257	195
393	0.53	784	13×10^{-13}	311	311	336	1222	190
413	0.58	889	3×10^{-13}	309	310	336	1179	183
428	0.62	896	3×10^{-13}	308	307	335	1162	181
438	0.65	1046	1×10^{-13}	303	303	333	1052	165

Table 5. 2- VFT parameters, glass transition temperature estimated equaling, $\tau = 1/2\pi f$, for 100 s, apparent activation energy at T_g, (E_g), fragility parameter, m and crystallinity degrees (χ_c) for all semi-crystalline PLLA specimens. T_0 was estimated both by Vogel law fit to the data ($T_{0,VFT}$) and by the derivative analysis ($T_{0,der}$).

To analyze more deeply the temperature dependencies, the derivative method is used (Equation 1.4). In the following this method is applied to the α_{SC}-relaxation (inset of Figure 5. 13) where the data for the different cold-crystallized specimens were compared close to T_g. First, it is concluded that indeed for all considered processes the temperature dependence of the relaxation rates follow a VFT law: all experimental data can be well described by straight lines. But as a second result it is obtained that the temperature T_0 can be influenced by the degree of crystallization. A similar trend as already obtained for the glass transition temperature is now observed for $T_{0,}$ which decreases with the T_c increase. All estimated T_0 values are in very good agreement with those obtained from the VFT fit to data (see, respectively, $T_{0,der}$ and $T_{0,VFT}$ in Table 5. 2).

5.6.2 The β- Relaxation

At first glance the dielectric loss curves included in Figure 5. 7 collected at the lowest temperatures seem to correspond to only one secondary process. However, while analyzing the dielectric spectra by the HN model function, a multi-component character is observed and thus a sum of HN-functions is employed. Figure 5. 14 gives an example of the fitting procedure of three individual HN-functions to the dielectric spectrum at 248 K for PLLA cold-crystallized at T_c= 368 K. The β process in the specimens studied is assigned to I, II and III related with increasing temperatures as emerging; thus process I is the one at lower temperatures/higher frequencies and so for the others, respectively.
The resulting shape parameters are summarized in Table 5. 3.

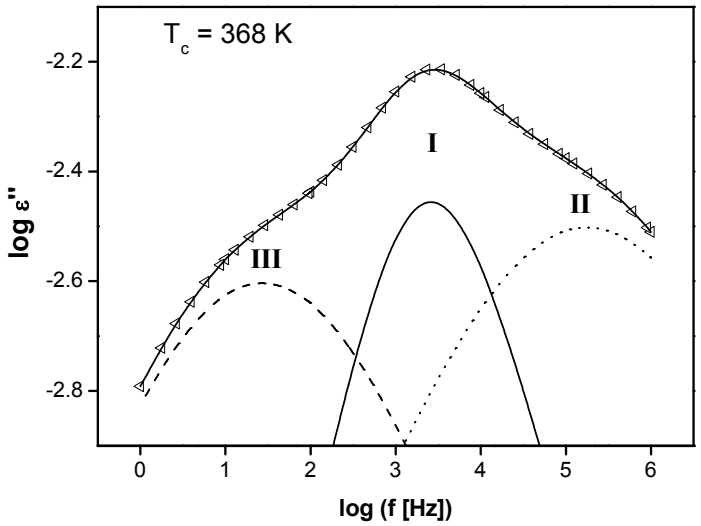

Figure 5. 14- Example of the fitting procedure for PLLA cold-crystallized at T_c = 368 K where three individual HN-functions are necessary to properly reproduce the experimental dielectric spectrum: overall fit – solid line, individual HN processes- are indicated above the respective fitting line.

Concerning the dielectric strength, the values obtained for the three individual processes are given in Annex 1.

The estimated relaxation times for each detected secondary process, after conversion to τ_{max}, show a temperature dependence described by an Arrhenius law (see Equation1.2 in Chapter I) as characteristic of local mobility. The respective linear plots are presented in Figure 5. 15 that also presents the temperature dependence of all cooperative α processes.

Table 5. 3- HN shape parameters (α_{HN}, β_{HN}) for β_I, β_{II} and β_{III} process obtained from the fitting of the complex permittivity data in two different temperature regions. Activation energies (E_A) and pre-exponential factors (τ_∞) estimated from the slopes of the linear plots at temperatures below 293 K.

β-relaxation $T < 293\ K^*$	α_{HN}	β_{HN}	E_A [kJ.mol^{-1}]	τ_∞ [s]	*β-relaxation* $T > 323\ K$ α_{HN}; β_{HN}
I	0.42±0.02	1.00	43±1	$(10 \pm 4) \times 10^{-16}$	0.30 ±0.03; 1.00
II	0.73 ±0.07; $T_c \leq 428$ K 0.85 ±0.03; $T_c = 438$ K	0.82 ±0.18	55±1	$(1.2 \pm 0.4) \times 10^{-16}$	
III	0.42 ±0.02	1.00	60±2	$(12 \pm 6) \times 10^{-16}$	

* In case of specimen crystallized at 438 K the same shape parameters were used until 323 K

The activation energies estimated from the Arrhenius equation (Equation 1.5) at temperatures below 293 K (see Table 5. 3) for processes II and III are relatively similar. This was expected, since the two processes evolve closely with the temperature increase. However, near below the glass transition in the temperature region where process II approaches the VFT dependence of the α_{sc}-relaxation, a particular effect occurs with the β_{II} trace bending towards the α-trace. Process III becomes unresolved at temperatures above 293 K for all specimens but T_c = 438 K, nevertheless it seems to be accelerated driven by the entrance of the α process. This is shown in the relaxation map (Figure 5. 15), where the respective activation plot, exhibits a slight change to higher slope; points are shown in gray since some uncertainty affects the fit.

Concerning processes I, it presents slightly lower activation energy, being not clear how it progresses with the temperature increase, since it leaves out from the frequency window. Nevertheless, a deviation of the β_I trace to high relaxation times seems to occur for instance in PLLA crystallized at 383 K were the three individual processes are well resolved in the raw data.

The different features found for the secondary process will be discussed in next section.

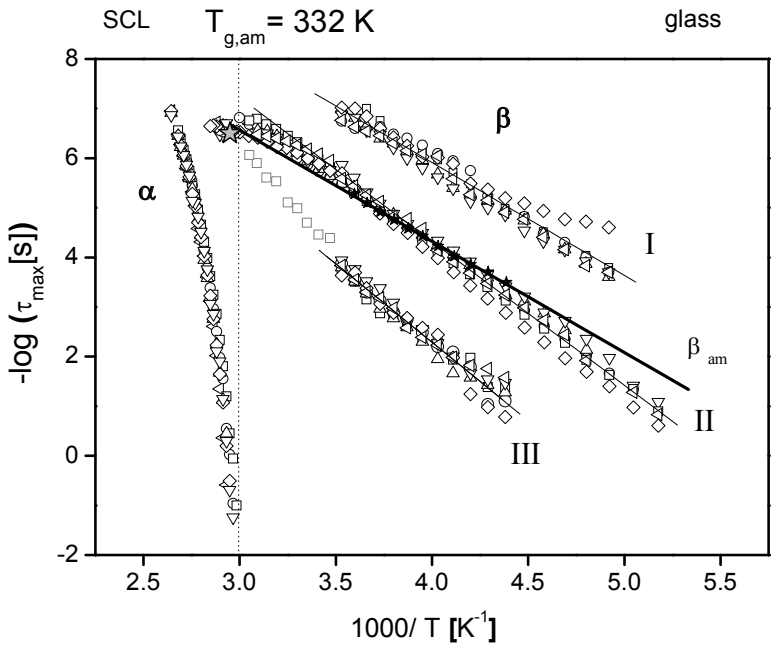

Figure 5. 15- Relaxation map for semi-crystalline PLLA showing all the processes detected covering supercooled and glassy states. The activation plot of the secondary process found in the amorphous sample was also included in the figure as full stars (★). The relaxation times of process III for specimen crystallized at 438 K (open squares) are in gray since some uncertainty affects the data. Solid lines are the Arrhenian fits taking in account all set of data for the respective process. The thicker solid line crossing process II is the linear temperature dependence of amorphous PLLA. Light gray star indicate the JG relaxation time, τ_{JG}, estimated from Coupling Model (Equation 1.40 in Chapter I). Vertical dashed lines are the dielectric glass transition temperature T_g^{diel} ($\tau = 100\ s$) = 332 K for amorphous PLLA.

5.7 Discussion

In general the crystalline phase is rigid and shows no dielectric relaxation processes. Therefore, the observed dielectric relaxation behavior is assigned to the amorphous phase exhibiting an α process related to the glass transition dynamics at lower frequencies and, at high frequencies, a β-relaxation, which, contrary to what is observed in the wholly amorphous PLLA, has multimodal character.

Figure 5. 16 gives an overview of the dielectric processes detected in an isochronal plot at 470 Hz that will be discussed separately.

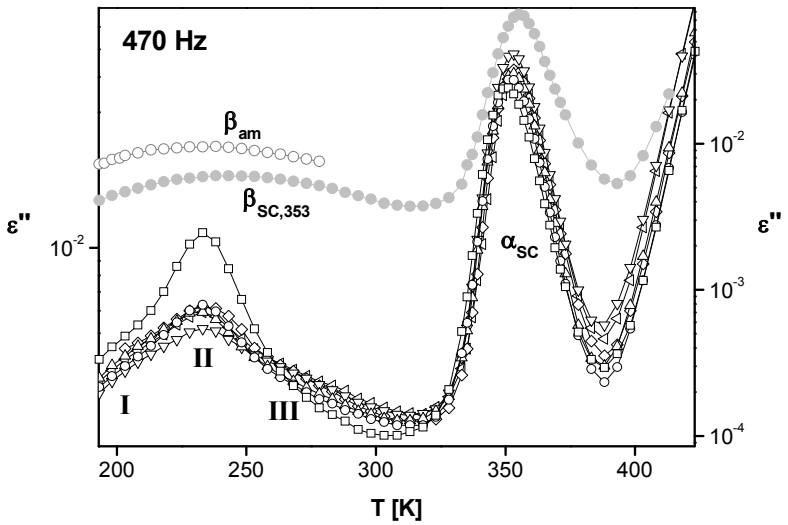

Figure 5. 16- – Isochronal plot taken at 470 Hz from isothermal measurements covering both glassy and supercooled states for all PLLA specimens: (◁) T_c=368 K, (◇) T_c=383 K, (▽) T_c=393 K, (△) T_c=413 K, (○) T_c=428 K, (□) T_c=438 K. Lines are guide for the eyes. Data for amorphous (open circles) and semi-crystalline PLLA crystallized at 353 K (full circles) are included in gray. The plots evidence the multi-modal character of the semi-crystalline PLLA β-relaxation for $T_c > 353$ K and the shift of the α process to lower temperatures with increasing T_c. Logarithmic scale was used in order to enhance the low-amplitude processes.

5.7.1.1 The α_{sc} process

The results obtained now by dielectric spectroscopy are compatible with what was found by both DSC [22] and dynamical mechanical analysis [23]. In fact, it is observed a consistent decrease of the glass transition temperature and of the temperature position of the mechanical tan δ peak with increasing crystallization temperature. Also, it was demonstrated that the overall crystallinity increases concomitantly with T_c, (crystallization degrees, χ_c, estimated in reference [22], included in Table 5. 2) while the content of the mobile amorphous phase decreases. It is assumed that not the entire amorphous phase contributes to the α_{sc} process [24,25]. This was understood by the decrease of the mechanical loss peak with increasing T_c [23]. In the present work, the dependence of the dielectric strength with the crystallization degree can be analyzed by normalizing $\Delta\varepsilon$ in regard to the value measured for the wholly amorphous sample, which for the later is known, at 353 K prior to crystallization.

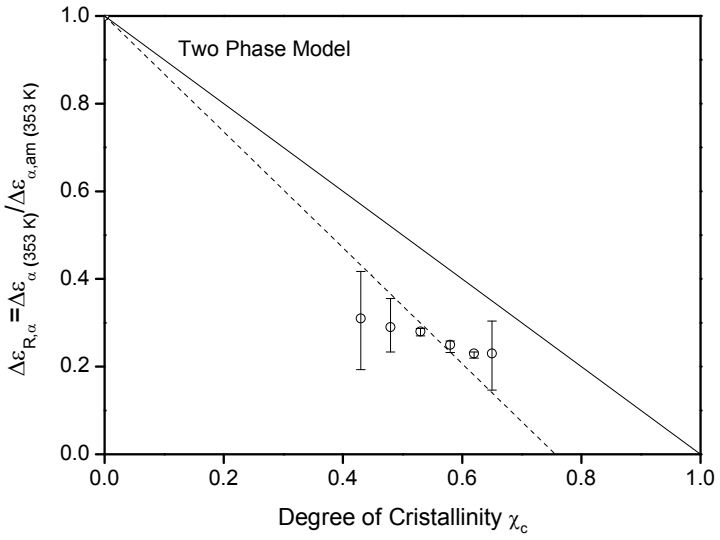

Figure 5. 17- Normalized dielectric strength for the α process $\Delta\varepsilon_{R,\alpha} = \Delta\varepsilon_{\alpha}/\Delta\varepsilon_{\alpha,am}$ at T=353 K plotted against the crystalline degree for the PLLA specimens studied. The solid line represents the theoretical two phase model. The dashed line shows the extrapolation to a $\Delta\varepsilon_{R,\alpha}$ value equal to zero of the data indicating an amount of rigid phase higher than 20% if strictly interpreted according a three phase model (see text).

In Figure 5. 17 the ratio $\Delta\varepsilon_{R,\alpha} = \Delta\varepsilon_{\alpha\,(353K)}/\Delta\varepsilon_{\alpha,am(353\,K)}$ is plotted against the crystalline degree where the line represents the behaviour assuming a two phase model. It is obvious that the behavior of the reduced dielectric strength does not follow this model and the extrapolation to a $\Delta\varepsilon_{R,\alpha}$ value equal to zero, reads a cristallinity value which is smaller than 1, confirming that a fraction of the amorphous phase does not participate in the dynamic glass transition process. A similar behavior was found for quite different semi-crystalline polymers ([24,26,27,28] and references therein) being taken as an evidence of the existence of the rigid amorphous phase. An alternative interpretation [18] for the changing of proportionality when diminishing the dielectric strength relative to the crystallinity is, besides the decrease in the number of dipoles due to immobilization, the decrease of the Kirkwood (g) correlation factor [29,30] upon crystallization. In fact, a reduction in g is observed in PET for crystalline samples relative to the wholly-amorphous specimen [31]. However, the difference between g_{am} and g_{sc} becomes less important with the temperature increase, those factors diverging less than 10% at T_g = +293 K. The analysis of the dielectric strength decrease in PLLA (Figure 5. 17) was carried 293 K above T_g, so if we assume a similar reduction in the g factor, this cannot explain the effective decrease in the dielectric strength: the extrapolation of the reduced dielectric strength to 0 can be taken as an indication of the fraction of non-crystalline immobile material [28], which in case of semi-crystalline PLLA gives more than 20%. The existence of the rigid amorphous phase for PLLA with χ_c higher than 0.4, was also established by Mano *et al*. [25] by using DSC where the incremental step change in the heat capacity at the glass transition was reduced to a greater extent then would be expected to the measured crystalline degree, leading to a fraction of rigid amorphous phase of the order of 20% for all specimens in good accordance with dielectric data. Therefore, the present

dielectric data, seem to support the existence of a finite rigid amorphous phase, RAP, in the semi-crystalline specimens studied. The RAP is amorphous in structure but rigid regarding the molecular mobility that originates the dynamic glass transition. However it was suggested that this phase may influence the α_{sc} process. Previous reported results emphasize the strong effect of this RAP on the glass transition. From WAXS and SAXS studies [22] the morphologies of the different semi-crystalline materials were characterized, and the thicknesses of each crystalline (L_c), rigid amorphous (L_{ra}) and mobile amorphous (L_{ma}) phases were determined. As a general trend, no significant influence on L_{ma}, but instead an increase in L_{ra} and L_c, was observed with the crystallization temperature increase. The thickness increase of the RAP is accompanied by a concomitant decrease in the glass transition temperature. In the present work, it was demonstrated by dielectric spectroscopy that an increase in the mobility is observed with the T_c increase, as revealed by the shift to higher frequencies of the α_{sc}-peak (or a deviation to lower temperatures as illustrated in Figure 5. 15).
Moreover, the enhancement of mobility is also accompanied by a decrease in the estimated glass transition and Vogel temperatures, seen in Figure 5. 18, the later decreasing even strongly with the crystallinity degree: the slope of T_0 *vs.* χ_c is more than two times the one that holds for $T_g(\chi_c)$. Thus, the Vogel temperature is a rather sensitive parameter to evaluate the influence of crystallinity in the α_{sc}-relaxation.

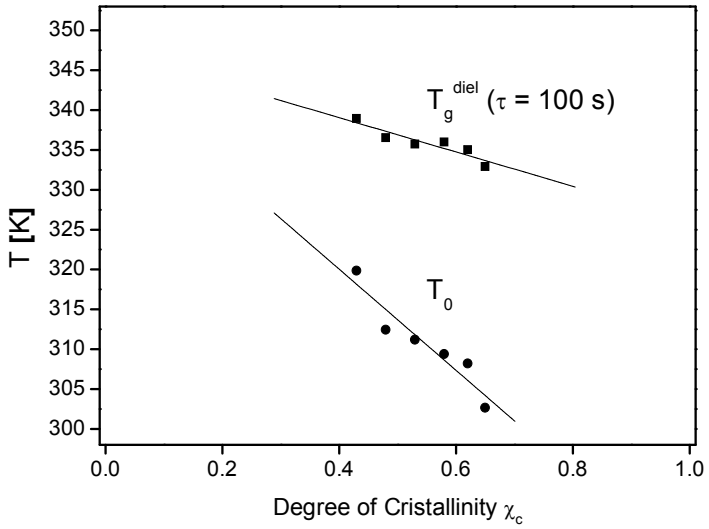

Figure 5. 18- The estimated glass transition (T_g) and Vogel (T_0) temperatures dependence on the degree of crystallinity (χ_c) for all the PLLA specimens; the Vogel temperature decreasing strongly with χ_c.

The decrease in the glass transition temperature was rationalized [23] by an enhancement of the mobility inside the mobile layer promoted by the adjacent rigid phase, where relatively local mobility persists, facilitating the conformational motions occurring in the former. This is just a hypothesis and should be confirmed, for example, by analyzing other semi-crystalline polymers. The rigid layer, with thicknesses between 2 nm and 4 nm [22], acts as relatively soft barrier impairing the direct contact of

the mobile amorphous phase, with thicknesses between 6 and 8 nm, with the stiff crystalline wall. The transition between the two amorphous layers should be gradual and the segmental motions will be increasing restricted as the chains are located more inside in the rigid region. Any influence of the rigid layer will be very limited due to the restriction on conformational mobility in this phase. At the same time, the enhanced mobility can arise from a density lowering of the mobile phase. As χ_c increases, mainly an increase of the rigid layer occurs, as proved by the dependence of L_{ra} with T_c [22]. Therefore, the mobile amorphous phase, MAP, that leftover can rearrange within a less dense packing. In fact, the absence of broadening of the α_{sc}-peak with T_c for all specimens seems to support that molecular rearrangements occurring in an analogous surrounding involving mainly the MAP. The width of the α_{sc}-peak is equivalent for the different specimens as clearly demonstrated by the superposition of the normalized isotherms collected at 353 K for all samples, previously shown in Figure 5. 12. Since local environments govern the conformational motions that are in the origin of the glass transition, the invariance of the α_{sc}-peak means that molecular rearrangements take place in equivalent surroundings independently of χ_c. The broadening of the glass transition as seen by DSC could lead to think that low-extent conformational adjustments inside RAP that engage in the cooperative motions within the MAP [23] will participate more and more deeply to the cooperative rearranging region (CRR) as defined by Adam and Gibbs [32]. The present results seem to rule out this hypothesis since the breath of the distribution of relaxation times between the different semi-crystalline specimens remains unchanged.

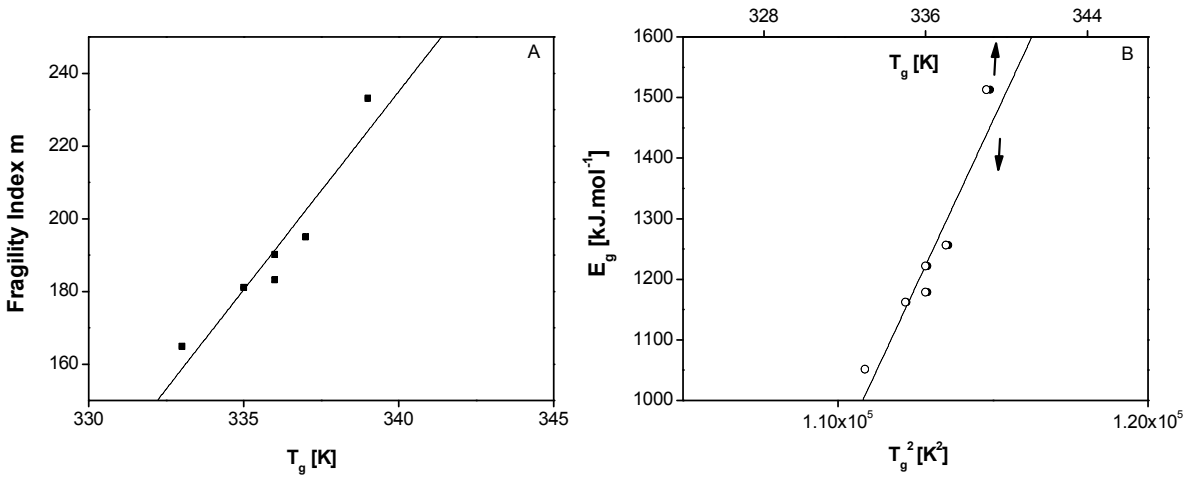

Figure 5. 19- Correlation between dynamic fragility m and apparent activation energy at T_g (E_g) and the glass transition temperature (T_g) (solid lines are linear regressions to the data): a) plot of m *vs.* T_g where the regression gives $m_{PLLAsc} \approx 10.9T_g - 3476$, b) Plots of E_g *vs.* both T_g (full circles) and T_g^2 (open circles), the regression of the later giving: $E_g(polymer) \approx 0.11T_g^2 - 11198$. All $r^2 = 0.91$.

However RAP can modify the temperature evolution of the mobile amorphous phase dynamics as seen by the change in the fragility index. For the amorphous PLLA the calorimetric fragility index was found to decrease with crystallinity [25]. In the present work, the same was found for a broader range of crystallinity degrees where an evolution towards a less fragile character is observed with χ_c. However this trend is less pronounced as the one observed in PET [25].

A correlation between fragility as well as between apparent activation energy at T_g (E_g) and the glass transition temperature, was verified in a variety of different systems by Qin and McKenna [33]. Figure 5. 19 shows the plot of a) the fragility index in function of T_g^{diel} (full squares) and b) the apparent activation energy at T_g (E_g) in function of both T_g(full circles) and T_g^2 (open circles). The correlation found for semi-crystalline PLLA is much stronger than the one obtained from the compiled data for polymers in respect to m (m_{PLLAsc}≈$10.9T_g - 3476$ against $m_{Polymers}$≈$0.28Tg + 9$) [33]. Regarding E_g, those authors found that in particular for polymers, hydrogen bonding organics and metallic glass formers, it varies approximately as T_g^2. Our apparent activation energy data, fit either in a linear correlation with T_g or T_g^2 (both correlation coefficients of 0.91). Once again, the dependence on T_g^2 ($E_g(PLLA_{sc})$≈ $0.11T_g^2 - 11198$) is much stronger then the observed for a variety of polymers ($E_g(polymer) \approx 0.006T_g^2 - 35$).

Additionally, the amount of RAP can be changed by temperature variation. This can be inferred from the temperature dependence of the dielectric strength that increases with temperature (remember insets in Figure 5. 11). Such behavior, found for a number of semi-crystalline polymers [24,34], has an opposite trend to what is usual in amorphous polymers. These results indicate that the rigid amorphous phase is not rigid at all temperatures but relaxes between the glass transition of the mobile amorphous phase and the melting point of the crystalline phase (~453 K). Therefore, segments previously immobilized in the RAP start participating in the relaxation process with increasing temperature. However, the effect is more pronounced for the lowest T_c which is compatible with a lower thickness of L_{ra} in these specimens and thus, with an easier activation of the rigid phase. It is also important to note that all specimens converge to a similar τ_∞ (Table 5. 2) as temperature increases. This can be understood as in the limit all phases becomes indistinguishable and crystallinity influences less and less the material.

5.7.1.2 The β-relaxation

It was shown that the secondary relaxation process in semi-crystalline PLLA has a multi-component character (see Figure 5. 16), which includes the plot at 470 Hz for the amorphous sample and the semi-crystalline PLLA crystallized at 353 K (χ_c~0.3) (see previous section), both showing only a single broad β process. As far as we know, the multi-modal nature of the secondary relaxation process detected in other semi-crystalline polymers (bisphenol-A polycarbonate, BPA-PC [35] and poly(aryl ether ether ketone), PEEK [36]) is already found in the amorphous material. By comparing the

isochronal data in PLLA, it becomes evident that the broad secondary peak in the amorphous sample is decomposed in three secondary processes after crystallization for T_c > 353 K.

The multi-component character of the secondary relaxation probably indicates that while the PLLA amorphous β-relaxation is characterized by a broad distribution of relaxation times, typically attributed by the existence of a large variety of environments felt by the relaxing species, the more restricted mobility of the cold-crystallized samples turned it possible to distinguish between these environments.

To understand the dependence of the dielectric strength on the crystallinity better for the complex β process, the discussion will be similar as before for the α_{sc} process. Figure 5. 20 shows $\Delta\varepsilon_\beta$ values normalized relative to the dielectric strength of the wholly amorphous state, *versus* the crystallinity degree at 253 K.

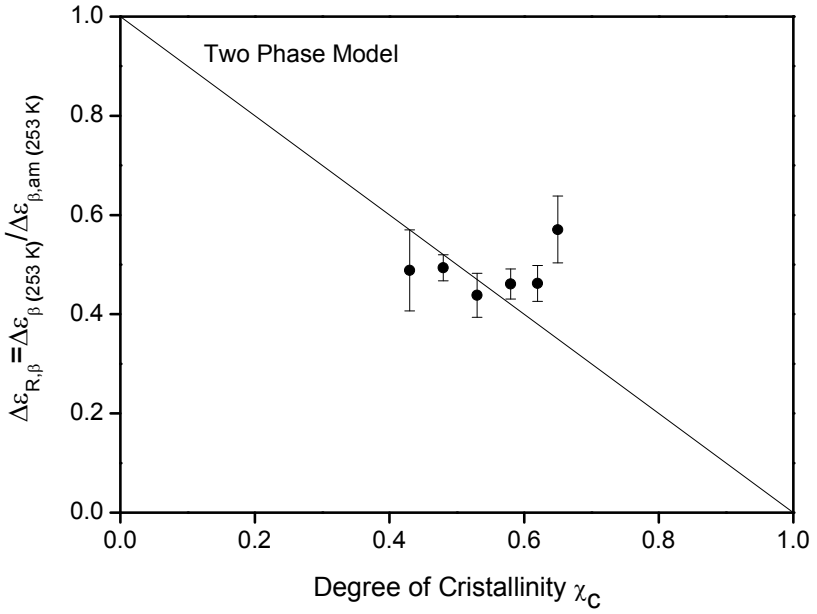

Figure 5. 20- Normalized β dielectric strength $\Delta\varepsilon_{R,\beta} = \Delta\varepsilon_\beta/\Delta\varepsilon_{\beta,am}$ at T= 253 K plotted against the crystalline degree for all the PLLA specimens studied. The line represents a two phase model.

For specimens with medium degrees of crystallinity, besides the expected general decrease of $\Delta\varepsilon_\beta$ with χ_c, the dependence follows more or less what is predicted by the two phase model (line in the graph). This can be taken as an indication that the whole amorphous phase including RAP contributes to the β process, as found in other semi-crystalline polymers [24,37,38]. The specimens with crystallinity degrees higher than 0.6 present a peculiar behavior with a positive shift relative to which is predicted by the two-phase model. This means that the relaxation strength determined from the raw data is higher than expected for the measured degree of crystallinity assuming a two-phase model. Thus, the over-determined values, especially for specimen crystallized at 438 K, can be a consequence of a preferential alignment of dipoles in some ordered arrangement promoted by a higher crystallinity, the main contribution to $\Delta\varepsilon_\beta$, being process II. This is also supported by the magnitude of the dielectric

strength of the α_{sc} process for this specimen which is comparable to the one of specimen at T_C = 368 K (remember insets of Figure 5. 11), even though it has half of amorphous mobile fraction [22]. Nevertheless further evidence to support this observation is needed.

In regard to the relaxation time temperature dependence of the β_{II} process, it shows an Arrhenius-like behavior with activation energy around 55 kJ.mol^{-1}, typical for local motional processes. This value is slightly higher than the one estimated for the amorphous one (50 kJ.mol^{-1}). The small activation energy increase is also found for other semi-crystalline polymers [24]. The activation plot of the secondary process found in the amorphous sample was included in Figure 5. 15 as full stars, evidencing a relatively inferior slope (thicker solid line). Additionally, above 323 K, processes II and III give rise to only one broad relaxation; the respective α_{HN} shape parameter being equal to (0.30±0.03), close to the value found to describe the β-relaxation of the wholly amorphous system (0.28) (shape parameters for temperatures higher than 323 K in last column of Table 5. 3). The uncertainty that affects the position of process III was the reason why no data was presented in the β_{III} trace above 293 K in relaxation map (remember Figure 5. 15), except for specimen crystallized at 438 K. The later, driven by the overlapping α_{sc}-relaxation seems to evolve in such a way that converges to process II leading to a single one, as found in the amorphous counterpart. The acceleration originated by the entrance of the α_{sc} process is reflected in a slight increase of the slope of process III, as observed in several glass formers [39], which is usually attributed to a Johari-Goldstein [40] β process taken as the precursor of the dynamic glass transition process. To test this in more detail for these systems, using β_{KWW} = 0.38, according to Alegría relation (Equation 1.39), Equation 1.40 (Chapter I) gives a value of τ_{JG} ($T_C = 438\,K$) at T_g of 3.15x10^{-7} s in good agreement with the experimental τ_β value at this temperature (see Figure 5. 15). However some care should be taken to interpret this process as a β_{JG} since this case is not a conventional behavior of a glass former: the temperature increase is not influencing only the localized thermal activated mobility but seems also to drive transformations in the RAP/crystalline fraction and therefore the acceleration of process III could be alternatively explained by an enhanced local mobility acting as precursor of the incoming melting transition.

As far as process β_I is concerned, as already mentioned, the way how it progresses with temperature is not clear due to its exit from the frequency window. However, having in mind that i) above 323 K only one process is necessary to well reproduce raw data in the high frequency side, and ii) the way how processes II and III merge in specimen crystallized at 438 K, it seems reasonable to conclude that the three processes become one.

Moreover, the convergence of the different processes seems to be supported by the similarity of the different pre-exponential factors (see Table 5. 3). The coalescence in a single process with the temperature increase can be taken as an indication that all the amorphous phase becomes indistinguishable in what concerns localized mobility, no matter what if molecular motions are originated in the rigid or mobile phases. Therefore, the local motions feel the progressive contribution

of the RAP to the dielectric response as the temperature is increased before the cooperative α_{sc} process, since in the former a lower length- scale is being probed.

The estimated pre-exponential values τ_∞ are lower than the value predicted for a Debye-type process, i.e, a process with only one characteristic relaxation time with relaxation times at infinite temperature of around 10^{-12}-10^{-14} s. Lower values than these mean an activation entropy greater than zero according to the Eyring formalism, which could indicate some cooperative nature of the secondary process [41].

5.8 Conclusions

Isothermal crystallization of PLLA at T_c = 353 K, coming from both the glassy or melt states, was monitored by DRS. During crystallization a shift of the main peak to lower frequencies around one decade is observed. Such behavior was observed in the two tested crystallizations (isothermal and non-isothermal) for PLLA with two molecular weights.

A linear combination of three loss peaks are able to fit the loss data during crystallization: (i) the beta secondary process at high frequencies; (ii) the α_{NA} process observed for nearly amorphous material and (iii) the loss peak for the fully transformed material (α_{SC}). The shape parameters and relaxation time are thus invariant during crystallization and were also found to be essentially independent of both molecular weight and thermal history that anticipates crystallization, providing that crystallization is promoted at the same temperature.

The invariance of shape and relaxation time of the two α −relaxation processes indicate that the two segmental dynamic process develops independently and the dynamics features of the (slower) confined amorphous phase do not change during crystallisation. The appearance of a clear contribution of α_{SC} in the initial stages of crystallinity development suggests that the confinement effect of the lamellae take places during primary crystallization. The $\Delta\varepsilon$ evolution upon crystallization is slower for the crystallization anticipated by melting and, for the same crystallization procedure, is retarded when M_w increases.

Relatively to the isothermally cold-crystallized specimens prepared at T_c, ranging between 368 K (χ_c= 0.43) and 438 K (χ_c= 0.65) , it was found that the mobility of the α-relaxation associated with the dynamic glass transition, becomes enhanced with the increase of crystallinity as revealed by the shift of the α loss peaks to higher frequencies/lower temperatures. Their temperature dependencies follow the VFT law from which the glass transition and Vogel temperatures were estimated, decreasing with the increase of χ_c. The Vogel temperature decreases faster with χ_c as compared with T_g suggesting that this is a useful quantity to evaluate the influence of crystallization in the α process. The dielectric strength dependence of the main relaxation relative to the crystalline degree does not follow a two-phase model, since, besides the crystalline fraction, a rigid and amorphous phase coexist, where the rigid one does not contribute to the α process, however influences it. The thicker rigid amorphous phase that diminishes the influence of the rigid crystalline wall and the less dense mobile

amorphous phase, are taken as the cause for the decrease of glass transition temperature and cooperative mobility enhancement in specimens with higher crystallization degree. The rigid amorphous phase is progressively activated with the temperature increase as seen by the increase in the dielectric strength of the α process. Contrary to what was observed previously in both amorphous and semi-crystalline PLLA crystallized at T_c = 353 K ($\chi_c \sim 0.3$), where a single broad relaxation process was observed, in the samples isothermally cold-crystallized at higher T_C, a multi-component secondary process was detected. This complex secondary process, results from different weighted contributions of three individual components. The overall dielectric strength for localized mobility obeys, for medium χ_c's, the two-phase model given that local motions can take part in the rigid amorphous fraction. Higher crystallinities ($\chi_c > 0.6$) deviated positively which can be a consequence of a more ordered arrangement within the amorphous phase imposed by the semi-rigid boundaries. The three processes that constitute the β −relaxation seem to merge in a single process, abnormally broad, close below T_g, revealing that the rigid and amorphous phases become progressively indistinguishable in what concerns localized mobility. This single process presents identical features to the one previously detected in both amorphous and PLLA crystallized at a lower temperature (T_c = 353 K, $\chi_c \sim 0.3$).

The decreasing of the dielectric strength with temperature in the specimens with higher χ_c's can point to a progressive involvement of several monomers, which were in the origin of a complex local motion with some cooperative character, in the cooperative motion that originates the α process.

While there are several examples in literature showing that the features of local mobility are little sensitive to the presence of crystallinity either in polymers with medium or high crystallization degree, this work demonstrates for the first time in PLLA that crystallization carried at $T_c \geq 368\,K$ has an important impact in the secondary β-relaxation, its complex nature acting as a probe of the morphology attained. In this context, dielectric relaxation spectroscopy proved to be a valuable tool able to bring additional information as compared with other conventional techniques.

5.9 References

[1] WUNDERLICH B (2005) MACROMOL. RAPID COMMUN. 26, 1521.

[2] BRÁS AR, VICIOSA MT, DIONISIO M, MANO JF (2007) J. THERM. ANAL. CAL. 88, 425.

[3] HAVRILIAK S, NEGAMI S (1967) POLYMER, 8, 161.

[4] VOGEL H (1921) PHYS. ZEIT. 22, 645.

[5] FULCHER GS (1925) J. AM. CERAM. SOC. 8, 339.

[6] TAMMANN G, HESSE (1926) G ANORG. ALLGEM. CHEM. 156, 245.

[7] ARNOULT M, DARGENT E, MANO JF (2007) POLYMER 48, 1012.

[8] KREMER F, SCHÖNHALS A (EDS.) (2003) "BROADBAND DIELECTRIC SPECTROSCOPY", SPRINGER, BERLIN.

[9] REN J, URAKAWA O, ADACHI K (2003) MACROMOLECULES 36, 210.

[10] DIONÍSIO M, VICIOSA MT, WANG Y, MANO JF (2005) MACROMOL. RAPID COMMUN. 26, 1423.

[11] MIJOVIC J, SY JW (2002) MACROMOLECULES 35, 6370.

[12] MANO JF, WANG Y, VIANA JC, DENCHEV Z, OLIVEIRA MJ (2004) MACROMOL. MAT. AND ENG. 289, 910.

[13] IANNACE S, NICOLAIS L (1997) J. APPL. POLYM. SCI. , 64, 911.

[14] LAREDO E, GRIMAU M, BARRIOLA P, BELLO A, MÜLLER AJ (2005) POLYMER 46, 6532.

[15] SANZ A, NOGALES A, EZQUERRA TA, LOTTI N, MUNARI A, FUNARI SS (2006) POLYMER 47, 1281.

[16] CHO J, BARATIAN S, KIM J, YEH F, HSIAO BS, RUNT J (2003) POLYMER 44, 711.

[17] BOYD RH (1985) POLYMER 26, 323.

[18] KALIKA DS, KRISHNASWAMY RK (1993) MACROMOLECULES 26, 4252.

[19] STARKWEATHER HW, AVAKIAN P, FONTANELLA JJ, WINTERSGILL MC (1993) MACROMOLECULES 26, 5084

[20] HENRY F, COSTA LC, DEVASSINE M (2005) EUROP. POLYM. J., 41, 2122.

[21] RICHERT R, BLUMEN A (1994) "DISORDER EFFECTS ON RELAXATIONAL PROCESSES" (EDS) SPRINGER, BERLIN.

[22] WANG Y, FUNARI SS, MANO JF (2006) MACROMOL. CHEM. PHYS. 207, 1262.

[23] PICCIOCHI R, WANG Y, ALVES NM, MANO JF (2007) COL. POLYM. SCI. 285, 575.

[24] SCHÖNHALS A (2003) "BROADBAND DIELECTRIC SPECTROSCOPY" (EDS.) SCHÖNHALS A, KREMER F, SPRINGER-VERLAG: BERLIN, CH. 7.

[25] ARNOULT M, DARGENT E, MANO JF (2007) POLYMER 48, 1012.

[26] KANCHANASOPA M, RUNT J (2004) MACROMOLECULES 37, 863.

[27] EZQUERRA TA, MAJSZCZYK J, BALTA´–CALLEJA FJ, LÓPEZ–CABARCOS R, GARDNER KH, HSIAO BS (1994) PHYS REV B 50, 6023, NOGALES A, EZQUERRA TA, GARCIA JM, BALTÁ-CALLEJA FJ (1999) J. POLYM. SCI.: PART B: POLYM PHYS. 37, 37–49.

[28] SANZ A, NOGALES A, EZQUERRA TA, LOTTI N, MUNARI A, FUNARI SS (2006) POLYMER 47, 1281–1290.

[29] BÖTTCHER CJF (1973) "THEORY OF DIELECTRIC POLARIZATION" 2ND ED., ELSEVIER, AMSTERDAM.

[30] FRÖHLICH H (1958) "THEORY OF DIELECTRICS" OXFORD UNIV. PRESS.

[31] COBURN JC, BOYD RH (1986) MACROMOLECULES 19, 2238.

[32] ADAM G, GIBBS JH (1965) J. CHEM. PHYS. 43, 139.

[33] QIN Q, MCKENNA GB (2006) J. NON-CRYST. SOLIDS 352, 2977.

[34] (A) HUO P, CEBE P (1992) MACROMOLECULES 25, 902. (B) HUO P, CEBE P (1993) POLYMER 34, 696. (C) HUO P, CEBE P (1994) THERMOCHIM. ACTA 238, 229.

[35] LAREDO E, GRIMAU M, MÜLLER A, BELLO A, SUAREZ N (1996) J. POLYM. SCI: PART B: POLYM. PHYS. 34, 2863.

[36] DAVID L, ETIENNE S (1992) MACROMOLECULES 25, 4302.

[37] BOYD RH, LIU F (1997) "DIELECTRIC SPECTROSCOPY OF DIELECTRIC MATERIALS" (EDS.) RUNT JP, FITZGERALD JJ, ACS-BOOKS, WASHIGHTON DC, PAGE 107.

[38] (A) KAKIZAKI M, KAKUDATE T, HIDESHIMA T (1985) J. POLYM. SCI. PHYS. ED. 23, 787 ; (B) KAKIZAKI M, KAKUDATE T, HIDESHIMA T (1985) J. POLYM. SCI. PHYS. ED. 23, 809.

[39] NGAI KL, PALUCH M (2004) J. CHEM. PHYS. 120, 857; NGAI KL, CAPACCIOLI S (2004) PHYS. REV. E 69, 031501 (1-5).

[40] JOHARI GP, GOLDSTEIN M (1970) J. CHEM. PHYS. 53, 2372.

[41] EYRING H (1936) J. CHEM. PHYS. 4, 283.

CHAPTER 6|CONCLUSIONS

The work developed in the scope of this thesis aimed to evaluate confinement effects. It was motivated by the previous knowledge that dynamical properties of condensed matter confined in space can be dramatically changed from those of the bulk state. These effects manifest when the dimensions of the confinement media are in the nanometer scale.

In the present study the dynamics under nano-confinement were mainly focused in the field of supercooled liquids, namely the liquid crystalline mixture of cyanobiphenyls, $E7$ and the pharmaceutical drug Ibuprofen, a rather small molecule from the Propionic acid family. Recently, the scope of the confinement notion has widened to several other systems embracing semi-crystalline materials. Such is the example also studied here which includes the dynamical characterization of the biopolymer PLLA, upon and after crystallization.

Each chosen material acts as a model system in its own category:

i) $E7$, due to its liquid crystalline properties is more sensitive to additional effects like ordering and/or phase transitions. Moreover $E7$ does not crystallize showing, besides the isotropic to nematic phase transition, a glass transition phenomenon being classified as a glass former. Therefore dielectric spectroscopy can be applied in a broad frequency and temperature range. This is not possible for related liquid crystals.

ii) Ibuprofen, one of the most widely known pharmaceutical drugs is usually tested when novel tools and strategies for controlled and efficient drug delivery are being implemented. For Ibuprofen it is also possible to circumvent crystallization allowing exploring its amorphous properties that can potentiate its therapeutic activity. Moreover, as an associating liquid via hydrogen bonding, with the peculiarity of not forming long chains structures like in monoalcohols, instead aggregating preferentialy as dimers or trimers, it is a suitable candidate to carry more fundamental studies on the nature of the D process for which correlated dipole orientations through hydrogen bonding are discussed to be its origin.

iii) PLLA is taken also as a model system in semi-crystalline biocompatible materials. In this context, the glass transition dynamics is particularly relevant by itself as the T_g of this material is not far above room or body temperatures. Therefore, the glass transition plays an important role in the general physical properties of PLLA during service. Moreover, it crystallizes slowly allowing preparing materials with tuned degrees of crystallinity and lamellar morphologies.

The confinement studies were preceded by a detailed characterization of bulk materials. While for the low molecular weight compounds, $E7$ and Ibuprofen, was possible to study in a wide temperature range covering the glassy, supercooled and liquid state, for PLLA mainly the sub-glass mobility was investigated for the full amorphous material since crystallization interferes with the detection of the α process.

Besides the relaxation process of the isotropic state, the two main processes of the liquid crystalline mesophase, δ- and tumbling, were characterized for bulk $E7$ from 10^{-2} Hz to 10^{9} Hz covering a temperature range of approximately 200 K. For the first time the origin of the glass transition was

elucidated in bulk $E7$ as being associated with the tumbling mode, by combining dielectric and heat capacity spectroscopy.

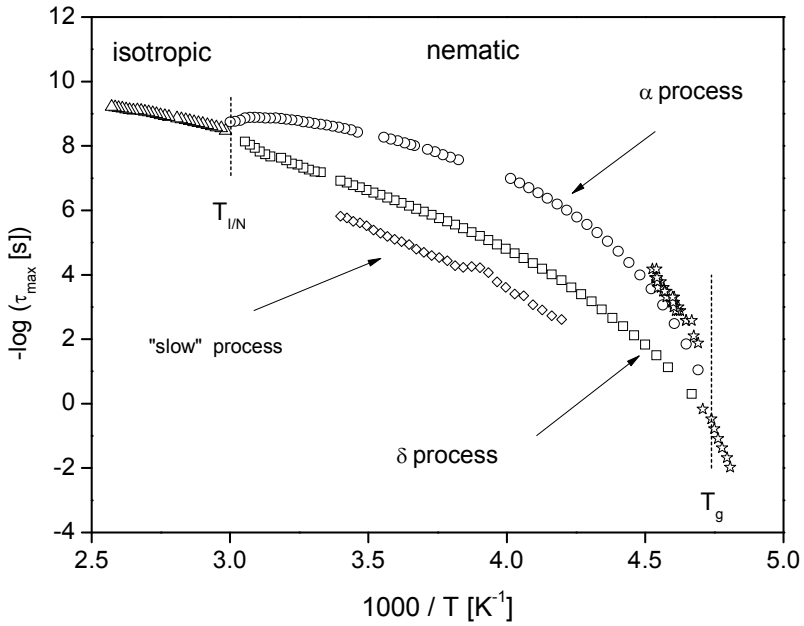

Figure 6. 1- Temperature dependence of the relaxation times, τ_{max}, for the different processes detected in bulk $E7$.

The exhaustive study of bulk Ibuprofen, covering again 11 decades of frequency, allowed to provide information on multiple relaxation process without the interference of crystallization as in the single previous work found in literature. The parameters that characterize its sub-glass relaxations and the D process were given for the first time; the same happened with the high frequency data for the α-relaxation. From the overall scanned frequency range, two dynamical different regions of the α process were distinguished. The tendency to aggregate of Ibuprofen was proved by DSC, HPLC, ESI Spectrometry and IR and predicted by molecular dynamics simulation.

In regard to the dynamical behavior under confinement of the target materials, when E7 is confined to the Anopore membranes with 20 nm pore diameter, both lecithin treated and untreated, an enhancement of mobility was found together with a slower surface relaxation. The relaxation time temperature dependence of the surface process can be described by an Arrhenius law with apparent activation energy that was discussed in terms of the different interaction of the molecules with the pore wall (lecithin layer > $E7$ in lecithin treated pores > $E7$ in untreated pores). Given the relatively high pore size, the higher mobility found for the α-relaxation was attributed, instead of a true confinement effect, to a lower density of E7 in the pore centre relative to the pore wall where the molecules are anchored in a dense packing arrangement. In the Anopore treated pores, the temperature dependence of the α process relaxation times is similar to the bulk state due to a lecithin layer which is settled at the pore wall.

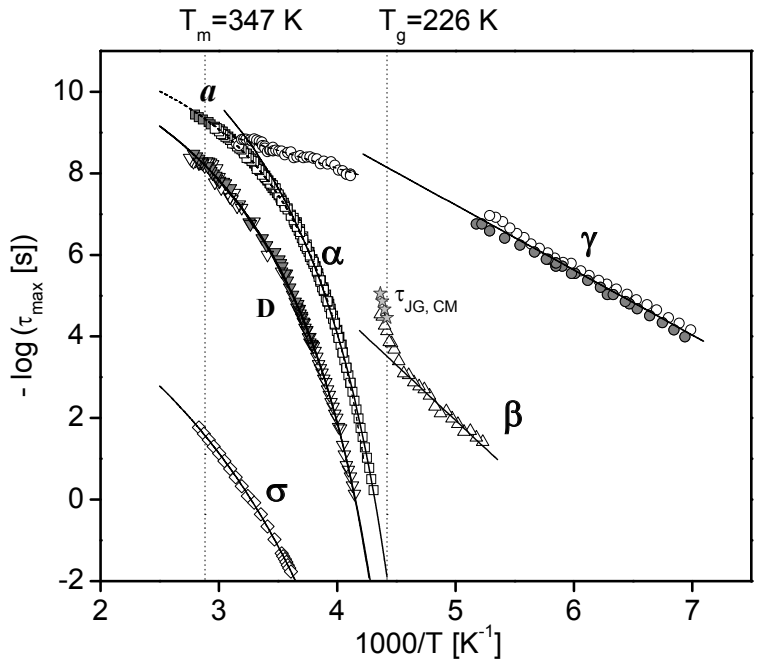

Figure 6. 2- Relaxation time, τ_{max}, *versus* 1/ T for all processes detected in bulk Ibuprofen.

The study of $E7$ confined in molecular sieves with pore sizes ranging from 3.6 to 7.8 nm, showed that besides the bulk-like processes, two additional relaxation processes were observed simultaneously for the first time, which are related to molecules interacting with the nanoporous hosts in different ways, by the inner or outer surfaces of the molecular sieves, S and I process, respectively. The FTIR analysis showed that strong interactions are present between the cyano group of the $E7$ constituents and the silica pore walls via hydrogen bonding. Moreover, a particular kind of confinement effect was found for $E7$ molecules adsorbed at the inner pore surface, since a step-like pore size dependence of the fragility and the Vogel temperature around 4 nm was observed, which can be taken as an indication of a transition from a strong to fragile behavior

For Ibuprofen this strong anchoring was not found, instead a relative weak interaction occurs with the pore walls when Ibuprofen is confined to the silica molecular sieves (3.6 and 6.8 nm pore sizes). The dynamical behavior of Ibuprofen revealed a significant variation from bulk properties. The glassy dynamics of bulk-like α process is faster than in bulk and changes from a VFT-like to an apparent Arrhenius behavior which originates from an inherent length scale of the underlying molecular motions, eventhough the minimal length is not yet reached for 3.6 nm. An S process assigned to the Ibuprofen molecules weakly adsorbed at the internal pore wall and a related Debye-like process (D_S -relaxation) is given for the first time.

The observation of two glass transitions for conventional glass-forming liquids confined in nanopores, was found to depend on the interaction between the wall of the pore and the confined liquid. Whereas one of the detected T_g's is close to the bulk, the second one is found to be lower than that for the bulk while for strong interactions the second T_g is higher. The first example seems to be the case of

Ibuprofen, due to the fact that it weakly interacts to the molecular sieves contrary to what was observed for $E7$ which follows the second example.

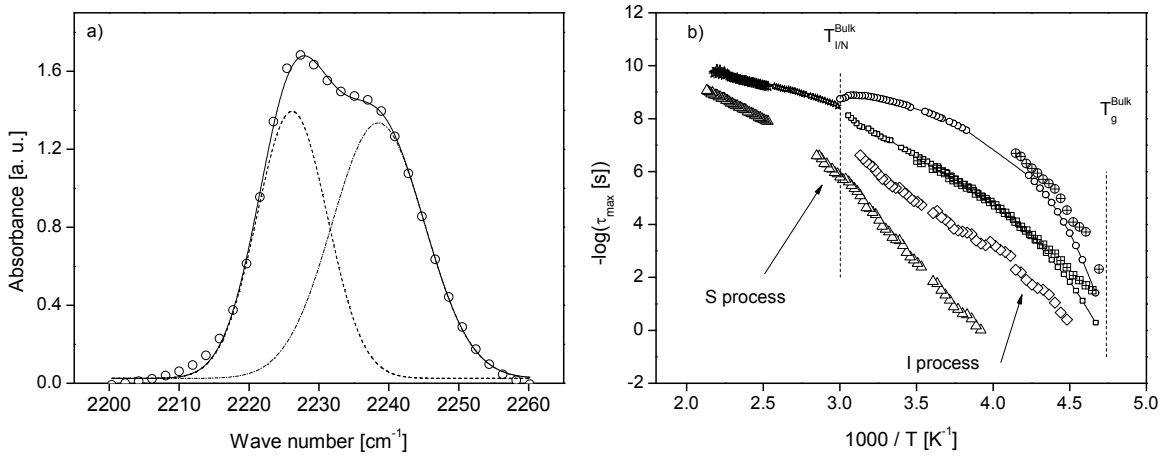

Figure 6. 3- a) FTIR spectrum for the CN-stretching vibration of $E7$ confined to the molecular sieve MCM-41-36; b) Relaxation times, τ_{max}, *vs.* $1/T$ for $E7$ embedded in the molecular sieve MCM-41-28 (sample $E7$/MCM-41-28) in comparison to the bulk.

Like for $E7$, confined Ibuprofen molecular dynamics is determined by a counterbalance of an adsorption and confinement effect.

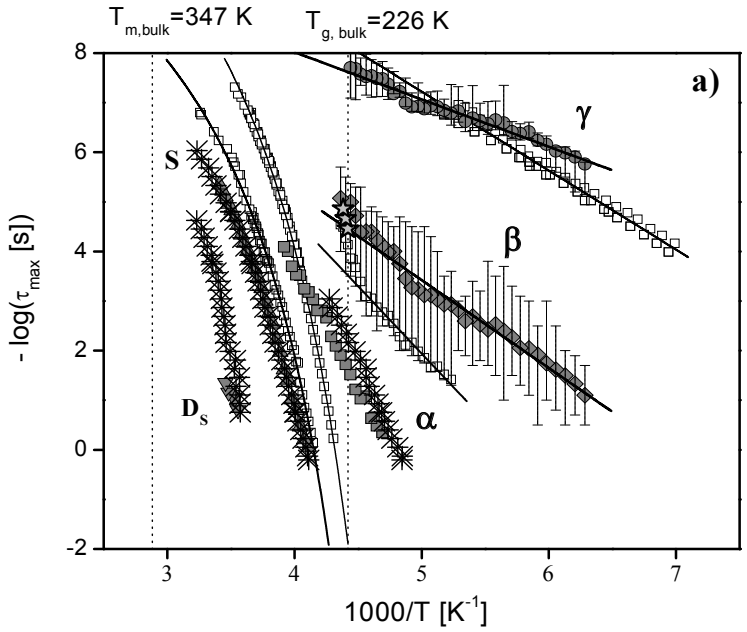

Figure 6. 4- Relaxation times, τ_{max}, *versus* $1/T$ for all processes detected in Ibuprofen: Open symbols – bulk isothermal loss data; Gray filled symbols - τ obtained from isothermal loss data for Ibu/MCM-41.

The semi-crystalline morphology of PLLA with different crystallization degrees (χ_C) was analyzed in terms of a three phase model consisting of crystalline, mobile amorphous and rigid amorphous phases, MAP and RAP, respectively. The dynamics of the constrained α process for the different χ_C is characterized by a broader relaxation time distribution shifted to higher values in comparison with amorphous α-relaxation. Nevertheless, between the specimens a mobility enhancement for the ones with higher χ_C was observed and rationalized in terms of both i) thicker rigid amorphous phase that decreases the influence of the rigid crystalline wall on the cooperative motions of the main relaxation process and ii) less dense mobile amorphous phase.

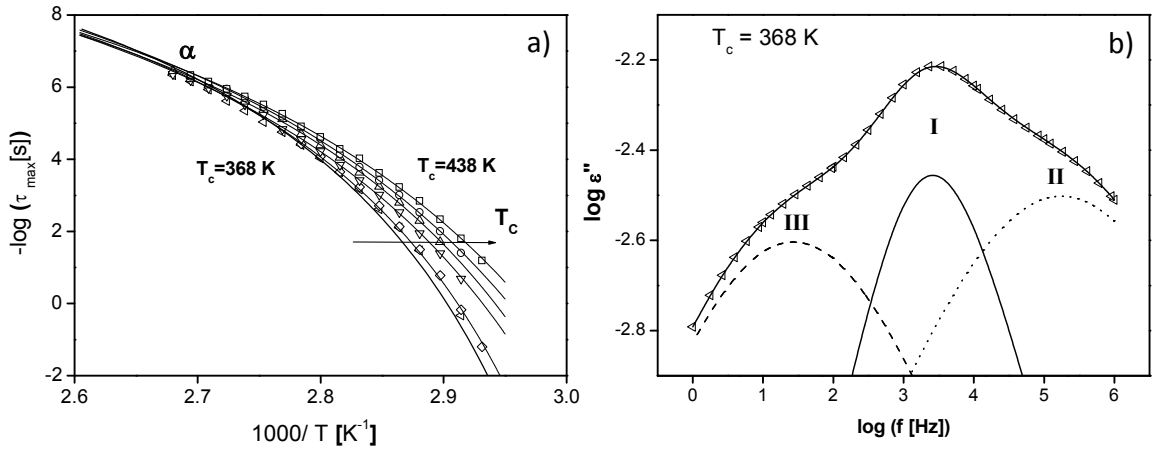

Figure 6. 5- a) Temperature dependence of the relaxation times for the α- relaxation processes for all PLLA specimens; b) Multi-modal nature of the secondary process detected in the semi-crystalline PLLA specimens.

It can be therefore seen the evident parallelism between all the systems. In the case of the confined glass formers here studied it is always observed at least one slower process due to the guest molecules interacting with the pore walls. The same happens for the semicrystalline polymers where this process is assigned to the presence of a highly confined amorphous fraction located within the spherulites and on their surfaces: a rigid amorphous region called α'-relaxation, also with a highly hindered dynamics in comparison with the α process.

Thus, it is shown that the interface is instrumental in determining the dynamics, giving rise to a relaxation time gradient across the cooperativity length scale of the guest. Depending on the guest-host interfacial conditions, dynamics can become faster or slower for guest at the same confinement size and identical experimental technique.

Another way of understanding all the results is to rationalize in terms of hard (molecular sieves) as well as soft (PLLA crystallites/RAP) confinement, where the length scale of the confinement competes with the spatial extent of cooperative motion. In the latter, the situation is more complex to rationalize since the same polymeric chain can participate simultaneously in the different phases. The

results point strongly towards the interface generating the main impact, while the pore or droplet size determines only the number of molecules which are at a certain distance away from the surface.

Finally, in face of the above stated it would be interesting as a future work to further investigate the guest's dynamical behavior in the case of hard confinement by modifying the inner pore surface by functionalization. In the case of the soft one, the study of the mixture of PLLA with another semicrystalline polymer as blend to test the influence on its morphology and dynamics would be also very attractive.

ANNEXES

Annex I.

a) Temperature dependence of the dielectric relaxation strength for the three secondary processes, β_I, β_{II} and β_{III}, of PLLA crystallized at the different studied T_C in Chapter V.

	Tc = 368 K			Tc = 383 K			Tc = 398 K			Tc = 413 K			Tc = 428 K			Tc = 438 K		
	Δε			Δε			Δε			Δε			Δε			Δε		
Temp. [K]	β_{III}	β_{II}	β_I	β_{III}	β_{II}	β_I	β_{III}	β_{II}	β_I	β_{III}	β_{II}	β_I	β_{III}	β_{II}	β_I	β_{III}	β_{II}	β_I
203	0.0100	0.0089	0.0193	0.0170	0.0065	0.0215	0.0100	0.0080	0.0173	0.0094	0.0083	0.0197	0.0067	0.0110	0.0185	0.0070	0.0248	0.0224
208	0.0100	0.0089	0.0200	0.0170	0.0066	0.0220	0.0130	0.0070	0.0175	0.0100	0.0086	0.0197	0.0079	0.0112	0.0185	0.0070	0.0247	0.0224
213	0.0109	0.0089	0.0200	0.0170	0.0064	0.0229	0.0130	0.0070	0.0175	0.0100	0.0101	0.0200	0.0091	0.0112	0.0187	0.0070	0.0243	0.0224
218	0.0109	0.0089	0.0199	0.0170	0.0065	0.0232	0.0140	0.0070	0.0180	0.0117	0.0107	0.0193	0.0101	0.0112	0.0187	0.0070	0.0245	0.0214
223	0.0117	0.0096	0.0196	0.0170	0.0069	0.0237	0.0130	0.0073	0.0180	0.0113	0.0114	0.0193	0.0112	0.0119	0.0183	0.0070	0.0248	0.0213
228	0.0122	0.0096	0.0196	0.0170	0.0070	0.0237	0.0130	0.0075	0.0183	0.0113	0.0114	0.0193	0.0108	0.0117	0.0187	0.0090	0.0235	0.0209
233	0.0122	0.0101	0.0196	0.0175	0.0060	0.0251	0.0130	0.0076	0.0190	0.0113	0.0114	0.0193	0.0119	0.0117	0.0187	0.0090	0.0233	0.0209
238	0.0125	0.0101	0.0196	0.0200	0.0060	0.0240	0.0130	0.0077	0.0193	0.0113	0.0114	0.0193	0.0122	0.0126	0.0179	0.0092	0.0227	0.0209
243	0.0131	0.0104	0.0201	0.0197	0.0075	0.0237	0.0130	0.0077	0.0193	0.0113	0.0114	0.0193	0.0122	0.0126	0.0179	0.0092	0.0227	0.0209
248	0.0142	0.0116	0.0194	0.0162	0.0093	0.0200	0.0130	0.0077	0.0195	0.0113	0.0116	0.0195	0.0122	0.0126	0.0179	0.0096	0.0223	0.0209
253	0.0137	0.0107	0.0207	0.0139	0.0105	0.0208	0.0133	0.0077	0.0195	0.0113	0.0118	0.0195	0.0122	0.0122	0.0183	0.0097	0.0221	0.0209
258	0.0136	0.0102	0.0213	0.0139	0.0105	0.0208	0.0135	0.0078	0.0197	0.0113	0.0116	0.0195	0.0122	0.0118	0.0188	0.0097	0.0216	0.0208
263	0.0137	0.0096	0.0211	0.0139	0.0107	0.0208	0.0137	0.0078	0.0195	0.0120	0.0110	0.0199	0.0122	0.0113	0.0192	0.0110	0.0206	0.0208
268	0.0140	0.0092	0.0214	0.0139	0.0107	0.0208	0.0143	0.0077	0.0197	0.0120	0.0108	0.0199	0.0122	0.0112	0.0192	0.0110	0.0206	0.0208
273	0.0140	0.0092	0.0214	0.0139	0.0107	0.0208	0.0143	0.0077	0.0197	0.0127	0.0107	0.0199	0.0122	0.0103	0.0192	0.0110	0.0201	0.0208
278	0.0144	0.0086	0.0214	0.0143	0.0100	0.0208	0.0153	0.0078	0.0197	0.0130	0.0103	0.0199	0.0122	0.0091	0.0198	0.0115	0.0194	0.0208
283	0.0151	0.0079	0.0214	0.0143	0.0100	0.0208	0.0153	0.0076	0.0198	0.0132	0.0101	0.0199	0.0129	0.0082	0.0199	0.0119	0.0184	0.0208